Multiparametric Quantitative MRI of the Cervical Spinal Cord to Measure Microstructure and Tissue Injury: Development, Validation, and Applications of a Clinically Feasible Protocol

by

Allan Russell Martin

A thesis submitted in conformity with the requirements
for the degree of Doctor of Philosophy

Institute of Medical Science
University of Toronto

Multiparametric Quantitative MRI of the Cervical Spinal Cord to Measure Microstructure and Tissue Injury: Development, Validation, and Applications of a Clinically Feasible Protocol

Allan Russell Martin

Doctor of Philosophy

Institute of Medical Science
University of Toronto

2017

Abstract

An array of spinal cord (SC) quantitative MRI (qMRI) techniques can measure aspects of microstructure and tissue injury. This research develops a clinically feasible multiparametric MRI protocol, including diffusion tensor imaging (DTI) fractional anisotropy (FA), magnetization transfer ratio (MTR), and measurement of SC cross-sectional area (CSA). A novel biomarker of white matter (WM) injury is also introduced, normalizing T2*WI WM signal intensity by grey matter (T2*WI WM/GM). A study of 40 healthy subjects establishes methods, normalization procedures, normative values, and reliability. 58 patients with degenerative cervical myelopathy (DCM) are studied, showing significant differences in 10 metrics. Combining these measures using multivariate methods overcomes the limitations of each technique, achieving good diagnostic accuracy and clinical correlation. T2*WI WM/GM shows strong potential as a novel biomarker, comparing favourably with established biomarkers FA and MTR. Our study of healthy subjects identifies an alarming rate of asymptomatic SC compression (ASCC) at 50%. Objective criteria and automated shape analysis are developed to create a new definition of SC compression, and qMRI demonstrates significant tissue injury in this group.

This finding suggests the potential for pre-symptomatic diagnosis of DCM and other spinal pathologies. Finally, a longitudinal study compares multiparametric qMRI with clinical measures for monitoring disease progression in DCM, indicating that modified Japanese Orthopedic Association (mJOA) score is insensitive to detect progression, whereas qMRI showed tissue progression more often than comprehensive clinical assessments. These results suggest that natural history studies employing mJOA underestimate progression, due to neuroplasticity and behavioural adaptation. Combined qMRI and clinical data are now being used to inform surgical decision-making for individual patients. Reliable multiparametric assessment of SC microstructure is possible using clinically suitable methods. This approach shows strong clinical utility for individual patients, including good diagnostic accuracy, correlations with impairment, detection of tissue injury in asymptomatic individuals, and detection of progressive tissue injury in DCM patients.

Acknowledgments

I received post-doctoral fellowship support from Canadian Institutes of Health Research (CIHR) and the Ministry of Health Clinician Investigator Program (MOH-CIP). This research received operational funding support from Rick Hansen Institute, as part of the Riluzole in Spinal Cord Injury Study – MRI (RISCIS-MRI) substudy, which is also supported by AOSpine North America, AOSpine International SCI Knowledge Forum, and the North American Clinial Trials Network (NACTN) of the Christopher and Dana Reeve Foundation. This research also received support from the Dezwirek Foundation, the Sherman Clinical Research Unit, and the Gerald and Tootsie Halbert Chair in Spinal Cord Research, for which I am grateful.

I would like to thank all of the patients and healthy subjects for their enthusiastic participation in this research. I would also like to acknowledge and thank the large group of individuals that made indispensable contributions to this work (see contributions section). I would like to personally thank my supervisor and mentor, Dr. Fehlings, for his personal interest in my well-being, his exceptional career mentorship, and his thoughtful academic guidance. Finally, I would like to highlight the commitment, sacrifice, hard work, and acceptance of delayed gratification that my beautiful wife, Kirsten Martin, has provided, in addition to the loving support of my wonderful children Zia, Scarlett, and Leo.

Contributions

The systematic review in Chapter 1, and the original research studies described in Chapters 2-5 were all primarily conceived of, designed by, and conducted by me (Allan Martin). However, the work was a collaborative effort with indispensible contributions from numerous individuals, most of all, Dr. Michael Fehlings and Dr. Julien Cohen-Adad, neither of whom this research would be possible without. The contributions of each individual involved in this research are as follows:

Supervisor: Dr. Michael Fehlings, who contributed leadership, knowledge, guidance, data interpretation, editing of manuscripts, and supervision over all aspects of this research, in addition to exceptional career mentorship and personal support.

Program Advisory Committee (PAC) Members: Dr. David Mikulis, Dr. Howard Ginsberg, Dr. Adrian Crawley, who contributed ideas, feedback, data analysis, editing of manuscripts, and guidance to all components of this research.

Technical Collaborators: Dr. Julien Cohen-Adad, who helped to set up and optimize all MRI protocols and analysis tools based on his previous experience and expertise, in addition to providing strategic guidance, technical support, and contributing to all aspects of the research (design, data analysis, interpretation, and manuscript writing); and Benjamin De Leener, who helped to create and enhance analysis tools (segmentation, registration algorithm, automated shape analysis tools), analyze data, edit manuscripts, and provide technical support for all original research.

Co-authors: Dr. David Cadotte, Dr. Lindsay Tetreault, Dr. Sukhvinder Kalsi-Ryan, Dr. Aria Nouri, Dr. Jefferson Wilson, Stefan Lange, who contributed to data collection, data analysis, interpretation, and writing of this research.

MRI Technicians: Keith Ta, Eugen Hlasny, for their patience and attention to detail in performing all MRI studies.

Undergraduate Students (Research Assistants): Samantha Smith, Justin Wang, Zenovia Tarmohamed, Nathaniel Smith, Stefan Lange, Elizabeth Fryer, Lauren Riehm, who assisted with various aspects of data collection and/or literature review.

Research Coordinators, Administrators, Research Managers: Natalia Nugaeva, Yuliya Petrenko, Christina Cherian, Amy Lem, Libertad Puy, Anoushka Singh, Yuriy Petrenko, Paul Bradshaw.

Table of Contents

List of Abbreviations

AD: axial diffusivity

ADC: apparent diffusion coefficient

AP: anterior-posterior

ASCC: asymptomatic spinal cord compression

AUC: area under the curve

BOLD: blood oxygen level dependent

CHESS: chemical selective water suppression

Cho: choline

COV: coefficient of variation

Cr: creatine

CR: compression ratio

CSA: cross-sectional area

CSF: cerebrospinal fluid

CSM: cervical spondylotic myelopathy

DCM: degenerative cervical myelopathy

DDE: double diffusion encoding

DKI: diffusion kurtosis imaging

DTI: diffusion tensor imaging

EPI: echo planar imaging

FA: fractional anisotropy

FC: fasciculus cuneatus

FG: fasciculus gracilis

FLAIR: fluid attenuated inversion recovery

fMRI: functional MRI

FOV: field of view

FSE: fast spin echo

GE: gradient echo

GM: grey matter

ihMT: inhomogenous magnetization transfer

kNN: k-nearest neighbors

L: left
Lac: lactate
LCST: lateral corticospinal tract
LDA: linear discriminant analysis
LR: logistic regression
MD: mean diffusivitiy
MERGE: multi-echo recombined gradient echo
MRI: magnetic resonance imaging
MRS: magnetic resonance spectroscopy
MS: multiple sclerosis
MT: magnetization transfer
MTR: magnetization transfer ratio
MTsat: magnetization transfer saturation
MWF: myelin water fraction
MyoI: myo-inositol
NAA: N-acetylaspartate
NEX: number of excitations
NODDI: neurite orientation and density dispersion imaging
OLF: ossified ligamentum flavum
OPLL: ossified posterior longitudinal ligament
PAC: program advisory committee
PCA: principal component analysis
PRESS: point resolved spectroscopy
qMRI: quantitative MRI
R: right
RD: radial diffusivity
rFOV: reduced field of view
ROC: receiver operating characteristic function
SC: spinal cord
SCI: spinal cord injury
SCT: Spinal Cord Toolbox
SE: spin echo

SL: spinal lemniscus

SNR: signal to noise ratio

SPGR: spoiled gradient echo

ssEPI: single shot echo planar imaging

STIR: short tau inversion recovery

STM: support tensor machine

SVM: support vector machine

T: Tesla

T1: longitudinal (spin-lattice) relaxation time

T1WI: T1-weighted imaging

T2: transverse (spin-spin) relaxation time

T2WI: T2-weighted imaging

T2*WI: T2*-weighted imaging

T2*WI WM/GM: T2*-weighted imaging white matter to grey matter signal intensity ratio

TE: echo time

TI: inversion time

TR: repetition time

TRCOV: test-retest coefficient of variation

VCs: ventral columns

WM: white matter

List of Tables

List of Figures

List of Appendices

Chapter 1
Background: The Limitations of Conventional MRI to Characterize Spinal Cord Tissue Injury in Degenerative Cervical Myelopathy, and the Potential Role of Quantitative MRI*

*This chapter includes content that was adapted from: (Martin et al., 2016) with permission. Dr. Martin was also a co-author of the following publications that involve related topics: (Nouri et al., 2016, Kurpad et al., 2017, Fehlings et al., 2017, Ahuja et al., 2016, Martin et al., 2017a).

This chapter begins with an overview of the pathological condition degenerative cervical myelopathy (DCM), which is the clinical population of interest in this dissertation. This is followed by a brief overview of conventional MRI and its limitations in providing detailed information about the health of the spinal cord. Then, a systematic review of the literature is included, entitled "Translating state-of-the-art spinal cord MRI techniques to clinical use: a systematic review of clinical studies utilizing DTI, MT, MWF, MRS, and fMRI," (Martin et al., 2016). Several of the tables from this manuscript are too large to conform to the formatting requirements for this document, and the reader is referred to Appendix A. This is followed by an update of research reports that were published after the electronic database search of the systematic review, and then a section that reviews T2*-weighted imaging. Finally, the objectives and specific aims of this research are presented, setting the stage for the ensuing chapters describing 4 original research studies that form the core of this dissertation.

1.1 Degenerative Cervical Myelopathy

1.1.1 Terminology

The term degenerative cervical myelopathy describes the collection of pathologies that arise from age-related degenerative changes in the cervical spine and cause extrinsic compression on the spinal cord (Nouri et al., 2015b). Specific pathologies included in this umbrella term include cervical spondylotic myelopathy (CSM), ossification of the posterior longitudinal ligament (OPLL), disk herniations, degenerative spondylolisthesis, and ossification of the ligamentum flavum (OLF). The terminology for these specific conditions has often been used interchangeably (e.g. CSM studies that include single-level disc herniations), leading to

confusion amongst clinicians, researchers, patients, and the general public. Much of the Japanese literature has used a similar umbrella term, “compressive cervical myelopathy” to describe this condition. For the remainder of this manuscript, the term DCM is used to describe all of these pathologies for the purpose of consistency.

1.1.2 **Prevalence and Diagnosis**

DCM is the most common cause of spinal cord dysfunction in adults (Kalsi-Ryan et al., 2013a, Karadimas et al., 2013, Nouri et al., 2015b). The prevalence has been estimated at 605 cases per million in North America, but this estimate was based only on subjects with severe motor deficits (paraplegia and quadriplegia), and is almost certainly an underestimate given that mild DCM is far more common. Regardless, DCM is a highly prevalent condition that frequently goes unrecognized by patients and primary care clinicians until severe deficits have developed, contributing to the burden of disability that it causes (Wu et al., 2013). Diagnosis is typically made based on the presences of 1 or more symptom and 1 or more neurological sign that localize to the spinal cord, in addition to MRI (or CT myelography) evidence of spinal cord compression. However, diagnosis is not always straightforward, as asymptomatic spinal cord compression (ASCC) is also a common entity (Wilson et al., 2013), indicating that MRI evidence of SC compression is not sufficient to make the diagnosis, and neurological symptoms and signs are often vague, transient, and subjective in nature. Some studies have used MRI T2-weighted imaging (T2WI) signal hyperintensity for diagnosis, but this is a poor choice as it is present in only 50-70% of DCM subjects, and it is also occasionally seen in asymptomatic individuals (Nouri et al., 2016). Electrophysiology studies such as somatosensory evoked potentials (SSEPs) and motor evoked potentials (MEPs) are not helpful to make the diagnosis of myelopathy, as they lack sensitivity and specificity (Bednarik et al., 1999, Kerkovsky et al., 2012, Wen et al., 2014b).

1.1.3 **Pathophysiology**

The pathophysiology of DCM involves a complex cascade of events that has been only partially elucidated, but typically begins with structural deterioration of the intervertebral disc, followed by collapse of disc height, disc protrusion into the spinal canal, joint hypermobility, hypertrophy of the ligamentum flavum, and osteophyte formation (Figure 1.1) (Karadimas et al., 2013). These changes culminate in canal stenosis, causing static spinal cord (SC) compression, ischemia, and

motion-related (dynamic) trauma. The chronic state of tissue ischemia causes endothelial cell loss and reduction of laminin, indicating a state of microvascular dysfunction, but the intricate molecular mechanisms underlying these changes have yet to be elucidated (Karadimas et al., 2013). Cadaver studies indicate that atrophy and neuronal loss occur in the ventral horns and intermediate zone first, followed by degeneration of the white matter (WM) in the lateral and dorsal funiculi in more advanced cases (Ito et al., 1996, Kameyama et al., 1994). The pathological processes also involve demyelination and remyelination, resulting in thin myelinated fibers (Ito et al., 1996).

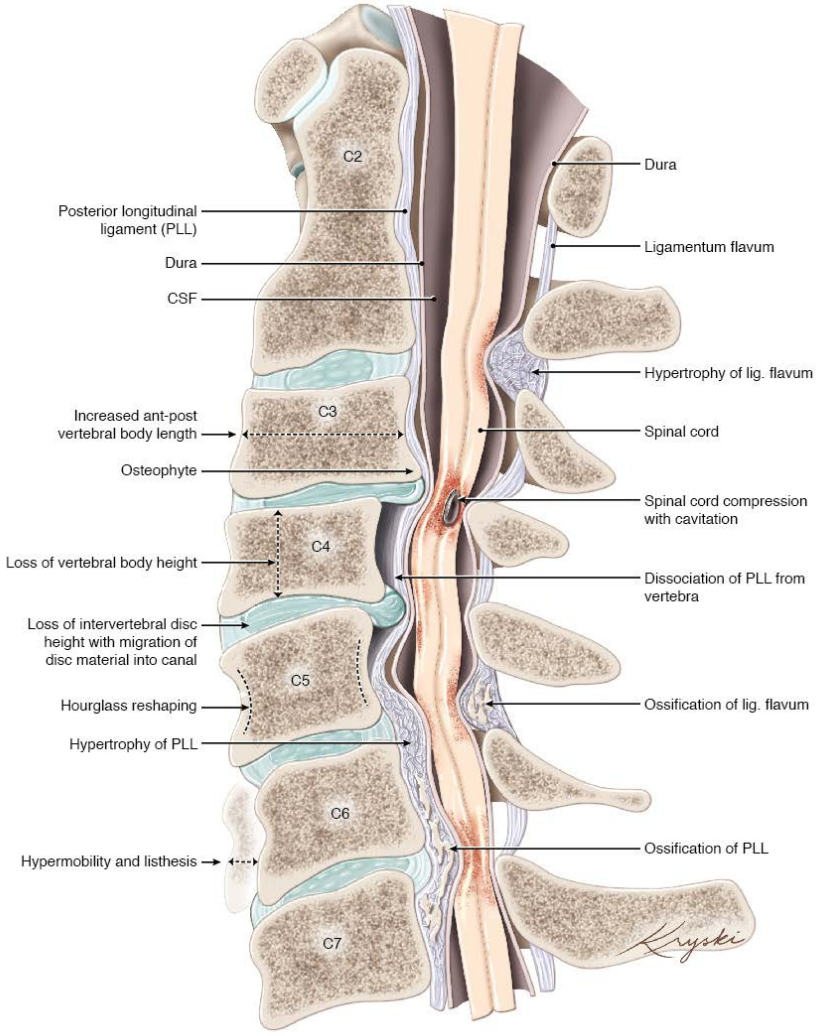

Figure 1.1: Pathophysiology of Degenerative Cervical Myelopathy. The pathological cascade of events is variable between subjects, but often begins with loss of intervertebral disc height, following by a host of changes including hypermobility, osteophyte formation, flattening and widening of the vertebral bodies (spondylosis), hypertrophy and/or ossification of the ligaments, and ultimately, spinal cord compression. Reproduced with permission from: (Nouri et al., 2015b).

1.1.4 **The Natural History of DCM**

The course of DCM is unpredictable, ranging from clinical stability for many years to rapid or stepwise decline to severe disability (Matz et al., 2009). However, the majority of individuals with DCM have stable symptoms or very slow progression. Several systematic reviews have been recently performed,(Matz et al., 2009, Karadimas et al., 2013, Rhee et al., 2013, Ghobrial and Harrop, 2015) finding low quality evidence that 20-62% of subjects will deteriorate in 3-7 years follow-up, although these studies used vague and variable definitions of deterioration and further prospective research is needed. Strong predictors of which patients will decline have not been identified, but 1 study suggested that longer duration of disease has worse outcome with non-operative management (Yoshimatsu et al., 2001). Non-operative treatments such as cervical collars and physiotherapy are alternatives to surgery, but these have also not been adequately studied (Rhee et al., 2013). As such, there are several knowledge gaps that make it difficult to provide non-operative DCM patients with an accurate prognosis.

1.1.5 **Surgical Treatment of DCM**

Cervical spinal cord compression can be relieved by either anterior or posterior surgery (or combined). These approaches have been used for decades, and both continue to be used in approximately equal proportions. Numerous variants of both approaches have been described and utilized; anterior procedures include anterior cervical discectomy (ACD), anterior cervical discectomy and fusion (ACDF) with or without metallic fixation, anterior cervical corpectomy and fusion (ACCF), multilevel ACDF (Figure 1.2), or multilevel hybrid (combination) techniques, and posterior procedures include laminectomy alone, laminectomy with instrumented fusion, and laminoplasty. Numerous factors influence surgical decision-making in terms of the approach and specific procedure, including direction of SC compression (anterior or posterior), number of levels, anterior access (to higher levels), kyphosis, and surgeon familiarity. Both anterior and posterior approaches are reasonably safe procedures and have roughly equivalent risk overall, although the risk of specific complications differs considerably such as dysphagia (greater with anterior surgery) and wound infection (greater with posterior surgery).

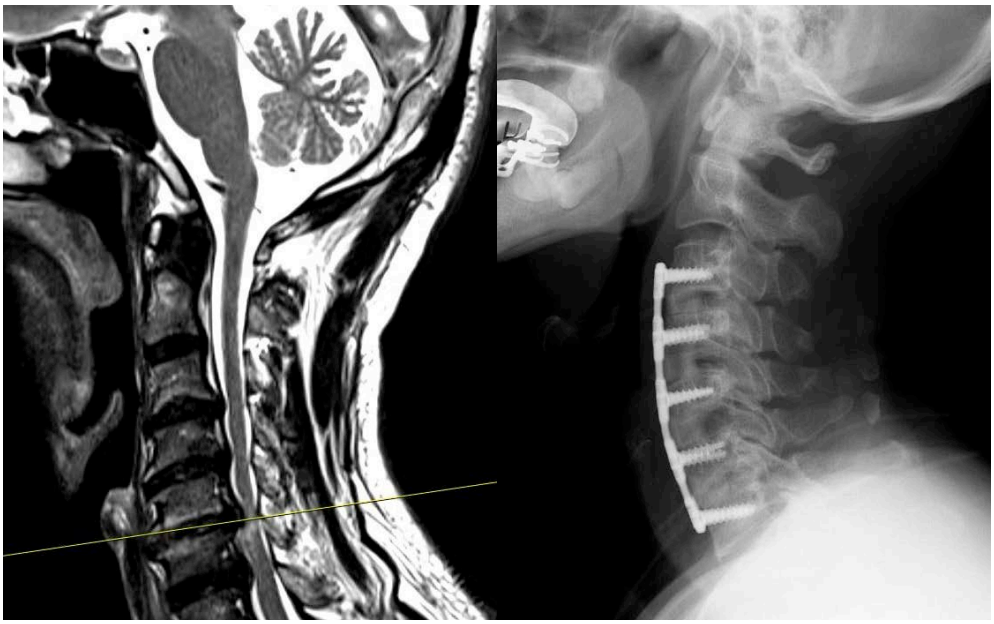

Figure 1.2: Surgical Treatment of Multilevel Degenerative Cervical Myelopathy. Sagittal T2-weighted image (left panel) showing multilevel degenerative changes with bulging discs, remodeled vertebrae, and ligamentum flavum hypertrophy causes spinal cord compression. Compression is maximal at C5-6, with intramedullary T2-weighted hyperintensity. Lateral radiograph (right panel) shows a 4-level anterior cervical discectomy and fusion with an anterior titanium plate.

However, the surgical treatment of DCM has been a topic of debate for decades. For many years the prevailing attitude was that surgery only halts the progression of DCM, while the vast majority of patients remain stable without surgery. This issue has also been clouded by conflicting results in the literature. Only 1 randomized controlled trial (RCT) has been performed, and this small study of 48 DCM patients (21 treated with surgery, 27 without) showed no difference in outcomes between groups at multiple follow-up periods out to 10 years (Kadanka et al., 2011, Kadanka et al., 2000, Kadanka et al., 2005). Of note, the non-operative group in this study showed minimal decline (at the low end of natural history estimates), while the subjects undergoing operative treatment showed no benefit following surgery. However, mounting evidence from more than a dozen large prospective studies indicates that surgery

provides considerable benefits. Our group recently performed a systematic review on this topic, and 27 studies were found, and all found statistically significant benefits of surgery (while the Kadanka et al. study did not meet inclusion criteria due to small sample size) ~~[INSERT GUIDELINES REF]~~.(Fehlings et al., 2017) The largest of these studies were the multi-center study by Fehlings et al. (2013) of 260 patients in North America, showing an average mJOA improvement of 2.88 points after 12 months, and the multi-center study by Fehlings et al. (2015) of 479 patients distributed globally, which showed a 2.40-point improvement of mJOA at 24-month follow-up. The systematic review concluded that moderate level evidence exists showing a benefit with surgery, but the level of evidence was not considered high due to the lack of an RCT. Based on the current evidence, attitudes are shifting toward a greater acceptance of surgery for DCM.

1.1.6 Guidelines for the Management of Degenerative Cervical Myelopathy

Recently, an effort to develop guidelines for the management of DCM was initiated, which was sponsored by CSRS and AOSpine North America and led by Dr. Michael Fehlings (of which I was a voting member) (Fehlings et al., 2017). This 3-year process began with the guidelines development group (GDG) performing numerous systematic reviews to characterize the natural history, efficacy of non-operative treatment, and efficacy of surgery. The GDG subsequently made a recommendation for surgical treatment of DCM for patients with moderate or severe impairment (Fehlings et al., 2017). However, for mild DCM, the GDG could not come to a consensus on the optimal treatment, due to the smaller improvements in neurological status obtained with surgery (due to ceiling effect), the risk of surgery, and the poorly characterized natural history without surgery. After vigorous discussion, we created a recommendation suggesting that surgical management is a treatment option in mild myelopathy; however, we made a clear recommendation for surgery in patients that show deterioration. However, the guidelines did not include an objective definition of deterioration (i.e. how much, and by what measure), and this was left up to individual practitioners to determine.

1.1.7 Knowledge Gaps for Future Research

The knowledge regarding DCM and its surgical treatment has evolved dramatically over the past decade, but further work is needed in several areas. First, the mild subgroup of DCM patients is

by far the most interesting from a research perspective because, arguably, there is equipoise between operative and non-operative treatment, whereas we have clear guidelines on how to manage moderate and severe patients. One approach to the mild subgroup would be to conduct a RCT to compare operative and non-operative treatments. This is, however, problematic because 1) large RCTs are costly, 2) the optimal non-operative treatment has not been identified, 3) a benefit of surgery has been established in large prospective studies, and 4) patient preferences need to be taken into account, and in this case patients likely have enough information about the risks and benefits of surgery to make an informed decision. Therefore, a new RCT is unlikely to happen for DCM. Instead, clinical tools that can predict which mild DCM patients are more likely to decline without surgery could help to inform decision-making, allowing surgery to be targeted to these individuals. Similarly, tools that can improve outcome prediction in surgical patients would also be beneficial, differentiating between those that are likely to improve or remain the same after decompression. Furthermore, improved monitoring of patients managed non-operatively with more objective assessment methods would also be beneficial, as this could help detect disease progression earlier and indicate the need for surgery before severe deficits develop. Finally, an additional area for future research involves the diagnosis of DCM, which is easy to make in moderate or severe cases but is often challenging to be confident of the diagnosis in mild subjects. Therefore, novel diagnostic tools that can discriminate whether or not mild symptoms are due to cervical spinal cord dysfunction would be valuable.

1.2 The Role of Conventional MRI in DCM

The advent of magnetic resonance imaging (MRI) in the mid-1980s transformed the field of spinal cord imaging and provided clinicians with high-resolution anatomical images, directly leading to improved clinical decision-making. MRI takes advantage of the fact that different biological tissues have different physical properties, including the longitudinal (or spin-lattice) relaxation time, known as T1, the transverse (or spin-spin) relaxation time, known as T2, and free induction decay time, known as T2* (Hashemi et al., 2010). T1 is the time constant that describes the relaxation rate (R1 = 1/T1) to reach equilibrium with an applied external magnetic field. T2 is the time constant that characterizes the rate (R2 = 1/T2) of dephasing that is specifically due to spin-spin interactions, whereas T2* describes the rate (R2* = 1/T2*) of dephasing that is due to both spin-spin interactions and magnetic field inhomogeneity. Thus, T2* is also affected by local perturbations of the magnetic field due to ferromagnetic and

paramagnetic materials, known as susceptibility. Conventional MRI typically involves a strong main magnetic field (B_0), which causes water protons to rotate (precess) around the B_0 vector at the Larmor frequency. This frequency is specific to water protons because of their local magnetic environment (including the covalent bond to oxygen). These water protons can then be manipulated to produce 2D and 3D images by using radiofrequency (RF) pulses at the Larmor frequency and by manipulating the magnetic field using gradients. Conventional MRI includes pulse sequences such as spin echo, gradient echo, and inversion recovery, which can yield images with different contrasts depending on the relaxation time (TR) and echo time (TE) that are used. In general, T1-weighted images (T1WI) are obtained with short TR and short TE, T2-weighted images (T2WI) with long TR and long TE, and proton density (PD) images with long TR and short TE. Spin echo begins with application of a 90° RF excitation (or induction) pulse at the Larmor frequency for a length of time ~~(1/4 of the period of the Larmor frequency), which~~ that changes the net magnetization vector from being parallel to the main magnetic field (labeled B_0) to being perpendicular and puts water proton spins into phase. The 90° pulse is then followed by one or more 180° refocusing pulses (e.g. at time TE/2) that counteract spin dephasing due to local magnetic field inhomogeneity, followed by the application of readout gradient (e.g. at time TE). Spin echo can produce T2-weighted images, as it removes/minimizes susceptibility effects, and it also has the advantage of producing relatively uniform images in spite of imperfections in the main magnetic field. Instead of 90° induction pulses, gradient echo uses a shorter RF pulse (i.e. flip angle less than 90°) and a negative polarity dephasing gradient, followed by an opposite rephasing gradient during readout (typically twice as long). The use of smaller flip angles leaves some longitudinal magnetization, allowing shorter TR than in spin echo. The contrast produced by gradient echo depends on the flip angle, in addition to TR and TE, including T1-weighting (large flip angle), PD-weighting (small flip angle), and T2*-weighting (small flip angle). Pure T2-weighting is not possible with gradient echo, but some variations of the sequence have been developed to provide relatively strong T2-weighting (i.e. minimizing T2*-effects). Inversion recovery is a variation of spin echo that begins with a 180° inversion pulse, following by a period of time called the inversion time (TI) before the 90° pulse that is selected to null the signal from certain tissues. Common applications of this approach including reducing fat signal in short tau inversion recovery (STIR) and water signal in fluid attenuated inversion recovery (FLAIR). Spin echo, gradient echo, and inversion recovery sequences have been refined over 3 decades of

clinical use and each are highly useful for different applications, making MRI the imaging modality of choice for most spinal disorders.

However, conventional MRI provides only modest information regarding the health and integrity of the spinal cord tissue itself. T2-weighted signal hyperintensity (T2WI-HI) is non-specific and corresponds with a variety of physiological processes, variably including edema, gliosis, demyelination, myelomalacia, and cavitation (Wada et al., 1995). This is reflected in relatively poor correlation of T2WI hyperintensity (T2WI-HI) with neurological and functional impairment in DCM and other spinal pathologies, and failure to provide reliable prognostic information (Matsuda et al., 1999; Yukawa et al., 2007, Cadotte et al., 2011)(Wada et al., 1995, Matsuda et al., 1999, Tetreault et al., 2013, Wilson et al., 2012, Nouri et al., 2015a, Nouri et al., 2015c, Tetreault et al., 2015a). In multiple sclerosis (MS), numerous studies have found that spinal cord lesion load (appearing as areas of T2WI-HI) is less important than atrophy, measured as the cross-sectional area (CSA) of the cord (Stevenson et al., 1998). In DCM, relatively weak correlates with clinical status have been identified between T2WI-HI and measures of cord compression (Wada et al., 1995, Matsuda et al., 1999, Tetreault et al., 2013). Wada et al. observed that T1 signal hypointensity is a more specific marker that suggests permanent changes such as gliosis, myelomalacia, and cavitation, suggesting a worse prognosis with or without surgical decompression (Wada 1999; Chibarro et al., 2006)(Nouri et al., 2015a, Nouri et al., 2015c). To improve upon the modest results observed with T2WI, Chen et al. (2001) proposed the categorization of T2WI-HI into type I, defined as “fuzzy” mild hyperintensity without a clear border, and type II, strong hyperintensity with a clearly defined border. This distinction showed improved correlations with impairment, primarily because type II T2WI-HI is usually associated with T1WI hypointensity, so it seems they tend to represent the same phenomenon of cavitation and myelomalacia. Nouri et al. (2015c) extended this work by making the distinction more objective, calculating a ratio of the average signal intensity within the hyperintense region to that of the normal spinal cord. However, the results of this approach were again modest, and this type of manual calculation is more suited for research than clinical use, as radiologists are unlikely to perform this extra measurement without a stronger impetus. There is also some indication that the post-operative regression of T2 signal hyperintensity following surgical decompression does correlate with a good outcome (Park et al., 2006; Mastronardi et al., 2007). Furthermore, there may be some additional value in combining the information from both T1 and T2 signal changes

(e.g. calculating the ratio of T2/T1 signal), which several authors have used to demonstrate a correlation with functional impairment and outcome following surgery (Suri et al., 2003; Suda et al., 2003; Kim et al., 2008; Vedantum et al., 2011; Tetreault et al., 2013). However, in spite of the many efforts to utilize T1WI and T2WI signal changes, they ultimately offer modest correlation with impairment and weak prediction of outcome, and they are only present in 10-20% and 50-70% of DCM patients, respectively, limiting their practical use. As a result, it can be concluded that intramedullary signal intensity changes on conventional MR images are of limited value as imaging biomarkers.

1.3 Translating state-of-the-art spinal cord MRI techniques to clinical use: A systematic review of clinical studies utilizing DTI, MT, MWF, MRS, and fMRI

1.3.1 Moving Beyond Conventional MRI

A 2013 international meeting of spinal cord imaging experts, sponsored by the International Spinal Research Trust (ISRT) and the Wings for Life (WfL) Spinal Cord Research Foundation, outlined 5 emerging MRI techniques that have the potential to revolutionize the field, by elucidating details of the microstructure and functional organization within the spinal cord (Stroman et al., 2014, Wheeler-Kingshott et al., 2014). This group highlighted the following techniques due to their ability to characterize microstructural features of the spinal cord: diffusion tensor imaging (DTI), magnetization transfer (MT), myelin water-fraction (MWF), and magnetic resonance spectroscopy (MRS). DTI measures the directional diffusivity of water, and several of the metrics that it produces correlate with axonal integrity, and to a lesser degree, myelination (Wheeler-Kingshott et al., 2002). MT involves an off-resonance saturating pre-pulse that takes advantage of the chemical and magnetization exchange between protons bound to lipid macromolecules and nearby water protons, and provides a surrogate measure of myelin quantity (Graham and Henkelman, 1997). This is most often expressed in a ratio between scans with and without the pre-pulse (MTR) or between the spinal cord and cerebrospinal fluid (MTCSF). MWF estimates the fraction of tissue water bound to the myelin sheath, by fitting the T2 relaxation curve to a multi-exponential model and identifying the fraction of the signal with a T2 parameter between 15 and 40 ms (Wu et al., 2006). MRS quantifies either the absolute or relative concentrations of specific molecules of interest within a single large voxel, including N-acetylaspartate (NAA), myo-inositol (Ins), choline (Cho), creatine (Cre), and lactate (Lac)

(Gomez-Anson et al., 2000). The expert panel also highlighted functional MRI (fMRI) of the spinal cord, due to its potential to characterize changes in neurological function, using either blood oxygen-level dependent (BOLD), which relies upon the concept of neuro-vascular coupling in which changes in neurological function produce corresponding changes in local blood flow, or signal enhancement by extravascular protons (SEEP), which is thought to detect neural activity indirectly through changes in the intracellular/extracellular volume ratio (Stroman et al., 2001). fMRI studies can involve a variety of designs, including motor tasks or sensory stimuli in block or event-related designs, and can visualize and provide indirect measures reflecting neuronal activity and connectivity occurring within the spinal cord (Stroman et al., 2014).

All 5 of these emerging MRI techniques are highly amenable to quantitative analysis, offering the opportunity to develop quantitative MRI biomarkers that correlate with disability and/or predict outcomes. The development of these techniques may also provide more sensitive and specific diagnostic tests. For example, in the earliest stages of CSM, symptoms may include vague complaints of numbness and neck pain, but the cause may be unclear between early myelopathy vs. musculoskeletal pain and peripheral nerve compression. Objective evidence of damage to the cord tissue could provide important information to prompt earlier surgery. Furthermore, quantitative biomarkers could act as surrogate outcome measures in clinical trials, such as therapeutic remyelination agents in MS or spinal cord injury (SCI), providing short-term end-points and reducing the time and costs associated with novel drug development (Cadotte and Fehlings, 2013). In acute SCI, these techniques could potentially discriminate reversible and irreversible components of damage (demyelination, axonal loss, grey matter loss) early after injury, and thus provide a more accurate prognosis to help guide therapeutic strategies and focus rehabilitation resources.

Unfortunately, the application of these advanced MRI techniques to image the spinal cord is far from trivial. These techniques were initially developed and validated in brain imaging, but the spinal cord is a far more challenging structure to obtain accurate data. In fact, the spine is among the most hostile environments in the body for MRI, due to magnetic field inhomogeneity at the interfaces between bone, intervertebral disc, and cerebrospinal fluid (CSF), and also because of the small size of the cord and its white matter tracts, and the relatively large motion of the cord during cardiac and respiratory cycles (Stroman et al., 2014). High-quality spinal cord imaging

using these methods has only recently been achieved, requiring specialized acquisition sequences, complex shimming, custom receive coils, long acquisition times, and substantial post-processing to correct for motion, aliasing, and other artefacts.

1.3.2 **Aims of this Review**

This systematic review aims to summarize the progress of clinical translation of these imaging techniques to date, and identify the most common technical methods employed. The review will also highlight the major barriers that are currently preventing the adoption of these techniques into clinical use. The search was designed to identify all studies that applied one or more of these MRI techniques to assess for clinical utility in one or more of the following 3 key questions:

1. Diagnostic Utility: Does the MRI technique provide metrics that demonstrate group differences or improved diagnostic accuracy (sensitivity/specificity) in the diagnosis of spinal pathologies?

2. Biomarker Utility: Does the advanced MRI technique generate metrics that quantify the amount of injury and thus correlate with neurological/functional impairment and/or show longitudinal changes over time that correlate with changes in disability in spinal pathologies?

3. Predictive Utility: Does the advanced MRI technique generate metrics that predict neurological, functional, or quality of life outcomes in spinal pathologies?

1.3.3 **Methods**

1.3.3.1 *Electronic Literature Search*

A systematic search of MEDLINE, MEDLINE-in-Progress, Embase, and Cochrane databases was conducted, with the results formatted in accordance with the PRISMA statement for systematic reviews and meta-analyses (Liberati et al., 2009). The search included literature published from January 1, 1985 to June 1, 2015 and sought all studies that describe the use of one or more of the state-of-the-art spinal cord MRI techniques (DTI, MT, MWF, MRS, and fMRI) on subjects with any clinical pathology (inclusion/exclusion criteria in Table 1.1). Studies that employed diffusion kurtosis imaging (DKI), an extension of DTI using multiple b-values,

were included as these studies typically also report DTI metrics in addition to measures of kurtosis. Studies that employed advanced MRI techniques to image only the brain were excluded (e.g. brain MRS in CSM). We also excluded studies utilizing diffusion-weighted imaging (DWI) that only calculated an apparent diffusion coefficient, but did not calculate tensors (which require the use of diffusion-sensitizing gradients in at least 6 directions) or tensor-derived metrics such as fractional anisotropy (FA), axial diffusivity (AD), and radial diffusivity (RD). The search was limited to human studies, but limits on study design were not placed. Abstracts identified in the initial search were reviewed by 3 of the authors (Allan R. Martin, Izabela Aleksanderek, Nathaniel Smith) to determine relevant manuscripts for full-text review. The inclusion criteria required that studies were original research that appeared to answer one or more of the key questions above and included a minimum of 24 total subjects, with at least 12 of these subjects with a specific spinal pathology. Thus, we included studies with at least 24 pathological subjects (with no control subjects), and studies with at least 12 pathological subjects and a total of at least 24 subjects (including controls). Studies that included 3 or more different groups for comparison (e.g. NMO vs. MS vs. healthy) were required to have at least 12 subjects with the primary pathology of interest. Case reports or smaller series, meeting abstracts, white papers, editorials, review papers, technical reports, or studies of only healthy subjects were excluded. The full text of each article was then analyzed by 2 of the authors (A.R.M, I.A.) in the context of each key question to determine suitability for final inclusion, with discrepancies resolved by discussion. If multiple articles were identified with redundant results based on the same group of subjects, only the most relevant article (larger sample size or more recent publication) was kept in the review. References of each full-text article and each review paper that were identified were also systematically checked to identify additional eligible articles (Figure 1.3).

	Inclusion	Exclusion
Patient	• Studies involving adult or pediatric human population (no age restriction) • Studies that include patients with a known or suspected pathological diagnosis affecting the spinal cord (SCI, CSM, MS, ALS, infarction, tumour, etc.)	• Animal subjects • Studies in only healthy subjects
Prognostic factors	• Metrics derived from spinal cord DTI: FA, MD, AD, RD • Metrics derived from spinal cord DTI tractography: fiber length, fiber density • Metrics derived from spinal cord MT imaging: MTR or MTCSF • Metrics derived from spinal cord MWF imaging • Metrics derived from spinal cord MRS: absolute or relative (expressed as a ratio) metabolite concentrations • Metrics derived fMRI signal conduction loss	• Studies involving brain imaging techniques
Outcome	• Diagnosis by disease specific criteria (e.g. McDonald criteria for MS) • Clinical severity by validated clinical tools/measures (e.g. ASIA for SCI, JOA/mJOA score for CSM, EDSS for MS, etc.) • Outcomes by disease-specific measures or quality of life measures (e.g. SF-36)	• Subjective or unvalidated outcome measures
Study Design	• Restrospective or prospective cohort studies designed to assess the ability of an imaging factor to: o Make a diagnosis o Correlate with neurological/functional impairment o Predict neurological/functional outcome after at least 3 months • Minimum 24 total subjects, with at least 12 having spinal pathological condition of interest	• Review articles • Opinions • Technical reports • Studies in healthy controls • Animal or biomechanical studies

Table 1.1: Study Inclusion and Exclusion Criteria.

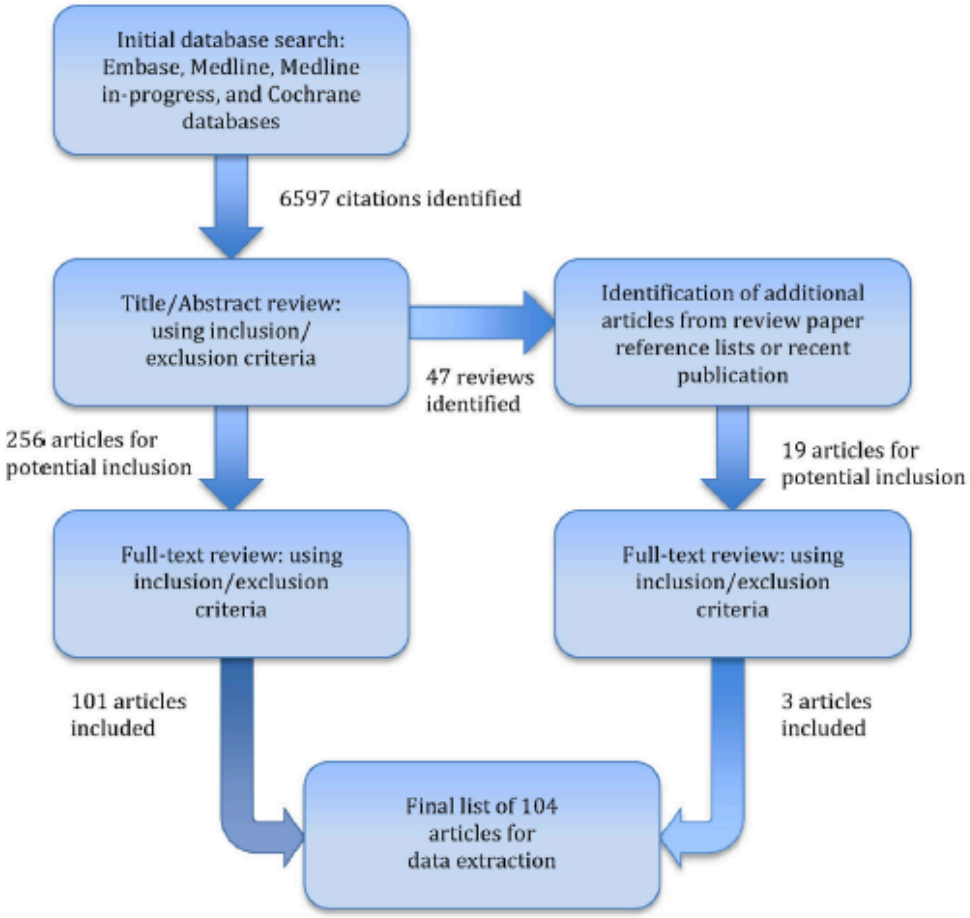

Figure 1.3: Flowchart showing results of literature search.

For key question 1 (diagnostic utility) we sought all articles that compared the presence or absence of a specific MRI feature or the value of a quantitative metric between patients and controls, relating to diagnosis. For question 2 (biomarker utility), we identified articles that identified relationships between MRI metrics and measures of clinical disability, including the calculation of correlation coefficients (Pearson, Spearman, or multivariate) or identification of differences between severity groups. To be relevant to key question 3 (predictive utility), studies needed to assess the relationship between baseline MRI metrics and follow-up clinical data at a specified time at least 3 months after the initial imaging.

1.3.3.2 *Data Extraction*

For each of the articles that met all inclusion/exclusion criteria after full-text review, the following data were extracted redundantly by 2 of the authors (A.R.M., Z.T.): study design, subject characteristics (age, gender, diagnosis, treatment(s) administered), follow-up duration, MRI sequences, MRI acquisition parameters, MRI data analysis methods, clinical data recorded, and results pertaining to diagnosis, correlation with disability, and correlation with outcomes. Differences in extracted data were resolved by discussion.

1.3.3.3 *Data Analysis and Synthesis*

Regarding diagnosis, we analyzed group differences and their statistical significance (P-value), and also the number of subjects with each specific MRI feature, present or absent (or a quantity above/below a threshold), that was reported for pathological and healthy subjects, to assess sensitivity (SE), specificity (SP), positive predictive value (PPV), and negative predictive value (NPV). For correlations with disability and prediction of clinical outcomes, we collected results that were reported as odds ratios, univariate or multivariate correlation coefficients, and P-values.

Although many of the studies identified in this systematic review reported results using the same quantitative metrics, a formal meta-analysis was not performed due to the wide variation in acquisition and data analysis techniques. Such a meta-analysis would only be relevant for a group of studies that showed substantial homogeneity in subject populations, MRI techniques, regions of interest (ROIs), and clinical measures. However, trends in the data were tabulated and summarized independently by 2 authors (A.R.M., I.A.) and discrepancies were resolved by discussion.

1.3.3.4 *Risk of Bias for Individual Studies*

Risk of bias was assessed for each article independently by 2 reviewers (A.R.M., I.A.). The risk of bias criteria were defined by the authors by consensus, combining criteria from the Center for Evidence-Based Medicine (CEBM) Diagnostic Study Appraisal Worksheet and *The Journal of Bone & Joint Surgery* for prognostic studies (Wright et al., 2003), in addition to the modifications described in (Skelly et al., 2013). The criteria were further modified to also consider potential sources of bias related to technical factors. The criteria are summarized in

Table 1.2. Factors that were considered to be potential sources of bias include retrospective, case series, or case-control study designs; failure to match or analyze differences in demographics (age, gender) or control for other confounders; heterogeneity in the diagnosis of the study population; non-random enrollment methods (e.g. convenience sampling or posters may have increased selection bias compared with consecutive enrollment); unreliable acquisition and analysis methods; and a narrow range of severity of illness. More specifically, acquisition techniques were considered to have a higher risk of bias if they produced wide confidence intervals for metrics (>20%), showed distortions/artefacts that frequently required the exclusion of slices/subjects (>5%), or were subject to potential systematic bias, such as acquisitions that have substantial partial volume effects due to in-plane resolution >1.5x1.5mm^2, or thickness >5mm. Analytical techniques were considered to confer a higher risk of bias if they involved manual processes (e.g. ROI selection) without blinding, or liberal statistical assumptions (e.g. uncorrected $p<0.05$ for activations in fMRI). For diagnostic studies, failure to calculate and report diagnostic accuracy was considered a potential source of reporting bias, as it conceals how many pathological subjects have an "abnormal" result on a given metric. Similarly, correlation studies that did not publish univariate or multivariate correlation coefficients do not disclose the strength of the correlation. Prognostic studies were also judged to have potential bias if the patients were not at a similar point in the course of disease (lacking internal validity), if the study did not achieve >80% clinical follow-up, if follow-up was not long enough for a majority of patients to show a clinical change, or if other known prognostic factors were not reported and analyzed. If an article failed to report important information for any of the aforementioned potential sources of bias, or technical details that are necessary to reproduce the image acquisition, it was considered to have an increased risk of bias. Following rating of each article for risk of bias by the 2 reviewers, discrepancies were resolved by discussion.

Risk of Bias	Study Design	Criteria for Diagnostic Studies	Criteria for Correlation (Biomarker) Studies	Criteria for Prognostic Studies
Low risk: Study adheres to commonly held tenets of high quality design, execution and avoidance of bias	Good quality cohort*	1. Prospective cohort design 2. Demographic and other potentially confounding information (age, gender, duration of disease) reported and matched/analyzed 3. Cohort includes patients with a homogeneous diagnosis 4. Patients have a range of severity of disease including mild/early (non-obvious) cases 5. Patients are randomly selected or recruited consecutively (on admission or in clinic) 6. Acquisition techniques likely to produce reliable results (acceptable SNR and distortions) 7. Quantitative MRI metrics derived using automated or blinded techniques 8. Objective criteria used for diagnosis based on presence/absence of distinct features or measurements 9. Appropriate reporting of SE, SP, PPV, NPV and/or ROC curves	10. Prospective cohort design 11. Demographic and other potentially confounding information (age, gender, duration of disease) reported and matched/analyzed 12. Cohort includes patients with a homogeneous diagnosis 13. Patients have a range of severity of disease including mild/early (non-obvious) cases 14. Patients are randomly selected or recruited consecutively (on admission or in clinic) 15. Acquisition techniques likely to produce reliable results (acceptable SNR and distortions) 16. Quantitative MRI metrics derived using automated or blinded techniques 17. Calculation of univariate correlation coefficients (Spearman or Pearson) or multivariate regression analysis on quantitative imaging features, related to clinical measures	18. Prospective longitudinal cohort design 19. Demographic and other potentially confounding information (age, gender, duration of disease) reported and matched/analyzed 20. Patients are randomly selected or recruited consecutively (on admission or in clinic) 21. Cohort includes patients with a homogeneous diagnosis 22. Patients at reasonably similar point in the course of their disease or treatment (**differs from diagnostic and correlation studies) 23. F/U rate of greater than 80% 24. Patients followed long enough for outcomes to occur 25. Accounts for other known prognostic factors 26. Acquisition techniques likely to produce reliable results (acceptable SNR and distortions) 27. Quantitative MRI metrics derived using automated or blinded techniques

Moderately low risk: Study has potential for some bias; does not meet all criteria for class I but deficiencies not likely to invalidate results or introduce significant bias	Moderate quality cohort	28. A cohort study that violates one of the criteria for low risk of bias	29. A cohort study that violates one of the criteria for low risk of bias	30. Prospective design, with violation of one of the other criteria for good quality cohort study 31. Retrospective design, meeting all the rest of the criteria for low risk of bias
Moderately high risk: Study has flaws in design and/or execution that increase potential for bias that may invalidate study results	Poor quality cohort, good quality case-control or cross-sectional (prognostic only)	32. A cohort study that violates two of the criteria for low risk of bias 33. A case-control study that violates one of the other criteria for low risk of bias	34. A cohort study that violates two of the criteria for low risk of bias 35. A case-control study that violates one of the other criteria for low risk of bias	36. Prospective design with violation of 2 or more criteria for good quality cohort 37. Retrospective design with violation of 1 or more criteria for good quality cohort 38. A good case-control study 39. A good cross-sectional study
High risk: Study has significant potential for bias; does not include design features geared toward minimizing bias and/or does not have a comparison group	Very poor quality cohort, poor quality case-control or cross-sectional (prognostic only), case series	40. A cohort study that violates three or more of the criteria for low risk of bias 41. A case-control study that violates two of the other criteria for low risk of bias 42. Any case series design	43. A cohort study that violates three or more of the criteria for low risk of bias 44. A case-control study that violates two of the other criteria for low risk of bias 45. Any case series design	46. Other than a good case-control study 47. Other than a good cross-sectional study 48. Any case series design

Table 1.2: Risk of Bias for Diagnostic, Correlation, and Prognostic Advanced MRI Studies.

1.3.3.5 *Overall Quality of the Body of Literature*

After individual article evaluation, the overall body of evidence with respect to each key question and specific finding was determined based upon precepts outlined by the Grading of Recommendation Assessment, Development and Evaluation (GRADE) Working Group (Schunemann et al., 2008). The possible ratings for overall quality of evidence are high,

moderate, low, very low, and insufficient. The initial quality of the overall body of evidence was considered high if the majority of the studies had low or moderately low risk of bias, and low if the majority of the studies had high or moderately high risk of bias. The body of evidence was then upgraded 1 or 2 levels (only if no downgrading occurred) on the basis of the following criteria: (1) large magnitude of effect or (2) dose-response gradient, or downgraded 1 or 2 levels on the basis of the following criteria: (1) inconsistency of results, (2) indirectness of evidence, (3) imprecision of the effect estimates (*e.g.*, wide confidence intervals [CIs] > 50% of the estimate), or (4) non-*a priori* statement of subgroup analyses. The final overall quality of evidence expresses our confidence in the estimate of effect and the impact that further research may have on the results (Schunemann et al., 2008). The overall quality reflects the authors' confidence that the evidence reflects the true effect and the likelihood that further research will not change this estimate of effect. For example, a high level of evidence suggests that the evidence reflects the true effect, and further research is very unlikely to change our confidence in the estimate. A grade of "insufficient" means that evidence either is unavailable or does not permit a conclusion.

1.3.4 **Results**

1.3.4.1 *Study Selection*

The literature search was designed to be highly inclusive and generated a total of 6597 unique citations (Figure 1.3). Following review of the title and abstract, 256 articles were retained for full-text review and 47 review papers were identified. The full-text review of the 256 articles excluded another 156, leaving 101 articles that met all inclusion/exclusion criteria and were relevant to one or more of the 3 key questions. The reference lists of these 101 articles and the 47 review papers identified another 18 articles for full-text review, and 1 additional study that was electronically published following the literature search was identified by the authors. Among these 19 articles, 3 were retained for a final total of 104 studies. Many of the articles excluded at the full-text stage employed advanced MRI techniques in the brain but not the spinal cord, or the number of subjects fell below the threshold. Several articles were also excluded that used MT as a method to enhance contrast between the spinal cord and surrounding tissues, but did not perform quantitative analyses such as computing MTR or MTCSF. Of the final 104 articles, 101 (97%) were identified by the electronic database search.

The systematic review identified 69 DTI studies, including 62 that performed ROI-based quantitative analysis and 16 that performed fiber tractography (FT), 25 MT studies, 1 MWF study, 11 MRS studies, and 8 fMRI studies. Ten of the studies employed multi-modal acquisition techniques, including DTI and MT (6 studies), DTI and fMRI (3 studies), or DTI and MRS (1 study). Eight studies that used DTI FT also performed ROI-based quantitative analysis. The chronological trends of each of these imaging techniques are displayed in Figure 1.4. The number of DTI studies that used ROI-based analysis sharply increased in recent years, whereas FT analysis decreased slightly. MT studies decreased after 2003, but saw a resurgence in recent years. MRS, MWF, and fMRI have been used in only a small number of studies, and recent use of these techniques has been limited. Tables in Appendix A (Tables 1.3-1.8) summarize the details of each study included in the review, separated by the imaging modality that was employed (with DTI divided by analysis technique).

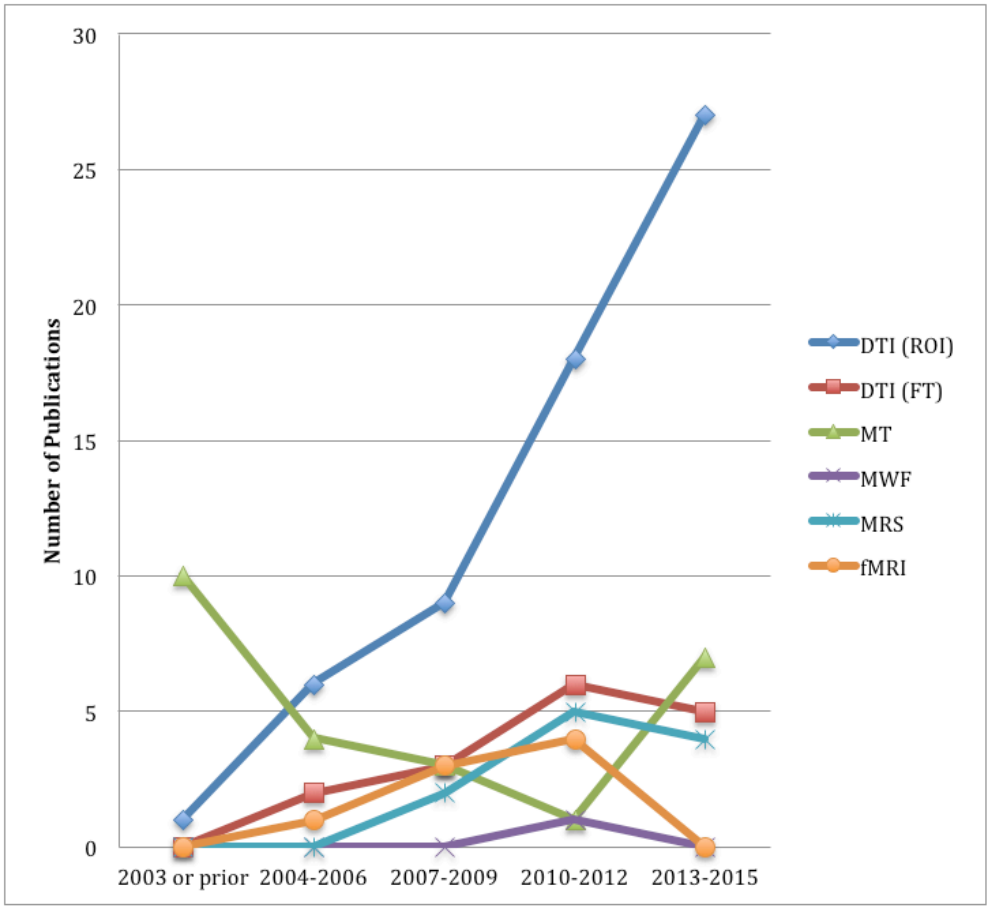

Figure 1.4: Chronological Trends in Clinical/Translational Studies Utilizing State-of-the-art Spinal Cord MRI Techniques.

1.3.4.2 *Methodology and Risk of Bias of Individual Studies*

Among the 104 studies, the risk of bias assessment found moderately low risk (with regards to at least 1 of the key questions) in only 6 studies, with the remainder of studies showing moderately high (24) or high (74) risk. Among the 69 DTI studies, the risk of bias was felt to be high in 52, moderately high in 14, and moderately low in only 3 studies. For MT studies this risk was high in 12, moderately high in 8, and moderately low in 5 studies. MRS studies showed high risk of bias in 7 studies and moderately high risk in 4. All of the fMRI studies and the single MWF study were all assessed to have high risk of bias. Most of the studies reviewed were exploratory in nature (i.e. early translational studies) and not clearly based on a priori hypotheses, frequently making many statistical comparisons without appropriate correction. Most were prospective cohort studies (101), and the remaining 3 were retrospective cohort studies. Furthermore, 43 of the 104 studies failed to account for confounding factors such as age and/or gender, either by ensuring age/gender-matched groups or by performing appropriate multivariate analyses. The vast majority of studies focused on a population with a homogenous diagnosis (98/104), avoiding possible issues with internal validity. However, only 15 of the 104 studies clearly reported the use of consecutive or random enrolment procedures to avoid possible selection bias, whereas the remaining 89 studies either used convenience sampling or failed to report enrolment methods in detail. Most of the studies (82/104) included patients with a range of severity of impairment, including mild/early cases that are more difficult to diagnose.

1.3.4.3 *Acquisition Techniques*

Among the reviewed studies, a large fraction utilized technical methods that could introduce significant bias in terms of quantitative results. The group of DTI studies used a wide range of pulse sequences, with the majority (41/69) employing a relatively straightforward single-shot EPI (ssEPI) sequence, whereas 3 studies used multi-shot EPI (msEPI), 9 studies used more complex reduced field of view (rFOV) techniques, 1 study used line scan DTI, 1 study utilized a fast spin echo (FSE) sequence, one study used a spectral adiabatic inversion recovery (SPAIR) sequence, and the remaining 13 studies did not provide sequence details. Acquisition parameters were also highly variable, including b-values, FOV, matrix, number of excitations (NEX), saturation bands, shimming, and the use of cardiac gating, which was employed in 16/69 (23%) studies. Two of the studies utilized multiple b-values and calculated measures of diffusion

kurtosis, such as mean kurtosis (MK) and root mean square displacement (RMSD) (Hori et al., 2012, Raz et al., 2013). 27 of 69 studies acquired images with very large voxels (greater than 1.5x1.5x5mm in at least 1 dimension) or failed to report resolution, potentially biasing the results due to increased partial volume effects. Several studies also performed analyses that could introduce a systematic bias against the pathological group, such as obtaining FA from an ROI in thinned spinal cord tissue at the level of syringomyelia or a hemorrhagic SCI lesion, which is more likely to include voxels with partial volume effects that artificially lower FA (Hatem et al., 2009, Hatem et al., 2010, Cheran et al., 2011, Koskinen et al., 2013, Yan et al., 2015). The group of MT studies tended to use more consistent acquisition methods with less variation, with 24/25 studies employing some form of gradient echo (GE) sequence, all studies using a sinc or Gaussian shaped saturating pre-pulse, and none of the studies utilizing cardiac gating. Only 2 studies computed MTCSF following a single MT acquisition. The remaining 23 studies acquired images with and without a saturation pre-pulse, coregistered the images, and calculated MTR. The study investigating MWF used a 32-echo sequence with inversion recovery (without cardiac gating) to measure the short T2 component using a multi-exponential model, but this technique only acquired a single axial slice with an acquisition time of 30 minutes. All of the MRS studies uniformly employed similar acquisition sequences, making use of point-resolved spectroscopy (PRESS) with chemical shift selective (CHESS) water suppression, while cardiac gating was employed in 5/11 (45%). Unfortunately, these studies all produced metrics with wide confidence intervals within subject groups. All of the spinal fMRI studies were based on a fast spin echo (FSE) acquisition, and none used cardiac gating. The fMRI studies appeared to suffer from challenges with reliable acquisitions, although reporting was not detailed enough to determine confidence intervals or measures of reliability, as the results typically involved processed data in terms of group activations and connectivity analyses.

1.3.4.4 *Analysis Methods*

Whole-cord ROIs were used in the vast majority of DTI, MT, and MWF studies. Among the 62 ROI-based DTI studies, 18 reported tract-specific metrics, 3 extracted metrics from WM, and 2 reported data from GM, with the remaining 39 reporting whole-cord metrics or non-specific ROIs (e.g. mixed GM and WM from a mid-sagittal slice). Among DTI FT studies, only 2 reported tract-specific metrics, with the remainder averaging results across all WM identified. 5/25 MT studies reported tract-specific metrics, 1 averaged results across all WM, and 2 offered

GM-specific metrics. All MRS results were whole-cord, and fMRI results were typically broken into cord quadrants (combining GM and WM). Only 5 of the ROI-based DTI studies performed automated (or semi-automated) selection of the ROI (Nair et al., 2010, Oh et al., 2013a, Oh et al., 2015, Oh et al., 2013b, Toosy et al., 2014), whereas the other 57 studies introduced potential bias by performing manual ROI selection without blinding procedures. The most common automated method was a simple segmentation procedure, followed by extraction from the whole cord. Nair et al. (2010) used FA values of each subject to create a WM skeleton, and then used this map to draw ROIs from C1 to C6, in a method that is somewhat similar to tractography-based ROI selection. Toosy et al. (2010b) performed automated segmentation and registration to a spinal cord template, and subsequently extracted whole-cord ROIs and also hyperintense lesions using an automated threshold-free cluster enhancement (TFCE) algorithm. In addition, 7 studies utilized a semi-automatic algorithm to perform spinal cord segmentation, but then performed manual exclusion of edge voxels that were subject to partial volume effects with contamination from CSF (Agosta et al., 2007, Agosta et al., 2009a, Agosta et al., 2009b, Agosta et al., 2008a, Manconi et al., 2008, Valsasina et al., 2007, Benedetti et al., 2010), which could introduce bias in the same manner as manual ROI selection. Another study performed random ROI placement to avoid issues of potential bias, but did not report the exact method of randomization (Kamble et al., 2011). Among the 16 DTI FT studies, 6 utilized automatic ROI selection based on the FT output, although 4 of these used manual seed points to initiate the FT algorithm and 1 did not report details on the use of seed points (Hatem et al., 2010). Budzik et al. (2011) performed semi-automated FT without manual seed points and extracted whole-cord ROIs automatically. Among the MT studies, 14 of the 25 studies utilized automatic or semi-automatic analysis methods to extract MTR or MTCSF, with only a minority of studies using manual ROI selection. Rather than exclude edge voxels manually, many of these studies excluded voxels based on a preset threshold of MTR < 10%. The single MWF study used manual ROI selection. The 11 MRS studies were all single-voxel ROIs, with relatively straightforward analysis methods. All of the fMRI studies used a complex series of steps in data analysis, and 7/8 of the reviewed studies made statistical assumptions without correcting for multiple comparisons, leading to potentially biased results. All of the fMRI studies manually divided the cord into quadrants or hemi-cords.

1.3.4.5 *Evidence Regarding Diagnostic Utility*

Ninety-five of the 104 studies included in the review made comparisons between pathological subjects and healthy controls. Among these 95 studies, 88 had a high risk of bias, and 7 had a moderately high risk. The vast majority of these studies (89/95) only reported group differences and did not calculate diagnostic accuracy in terms of SE, SP, PPV, or NPV. Group comparisons between pathological subjects and healthy controls frequently showed similarities across different diseases including decreased FA, increased MD, increased RD, decreased MK, decreased MTR, increased MTCSF, and decreased NAA concentration, suggesting various clinical pathologies share common underlying injury mechanisms of demyelination, axonal loss, and GM loss. All 6 of the studies that reported diagnostic accuracy (SE, SP) results utilized DTI, with 4 showing moderate utility of DTI metrics in diagnosing CSM, 1 in CM, and 1 in MS. In CSM, the reported values of SE and SP of DTI metrics ranged from 50-100%, but tended to exceed those reported for T2w-HI. However, none of the reported values for diagnostic accuracy were sufficiently high to compete with the gold standard for CSM diagnosis, which is based upon clinical signs of myelopathy along with imaging evidence of any amount of cord compression (typically using conventional MRI). The evidence for diagnostic utility in the CM and MS studies was also not sufficient to consider DTI superior to existing diagnostics. Two studies (both using DTI) computed z-statistics for metrics at each vertebral level to determine if an individual measurement was normal or abnormal. Results pertaining to diagnostic utility are summarized for each clinical pathology in Table 1.9.

Table 1.9: Summary of Studies by Clinical Pathology.

Clinical Pathology	Number of Studies by Imaging Technique						Key Findings		
	ROI DTI	DTI FT	MT	MWF	MRS	fMRI	Diagnostic Utility	Biomarker Utility (Correlation with Disability)	Predictive Utility
ALS	7		2		3		• FA decreased (7/7 studies), specifically in LCSTs (4/4 studies) • MTR (in LCSTs) was decreased in ALS (1 study) • NAA decreased in ALS (3/3 studies)	• FA correlated with ALSFRS (r=-0.55-0.74, R=0.38, 4/6 studies) • NAA/Cre correlates with ALSFRS (r=0.79, 1/2 studies) and FVC (r=0.66, 1 study) • FA, MD changes over 1y not correlated with change in ALSFRS (2/2 studies) • MTR does not correlate with ALSFRS (1 study)	• FA predicted ALSFRS at 1y (1 study) • NAA/Cre and NAA/Myo predict ALSFRS at 1y (r=-0.70-0.78, 1 study)
aSCI	3						• MD decreased (2/3 studies) • FA decreased (2/3 studies)	• FA correlates with one or more components of ASIA motor score (2/2 studies)	
CM	3	3					• FA decreased and MD increased at MCL (2/3 studies) • FA had higher SE (73%) and SP (100%) than T2w-HI (1 study)	• No correlation of FA, MD, FT with JOA (1 study)	• FA, MD did not predict JOA outcome (1 study)
cSCI	4		1			2	• FA decreased above (4/4 studies) and below (3/3 studies) injury site • FA at lesion correlates with ASIA motor score (r=0.67, 1 study)	• MTR correlates with ASIA motor/sensory score (r=0.59, 1 study) • Number of active voxels correlates with sensory impairment (R=0.96, 1 study)	

							• FA, RD outside lesion correlates with ASIA motor/sensory scores (r=0.66-0.74, 1 study) • MTR decreasd above/below injury (1 study) • fMRI shows increased bilateral activation in cSCI vs. HCs (2/2 studies)		
CSM	18	5			3		• FA had SE=72-95%, SP=50-100% to detect myelopathy (4 studies) • MD had SE=13-100%, SP=50-80% to detect myelopathy (3 studies) • OE had SE=81%, SP=67% to detect myelopathy (1 study) • FA reduced at compressed level (12/12 studies), above compression (2/5 studies), and below compression (1/3 studies) • MD increased at compressed level (8/10 studies), above compression (1/4 studies), and below compression (1/3 studies) • MK decreased in overall cord (1 study) • NAA/Cre reduced (2/3 studies),	• FA correlates with JOA/mJOA (r=0.48-0.88, R=0.57-0.64, 5/5 studies) • SD(θ) correlates with mJOA (R=0.64, 1 study) • Tractography pattern only correlated with clinical scale (JOA/Nurick) in 1/3 studies • NAA/Cre ratio not correlated with mJOA (1 study) • Cho/NAA correlated with mJOA (R=-0.45, 1 study)	• FA predicts improvement on NDI (r=-0.61) but not mJOA (1 study) • FA predicts mJOA Recovery Ratio > 50% (P=0.03, 1 study)

							Cho/NAA increased (1 study) • Lactate peak present in 33% of subjects (1 study)		
MS	19	3	16	1	5	5	• FA has SE=87%, SP=92% for diagnosis (1 study) • FA reduced in whole-cord (11/12 studies), NAWM (6/8 studies), and in lesions (3/3 studies) • MD increased in whole-cord (7/10 studies), NAWM (2/5 studies), lesions (2/3 studies) • RD increased in whole-cord (4/6 studies) • FA decreased in progressive MS vs. RRMS (4 studies) • MK decreased in NAGM and lesions (1 study) • MTR decreased in whole-cord (8/11), WM (2/2), GM (1/2 studies) • MTR decreased in progressive MS vs. RRMS (2/3 studies) • MTCSF increased in WM (1 study) • MWF not different vs. HCs (1 study) • Decreased NAA (4/4 studies) • Increased number of active voxels	• FA correlates with EDSS (r=-0.37-0.51, R=-0.60, 7/15 studies), TWT (R=0.70, 1 study) • FA of LCST correlates with MEPs (r=-0.93, 1 study) • MD correlates with EDSS (r=0.37, 3/13 studies) • RD correlates with EDSS (R=0.7, 4/8 studies) and TWT (R=-0.6, 1 study) • MK does not correlate with EDSS (1 study) • MTR correlates with EDSS (r=-0.25-0.48, 6/15 studies) • MTCSF of LCs correlates with EDSS (r=0.59), walk speed (r=-0.51), ankle strength (r=-0.45) (1 study) • MTCSF of DCs correlates with EDSS (r=0.59), vibration (r=0.58), postural sway (r=0.32) (1 study) • Change in MWF over 1y, 2y not correlated with change in EDSS (1 study) • NAA does not correlate with EDSS (5	• FA predicts EDSS at 6m-3y FU (r=-0.40, 2/2 studies) • RD predicts EDSS, 9 hole peg, and TWT at 6m FU (P<0.05, 1 study) • MWF not predictive of EDSS at 1y, 2y (1 study) • NAA predicts decrease in EDSS at 6m-1y FU (1/2 studies)

							(2/6 studies) • Increased mean SI change in active voxels (3/3 studies) • Increased distribution of activation outside expected ipsilateral dorsal horn (2/2 studies)	studies) • Number of active voxels correlates with EDSS (1/3 studies)	
Myelitis	2	2	1				• Diagnostic utility: • FA decreased at lesion site (3/3 studies) • MTR decreased at lesion site (1 study)	• FA, RD correlate with EDSS (P<0.0001) and 9 hole peg (P<0.0001) (1 study) • FA correlates with sensory score (r=-0.40, 1 study) • MTR does not correlate with clinical measures EDSS, 9 hole peg, finger-tapping (1 study)	
NMO	2						• FA decreased in NAWM (2/2) and lesions (1/1) • FA decreased in NAWM vs. MS (1 study) • MD increased in NAWM (1/1) and lesions (1/1)	• FA correlates with EDSS (r=-0.80, 1 study)	
Syringo-myelia	1	2					• FA decreased at syrinx vs. HCs (2/2 studies) • FA decreased between symptomatic vs. asymptomatic subjects (1 study) • FA not different above/below syrinx (1 study)	• FA correlates with thermal sensation in 1/2 ROIs (r=-0.63, 1/2 studies) • FA (r=-0.64, P=0.02) and number of FT fibers (r=-0.75, P=0.02) correlate with average daily pain scores (1 study)	

1.3.4.6 *Evidence Regarding Biomarker Utility*

A total of 67 studies assessed correlation of MRI metrics with measures of clinical impairment. The risk of bias was high in 40 of these studies, moderately high in 21, and moderately low in 6. Most of these studies (57/67) performed univariate or multivariate correlations, although 10 studies took the simplistic approach of dividing subjects into categories of severity (above/below artibrary thresholds) and then comparing group differences in metrics. Among these studies, the majority (38/67, 57%) only investigated correlations with a single coarse clinical measure, such as Expanded Disability Status Scale (EDSS), Japanese Orthopedic Association (JOA), modified JOA (mJOA), amyotrophic lateral sclerosis (ALS) Functional Rating Scale (ALSFRS), or ASIA Impairment Scale (AIS), rather than employing a battery of assessments or using more detailed measures of impairment such as ASIA motor/sensory scores. The majority of DTI studies reporting biomarker utility results focused on the metric FA, which was particularly successful in CSM with significant results in 5/5 studies correlating with JOA or mJOA (Spearman r=0.48-0.88, Pearson R=0.57-0.64) (Gao et al., 2013, Jones et al., 2013, Ellingson et al., 2014, Wen et al., 2014a, Maki et al., 2015) and in SCI in 4/4 studies correlating with ASIA motor/sensory scores(r=0.59-0.74, R=0.78-0.92) (Cheran et al., 2011, Cohen-Adad et al., 2011, Koskinen et al., 2013, Vedantam et al., 2015), but slightly less successful in MS with significant results in only 7/15 studies correlating with EDSS (r=-0.37-0.51, R=-0.60), with negative results in 8 studies. Other metrics had limited success in MS correlating with EDSS, with significant results for MD in 3/13 studies, RD in 4/8 studies, MTR in 6/15 studies, MTCSF in 2/2 studies, and the number of active voxels using fMRI in 1/3 studies, whereas no correlation was found between EDSS and the DKI metric MK (1 study) and the MRS metric NAA (or relative NAA concentration) in 5/5 studies. Three studies used longitudinal imaging and clinical data collection to assess if changes in MRI metrics over time reflected changes in clinical status, but the results were negative in 2/2 studies using DTI in ALS and 1 study using MWF in MS. Results for biomarker utility, divided by clinical pathology, are summarized in Table 1.9.

1.3.4.7 *Evidence Regarding Predictive Utility*

Longitudinal studies that assessed predictive utility of advanced MRI metrics were only conducted in a total of 10 studies involving MS (5), ALS (2), CSM (2), and CM (1). Among these, 6 utilized DTI, 3 used MRS, 1 used MT, and 1 used MWF. The risk of bias among these studies was assessed as high in 8 and moderately high in 2. Four additional studies collected longitudinal clinical data but did not report prediction of outcomes using baseline MRI metrics. Among the 10 studies investigating predictive utility, 5 employed a detailed battery of clinical assessments (Freund et al., 2010, Bellenberg et al., 2013, Ikeda et al., 2013, Jones et al., 2013, El Mendili et al., 2014). Baseline FA showed weak to moderate correlations with clinical outcomes such as ALSFRS in ALS (1 study), mJOA recovery ratio in CSM (1/2 studies), and EDSS in MS (2/2 studies), but not mJOA in CSM (1 study). Ratios involving NAA were predictive of outcome in ALS (1 study) and MS (1/2 studies). Results for predictive utility are summarized in Table 1.9.

1.3.4.8 *Evidence Summary*

The vast majority of studies included in this review had high or moderately high risk of bias, leading to a low baseline quality of evidence for each of the specific findings listed in Table 1.10. For the specific finding that FA is decreased in terms of group differences between patients and healthy controls in ALS, CSM, myelitis, MS, neuromyelitis optica (NMO), and SCI, the overall quality of evidence was neither upgraded nor downgraded, and remained low. Other metrics MD, RD, MK, MTR, MTCSF, and NAA also showed group differences between patients and healthy subjects in various clinical conditions, but the quality of evidence for these metrics was downgraded to very low due to a low level of evidence (MK, MTCSF) or inconsistent results between studies (MD, RD, MTR, NAA. There was insufficient evidence available to make any recommendations regarding the diagnostic utility (in terms of detecting group differences) of AD, standard deviation of primary eigenvector orientation (SD(θ)), orientation entropy (OE), tractography pattern, MWF, and fMRI-based metrics due to a lack of evidence, inconsistent results, and wide confidence intervals in many of the studies. The overall quality of evidence for diagnostic accuracy (sensitivity and specificity) was also insufficient, which was downgraded 2 levels due to highly inconsistent results. In terms of biomarker utility, only FA demonstrated consistent results, and the quality of evidence was upgraded 1 level to moderate for showing a dose-response gradient. The evidence for other MRI metrics as biomarkers was

inconsistent and imprecise, leading to a finding of insufficient evidence. Finally, the evidence regarding the predictive utility for all MRI metrics was inconsistent and imprecise, leading to a rating of insufficient.

Table 1.10: Evidence Summary.

Key Question	Specific Finding	Quality of Evidence		
		Baseline	Upgrade/ Downgrade	Final
1) Diagnostic Utility: Does the MRI technique provide metrics that demonstrate group differences or improved sensitivity/specificity in the diagnosis of spinal pathologies?	FA is decreased in terms of group differences between patients and healthy controls in the clinical conditions ALS, CSM, myelitis, MS, NMO, and SCI	Low	None	Low
	MD, RD, MK, MTR, MTCSF, and NAA demonstrate group differences between patients and healthy controls in various clinical conditions	Low	Downgrade: inconsistency (1)	Very low
	AD, SD(θ), OE, tractography pattern, MWF, and fMRI metrics demonstrate group differences between patients and healthy controls in various clinical conditions	Low	Downgrade: inconsistency (1), imprecision of estimates (1)	Insufficient
	Quantitative metrics based on state-of-the-art MRI techniques can be used for diagnosis with high diagnostic accuracy (sensitivity and specificity)	Low	Downgrade: inconsistency (2)	Insufficient
2) Biomarker Utility: Does the advanced MRI technique generate quantitative metrics that correlate with neurological/functional impairment and/or show longitudinal changes that correlate with changes in impairment in spinal pathologies?	FA shows moderate correlation with clinical impairment in a number of clinical conditions: ALS, CSM, MS, myelitis, NMO, and SCI	Low	Upgrade: dose-response gradient	Moderate
	MD, RD, MTR, MTCSF, NAA are weak-moderate biomarkers for clinical impairment in various clinical conditions	Low	Downgrade: inconsistency (1), imprecision of estimates (1)	Insufficient
3) Predictive Utility: Does the advanced MRI	FA, RD, and NAA are predictive of outcome in MS, ALS, and CSM	Low	Downgrade:	Insufficient

technique generate metrics that predict neurological, functional, or quality of life outcomes in spinal pathologies?			inconsistency (1), imprecision of estimates (1)	

1.3.5 **Discussion**

1.3.5.1 *Summary of Results*

It is an exciting time in spinal cord imaging, as the emergence of powerful new MRI techniques has inspired a large number of early clinical studies of pathological spine conditions. The excellent research conducted to date has demonstrated tremendous potential for all of these techniques to elucidate aspects of the microstructure or function within the human spinal cord, adding numerous insights into the pathophysiology of several neurological diseases. Among the 5 new techniques addressed in this review, DTI has thus far generated the most research, comprising 66% of the included studies and showing a sharp increase within the past 6 years, particularly using ROI-based analysis (Figure 1.4). This increase in interest is most likely related to the promising results that DTI studies have demonstrated, particularly with moderate evidence that FA is a biomarker for disability in numerous pathologies (Table 1.10). The correlation of FA with impairment appears to be strongest in diseases that are confined to the spinal cord (e.g. CSM), which is consistent with the concept that disability in more distributed diseases (e.g. MS) is caused by injury to both the brain and the spinal cord. Low evidence was also found suggesting that FA shows group differences compared with healthy controls in several conditions, but insufficient evidence was available to suggest that DTI provides improved diagnostic accuracy or prediction of outcomes over established methods. A very low level of evidence was found for group differences using other DTI metrics MD and RD, MT metrics MTR and MTCSF, and the MRS metric of NAA concentration. It is unclear based on the current body of evidence if these metrics have substantial diagnostic value, due to a lack of strong evidence and substantial inconsistencies in results to date. The lack of well-designed studies to determine the diagnostic utility of the advanced MRI techniques, with 93% having a high risk of bias and only 6% reporting sensitivity and specificity, suggests a profound knowledge gap for future research. Furthermore, several studies in the review suggested that the simple quantitative measure of spinal cord CSA (quantifying atrophy) outperforms all of the advanced MRI metrics in terms of diagnostic and biomarker utility (Oh et al., 2013b, Kearney et al., 2014a, Kearney et al., 2015a, Oh et al., 2015), suggesting that stronger results are still needed to contemplate the clinical uptake of these techniques.

1.3.5.2 *Interpreting the Evidence in the Context of Risk of Bias*

Unfortunately, the vast majority of studies (98/104, 94%) completed to date have a high or moderately high risk of bias, indicating the relative immaturity of the research in the field thus far. Although we were unable to determine precisely how many of the studies were based on a priori hypotheses (often due to ambiguous reporting of methods), it was obvious that most studies were highly exploratory, as they frequently analyzed numerous metrics and ROIs/levels without statistical correction to avoid type I errors. The early nature of the body of evidence is also apparent in the fact that 86% of studies failed to explicitly use randon/consecutive enrolment methods, and 41% did not perform age/gender matching in group comparisons or analysis for these potential confounders when assessing correlations or prediction of outcomes. Comparing the risk of bias between the 5 advanced MRI techniques, it was found to be lowest in MT studies, rated as moderately low in 20%, moderately high in 32%, and high in 48%, primarily as a result of more reliable, consistent acquisition methods and a tendency to more frequently utilize automated analysis techniques. However, in spite of these advantages, the results of the MT studies (most commonly using the metric MTR) showed considerably less consistent results compared with the DTI metric FA in terms of detecting group differences and correlating with impairment. As a result, the overall quality of evidence for MTR (and MTCSF) to demonstrate group differences in various clinical conditions was considered very low, and the evidence for their utility as biomarkers was insufficient (Table 1.10). This is suggestive that MTR is, overall, a weaker marker of pathological changes in the diseases studied than FA, although these metrics appear to measure separate components of microstructural change (Wheeler-Kingshott et al., 2002, Cohen-Adad et al., 2011), and the differences in consistency of results could alternatively be explained by technical factors. The risk of bias among DTI studies was assessed as high in 75% and moderately high in another 20%, largely as a result of problems with acquisition methods such as very large voxels (39%) and a lack of automated/objective analyses (86%). The lack of a substantial number of high quality DTI studies led to a low baseline level of evidence for FA, MD, RD, and MK to demonstrate group differences and utility as a biomarker (Table 1.10). The quality of evidence for FA as a biomarker was upgraded to moderate due to a “dose-response gradient” (a term used in GRADE) as it shows consistent and relatively strong correlations with impairment, whereas the evidence for MD, RD, and MK were downgraded to very low in terms of diagnostic utility (showing group differences) and insufficient in terms of

value as biomarkers. The risk of bias in MRS studies was high in 64% and moderately high in the remaining 36%, related to technical problems with acquisitions that resulted in the exclusion of subjects and wide confidence intervals in reported metrics. NAA showed very promising results in some studies, but the overall evidence was again downgraded to very low in terms of group differences and insufficient for correlation with impairment due to inconsistent results and imprecise estimates of effect. The single MWF study and all of the spinal fMRI studies were deemed to have a high risk of bias, primarily relating to difficulties in acquiring reliable images and the use of liberal statistical assumptions. As a result, none of the metrics investigated in these studies were deemed to have thus far demonstrated utility in terms of the three key questions.

1.3.5.3 *The Design of Imaging Studies for Clinical Translation*

The incorporation of detailed clinical assessments into translational study protocols provides a richer and more objective characterization of patients' functional impairments compared with coarse clinical tools such as EDSS, JOA, mJOA, ALSFRS, and AIS. The majority of studies that investigated biomarker utility (57%) and half of the prognostic studies employed only a single coarse measure of impairment. The use of these summary measures of disability risks misrepresenting the degree to which the spinal cord and specific WM tracts are truly injured, as these measures are imprecise, and results can be strongly influenced by confounding factors, such as reporting bias (in self-reported measures) or brain involvement in distributed CNS diseases (e.g. MS). If considerable noise and inaccuracies are present in the clinical assessments, the process of trying to identify meaningful correlations with MRI metrics can become futile. The additional use of electrophysiology (EP) tests can be used to augment the clinical information, although it is important that these test do not replace detailed neurological/functional assessments, as in some cases they may not be sufficiently sensitive or specific (Kerkovsky et al., 2012). However, it should be noted that a trend appears to be emerging, with many recent studies employing a broader array of clinical tests. Future studies that generate fine-grained clinical data using a battery of assessments are more likely to identify important correlations with disability, and such high fidelity data may even have the power to show strong relationships between MRI changes in individual WM tracts and focal neurological deficits that uniquely occur in each specific disease.

1.3.5.4 *State-Of-The-Art Spinal Cord MRI Acquisition Techniques: A Work in Progress*

"The only thing that is constant is change." – Heraclitus, 500BC. Although many technological advances have been made, the state-of-the-art spinal cord MRI techniques addressed in this review remain a work in progress, with many technical hurdles remaining. All of these imaging techniques are much more difficult to implement in the spinal cord than other regions, such as the brain, which has attracted many talented MRI physicists and engineers to take on this challenge. The issues of magnetic field inhomogeneity and physiological motion, leading to various artefacts and image distortions, remain significant barriers to high quality data collection for all of the techniques. DTI, most commonly based on spin echo EPI sequences, is an inherently noisy technique that typically requires large voxels and/or the use of multiple excitations to achieve acceptable SNR, both of which can increase partial volume effects at the cord periphery. The substantial variability in acquisition methods used by spinal cord DTI research groups indicates that this community is far from reaching consensus on the optimal approach to this difficult problem. The most common DTI sequence employed was ssEPI (59%), which tends to allow short acquisition times (<5 minutes in the majority of reviewed studies; Table 1.3, 1.4). 11/69 studies took advantage of these short scan times and used the approach of performing multiple ssEPI acquisitions and averaging the results offline to improve SNR, using coregistration and motion correction tools. However, it should be noted that EPI involves important tradeoffs, as it is strongly affected by susceptibility artefact due to inhomogeneity in the magnetic field. This effect can cause image distortions, particularly at the level of intervertebral disc spaces, which is exaggerated when herniated discs obliterate the anterior CSF, potentially introducing bias or invalidating metrics calculated in the compressed portion of the spinal cord in conditions such as CSM. For example, Kerkovsky et al. (2012) report decreased FA in patients with spinal cord encroachment (effacement on the CSF) that have neck pain or radiculopathy but no objective signs of myelopathy. This result could represent sub-clinical changes in the spinal cord microstructure, but could alternatively be explained by increased susceptibility artefact. In recent years, there has been increased use of rFOV techniques, although this approach was only utilized in 13% of the reviewed studies. These sequences are based on 2D radiofrequency (RF) excitation (Saritas et al., 2008, Finsterbusch, 2009) or oblique refocusing pulses (Dowell et al., 2009, Wilm et al., 2009), and allow the use of a smaller FOV with higher resolution while avoiding aliasing problems and decreasing distortions, albeit at a cost of

increased acquisition time. Only a fraction of DTI studies (23%) employed cardiac gating, likely because most groups felt that the reduction in motion artefacts is not worth the increased acquisition time and added complexity of setting up cardiac monitoring equipment. Two diffusion studies collected data with multiple b-values and computed measures of diffusion kurtosis, which is a dimensionless measure of the deviation from a Gaussian probability curve, with a positive value reflecting a sharper peak and heavier tails (Hori et al., 2012, Raz et al., 2013). Both studies identified positive MK in all subjects, with pathological subjects in CSM (Hori et al., 2012) and MS (Raz et al., 2013) showing group decreases in MK. However, it is unclear if DKI measures are sufficiently more powerful than simple DTI metrics to justify the added acquisition time required for multiple b-values. However, the optimal number of diffusion-sensitizing directions has not been established for DKI, but it may be possible that DKI can be performed with a smaller number of directions, possibly offsetting the need for multiple b-values. As mentioned above, all of the MT studies utilized similar acquisition methods such as GE sequences (except for the earliest study (Silver et al., 1997), MT pre-pulse parameters, and resolution. The single WMF study was exploratory in nature, and further refinements in spinal cord MWF image acquisition, including decreased scan time, are needed prior to the initiation of more advanced clinical studies using this method. MRS, particularly of the spinal cord, is prone to motion artefact and low SNR, typically requiring relatively long acquisition times due to the use of complex shimming methods, a high number of signal averages, and cardiac gating to obtain useful data. The magnetic field inhomogeneity within the spinal canal makes it difficult to shim the B0 field, usually requiring high-order shimming procedures to attempt to compensate. As a result, there is line broadening in the metabolite peaks and decreased amplitude, making detection difficult. MRS studies had the highest use of cardiac gating at 45% compared to other techniques in this review. The MRS results demonstrate significant variations in metabolite concentrations and ratios, even among healthy individuals (Holly et al., 2009, Ikeda et al., 2013, Salamon et al., 2013), suggesting that noise may still be a major limitation. However, it may also be the case that there naturally exists a wide range of normal in the concentrations and ratios of the molecules that MRS captures, in which case it will be difficult for MRS to make strong assertions about individual patients, even with further technical improvements. However, MRS provides unique information compared with the other advanced MRI techniques, and further development may allow quantification of important CNS molecules such as glutamate (not reliably detected with current methods), which may suggest an important role for MRS to

compl~~e~~ment the other more anatomically specific techniques. All 8 of the spinal fMRI studies used a fast or turbo SE pulse sequence with SEEP contrast, compared with T2*-weighted EPI that is typically used in brain fMRI based on BOLD contrast. FSE is commonly employed in spinal fMRI to compensate for severe inhomogeneity of the magnetic field within the spinal canal, but the readouts from this technique are considerably slower than EPI, increasing the effects of physiological motion artefacts. The time to acquire each volume of images in the reviewed studies ranged from 8 to 13 seconds, collecting between 5 and 9 slices (axial orientation in 7 studies, sagittal in 1) per volume, indicating the relatively low temporal resolution compared with brain fMRI, in which an entire brain volume can be acquired in 2 to 4 seconds. Furthermore, the signal change relating to altered neural activity is frequently only 2-3% (Stroman et al., 2004), requiring high SNR to reliably differentiate active voxels from background noise. The overall results of the spinal fMRI studies did not show convincing changes in activation patterns in specific pathologies (only minor loss of ipsilateral focal activation), possibly due to technical problems achieving sufficient SNR. If, however, reliable activations can be detected with better temporal resolution and shorter acquisition time, fMRI will likely make a significant impact, with obvious applications in conditions such as SCI to detect new activity and connectivity as regeneration therapies (e.g. stem cells) are studied. In summary, all 5 of the state-of-the-art spinal cord MRI techniques continue to face technical issues that require further innovations, and clinical studies face the limitation of needing to freeze on a specific acquisition methodology over the period of time required to complete data collection, even if it may not include the latest and greatest technical advances.

1.3.5.5 *State-Of-The-Art Imaging Deserves State-Of-The-Art Analysis*

The majority of DTI, MT, MWF, and fMRI studies included in this review used manual methods of ROI selection to extract quantitative metrics, with only 25/93 (27%) using automated or semi-automated ROI selection. In addition to being slow and imprecise, unblinded manual ROI selection is an obvious source of potential bias in studies, as the technician selecting the ROI can arbitrarily include or omit pixels of high or low signal (often present at the edge of the cord due to partial volume effects), and it is impossible to blind the technician in many scenarios (e.g. compressive myelopathy). The very low rate of objective analysis techniques for DTI studies (14%), compared with 56% of MT studies, is possibly due to greater problems with partial volume effects at the edge of the cord in DTI, where contamination with CSF causes an increase

in isotropic diffusion and a corresponding decrease in FA, prompting 7 DTI studies to employ manual exclusion of edge voxels after performing semi-automated segmentation to identify the spinal cord. Furthermore, most studies (73/104, 70%) included in this review reported whole-cord metrics, which average the effects of a specific disease process across all GM and WM. Analyzing whole-cord metrics lacks the specificity of measuring changes in individual anatomical areas, such as WM tracts (which might be differentially affected in a certain disease), and it also potentially dilutes the sensitivity to detect small changes: a 10% change present in the WM might only may show a 5% change in the whole-cord metric, which may no longer be statistically significant. To optimize the sensitivity and specificity of these techniques, the ideal solution is to analyze only the tissue that is most affected by a certain disease, such as the anterior horn GM and/or the lateral corticospinal tracts in ALS. Several groups are actively developing tools for this purpose, which can perform a series of complex data processing steps and automatically extract quantitative metrics from GM, WM, and specific WM-tracts (Cohen-Adad J, 2014), even correcting for partial volume effects at the cord periphery (Levy et al., 2015). Tract-specific metrics, which were available in only 22/104 studies (21%), also have the advantage of potentially characterizing gradations of injury to each anatomical area within the cord, potentially correlating with or predicting focal neurological deficits. Fiber tractography (FT) is an interesting alternative to ROI-based quantitative analyses of DTI data. The DTI studies that employed FT were listed separately from ROI studies in Table 1.4, primarily to identify trends and commonalities among the methods used within FT studies. Among the FT studies reviewed, only 38% extracted quantitative metrics from the region defined by the FT results. The utility of FT in quantitative assessment of the spinal cord is controversial, as some have suggested that using FT to automatically define ROIs is inherently biased (Cohen-Adad et al., 2011), and most FT algorithms require manual seed points, as was identified in our review (only 1/16 studies did not require seed points). However, one study in this review reported improved measures of inter-observer reliability using FT-based ROIs vs. manual ROIs, again supporting the importance of automated, objective analysis methods (van Hecke et al., 2009). Other studies derived quantitative measures from the FT output, such as number of fibers, fiber density, or fiber length (as surrogates for number of intact axons). However, the FT analysis is typically based on liberal assumptions of what constitutes a fiber, using low thresholds for minimum FA of 0.10-0.30 and angle of < 20-70° when calculating connections between voxels. The result is a very loose representation of the actual white matter that should be interpreted with

caution. An alternative to using tractography to measure the organization of the white matter is to perform quantitative analysis of the directionality of the eigenvectors, which was performed in 2 studies using OE and SD(θ). These alternative methods are highly quantitative, and may turn out to be more reliable than tractography in characterizing white matter changes, but greater data is needed to fully define their value. Half of the FT studies, all of which involved various forms of compressive myelopathy, only reported descriptions of the pattern of tracked fibers such as the degree of deformation or disruption. However, assignment of these descriptors is highly subjective and WM compression may be more accurately represented by geometric measurements (e.g. maximum spinal cord compression ratio). In comparing MT techniques, the use of MTR may have a theoretical advantage over MTCSF, as the CSF is prone to flow artefact that causes signal dropout, which could potentially bias results, but this was not an obvious drawback in the 2 studies that employed MTCSF. The calculation of MTR requires an added post-processing step, as images with and without an MT prepulse need to be co-registered accurately, but this is relatively straightforward with modern tools. No major technical challenges were identified in the analysis techniques employed by MWF and MRS studies, except for the use of manual ROIs in the WMF study (Laule et al., 2010). In all of the reviewed fMRI studies, time-series data were analyzed by convolving with a canonical hemodynamic response function, and activation maps (based on a p-value threshold or a clustering algorithm) were created. Due to challenges in obtaining robust activations, most of the spinal fMRI studies used an uncorrected threshold of $P<0.05$ for each voxel so that a greater number of activations could be identified, with the exception of one study (Cadotte et al., 2012a). This uncorrected analysis runs a high risk of identifying false activations, particularly when hundreds of voxels are included, and therefore the results of these studies must be interpreted with caution. All of the fMRI studies also used manual ROI selection, typically dividing the cord into quadrants manually, contributing another potential source of bias to the analysis.

1.3.5.6 *Statistical Analysis: A Big Data Problem*

Appropriate statistical analysis for complex clinical studies using quantitative MRI techniques is far from straightforward. This data can involve a large number of metrics, including multiple DTI indices or the output from multi-modal acquisitions, and the values might be extracted from numerous ROIs located in individual WM tracts at many rostro-caudal levels of the spinal cord. Furthermore, the above-mentioned trend toward using multiple clinical measures to fully

characterize disability suggests that future studies will need to employ multivariate analyses with an increasing number of independent and dependent variables. The analysis of these studies quickly becomes a big data problem, and help from an experienced statistician is advisable to correctly design robust multivariate analyses that incorporate a priori variables of interest and potential confounding factors such as age and gender. It is of paramount importance that a priori hypotheses are clearly stated beforehand, to avoid an excess number of comparisons and misrepresentation of the complex data to make unfounded conclusions. Among the studies reviewed, there were many cases where no correction was made for multiple comparisons, leading to findings that would not have been identified as significant with proper correction. In some cases, studies went as far as reporting conclusions that were clearly overstated or unfounded, which must be avoided in future translational research that will form the basis for clinical adoption of these techniques.

1.3.5.7 *Limitations of this Study*

This systematic review attempted to perform an exhaustive review of all clinical studies utilizing the 5 advanced spinal cord MRI techniques. A large number of citations were analyzed in an attempt to identify all relevant articles, but it is still possible that relevant studies were missed, including those not available in English. On the other hand, the large scope of this review made it more difficult to discuss all of the subtleties involved in these MRI techniques. Also, the inclusion criteria arbitrarily excluded cohorts with fewer than 24 subjects or fewer than 12 pathological subjects. This threshold was originally set at 20 total subjects and 10 pathological subjects, but it was increased because the number of studies identified using the lower threshold was far greater than 100, which would have made the tables excessively long and the discussion even more difficult. However, we did not increase the threshold higher than 24 as we felt that several key studies would have been excluded. Studies that only analyzed the quantitative metrics apparent diffusion coefficient (ADC), generated from DWI, or CSA, derived from anatomical images, were also excluded for the purpose of focusing this review on new techniques. Spinal cord DWI has been in clinical use for many years for the detection of infarction and abscess, but the simple metric of ADC (equivalent to MD in DTI) may have value in specific applications as a measure of microstructural tissue changes. CSA is clearly a powerful quantitative metric that relates to cord atrophy, which should be considered for use in addition to the advanced MRI metrics in multivariate models. The search strategy excluded research that

only studied healthy subjects, as these studies and those with smaller cohorts of pathological subjects tended to show less robust methodology and clinical relevance. This review also focused solely on advanced spinal cord imaging techniques, but several groups studying spinal cord pathologies have investigated imaging changes in brain microstructure and function, in part due to the relative simplicity of implementing these imaging protocols in the brain (Mikulis et al., 2002, Kowalczyk et al., 2012, Freund et al., 2013). Furthermore, this review was focused on the 5 most promising spinal cord imaging techniques identified by the recent expert panel, but several others are emerging that may make a substantial impact to this field, including perfusion imaging, susceptibility weighted imaging, T1 relaxometry, neurite orientation dispersion and density imaging (NODDI), and myelin g-ratio (Stikov et al., 2015).

1.3.5.8 *Future Directions*

The path to clinical translation of technological innovations, such as new MRI techniques, invariably includes numerous challenges and there remains significant work to successfully bring these techniques into clinical use. Translational research typically involves a process that begins with small exploratory studies and transitions to large, carefully designed clinical trials, and several of the state-of-the-art spinal cord MRI techniques reviewed in this paper have demonstrated sufficiently strong results and are ready for this next step. Looking forward, the spinal cord imaging community will continue to drive these powerful techniques forward, with several key steps happening concurrently: 1) larger clinical studies with specific hypothesis-driven research questions will be designed and conducted to assess for clinical utility; 2) acquisition techniques will continue to evolve and be refined to maximize signal-to-noise ratio (SNR) and resolution while minimizing distortions, artefacts, and acquisition times; and 3) powerful data analysis tools will be developed that can automatically extract quantitative data from the GM, WM, and specific WM tracts. The long path to clinical translation is not easy, but in the coming years, we can expect many further innovations in this burgeoning field, which will hopefully lead to major improvements in the diagnosis and management of patients with spinal cord pathologies.

New techniques and innovations are also emerging that could dramatically alter the course of research in this field, but were not utilized by any of the studies in this review. For example, the development of high strength gradients for DTI, highlighted by the human connectome project

that uses 300mT/m gradients (200mT/m/ms slew rate) - 8 times stronger than most clinical hardware, have provided new insights, such as mapping the axon diameter distribution in the human spinal cord (Duval et al., 2015). Recently, the introduction of inhomogenously broadened MT (ihMT) imaging has demonstrated much higher specificity for myelin imaging than previous MT techniques (although the signal dropout is less pronounced requiring subtraction between images, which decreases SNR substantially), which will likely spur new clinical studies to investigate its utility (Girard et al., 2015). Chemical Exchange Saturation Transfer (CEST) effect is a particular case of MT imaging, which can quantify the biochemical composition of tissues based on labile protons (hydroxyl, amide, amine, and sulfhydryl moieties). Feasibility in the human spinal cord and application in MS patients have recently been demonstrated (Kim & Cercignani, 2014). In addition, none of the 104 studies that were reviewed used 7T field strength, but with the proliferation of 7T research systems and the recent announcement of 7T clinical scanners, it is inevitable that new clinical studies at ultra-high field strength are coming soon and these could potentially show substantial improvements that strengthen the case for clinical utility. Analysis techniques may also undergo a revolution with the introduction of machine learning, as complex multivariate data from healthy and pathological subjects could be used to train classifiers, potentially increasing diagnostic sensitivity and specificity.

However, optimism for novel MRI methods must be tempered with practicality. Even if the clinical utility of one or more of these quantitative MRI techniques is clearly demonstrated, a considerable hurdle will still remain before widespread clinical adoption will occur. The concept of quantitative MRI has been used in the research domain for several years (e.g. CSA for MS), but is largely foreign to clinicians, and the exact method and workflow for its use needs to be carefully considered, or these new techniques will be quickly abandoned. Radiologists, neurologists, and spine surgeons that have busy clinical practices are unlikely to sit at an imaging workstation and perform manual tasks to generate quantitative metrics, so data analysis will need to be fully automated, robust, and seamlessly integrated. The perception that new analysis methods are time consuming, unreliable, or inaccurate will render these new methods unacceptable. Thus it is essential that sophisticated, automatic analysis tools be developed in parallel with advances in the imaging techniques themselves.

1.3.6 Conclusions

The current body of evidence of clinical studies using spinal cord DTI, MT, MWF, MRS, and fMRI is relatively limited, indicating the early stage of this translational research effort. However, moderate evidence indicates that the quantitative DTI metric FA successfully correlates with impairment in a number of neurological disorders. Low evidences suggests that FA shows tissue injury (in terms of group differences) in a number of disorders, but the evidence is insufficient to support its use as a diagnostic test or as a predictor of clinical outcomes. Very low evidence exists for other metrics to show pathological changes in terms of group differences in the spinal cord, including MD, RD, MK, MTR, MTCSF, and NAA, and the evidence is insufficient to determine if they can be used as a diagnostic test, biomarker, or prognostic marker in a clinical context. DTI has produced the most substantial results to date, but acquisition methods, data processing, and interpretation require further refinement, followed by standardization and cross-vendor validation, before this technology is ready for widespread clinical adoption. The path to clinical translation of these complex MRI techniques is not straightforward, and future translational studies are required that have clear a priori hypotheses, large enrolment numbers, short scan times, high quality acquisition techniques, detailed clinical assessments, automated analysis techniques, and robust multivariate statistical analyses. It is also important to keep in mind that the definition of clinical utility is to be able to make assertions about individual patients, not just achieve significant group differences, setting a very high standard for success. However, much progress has already been made, and the spinal cord imaging community will undoubtedly make many great achievements in the years to come.

1.4 Recent Publications (June 2015 to January 2017) Not Captured by the Systematic Review

The systematic review presented in section 1.3 captured research articles up to June 1, 2015. This section discusses additional research reports that have become available in the past 20 months.

1.4.1 Methods

An electronic search was performed using PubMed (pubmed.gov) for publications between June 1, 2015 and February 6, 2017. Search terms included synonyms of the 5 MRI techniques involved in the earlier systematic review, in addition to synonyms for the spinal region (Appendix B). The title and abstract of each citation were reviewed, and studies that met

eligibility criteria for the previous systematic review were retrieved for full-text review. Each article was read, and pertinent MRI techniques and findings are summarized and discussed below.

1.4.2 **Results**

The electronic search returned 374 citations, and following review of titles and abstracts, 25 relevant studies were identified (Table 1.11).

Study	Subjects	MRI Techniques/ Metrics	Clinical Data	Key Findings
Ellingson et al. (2015a)	21 DCM, 6 ASCC	rFOV DTI: FA, MD at MCL, C2 (whole cord, manual ROI) DTT: fiber density, ratio (MCL/C2) MRS: NAA, Cho, Cr, and ratios	mJOA	Numerous variables correlated with mJOA: MCL FA (R^2=0.70), MCL MD (R^2=0.47), fiber density ratio (MCL/C2, R^2=0.59), Cho/NAA (R^2=0.46). Multivariate model retained fiber density ratio, MD, and Cho/NAA (R^2=0.83).
Ellingson et al. (2015b)	Same as Ellingson et al. (2015a)	rFOV DTI with DTT: fiber density	mJOA	Data reported overlaps with Ellingson et al. (2015a). Maximum fiber density at MCL correlates with mJOA (R^2=0.63).
Grabher et al. (2015)	14 subacute SCI patients, 18 HCs	MRI at baseline, 2, 6, 12 months post injury: MPM (brain and upper cord): CSA, MTsat, R1 (whole cord)	ISNCSCI motor and sensory, pain, 12-month FU	MTsat and R1 reduced in patients vs. controls at 12 months (p=0.003, p=0.012, respectively) AP and LR diameter at C2 reduced (p<0.05)
Kearney et al. (2015b)	62 MS, 21 CIS, and 30 HCs	rFOV DTI: FA, MD, AD, RD in GM, LCs, DCs; manual ROI after semi-automated segmentation	EDSS, MSFC, 9-hole peg, TWT	GM showed decreased FA, increased MD, RD in SPMS>RRMS>CIS>HC. GM RD showed indepdent relationships with EDSS, 9-hole peg, and TWT.
Kim et al. (2015)	17 cSCI (all managed non-operatively, 21 HCs	DTI (sequence NR): FA, MD in GM, WM; manual ROI Phase-contrast: CSF	AIS, SCIM, MBI, SSEPs, MEPs	Decreased WM FA and increased MD at all levels (p<0.05). Higher peak CSF flow in cSCI (p<0.05). FA showed inconsistent correlations with clinical measures (many

		velocity		comparions, not corrected)
Lee et al. (2015)	14 DCM, 50 ASCC	Sagittal rFOV DTI: FA, MD, AD, RD; manual ROI	None	Subgroup without T2WI hyperintensity (N=33, 4 with DCM) showed moderate diagnostic accuracy that improved with FA was combined with MD, AD, or RD
Maki et al. (2015)	20 DCM, 10 HCs	rFOV DTI: FA of the LCs, DCs; manual ROIs	JOA	FA correlated with JOA (r=0.48 for both LC, DC), but stronger for LE subscore (LC: r=0.76, DC: r=0.74)
Wang et al. (2015)	16 DCM, 58 HCs (possibly same population as Li et al. (2014))	DTI (sequence NR): FA; manual ROI	Symptomatic level diagnosis by sensation, weakness, reflexes	Support tensor machine (STM) outperformed Bayesian and support vector machine (SVM) classifiers for symptomatic level: SE=85%, SP=97%.
Bosma et al. (2016)	14 Fibromyalgia, 15 HCs	HASTE BOLD fMRI: activations in brain, brainstem, cord; manual ROI	Pain threshold, after-sensation	Small differences in dorsal horn and brainstem activity following pain stimuli
Budrewicz et al. (2016)	15 ALS, 10 HCs	ssEPI DTI: FA of VCs, LCs, DCs; manual ROI	None	All WM regions showed similar degeneration in ALS ($p<0.00001$).
Casseb et al. (2016)	28 sensory neuronopathy, 14 diabetic neuropathy, 20 HCs	DTI (sequence NR): FA, MD in DCs; manual ROI	LANSS, ISSS, SARA	FA discriminates between SN and other subjects with AUC=0.838. FA correlates with LANSS (r=0.50) but not ISSS, SARA.
Castellano et al. (2016)	13 AML, 12 HCs	WM and GM CSA DTI (sequence NR): FA extracted from GM; semi-automatic ROI	EDSS, ALD, ambulation index	Cord CSA showed strong differences vs. HCs. WM FA decreased in AML, GM FA not significantly affected. MRI measures did not correlate with clinical measures.
Egger et al. (2016)	25 intramedullary tumour patients	Multishot DTI Siemens streamlines DTT: normal, displaced, or terminated	None	All 6 patients with normal DTT showed inflammatory/demyelinating pathology; 10 subjects had displaced DTT: 6 tumours, 4 NYD; 9 showed terminated DTT: 5 tumours, 2 reactive gliosis, 2 NYD.

Grabher et al. (2016)	20 DCM, 18 HCs	ssEPI DTI: FA, MD, AD, RD in WM, GM, DCs, LCSTs; manual ROI CSA of rostral WM, GM, DCs, LCs	mJOA, UELT, UEPP, GRASSP, SCIM	Decreased FA in LCST (p=0.01) and DCs (p=0.006). DCM showed decreased CSA of GM (7.2%), WM (13.9%), DCs (16.1%).
Jain et al. (2016)	34 Pott's disease	DTI (sequence NR): FA, MD; manual ROI (central, mixed GM/WM) DTT: subjective pattern	Motor score (details NR)	MCL FA showed no difference vs. rostral (used as control). Caudal FA showed decrease vs. control. Unclear if data was normalized for level.
Lema et al. (2016)	134 MS	MTR: GE ± MT prepulse MTsat: derived from PD, T1WI, and MT images	EDSS, TWT	MTsat showed stronger correlations with EDSS and TWT than MTR.
Lindberg et al. (2016)	16 DCM (minimally symptomatic), 20 HCs	Sagittal ssEPI DTI: FA, MD, AD, RD, manual ROI	EMS, FIM, grip strength, Moberg dexterity test	None had overt SC compression; DCM subjects and 5 subjects with ASCC (but with deficits on clinical testing) had reduced FA compared to controls; few voxels used and certain conclusions are not founded: lateral ROI shows greater changes likely because it reflects more WM than medial ROI.
Lindemann et al. (2016)	25 RLS, 25 HCs	DTI (sequence NR): FA from C1-C5; manual ROI	RLS scale, disease duration	Decreased FA in RLS ($p<0.05$) but not after Bonferroni correction
Liu et al. (2016)	18 DCM, 25 HCs	Resting-state fMRI with GE-EPI (BOLD): ALFF	JOA	Not age matched; amplitude of low frequency fluctuations (ALFF) differed in DCM ($p<0.001$) and severe DCM had greater ALFF than mild DCM ($p<0.05$)
Maki et al. (2016)	40 DCM, 10 HCs	rFOV DTI: FA; manual ROI in LCs	ASIA MS	FA lower in DCM than HCs; motor score correlated with FA (r=0.64-0.67); Assymetry index between L/R FA values had AUC=0.86, for CSA: AUC=0.54 (hemi-cord CSA was based on bony landmarks, not the cord itself)
Wang et al. (2016)	93 DCM, 36 HCs	ssEPI DTI: FA, MD; manual ROI; DTT with	JOA, JOA RR at 1-year FU	FA and MD ratios showed less age-variation; MRI grading (T1WI/T2WI hyperintensity)

		manual grading		correlated with JOA (r=-0.67) but not JOA RR; high correlations between FA ratio and JOA (r=0.75-0.85); modest prediction of outcomes (r=0.35-0.43)
Ying et al. (2016)	32 DCM, 21 HCs	ssEPI DTI: FA, MD; manual ROI	mJOA	FA correlates with mJOA (r=0.51) better than MSCC (-0.36).
Kerkovsky et al. (2017)	37 DCM, 93 ASCC, 71 HCs	ssEPI DTI: FA, MD; manual ROI	None	FA lower in DCM vs. ASCC ($p<0.05$) but diagnostic accuracy NR; ASCC and HCs not directly compared but FA values appear similar
Rajasekaran et al. (2017)	35 DCM (26 with FU)	ssEPI DTI: FA, MD, E1, E2, E3; ROI selection NR	Nurick, 1-year FU	DTI not predictive of Nurick recovery; MD, E1, and E2 were responsive to recovery
Vedantam et al. (2017)	27 DCM	1.5T ssEPI DTI: FA; manual ROI	mJOD, NDI, SF-36, 3-month FU	FA correlates with baseline mJOA (r=0.65) and predicts mJOA change at 3 months (r=-0.42); outcome prediction not analyzed wrt baseline mJOA (i.e. baseline FA likely provides redundant information as baseline mJOA)

Table 1.11: Summary of Recent Quantitative MRI Studies. The studies listed were captured in a PubMed search of DTI, MT, MRS, MWF, and fMRI studies between June 1st, 2015 and February 6th, 2017.

1.4.2.1 *Acquisition Techniques*

Among these, 21 utilized DTI as a quantitative MRI technique, including 20 that performed ROI-based analysis and 6 that employed DTT for analysis. 1 studies employed MTR imaging. An additional 2 studies investigated the use of fMRI, with one using a thermal pain stimulation paradigm and the other using resting-state fMRI (rsfMRI), a popular technique in brain studies but implementation in the spinal cord is relatively new. 1 study employed MRS, in addition to DTI.

Several studies investigated new qMRI techniques that were not discussed in the "State-of-the-Art" NeuroImage papers and were not part of our earlier systematic review (Stroman et al., 2014, Wheeler-Kingshott et al., 2014, Martin et al., 2016). 2 studies used an emerging technique called

MT saturation (MTsat), that is reported to be more specific to myelin, independent of T1-relaxation and B1 inhomogeneity effects, and showing greater grey-white contrast than MTR (Lema et al., 2016). Another study used multiparametric mapping (MPM) of the brain and rostral cord, collecting MTsat, longitudinal relaxivity (R1) maps, and CSA (Grabher et al., 2015). Finally, 1 study employed phase-contrast MRI to quantify CSF flow (Kim et al., 2015).

1.4.2.2 *Analysis Techniques*

Among the ROI-based DTI studies, only 1 performed template-based analysis using a probabilistic atlas (Castellano et al., 2016), 18 used manually selected ROIs, and 1 did not report ROI selection. None of the DTT studies used the tractography maps to define ROIs. 2 studies (from the same group, same subjects) reported fiber density of the tractography maps (Ellingson et al., 2015a, Ellingson et al., 2015b). The remaining 4 studies used subjective visual grading of the reconstructed tractography fibers to assign subjects to categories such as “normal”, “partially disrupted”, and “disrupted”.

1.4.2.3 *Clinical Populations and Assessments of Disability*

The majority of clinical qMRI studies in the past 20 months have focused on DCM as the clinical population of interest, including 14 studies. Whereas MS was previously the most commonly studied pathology with spinal cord qMRI, it was the subject of only 2 new studies. The remainder of studies investigated RLS (1), Pott’s disease (1), sub-acute SCI (1), cSCI (1), sensory neuropathy (1), ALS (1), AML (1), fibromyalgia (1), and intramedullary tumours (1).

Clinical data included multiple measures of disability in 10 studies, a single measure in 10 studies, and no clinical assessments (other than diagnosis) in 5 studies. Diagnosis was the explicit focus in 4 studies, including diagnosis of DCM in 1 study, identification of the symptomatic level in multilevel DCM in 1 study, and differentiation between intramedullary SC tumour types in 1 study.

1.4.3 **Discussion**

The field of spinal cord qMRI has continued to evolve over the past 20 months, with several new approaches to acquisition techniques being introduced. The MPM protocol employed by Grabher et al. (2015) that produces an array of quantitative tissue parameters is an exciting development,

representing an incremental advance from similar techniques that was previously used in the brain and spinal cord by several of the same authors (Samson et al., 2013, Freund et al., 2013). This longitudinal study showed that R1 and MTsat provide myelin-sensitive measures of tissue degeneration that can be detected in the C2-3 region of the cervical cord. However, these results need to be validated in DCM and other clinical populations, as the cohort of sub-acute patients in this study included a majority of severe (motor-complete) injuries, in which severe changes in spinal cord microstructure are expected. Thus, it remains to be seen if this protocol can produce the same quality of data in the cervical spinal cord as other qMRI techniques, as magnetic field inhomogeneity, physiological noise, and the small size of the spinal cord pose substantial challenges, and further data is needed to determine the clinical utility of this approach. The study by Lema et al. (2016) comparing MTsat to MTR in MS patients was also of great interest, reporting that spinal cord MTsat shows superior clinical correlations compared with MTR. The applicability of this technique to detect more subtle demyelination in DCM should be investigated, ideally in comparative studies that also use MTR and/or DTI.

Perhaps the most interesting new reports were 7 studies that explored the utility of qMRI to solve specific clinical problems, with 4 of these related to various forms of diagnosis and 3 involving prediction of outcomes. Lee et al. (2015) compared diagnostic accuracy between various DTI metrics and found that the combination of FA and AD (logical AND of dichotomized values) outperformed individual metrics and other combinations, achieving SE=100% and SP=68.9%. However, this study had a small sample size (N=33), including only 4 DCM patients, and the results are not convincing that this approach is likely to surpass the current diagnostic “gold standard” of cord compression on anatomical MRI and neurological deficits that localize to the cervical cord. Wang et al. (2015) used DTI parameters in a slightly different approach, to attempt to localize the most symptomatic level in cases of multilevel DCM, using clinical examination of sensory deficits (dermatomes), motor weakness (myotomes), and diminished deep tendon reflexes. This study appears to be related to Li et al. (2014), using more complex analysis methods to investigate the same topic with a similar sample size and many of the same authors, but the earlier study was not cited. They reported that a support tensor machine (STM) classifier outperformed naïve Bayesian and support vector machine (SVM) algorithms, and identified the clinically symptomatic level with SE=85% and SP=97%. It is, however, unclear if this is sufficient to be clinically useful, as the use of qMRI in this application does not clearly improve

the information gleaned from clinical methods, and furthermore, many surgeons prefer to treat all compressed levels in multilevel DCM. Casseb et al. (2016) used DTI with manual ROI analysis to determine if patients with the diagnosis of sensory neuronopathy (SN) could be reliably distinguished from those with diabetic neuropathy and healthy subjects. This has potential clinical utility, as SN is difficult to distinguish on clinical grounds from other length-dependent sensory neuropathies, the most common of which is diabetic neuropathy. SN involves primary degeneration of the dorsal root ganglia and projections, leading to severe sensory deficits and afferent ataxia, and is thus an important clinical entity to distinguish for prognosis, patient education, and management. FA showed good discrimination between SN and other subjects (AUC=0.838), but the authors did not report the more important discrimination between SN and other sensory neuropathies, which is presumably lower. Thus, the results are not sufficient to show clinical utility of FA for diagnosis in this disease. Finally, Egger et al. (2016) performed DTT in 25 patients with intramedullary cervical SC tumours, and the results were suggestive that this technique was helpful in differentiating between demyelinating or inflammatory pathologies (showing normal fiber pathways), tumours (showing displaced or terminated fibers), and reactive gliosis (showing terminated fibers). This is a similar approach as previously described by Vargas et al. (2008), but the earlier study was too small to be captured by our large systematic review. Egger et al. (2016) propose an algorithm in which patients with a DTT study that shows normal fiber pathways do not undergo biopsy, but rather have a short-term follow-up DTT study instead. However, the authors do not report that the proposed method of using this information has been implemented to actually inform decision-making.

Three studies involving the DCM population investigated the capability of DTI parameters to predict outcomes. Rajasekaran et al. (2017) found that DTI parameters were not predictive of post-operative recovery in univariate analysis of 35 patients. Vedantam et al. (2017) similarly studied 27 patients with DTI to predict post-operative outcome, and found that baseline mJOA predicts the mJOA change score at 3 months (r=-0.42) in univariate analysis. However, this is not a surprising finding, as it has been well established that more severe cases of DCM show greater improvement following surgery (Fehlings et al., 2013), and these results are likely explained by the fact that baseline FA correlates well with baseline mJOA (r=0.65 in the same report). Thus, this analysis requires multivariate analysis that, ideally, includes all known predictors of outcome, of which baseline neurological status has been demonstrated to show the

strongest relationship (Nouri et al., 2015c, Tetreault et al., 2015b). Wang et al. (2016) completed a large study with 93 DCM subjects, and found modest correlations (Pearson r=0.35-0.45) between baseline DTI parameters and JOA recovery ratio (RR), which is calculated using the Hirabayashi method: recovery rate (%) = (follow-up JOA score – baseline JOA score)/(17 – baseline JOA score)×100%. This again was a univariate analysis, but the use of JOA RR as the outcome measure helps to reduce the impact of baseline neurological status, as it has been shown that all severity categories in DCM recovery approximately half of their deficits post-operatively (Fehlings et al., 2013). In addition to these 3 studies DTI studies, 1 small study was found incidentally that was not included in the electronic search, which used MRS to predict outcomes in 16 DCM patients (Holly et al., 2016). This study found a very strong relationship between preoperative mJOA and postoperative mJOA ($p<0.0001$). The results also found that NAA/Cr and Cho/NAA ratios were weakly related with mJOA change, but the authors did not perform multivariate analysis to determine if these were independent of the effect of baseline mJOA (which both are known to correlate with). This highlights how important multivariate analysis is to determine if new prognostic factors provide additional information beyond what is already known with established ones.

Unfortunately, little progress has been achieved in clinical qMRI studies in terms of analysis techniques, with almost all ROI-based DTI studies still using manual ROI placement. This approach is quite simply not appropriate for clinical use, as it is slow, does not isolate WM or GM, and has a high risk of bias (e.g. one can produce lower FA measurements by including more GM).

1.4.4 **Conclusions**

In spite of several new advances in the acquisition of high-quality quantitative MRI data, much work remains to successfully translate these methods to clinical use. Although several studies have demonstrated some potential for qMRI techniques to be useful in a clinical setting, no studies have thus far demonstrated cases in which qMRI has been used to inform decision-making and alter patient care.

1.5 T2*-weighted Imaging of the Spinal Cord

T2*-weighted imaging (T2*WI) is an MRI technique that is weighted based on the rate of dephasing of protons, known as the transverse relaxation rate. T2* decay includes the effects of spin-spin interactions (what is measured by T2-weighted imaging) and also magnetic field inhomogeneity that causes protons to precess at slightly different frequencies (Levitt, 2008). Gradient echo sequences with long repetition time (TR) and echo time (TE) are inherently T2*-weighted because they do not employ the 180° rephasing pulses that are employed in spin echo. The use multiple echoes are helps to improve signal to noise ratio (SNR) and provide higher quality images. T2*WI is available on all major MRI vendors, including the GE MERGE, Siemens MEDIC, Philips M-FFE, and Hitachi ADAGE sequences, although differences may exist between implementations (White et al., 2011).

T2*-weighted imaging (T2*WI) of the SC provides high resolution and strong contrast between GM and WM, particularly at 3T or higher field strength, allowing accurate segmentation between these structures (Yiannakas et al., 2012). Several groups have employed T2*WI to measure CSA of specific structures within the SC, including WM (Taso et al., 2016, Grabher et al., 2016, Taso et al., 2015, Yiannakas et al., 2012), GM (Taso et al., 2016, Grabher et al., 2016, Taso et al., 2015, Yiannakas et al., 2012), and individual funiculi (e.g. the dorsal columns) (Grabher et al., 2016). It has also been established that T2*WI shows hyperintensity of the WM in various pathologic conditions (Cohen-Adad et al., 2012, Cohen-Adad et al., 2013b). In one study, a pattern consistent with Wallerian degeneration of fasciculus gracilis could be visualized rostrally following a cervical SC needle injury (Figure 1.5) (Cohen-Adad et al., 2012). Another study found hyperintensity in bilateral LCSTs in a patient with amyotrophic lateral sclerosis (ALS), presumably related to the degeneration of descending upper motor neurons (Cohen-Adad et al., 2013b).

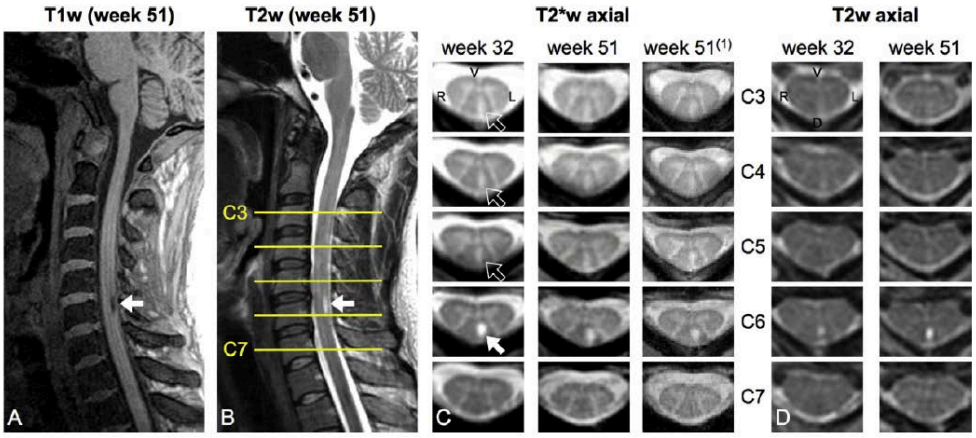

Figure 1.5: Example of T2*WI WM Hyperintensity. Sagittal T1-weighted (T1w, A) and T2-weighted (T2w, B) images show an intramedullary cavitation at C6 related to an accidental needle injury during an epidural steroid injection. Axial T2*-weighted (T2*w) images (C) clearly reveal ascending Wallerian degeneration of the left fasciculus gracilis up to C3, whereas axial T2-weighted images (D) show only a minimal trace of the injured white matter rostral to the injury. Reproduced with permission from Cohen-Adad et al. (2012).

The pathophysiological processes that underlie T2*WI WM hyperintensity, revealed primarily from brain MRI studies, include demyelination, gliosis, increased calcium concentration, and non-heme iron stored in ferritin, but signal intensity also depends on water content and local concentration of deoxyhemoglobin (used in BOLD fMRI) (Cohen-Adad, 2014, Lee et al., 2012, Fukunaga et al., 2010, Haacke et al., 2005, Marques et al., 2009). However, T2*WI signal intensity is itself not a meaningful quantity, as it is a relative value that varies between subjects due to a number of factors (e.g. tissue susceptibility differences). Thus, it requires normalization for use as a quantitative biomarker, which we propose and discuss in Chapter 2 and 3. In summary, T2*WI shows promise as an additional qMRI technique, warranting further investigation.

1.6 Moving Quantitative Spinal Cord MRI Closer Toward Clinical Translation: Objectives, Aims, and Hypotheses of This Research

1.6.1 The Current Progress of the Field

Great progress has been made to develop an array of qMRI techniques that measure various aspects of tissue microstructure and function. This effort, to date, has primarily been led by the MR physicists and engineers who have developed the techniques. This has led to more than a hundred of studies that have largely shown group differences and demonstrated interesting physiological findings, but none of these studies shows an application of qMRI to directly alter clinical management in individual patients. At present, the field is at a transition point where greater contributions from clinicians and clinical researchers are needed. These clinicians will need to have a strong understanding of the technological aspects of the work to help guide its development, and strong collaboration is needed to bridge the gap between clinical and technological disciplines. These next steps include 1) the simplification and standardization of qMRI acquisition and analysis methods such that they can be realistically applied in a clinical setting, 2) the identification of specific clinical problems that qMRI approaches might be able to solve for individual patients, 3) the design of high-quality prospective hypothesis-driven studies that investigate clinical utility, 4) the completion of these studies and critical interpretation of their results, including the identification of any barriers that would preclude clinical use, and 5) the implementation of qMRI into clinical decision-making algorithms at a small scale, followed by knowledge translation activities to disseminate the approach more widely.

1.6.2 Overarching Objective

The overaching objective of this research was to identify specific clinical problems in the management of DCM patients that could be solved with quantitative MRI techniques, and perform clinical research with a low risk of bias to determine the utility of clinically feasible qMRI techniques for these specific applications.

1.6.3 Specific Aims and Hypotheses

Table 1.12 displays the specific aims of this research, and the corresponding hypotheses that were tested. Hypotheses 1-11 and 14 were specifically tested in the original research studies

described in chapters 2-5, whereas hypotheses 12, 13, and 15 are currently under investigation and are discussed in Chapter 6 (Section 6.2, Future Directions). This research was driven by a number of hypotheses that relate closely to the specific aims, in addition to several other hypotheses that were tested:

	Aim	Hypothesis	Chapter
1	To develop a multiparametric MRI protocol that captures several measures of microstructure and tissue injury using techniques suitable for clinical use, including MRI vendor-independent pulse sequences, standard clinical hardware, and short acquisition time.	A clinically feasible multiparametric quantitative MRI protocol could be developed that shows similar or better performance compared to previous studies that employ more complex and less portable methods.	2
2	To develop a template-based analysis framework that uses automated tools to minimize bias and analysis time, while providing readouts from the whole SC, WM, GM, and individual WM tracts at various levels of the cervical spinal cord.	A semi-automated image processing pipeline using the spinal cord toolbox (SCT) could be developed to analyze data efficiently and accurately.	2
3	To analyze the variation of quantitative MRI metrics with subject characteristics and rostrocaudal level, and subsequently develop appropriate normalization procedures to generate more accurate measures of tissue integrity.	Normalization procedures could be developed that reduce the inter-subject variability of the healthy population and produce more accurate measures of tissue injury.	2
4	To characterize the test-retest reliability of quantitative measures in healthy subjects and patients with DCM.	The test-retest reliability of our clinically feasible protocol would be similar to or better than those previously reported for each technique.	2, 6
5	To measure the differences in DTI metrics and test-retest reliability with and without cardiac triggering.	DTI without cardiac triggering would produce approximately equivalent results as DTI with cardiac triggering, when collecting extra data without triggering (due to its shorter scan time) and using outlier rejection to remove spurious motion-related values.	2, 6

6	To investigate the clinical utility of qMRI measures for diagnosis of DCM.	Our multiparametric qMRI protocol can provide an accurate diagnostic tool that discriminates between DCM and healthy subjects, including cases with diagnostic uncertainty.	3, 4, 6
7	To compare the performance of qMRI metrics in terms of group differences and diagnostic accuracy (DCM vs. healthy), and correlations with a suite of clinical measures.	qMRI metrics would show similar group differences and diagnostic accuracy between DCM and healthy subjects, and clinical correlations compared with previous studies in univariate analyses.	3
8	To investigate or develop new qMRI measures for their potential use as biomarkers of disease in DCM.	We can identify one or more novel biomarkers of SC tissue injury that are useful in DCM and other spinal pathologies.	3, 6
9	To develop multivariate models and/or composite scores that combine qMRI measures to increase their statistical power.	Multivariate models and/or composite scores that incorporate our multiparametric data would show stronger group differences and diagnostic accuracy between DCM and healthy subjects, and clinical correlations compared with univariate approaches.	3, 4, 5, 6
10	To investigate the clinical utility of qMRI measures for diagnosis of subclinical tissue injury in asymptomatic subject that have an element of spinal cord compression.	Multiparametric qMRI can detect subclinical tissue injury in asymptomatic subject that have an element of spinal cord compression. Morphological analysis of the spinal cord can objectively diagnose mild indentation, flattening, and torsion of the cord, which imply the presence of static or dynamic compression.	4
11	To investigate the clinical utility of qMRI measures for serial monitoring of disease progression (to	Neuroplasticity and behavioural adaptation are factors that act to mask	5

	detect deterioration) in DCM patients managed non-operatively.	progressive tissue injury in DCM, and serial qMRI assessments would show a greater rate of progression of tissue injury compared with comprehensive clinical measures that detect functional/neurological deterioration in DCM patients managed non-operatively.	
12	To investigate the clinical utility of qMRI measures to predict outcomes in DCM patients managed non-operatively, looking for specific risk factors for deterioration.	qMRI ~~To investigate the clinical utility of qMRI measures to predict outcomes in DCM patients managed non-operatively, looking for specific risk~~prognostic factors can be identified that portend an increased risk for myelopathic deterioration in non-operative DCM patients.~~.~~	6
13	To investigate the clinical utility of qMRI measures to predict outcomes in DCM patients managed operatively, looking for specific prognostic factors of recovery.	qMRI prognostic factors can be identified that portend an increased likelihood of good recovery in operative DCM patients~~To investigate the clinical utility of qMRI measures to predict outcomes in DCM patients managed operatively, looking for specific prognostic factors of recovery~~.	6
14	To investigate the feasibility of acquiring qMRI data in post-operative DCM patients with metallic implants and identifying the distance at which we can obtain useful data.	~~To investigate the feasibility of acquiring qMRI data in post-operative DCM patients with metallic implants and identifying the distance at which we can obtain useful data.~~qMRI data obtained above the levels of hardware (e.g. C1-2) shows minimal artifacts and acceptable results.	3, 6
15	To determine the responsiveness of qMRI measures to monitor post-operative recovery in DCM patients following surgical treatment.	~~To determine the responsiveness of~~ qMRI measures are responsive to ~~to monitor~~ post-operative recovery in	6

		DCM patients following surgical treatment.	

Table 1.12: Specific Aims and Hypotheses of this Research.

1.6.4 **Research Strategy**

The overall strategy for this research was to begin with a large systematic review of the literature, which was useful to gain an overall understanding of the techniques and their clinical potential. In parallel, discussions my supervisor (Dr. Fehlings), thesis program advisory committee (PAC) members (Dr. Mikulis, Dr. Ginsberg, Dr. Crawley), key collaborators (Dr. Cohen-Adad, Dr. Kalsi-Ryan) were held to determine the clinical questions that could be answered, design the clinical data that would be collected, and plan the MRI acquisition. Dr. Cohen-Adad travelled to Toronto on 2 occasions to help design and set up the acquisition protocol. The clinical study design, MRI acquisitions, and analysis methods were iteratively refined over the next several months. Finally, a clear study design emerged with specific aims and hypotheses, and these mostly remained fixed for the remainder of the study (except for the study of asymptomatic spinal cord compression, which was conceived of after analyzing healthy subject data entirely (Chapter 2).

Chapter 2
Clinically Feasible Microstructural MRI to Quantify Cervical Spinal Cord Tissue Injury using DTI, MT, and T2*-weighted Imaging: Assessment of Normative Data and Reliability*

*This chapter is based upon the following published article: (Martin et al., 2017b), and is reproduced with permission.

DTI, MT, T2*WI, and CSA can quantify aspects of spinal cord microstructure. However, clinical adoption remains elusive due to complex acquisitions, cumbersome analysis, limited reliability, and wide ranges of normal values. We propose a simple multiparametric protocol with automated analysis and report normative data, analysis of confounding variables, and reliability. 40 healthy subjects underwent T2WI, DTI, MT, and T2*WI at 3T in <35 minutes using standard hardware and pulse sequences. CSA, fractional anisotropy (FA), MT ratio (MTR), and T2*WI WM/GM signal intensity ratio were calculated. Relationships between MRI metrics and age, sex, height, weight, cervical cord length, and rostrocaudal level were analyzed. Test-retest coefficient of variation (TRCOV) measured reliability in 24 DTI, 17 MT, and 16 T2*WI datasets. DTI with and without cardiac triggering was compared in 10 subjects. T2*WI WM/GM showed lower inter-subject coefficient of variation (COV, 3.5%), compared with MTR (5.8%), FA (6.0%), and CSA (12.2%). Linear correction of CSA with cervical cord length, FA with age, and MTR with age and height led to decreased COV (4.8%, 5.4%, and 10.2%, respectively). Acceptable reliability was achieved for all metrics/levels (TRCOV<5%), with T2*WI WM/GM comparing favourably with FA and MTR. DTI with and without cardiac triggering showed no significant differences for FA and TRCOV. Reliable multiparametric assessment of SC microstructure is possible using clinically suitable methods. These results establish normalization procedures and pave the way for clinical studies, with potential for improving diagnostics, objectively monitoring disease progression, and predicting outcomes in spinal pathologies.

2.1 **Background**

The era of quantitative MRI (qMRI) has arrived, allowing in vivo measurement of specific physical properties reflecting spinal cord (SC) microstructure and tissue damage (Wheeler-

Kingshott et al., 2014, Stroman et al., 2014). Such measures have potential clinical applications, including improved diagnostic tools, objective monitoring for disease progression, and prediction of clinical outcomes (Martin et al., 2016). However, technical challenges such as artefacts, image distortion, and achieving acceptable SNR have led to limited reliability. Specialized pulse sequences and custom hardware have advanced the field, but incur costs of increased complexity and acquisition time while creating barriers to portability and clinical adoption. Furthermore, qMRI metrics often show wide ranges of normal values and confounding relationships with subject characteristics such as age (Uda et al., 2013b, Mamata et al., 2005, Budzik et al., 2011, von Meyenburg et al., 2013, Taso et al., 2016), which most previous studies have not accounted for (Martin et al., 2016).

Among the most promising SC qMRI techniques are DTI and magnetization transfer (MT)(Stroman et al., 2014, Wheeler-Kingshott et al., 2014, Martin et al., 2016). These provide measures of axonal integrity and myelin quantity that correlate with functional impairment in conditions such as degenerative cervical myelopathy (DCM)(Uda et al., 2013a, Mamata et al., 2005, Budzik et al., 2011, von Meyenburg et al., 2013) and MS (Martin et al., 2016, Oh et al., 2013b), albeit with limited physiological specificity (e.g. fractional anisotropy, FA, reflects both demyelination and axonal injury) (Harrison et al., 2015, Vavasour et al., 2011). SC cross-sectional area (CSA) computed from high-resolution anatomical images can measure atrophy (e.g MS) (Kearney et al., 2014a) or the degree of SC compression in DCM (Nouri et al., 2015c). T2*-weighted (T2*WI) imaging at 3T or higher field strength offers high-resolution and sharp contrast between SC WM and GM, allowing segmentation between these structures similar to phase-sensitive inversion recovery (PSIR) (Grabher et al., 2016, Datta et al., 2016). T2*WI also demonstrates hyperintensity in injured WM (Cohen-Adad et al., 2012, Cohen-Adad et al., 2013b, White et al., 2011), reflecting demyelination, gliosis, and increased calcium and non-heme iron concentrations (Cohen-Adad, 2014). T2*WI signal intensity is not an absolute quantity, so we normalize its value in WM by the average GM signal intensity in each axial slice, creating a novel measure of WM injury: T2*WI WM/GM ratio (Martin AR, 2017b).

We propose a multiparametric approach to cervical SC qMRI with clinically feasible methods, including acceptable acquisition time, standard hardware/pulse sequences, and automated image analysis. Our protocol yields 4 measures of SC tissue injury (CSA, FA, MT ratio (MTR), and T2*WI WM/GM), for which this study establishes normative values in numerous ROIs. We

characterize the variation of these metrics with age, sex, height, weight, cervical cord length, and rostrocaudal level and propose normalization methods. Finally, we assess test-retest reliability of FA, MTR, and T2*WI WM/GM and compare our DTI results against those with cardiac triggering.

2.2 Materials and Methods

2.2.1 Study Design and Subjects

This study received approval from the University Health Network (Toronto, Ontario, Canada) and written informed consent was obtained from all participants. 42 subjects were recruited between October 2014 and December 2016 with a broad range of ages and balanced between sexes. A physician (ARM) assessed all subjects to rule out symptoms and signs of neurological dysfunction and T2WI images were screened for abnormalities suggestive of multiple sclerosis, tumour, or severe cord compression. Two subjects were excluded from the study with clinical and imaging findings of DCM, leaving 40 healthy subjects for analysis. Data from 18 DCM patients were included for analysis of test-retest reliability and 6 DCM patients were included in a cardiac triggering comparison, but DCM subjects were excluded from other analyses.

2.2.2 MRI Acquisitions

MR images were acquired on a 3T clinical scanner (GE Signa Excite HDxt, peak gradients 50mT/m, slew rate 150 T/m/s) using a body coil for transmission and the top 2 elements of a standard 8-element spine coil (USA Instruments) for reception. Subjects were positioned head-first, supine with the head tightly padded to prevent movement and neck flexed to straighten the cervical SC.

The MRI protocol was developed based on methods previously employed by one of the authors (JCA) (Cohen-Adad et al., 2012, Cohen-Adad et al., 2011, Cohen-Adad et al., 2013b). ~~T2WI~~ Anatomical imaging was performed using ~~esa employed~~ sagittal FIESTA-C sequence with 0.8mm^3 isotropic resolution covering brainstem to T4, which is known to produce images with T2/T1-weighting.~~.~~ DTI, MT, and T2*WI images had 13 axial slices positioned perpendicular to the spinal cord (at C3), covering C1 to C7 using a variable gap, alternating between mid-vertebral body and intervertebral disc (Figure 2.1). Parameters for each sequence are listed in Table 2.1. DTI employed a spin echo single shot EPI (ssEPI) sequence with 80x80 mm^2 FOV to

minimize susceptibility distortions, anterior/posterior saturation bands to achieve outer volume suppression (OVS), and no cardiac triggering. Second order localized shimming was performed prior to DTI by positioning a VOI encompassing the SC from C1-C7. T2*WI images used the multi-echo recombined gradient echo (MERGE) sequence, with 3 echoes that are magnitude reconstructed and combined using a sum of squares algorithm (White et al., 2011). Each session required 30-35 minutes, including subject positioning, slice prescription, pre-scanning, and shimming.

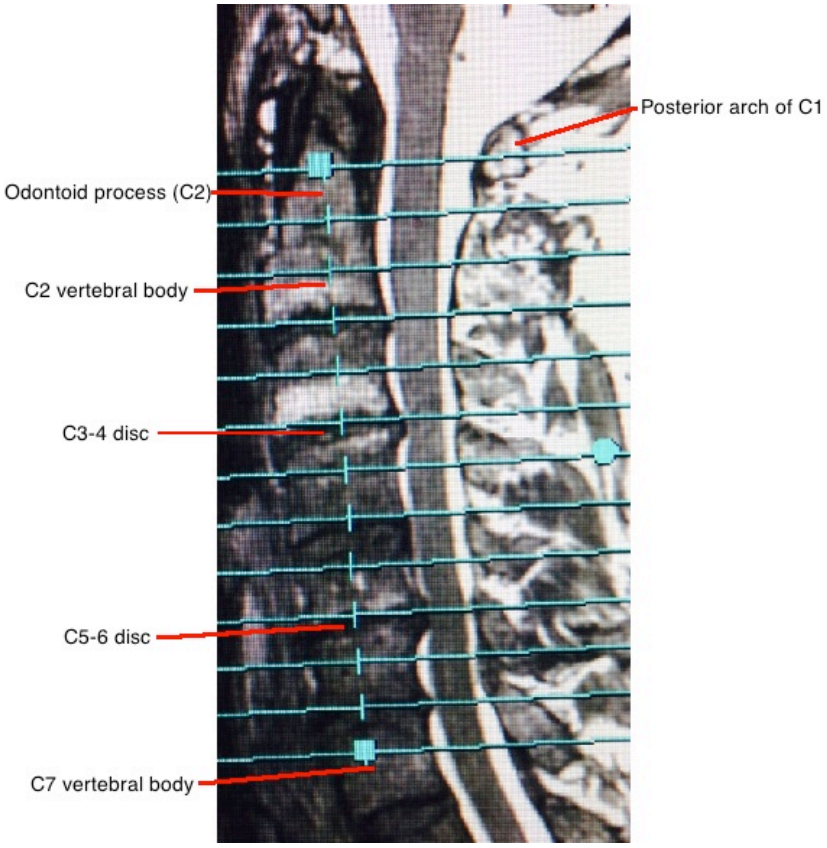

Figure 2.1: Slice Prescription. 13 axial slices positioned from C1 to C7 perpendicular to SC, using a variable gap to align alternating slices with mid-vertebral body and mid-intervertebral

disc. Note that this subject has substantial Modic type II endplate changes reflective of degenerative disc disease and conversion to fatty yellow marrow.

Imaging Type	Pulse Sequence; Orientation	Technical Details	Acquisition Time	Metric
~~T2WI~~Anatomical (T2/T1-weighted)	3D FIESTA-C; sagittal	TR/TE=5.4/2.6 ms, FOV=200x200 mm^2, matrix=256x256, resolution=0.8x0.8x0.8 mm^3, NEX=2, flip angle=35°	6m56s	CSA
DTI	Spin echo ssEPI with OVS; axial	TR/TE=4050/91.2 ms, FOV=80x80 mm^2, matrix=64x64, resolution= 1.25x1.25x5mm^3, 25 directions (b=800 s/mm^2), 5 b=0 s/mm^2 images, anterior/posterior saturation bands, phase encoding=AP, 2nd order shimming	3 x 2m6s, 1m30s for shimming	FA
MT	2D SPGR with/without pre-pulse; axial	TR/TE=32/5.9 ms, FOV=190x190 mm^2, matrix=192x192, resolution=1x1x5mm^3, NEX=3, flip angle=6°, flow compensation, phase encoding=AP, pre-pulse: Gaussian, duration=9984 µs, offset=1200 Hz	3m45s each, with and without pre-pulse	MTR
T2*WI	2D MERGE; axial	TR/TE=650/5,10,15 ms, FOV=200x200 mm^2, matrix=320x320, resolution=0.6x0.6x4mm^3, NEX=1, flip angle=20°, BW=62kHz per line	3m33s	WM/GM ratio

Formatted Table

Table 2.1: Acquisition Protocol. Technical specifications of our multiparametric cervical SC MRI protocol, with acquisition time of 25 minutes (30-35 minutes including positioning, slice prescription, shimming, and pre-scans). BW: bandwidth, CSA: cross-sectional area, FA: fractional anisotropy, FIESTA-C: fast imaging employing steady-state acquisition – cycled phases, MERGE: multi-echo recombined gradient echo, MT: magnetization transfer, MTR: MT ratio, OVS: outer volume suppression, SC: spinal cord, T2*WI: T2*-weighted imaging.

Test-retest reliability was assessed by removing the subject from the scanner and repositioning before re-scan. This was performed in a subset of subjects (DTI: 17 healthy, 9 DCM; MT: 13 healthy, 4 DCM; T2*WI: 5 healthy, 11 DCM) extemporaneously depending on scanner availability and subject willingness. Reliability was not assessed for SC CSA measurement due to time constraints.

A comparison of DTI with and without cardiac triggering was also performed in 10 subjects (4 healthy, 6 DCM). Cardiac triggered DTI was performed with pulse oximetry triggering, trigger delay of 310ms, window of 250ms, and TR=7 RR. Two acquisitions were performed that were analyzed individually for TRCOV and then concatenated and averaged for comparison with non-triggered DTI.

2.2.3 **Image Analysis Techniques**

Imaging data were analyzed using Spinal Cord Toolbox (SCT) v2.3 (Cohen-Adad J, 2014). Each axial image was visually inspected by 1 rater (ARM) and excluded if low signal or artefacts (motion, aliasing) were present. SC segmentation was automatically performed using native anatomical ~~T2WI~~ and T2*WI images, the mean diffusivity map for DTI, and the MT image with prepulse. Segmentation errors were resolved by providing seed points for automatic segmentation or manual editing. Images were non-linearly registered to the MNI-Poly-AMU template/atlas (Fonov et al., 2014). Anatomical ~~T2WI~~ images were used to automatically calculate cervical cord length (from the top of C1 to the bottom of C7 vertebral levels) and SC CSA. DTI images were motion corrected with regularized registration and diffusion tensors were calculated with outlier rejection using the RESTORE method (Chang et al., 2005). MT images with and without pre-pulse were co-registered and MTR was computed. T2*WI data were further analyzed with automatic segmentation of GM and WM (Asman et al., 2014), which was used to refine the registration of T2*WI images to the template. FA, MTR, and T2*WI WM/GM ratio were extracted from various ROIs using the SCT probabilistic atlas with automatic correction for partial volume effects using the *maximum a posteriori* method (Levy et al., 2015). ROIs included the SC, WM, GM, and left/right lateral corticospinal tract (LCST), fasciculus cuneatus (FC), fasciculus gracilis (FG), and spinal lemniscus (SL) in each axial slice (Figure 2.2). Metrics were averaged at rostral (C1-C3), middle (C4-5) or maximally compressed level (MCL, DCM subjects), and caudal (C6-C7) levels.

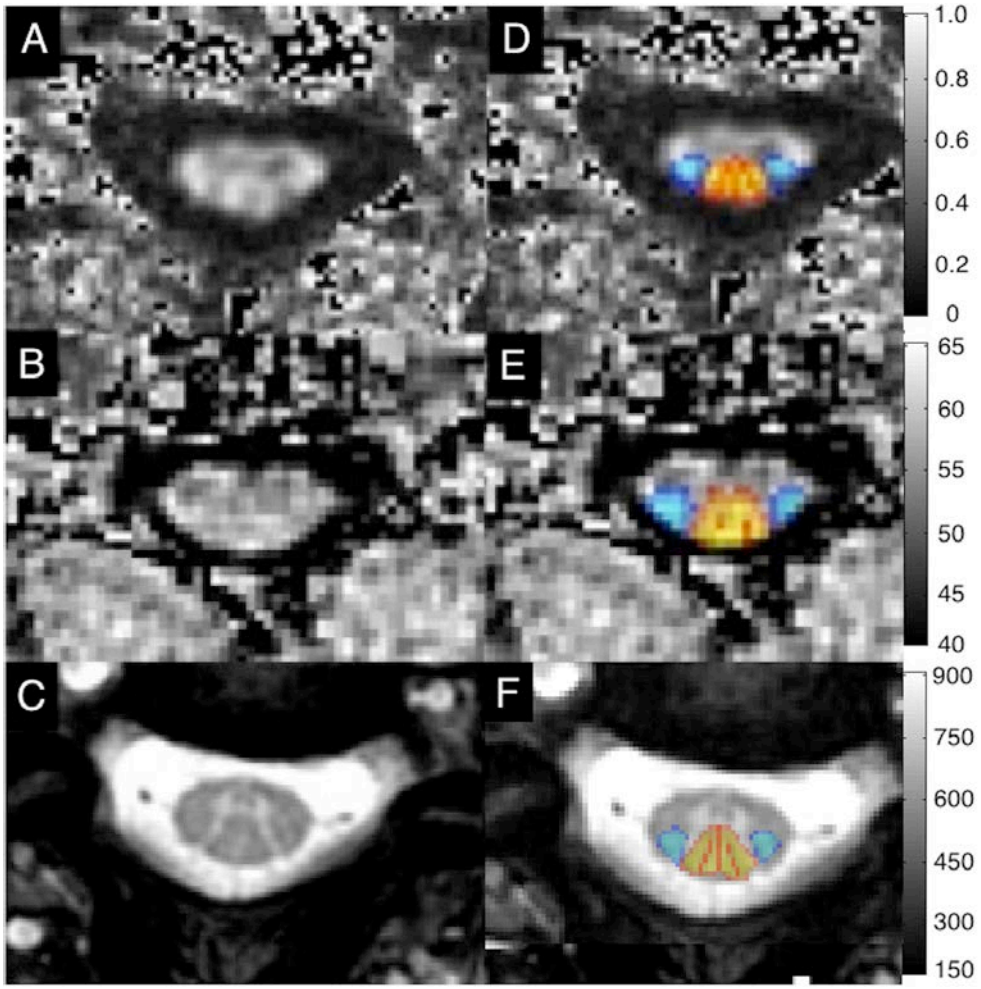

Figure 2.2: Representative Images. Images showing FA maps (A), MTR maps (B), and T2*WI (C) with probabilistic maps of LCSTs (blue) and dorsal columns (red-yellow) overlaid (D-F) following registration to the SCT atlas. FA: fractional anisotropy, LCST: lateral corticospinal tract, MTR: magnetization transfer ratio, SCT: spinal cord toolbox.

2.2.4 **Statistical Analysis**

Statistical analysis was performed with R v3.3. Normative data were summarized with mean, standard deviation (SD), and inter-subject coefficient of variation (COV). Relationships between MRI metrics (averaged from C1-C7) and patient characteristics (age, sex, height, weight,

cervical cord length) were assessed with Pearson correlation coefficients and backward stepwise linear regression to determine significant independent relationships and their coefficients. Differences by rostrocaudal level were assessed with ANOVA. If differences were found, we calculated Spearman coefficients (between mean values and numbered levels) to identify monotonic relationships. To determine if non-linear relationships were present, we performed a likelihood ratio test on linear regression models with and without a 5-knot restricted cubic spline. Paired T tests compared WM and GM differences, and ANOVA was used to identify differences between individual WM tracts (averaged bilaterally). Reliability was assessed using test-retest COV (TRCOV), and differences between healthy and DCM subjects were assessed with Welch's T tests, as were pairwise comparisons between techniques at each rostrocaudal level. Statistical significance was set to p=0.05 and was not corrected for multiple comparisons due to the exploratory nature of this study.

2.3 Results

2.3.1 Subject characteristics

Characteristics of 40 healthy subjects and 18 DCM subjects included in this study are listed in Table 2.2.

Characteristic	Healthy Subjects (N=40)	DCM Subjects (N=18)
Age	47.1 ± 15.3 years (range 19-79)	56.4 ± 11.0 years (range 36-76)
Sex	21 male, 19 female	11 male, 7 female
Height	171.4 ± 8.6 cm	172.8 ± 8.9 cm
Weight	74.6 ± 11.5 kg	79.0 ± 15.1 kg
Cervical cord length	10.6 ± 1.0 cm	11.1 ± 0.9 cm

Table 2.2: Subject Characteristics. Demographics and characteristics of 40 healthy and 18 DCM subjects are displayed. DCM: degenerative cervical myelopathy.

2.3.2 **Image Acquisition**

Acceptable image quality was achieved in all subjects and techniques. For DTI, 27 out of 520 axial images (5.2%) were excluded, due to artefacts or poor signal. For MT and T2*WI, 6 (1.2%) and 4 (0.8%) slices were excluded due to artefacts, respectively.

2.3.3 **Automated Analysis**

Automated segmentation was frequently successful, with manual editing required in 8 ~~T2WI~~anatomical datasets (20%), 14 MT datasets (35%), 4 DTI datasets (10%), and 20 T2*WI datasets (50%). Manual segmentation editing was usually restricted to a small number of slices and required <5 minutes per dataset. Automatic registration to the template and data extraction were successful in all cases.

2.3.4 **Normative Values for MRI Metrics**

Normative data extracted from C1-C3 showed T2*WI WM/GM had the smallest inter-subject COV at 3.5% (0.848 ± 0.028), compared with 5.8% for MTR (52.8 ± 3.1%), 6.0% for FA (0.706 ± 0.042), and 12.2% for CSA (78.5 ± 9.6 mm^2) (Figure 2.3). The strongest contrast between WM and GM was found for T2*WI signal intensity (mean GM-WM difference ± standard error: 83.9±4.72, $p=3x10^{-20}$), which exceeded that of FA (-0.110±0.0083, $p=2x10^{-15}$), and MTR (-2.1±0.28, $p=4x10^{-9}$). Individual WM tracts showed significant variations for T2*WI WM/GM (ANOVA $p=2x10^{-9}$), FA ($p=3x10^{-7}$), and MTR (p= 0.01).

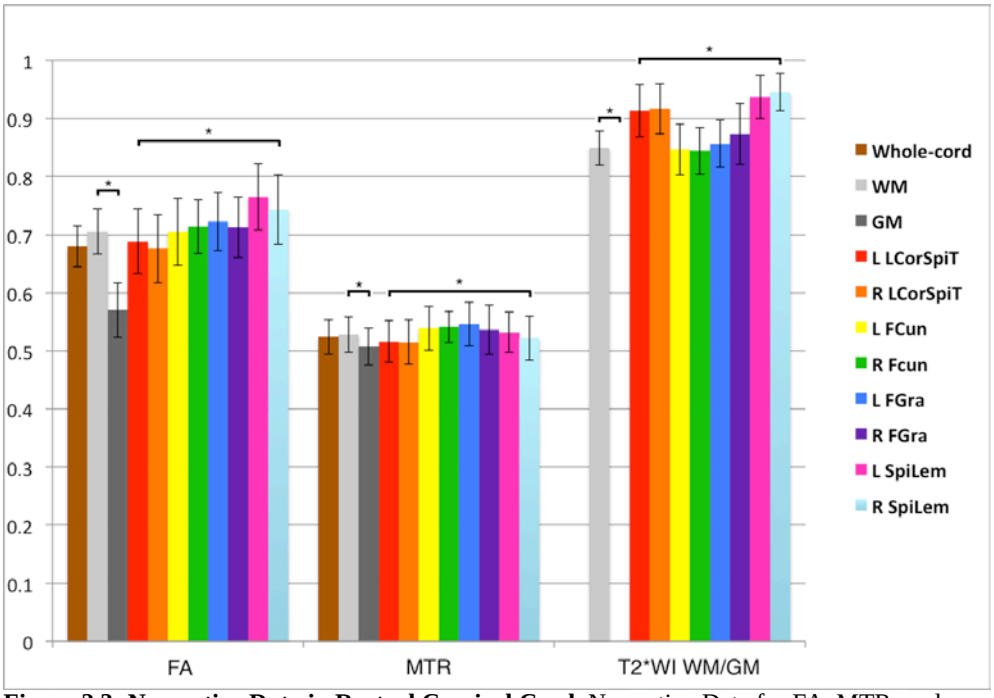

Figure 2.3: Normative Data in Rostral Cervical Cord. Normative Data for FA, MTR, and T2*WI WM/GM ratio. Metrics are extracted from SC, WM, GM, and key WM tracts averaged over rostral slices (C1-C3). Values are displayed as mean ± inter-subject SD (error bars). * denotes $p < 0.05$ using paired t-tests between WM and GM and ANOVA between WM tracts. FA: fractional anisotropy, FC: fasciculus cuneatus, FG: fasciculus gracilis, LCST: lateral corticospinal tract, MTR: magnetization transfer ratio, SC: spinal cord, SD: standard deviation, SL: spinal lemniscus, T2*WI: T2*-weighted imaging.

2.3.5 Variations with Subject Characteristics

Univariate relationships between MRI metrics and subject characteristics included the following: CSA increased with cervical cord length ($p=8x10^{-4}$), weight ($p=0.03$), and male sex ($p=0.03$), FA decreased with age ($p=0.009$), and MTR decreased with height ($p=0.008$), weight ($p=0.01$), and male sex ($p=0.006$) (Table 2.3). Trends were also present for CSA increasing with height ($p=0.06$) and T2*WI WM/GM increasing with age ($p=0.06$) and weight ($p=0.06$). In multivariate analysis, CSA varied only with cervical cord length ($\beta=+5.3690$), FA with age ($\beta=-0.0012053$),

and MTR with height (β=-0.17410, p=0.001) and age (β=-0.074131, p=0.01), while T2*WI WM/GM did not require normalization. Following linear corrections, inter-subject COV decreased to 4.8% for MTR, 5.4% for FA, and 10.2% for CSA.

Metric	Age	Sex (M vs. F)	Height	Weight	Cervical Cord Length
CSA ~~())~~ (mm^2)	r = -0.25 (p=0.12)	80.0 ± 11.2 vs. 73.5 ± 8.5 (p = 0.03**)	r = 0.31 (p = 0.06*)	r = 0.34 (p = 0.03**)	r = 0.51 (p = $8x10^{-4}$**)
FA	r = -0.43 (p=0.009**)	0.658 ± 0.037 vs. 0.663 ± 0.034 (p = 0.75)	r = -0.02 (p = 0.89)	r = -0.26 (p = 0.12)	r = 0.11 (p = 0.53)
MTR	r = -0.25 (p = 0.11)	48.8 ± 2.5 vs. 51.4 ± 2.7 (p = 0.006**)	r = -0.41 (p = 0.008**)	r = -0.40 (p = 0.01)	r = -0.18 (p = 0.26)
T2*WI WM/GM	r = 0.31 (p = 0.06)	0.863 ± 0.034 vs. 0.858 ± 0.031 (p = 0.64)	r = -0.12 (p = 0.48)	r = 0.31 (p = 0.06*)	r = -0.09 (p = 0.55)

Table 2.3: Univariate Relationships of MRI metrics with Healthy Subject Characteristics. Mean ± SD (for each sex) and Pearson coefficients are displayed (p values in parentheses). FA, MTR, and T2*WI WM/GM ratio are extracted from WM, while CSA of the spinal cord is measured, averaged across C1-C7. * denotes trends (p<0.10) and ** denotes significance (p<0.05). CSA: cross-sectional area, FA: fractional anisotropy, MTR: magnetization transfer ratio, SD: standard deviation, T2*WI: T2*-weighted imaging.

2.3.6 **Metrics by Rostrocaudal Level**

ANOVA detected significant differences (p<0.05) across rostrocaudal levels for all metrics. Monotonic variations were present (p<0.05) for MTR (ρ=-0.98), FA (ρ=-0.90), and CSA (ρ=-0.55), which all decreased from rostral to caudal levels, whereas T2*-WM/GM showed a trend toward increasing (ρ=0.53, p=0.06),(Figure 2.4). CSA, FA, and T2*WI WM/GM showed non-linear rostro-caudal variation (p<0.05), whereas MTR did not (p=0.58).

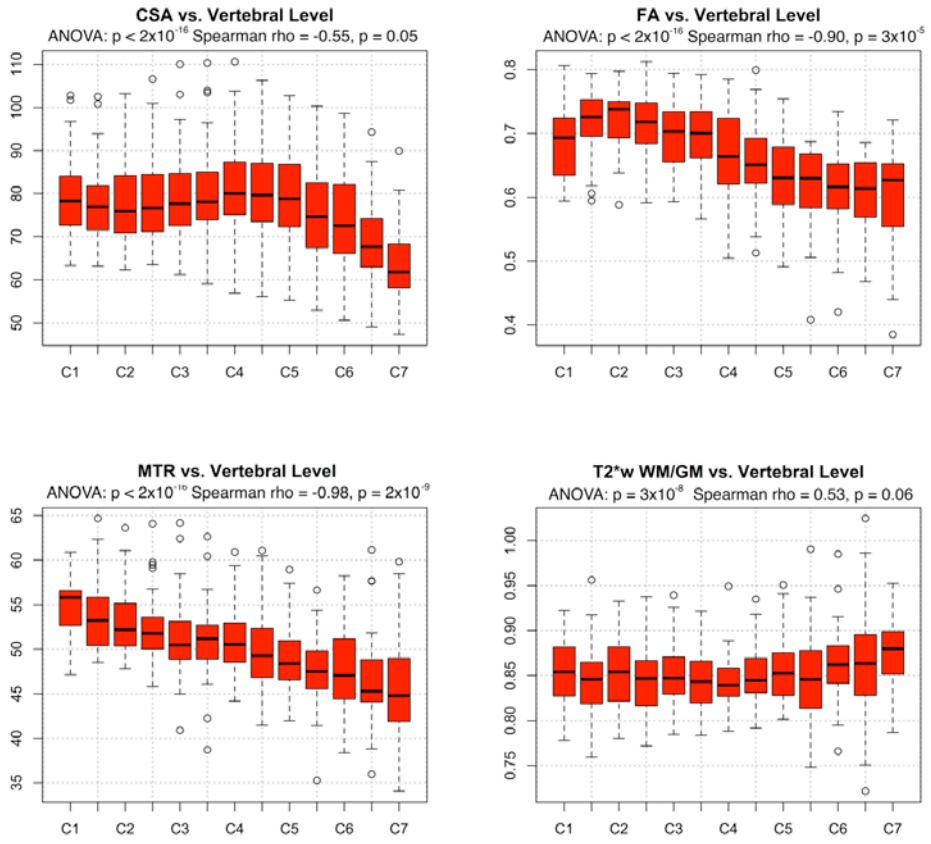

Figure 2.4: Variations by Rostrocaudal Level. MRI metrics displayed for each vertebral and intervertebral level from C1 to C7. FA, MTR, and T2*WI WM/GM ratio are extracted from WM. ANOVA shows significant differences by level for all metrics. Monotonic variations are present for CSA, FA, and MTR. CSA: cross-sectional area, FA: fractional anisotropy, MTR: magnetization transfer ratio, T2*WI: T2*-weighted imaging.

2.3.7 **Reliability**

T2*WI WM/GM ratio was the most reliable metric (pooled TRCOV: rostral: 0.9%, MCL: 2.9%, caudal: 2.6%), comparing favourably with FA (rostral: 2.6%, MCL: 3.6%, caudal: 3.2%) and MTR (rostral: 2.4%, MCL: 3.7%, caudal: 4.2%), although these differences were only significant for rostral metrics ($p<0.05$) (Table 2.4). Reliability measures were comparable between healthy and DCM subjects rostrally (C1-C3), but DCM subjects trended toward increased TRCOV for MCL MTR (6.1% vs. 3.2%, $p=0.08$) and caudal FA (4.6% vs. 2.2%, $p=0.06$). Reliability of data from individual WM tracts was acceptable (TRCOV <5%) except for FA of the right and left SL (5.3%, 5.6%, respectively; Figure 2.5).

Level	Metric	Healthy	DCM	P Value	Pooled
Rostral (C1-C3)	FA	2.5 ± 2.0%	2.8 ± 1.8%	0.71	2.6 ± 1.9%
	MTR	2.7 ± 1.9%	1.3 ± 0.5%	0.17	2.4 ± 1.9%
	T2*WI WM/GM	0.9 ± 0.6%	1.0 ± 0.7%	0.77	0.9 ± 0.7%§§
Mid-Cervical (C4-C5) or MCL	FA	3.0 ± 2.2%	5.0 ± 5.7%	0.21	3.6 ± 3.6%
	MTR	3.2 ± 3.0%	6.1 ± 0.9%	0.08*	3.7 ± 3.2%
	T2*WI WM/GM	1.4 ± 1.1%	3.5 ± 2.2%	0.11	2.9 ± 2.2%
Caudal (C6-C7)	FA	2.2 ± 1.6%	4.6 ± 4.7%	0.07*	3.2 ± 3.5%
	MTR	4.4 ± 3.8%	3.1 ± 3.9%	0.56	4.2 ± 3.7%
	T2*WI WM/GM	3.4 ± 3.0%	2.2 ± 2.1%	0.37	2.6 ± 2.4%

Table 2.4: Test-Retest Reliability Across Rostrocaudal Levels. TRCOV ± SD is displayed for healthy and DCM subjects at rostral (C1-C3), mid-cervical (C4-5) or maximally compressed level (MCL) in DCM subjects, and caudal (C6-C7) levels. Sample size was 26 subjects (17 healthy, 9 DCM) for DTI, 17 subjects (13 healthy, 4 DCM) for MT, and 16 subjects (5 healthy, 11 DCM) for T2*WI imaging. * denotes trends ($p<0.10$) and ** denotes significant differences ($p<0.05$) in reliability between healthy and DCM subjects for each level/metric, and pooled reliability was calculated if no significant differences were found. § denotes trends ($p<0.10$) and §§ denotes significant differences ($p<0.05$) between pooled TRCOV of metrics at each level. DCM: degenerative cervical myelopathy, FA: fractional anisotropy, MCL: maximally compressed level, MTR: magnetization transfer ratio, SD: standard deviation, TRCOV: test-retest coefficient of variation, T2*WI: T2*-weighted imaging.

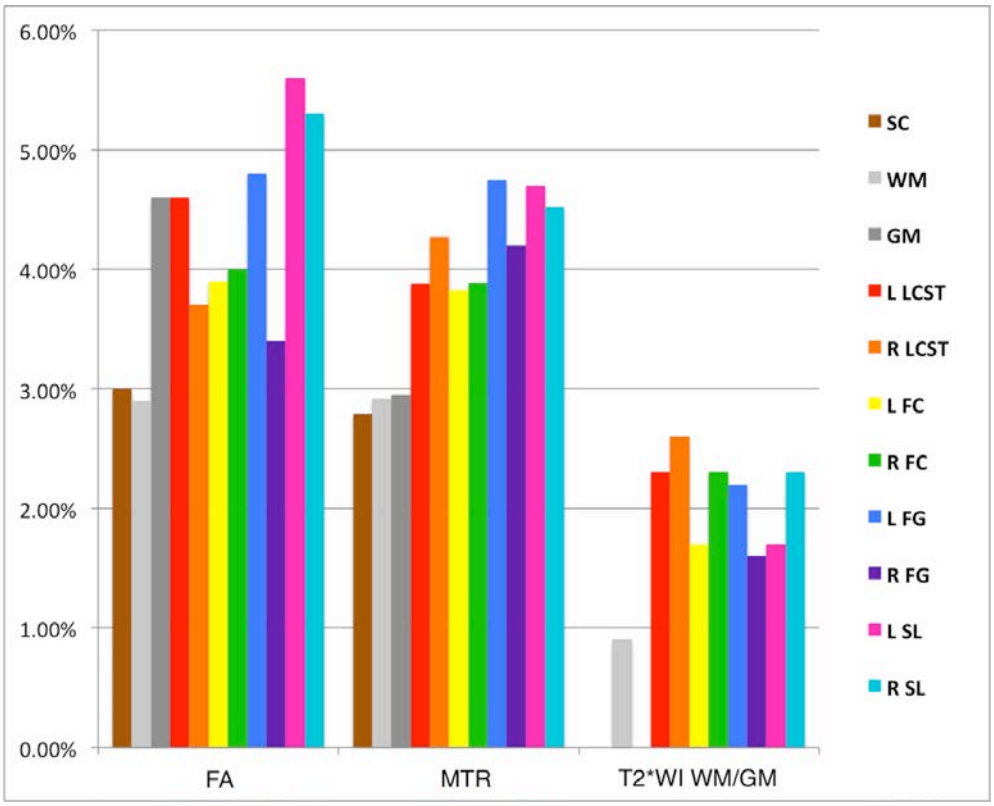

Figure 2.5: Reliability of FA, MTR, and T2*WI WM/GM. Reliability of FA, MTR, and T2*WI WM/GM extracted from SC, WM, GM, and key WM tracts in rostral slices (C1-C3) is displayed are TRCOV. T2*WI WM/GM ratio shows better reliability than FA and MTR. Metrics derived from SC and WM show TRCOV < 3%, while GM and key WM tracts show TRCOV < 5% except for FA of the Spinal Lemniscus. CSA: cross-sectional area, FA: fractional anisotropy, FC: fasciculus cuneatus, FG: fasciculus gracilis, LCST: lateral corticospinal tract, MTR: magnetization transfer ratio, SC: spinal cord, SD: standard deviation, SL: spinal lemniscus, TRCOV: test-retest coefficient of variation, T2*WI: T2*-weighted imaging.

2.3.8 **Cardiac Triggering in DTI**

FA did not differ significantly between DTI acquisitions with and without cardiac triggering, although triggering showed a trend toward higher FA at MCL (0.558 vs. 0.514, p=0.06) and caudal (0.562 vs. 0.534, p=0.07) levels (Table 2.5). No significant differences in TRCOV were observed, although cardiac triggered DTI provided approximately 1% lower TRCOV at all levels.

Measure	Level	No Triggering	Triggering	P Value
FA	Rostral	0.651 ± 0.054	0.664 ± 0.064	0.41
	Mid/MCL	0.514 ± 0.068	0.558 ± 0.081	0.06*
	Caudal	0.534 ± 0.057	0.562 ± 0.044	0.07*
TRCOV	Rostral	2.6 ± 1.9%	1.5 ± 1.2%	0.11
	Mid/MCL	3.6 ± 3.6%	2.2 ± 2.3%	0.27
	Caudal	3.2 ± 3.5%	2.4 ± 2.3%	0.52

Table 2.5: DTI With and Without Cardiac Triggering. Paired T tests were used to compare FA values extracted from WM at rostral (C1-C3), mid-cervical (C4-5, healthy subjects) or MCL (DCM subjects), and caudal (C6-C7) levels between no triggering vs. triggering in 10 subjects (4 healthy, 6 DCM). Welch's T tests were used to compare test-retest coefficient of variation (TRCOV) between no triggering (N=26) and triggering (N=10). * denotes trends ($p < 0.10$) and ** denotes significance ($p < 0.05$). DCM: degenerative cervical myelopathy, FA: fractional anisotropy, MCL: maximally compressed level, TRCOV: test-retest coefficient of variation.

2.4 **Discussion**

2.4.1 **Summary of Findings**

This study establishes a multiparametric MRI protocol and analysis framework to assess microstructure of the entire cervical SC using simple methods that are feasible for clinical

adoption, requiring only 20 minutes of acquisition time in addition to anatomical imaging. Image acquisition was successful in all subjects and automated analysis provided robust readouts from multiple ROIs, with the results validated by acceptable reliability data. Our results establish normative data for CSA, FA, and MTR that are consistent with previous reports at 3T (Samson et al., 2013, Cohen-Adad et al., 2011, Smith et al., 2010, Ellingson et al., 2014, Kearney et al., 2014a), in addition to our novel T2*WI WM/GM metric. T2*WI WM/GM, FA, and MTR all showed strong grey-white contrast and differences between individual WM tracts. FA and MTR showed moderate inter-subject and test-retest variability, with similar or better reliability than previous reports in spite of differences in acquisition and analysis techniques (Kerkovsky et al., 2012, Samson et al., 2016, Smith et al., 2010, Ellingson et al., 2014, Samson et al., 2013, Taso et al., 2016). T2*WI WM/GM demonstrates low inter-subject and test-retest variability, which are favourable statistical properties as they make it more likely that a pathological subject will show abnormal results (confirmed by encouraging results reported in companion paper (Martin AR, 2017b)). CSA showed greater inter-subject variation than other metrics, although this improved slightly following normalization with cervical cord length. Reliability of CSA measurement was not assessed due to time constraints, but it likely surpasses that of our other measures, as it has been previously reported to have TRCOV under 0.5% using similar techniques (Kearney et al., 2014a). Reliability was greatest in the rostral region for all techniques, where healthy and DCM patients showed similar results. In contrast, DCM patients showed trends toward diminished reliability at MCL and caudal levels, likely related to distorted anatomy, increased partial volume effects, increased susceptibility artefact, and less accurate registration to the SCT template. However, these differences were not significant, and pooled reliability results were all considered acceptable (TRCOV < 5%). Our clinically feasible multiparametric approach provides 4 unique quantitative measures in multiple ROIs that reflect aspects of macrostructure and microstructure, with the benefit that these measures cross-validate each other to overcome limitations (reliability, inter-subject variability, sensitivity to pathology) of each individual technique. We anticipate that this multivariate approach can accurately characterize tissue injury in various SC pathologies, which could enable qMRI of the SC to achieve clinical translation in the near future.

2.4.2 **Normalization for Confounding Factors**

To move toward clinical utilization of SC qMRI, it is essential that quantitative readouts reflect pathological changes and eliminate confounding effects as much as possible. In keeping with prior reports, significant relationships were found between age and FA (Mamata et al., 2005, von Meyenburg et al., 2013, Taso et al., 2016) and MTR (Taso et al., 2016), but not CSA (Taso et al., 2016, Fonov et al., 2014). However, we also identified univariate relationships between MRI metrics and sex, height, weight, and cervical cord length, for which we are not aware of previous reports. The relationship between CSA and cervical cord length likely indicates that CSA is related to overall body size, since height and weight also showed positive (non-significant) correlations. It is unclear why MTR decreases with height, but weak negative trends were also seen with weight and cervical cord length, suggesting MTR (reflecting myelin density) is negatively related to overall body size. However, no relationship was present between MTR and CSA in a post hoc test ($r=0.01$, $p=0.94$). Strong relationships were also found between all 4 metrics and rostrocaudal level, with CSA, FA, and MTR showing non-linearity (Figure 2.4). CSA increased between C3 and C6 vertebral levels, reflecting the cervical enlargement that contains increased GM for C5 to T1 neurological levels, and our CSA measurements were highly similar to previous reports (Cadotte et al., 2015, Kato et al., 2012). WM FA peaked at C2 and locally at C7, where the orientations of axons are almost purely rostrocaudal. In contrast, decreases were seen at C1 (likely due to decussation of corticospinal fibers) and in the cervical enlargement (where a fraction of axons turn and form synapses within GM). T2*WI WM/GM ratio was nearly invariant from C1 to C6 but increased at C7, likely due to increased susceptibility artefact from the lungs, decreased SNR, and respiratory motion. We suggest a normalization scheme where CSA, FA, and MTR are linearly corrected for relationships (cervical cord length, age, and age/height, respectively), and all metrics are converted to Z scores per rostrocaudal level, as proposed by Uda et al. for DTI metrics (Uda et al., 2013a). Although normalization procedures add complexity to data post-processing, these methods facilitate fair comparisons, decrease nuisance variability, and produce more accurate biomarkers of SC tissue injury.

2.4.3 **Quantitative MRI Techniques: Specificity, Accuracy, Feasibility**

The rapidly evolving field of qMRI includes a rich array of acquisition techniques, including strict quantitative methods that attempt to measure a specific physical property, such as

quantitative MT (qMT), longitudinal relaxation rate (R1) and apparent transverse relaxation rate (R2*) mapping (Levesque et al., 2010, Freund et al., 2013, Samson et al., 2013). However, such techniques are inherently complex and require specialized pulse sequences, while typically requiring lengthy scan times. Furthermore, these methods face challenges in achieving acceptable SNR and reliability, particularly in the SC, which is considerably more difficult to image than the brain due to magnetic field inhomogeneity and physiological motion. Similarly, reduced FOV (rFOV) DTI has become available offering increased SNR and reduced distortions, but often requiring increased acquisition time and involving proprietary pulse sequences (Samson et al., 2016). Our protocol purposefully employed standard sequences that are available on all major MRI vendors, making it an attractive approach for multi-centre studies and clinical use. A recent study comparing rFOV to OVS for cervical SC DTI found only minimal differences in reliability (inter-subject COV: rFOV=3.98% vs. OVS=4.59) (Samson et al., 2016). Unfortunately this study did not report p values for these comparisons, nor did it assess intra-subject reliability, but the findings suggest that OVS provides acceptable reliability.

2.4.4 **Cardiac Triggered DTI**

Previous research suggests that cardiac triggering reduces variance in diffusion time series by acquiring data during the quiescent phase of cardiac-related SC motion (Summers et al., 2006). However, to our knowledge no studies have directly compared the test-retest reliability of SC DTI acquisitions with and without cardiac triggering, particularly in the context of multiple acquisitions and outlier rejection during post-processing. Our pilot data in 10 subjects suggest roughly equivalent results with and without triggering, although trends toward higher FA and lower TRCOV (approximately 1%) were observed with triggering. Further investigation is needed, but the ungated acquisition used in this study is validated by its acceptable reliability, and this simpler approach avoids difficulties with triggering such as variable TR and cardiac irregularities (arrhythmias, tachycardia) that are more common in older or critically ill patients.

2.4.5 **Limitations**

Further studies with larger sample sizes would allow greater accuracy for normative data, influences of confounding variables, and differences in DTI with and without cardiac triggering. The normative data are specific to our methodology, and cross-site and cross-vendor validation is required. Our use of automated analysis aimed to reduce bias, but manual editing of

segmentations was frequently required. Other DTI metrics were not analyzed due to an *a priori* decision to focus on FA, due to its consistent results in previous studies (Martin et al., 2016). Our test-retest reliability experiment does not account for scanner drift, but this is unlikely a large source of error as the 3 metrics are ratios rather than absolute signal intensity values. Neurologically intact subjects with mild SC compression were considered healthy subjects; these changes are evident in 8-26% of asymptomatic individuals (Wilson et al., 2013, Kato et al., 2012), and we feel the spectrum of "normal" includes this subgroup, but previous studies have excluded such subjects.

2.4.6 **Conclusions**

Reliable multiparametric assessment of SC microstructure is possible with standard hardware, acceptable acquisition time, and automated analysis that provides high-fidelity readouts of tissue injury from numerous ROIs. Normalization procedures can be implemented to mitigate confounding effects such as age, height, cervical cord length, and rostrocaudal level, producing more meaningful quantitative metrics. Our clinically-suited approach paves the way for translational studies to evaluate potential uses such as improved diagnostics, monitoring of disease progression, and prediction of outcomes.

Chapter 3
A Novel MRI Biomarker of Spinal Cord White Matter Injury: T2*-weighted White Matter to Grey Matter Signal Intensity Ratio*

*This chapter is based upon the following published article: (Martin et al., 2017c), and is reproduced with permission.

T2*-weighted imaging (T2*WI) provides sharp contrast between spinal cord GM and WM, allowing their segmentation and cross-sectional area (CSA) measurement. Injured WM demonstrates T2*WI hyperintensity, but requires normalization for quantitative use. We introduce T2*WI WM/GM signal intensity ratio and compare it against CSA, the DTI metric fractional anisotropy (FA), and magnetization transfer ratio (MTR) in degenerative cervical myelopathy (DCM). 58 DCM patients and 40 healthy subjects underwent 3T MRI, covering C1-C7. Metrics were automatically extracted at maximally compressed (MCL) and uncompressed rostral/caudal levels. Normalized metrics were compared with T tests, area under the curve, (AUC), and logistic regression. Relationships with clinical measures were analyzed using Pearson correlation and multiple linear regression. MCL CSA demonstrated superior differences (p=1x10-13), diagnostic accuracy (AUC=0.890), and univariate correlation with mJOA (0.66). T2*WI WM/GM showed strong differences (rostral: $p=8x10^{-7}$, MCL: $p=1x10^{-11}$, caudal: $p=1x10^{-4}$), correlations (mJOA: rostral: -0.52, MCL: -0.59, caudal: -0.36), and diagnostic accuracy (rostral: 0.775, MCL: 0.860, caudal: 0.721), outperforming FA and MTR in most comparisons, and CSA at rostral/caudal levels. Rostral T2*WI WM/GM showed the strongest correlations with focal motor (-0.45) and sensory (-0.49) deficits, and was the strongest independent predictor of mJOA (p=0.01) and diagnosis (p=0.02) in multivariate models (R2=0.59, $p=8x10^{-13}$; AUC=0.954, respectively). T2*WI WM/GM shows promise as a novel biomarker of WM injury. It detects damage in compressed and uncompressed regions and contributes substantially to multivariate models for diagnosis and correlation with impairment. Our multiparametric approach overcomes limitations of individual measures, holding potential to improve diagnostics, monitor progression, and predict outcomes.

3.1 Introduction

Quantitative MRI (qMRI) techniques have the potential to provide in vivo measurement of specific tissue properties, including characterizing aspects of spinal cord (SC) microstructure and tissue injury (Stroman et al., 2014, Wheeler-Kingshott et al., 2014). However, efforts to apply qMRI in clinical studies have thus far achieved only modest success (Martin et al., 2016). The strongest results include cross-sectional area (CSA) as a measure of spinal cord atrophy, the DTI metric fractional anisotropy (FA) to evaluate axonal integrity, and magnetization transfer ratio (MTR) as a measure of demyelination (Martin et al., 2016). Spinal cord CSA has shown moderate to strong correlation with disability in MS (Oh et al., 2014, Kearney et al., 2014a, Kearney et al., 2015a), but is a non-specific measure of tissue injury and shows high inter-subject variability in healthy subjects (Martin AR, 2017a, Kato et al., 2012), somewhat limiting its utility. FA has demonstrated moderate correlation with global and focal disability in dozens of studies involving various pathologies (Martin et al., 2016)(Uda et al., 2013a, Budzik et al., 2011, Ellingson et al., 2014, Grabher et al., 2016, Jones et al., 2013, Wen et al., 2014a), but has yet to achieve clinical uptake due to a lack of standardized/portable acquisition methods and cumbersome analysis techniques. MTR has also shown correlation with impairment in MS and spinal cord injury (SCI) studies(Cohen-Adad et al., 2011, Oh et al., 2013a, Oh et al., 2013b), but results have been inconsistent, in part due to T1 and frequency offset dependencies, and thus insufficient to drive clinical adoption (Martin et al., 2016).

At 3T or higher field strength, T2*-weighted imaging (T2*WI) of the SC provides high resolution and strong contrast between GM and WM, allowing segmentation between these structures and calculation of their CSA (Yiannakas et al., 2012). It has also been established that T2*WI shows hyperintensity in injured SC WM in various pathologic conditions (Cohen-Adad et al., 2012, Cohen-Adad et al., 2013b). We hypothesized that T2*WI hyperintensity is a general phenomenon in WM injury leading to decreased grey-white contrast, and can be quantified by normalizing the WM signal intensity within each axial slice by that of the GM, as T2*WI WM/GM signal intensity ratio. Our investigation in 40 healthy subjects established that T2*WI WM/GM has lower inter-subject variability compared with CSA, FA, and MTR and superior reliability to FA and MTR (Martin AR, 2017a), although the latter metrics showed acceptable results, in keeping with prior reports (Taso et al., 2016, Samson et al., 2016, Ellingson et al., 2014, Kerkovsky et al., 2012, Smith et al., 2010, Samson et al., 2013).

These encouraging findings prompted the current study in degenerative cervical myelopathy (DCM), a common condition involving degeneration of the discs, ligaments, and vertebrae resulting in cervical spinal cord compression and functional impairment (Figure 3.1) (Fehlings et al., 2013, Nouri et al., 2016). We aimed to determine how well T2*WI WM/GM (i) differs between patients with DCM and healthy subjects, and (ii) correlates with global disability and focal neurological deficits when extracted from corresponding regions of WM, in comparison with FA, MTR, and CSA of the SC.

Figure 3.1: Anatomical Imaging~~T2WI~~ Showing DCM Subject with Spinal Cord Compression. Sagittal ~~T2WI~~ T2/T1-weighted images in a DCM subject with severe impairment

showing multi-level disc degeneration, spondylosis, and spinal cord compression at C5-6 with focal hyperintensity.

3.2 Materials and Methods

3.2.1 Study Design and Subjects

This study received institutional approval from the University Health Network (Toronto, Ontario, Canada) and all participants provided written informed consent. Fifty-eight DCM patients were consecutively recruited from outpatient spine neurosurgery clinic, and 42 healthy subjects were recruited between October 2014 and December 2016. DCM patients with confounding neurological impairment, such as diabetic neuropathy or symptomatic lumbar radiculopathy, were excluded. All subjects were examined by an experienced physician (MGF, ARM). Two subjects recruited as healthy volunteers were found to have clinical and imaging evidence of mild DCM, and were analyzed as DCM subjects. Two DCM subjects failed to complete the MRI study due to pain/claustrophobia and were excluded from analysis. This left a total of 58 DCM patients and 40 healthy subjects for analysis. DCM severity was categorized based on modified Japanese Orthopedic Association (mJOA) score (normal=18 points) into mild (mJOA 15-17), moderate (mJOA 12-14), and severe (mJOA < 12) (Fehlings et al., 2013). Three DCM patients had undergone previous cervical surgery with metallic implants and had achieved a complete or near-complete recovery (to mJOA >= 17) followed by new cord compression at another cervical level.

3.2.2 Clinical Assessments

DCM subjects were assessed with 1) mJOA to determine overall functional impairment, 2) International Standards for Neurological Classification of Spinal Cord Injury (ISNCSCI) Upper Extremity (UE) Motor Score consisting of power testing (5 point score) in 10 upper extremity muscle groups (maximum score=50) on both sides(Kirshblum et al., 2011), and 3) UE Sensory Score consisting of Semmes Weinstein monofilament testing in C6, C7, and C8 dermatomes (4 points each, maximum score=12). Healthy subjects all had mJOA=18, and were assumed to have full motor (50/50) and sensory (12/12) scores for analyses.

3.2.3 **MRI Acquisitions**

Subjects underwent high resolution isotropic ~~T2WI~~anatomical imaging (FIESTA-C sequence, T2/T1-weighted), DTI using single shot EPI, spoiled gradient echo imaging with and without magnetization transfer (MT) pre-pulse, and T2*WI using multi-echo recombined gradient echo (MERGE) at 3T (GE Signa Excite HDxt), as described in ~~companion paper (Martin AR, 2017a)~~Chapter 2. The MERGE sequence uses 3 echoes that are magnitude reconstructed and combined using a sum of squares algorithm. Total imaging time was approximately 30-35 minutes including subject positioning, slice prescription, and 2nd order localized shimming.

3.2.4 **Image Analysis Techniques**

Template-based analysis was performed using Spinal Cord Toolbox (SCT) v2.3 (Cohen-Adad J, 2014), as described in companion paper (Martin AR, 2017a). Metrics included CSA from anatomical ~~T2WI~~ images, FA, MTR, and T2*WI WM/GM signal intensity ratio, extracted from the rostral uncompressed SC (C1-C3), maximally compressed level (MCL), and caudal uncompressed cord (C6-C7). For MCL metrics, CSA was extracted from a single slice whereas FA, MTR, and T2*WI WM/GM were averaged over 3 slices centered at the compressed level. In subjects with motion artefact on ~~T2WI~~ anatomical (FIESTA-C) images, T2*WI was used to calculate CSA with correction for oblique angle. For FA, MTR, and T2*WI, ROIs included total WM, GM (T2*WI only), and left/right fasciculus cuneatus (FC) and lateral corticospinal tract (LCST) (Figure 3.2). Sagittal and reformatted axial T2/T1-weighted~~WI~~ images were visually assessed for SC hyperintensity by 2 raters (ARM, AN), with disagreements resolved by discussion. These findings were confirmed by comparing with T2-weighted images of each patient that had been obtained for clinical purposes (not under study protocol).

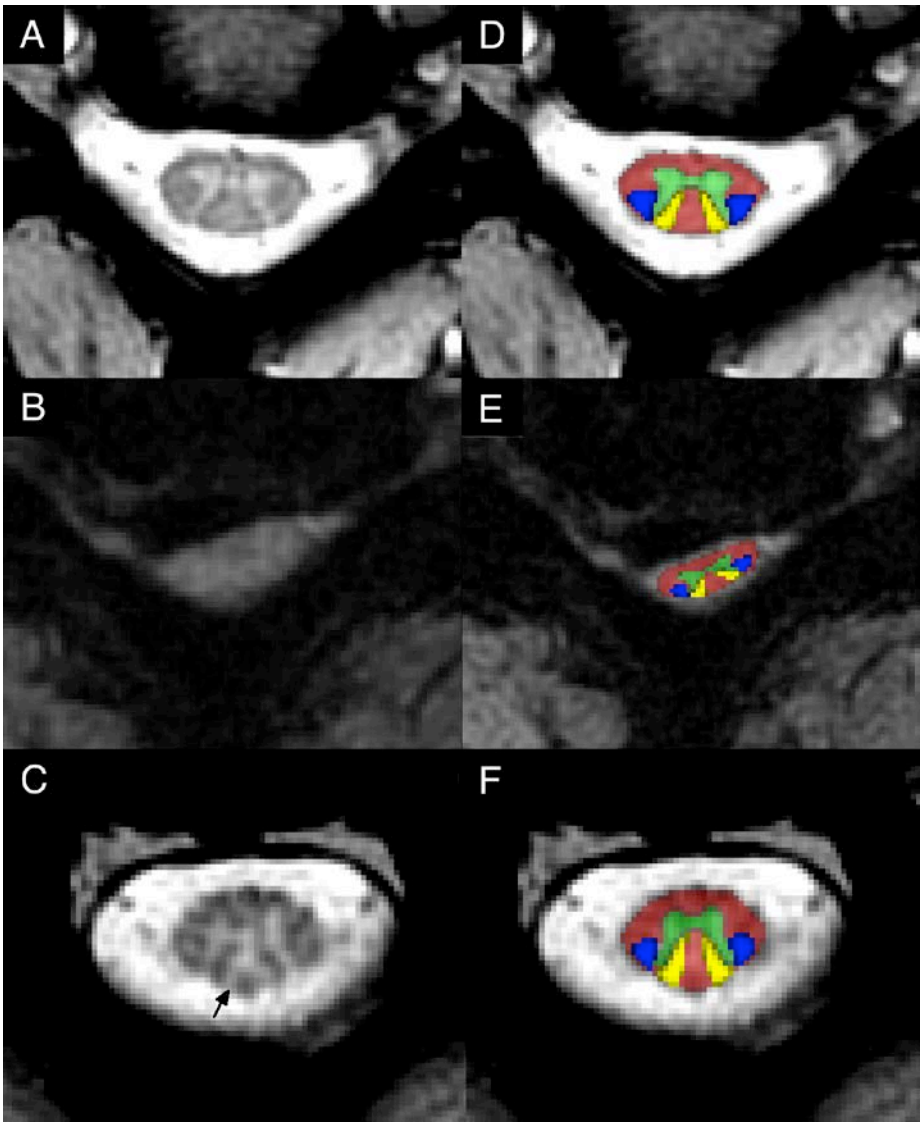

Figure 3.2: T2*WI Demonstrating Loss of Grey-White Contrast and Wallerian Degeneration. A: Axial T2*WI at C3-4 in a healthy subject showing strong contrast between GM and WM (T2*WI WM/GM=0.791 for this image). B: T2*WI at C5-6 in severe DCM subject showing SC compression from a lateral disc herniation, with loss of grey-white contrast (T2*WI WM/GM=0.967). C: T2*WI at C3 in same DCM subject showing focal hyperintensity

(arrow) within the dorsal columns suggesting Wallerian degeneration (T2*WI WM/GM=0.923). D-F: Same images as A-C with SCT probabilistic atlas representations of WM (red), GM (green), LCSTs (blue), and FCs (yellow) overlaid. DCM: degenerative cervical myelopathy, FC: fasciculus cuneatus, LCST: lateral corticospinal tract, T2*WI: T2*-weighted imaging.

3.2.5 **Statistical Analysis**

Statistical analysis was performed with R v3.3. Metrics are reported as mean ± standard deviation (SD). Comparisons between healthy and DCM subjects' characteristics were made using 2-sample T tests and X^2 tests. MRI metrics were normalized to correct for confounding relationships according to the following linear equations, developed from data in 40 healthy subjects (Martin AR, 2017a):

Equation 1: $CSA_{corr} = CSA_{raw} - 5.3690 * (\text{Cervical Cord Length} - 10.6)$

(CSA in mm^2, Cervical Cord Length in cm)

Equation 2: $FA_{corr} = FA_{raw} + 0.0012053 * (\text{Age} - 47.1)$

(Age in years)

Equation 3: $MTR_{corr} = MTR_{raw} + 0.17410 * (\text{Height} - 171.6) + 0.074131 * (\text{Age} - 47.1)$

(MTR as percentage, Height in cm, Age in years)

Metrics were then converted to Z scores to normalize across rostrocaudal levels (e.g. for comparisons at MCL). Comparisons of normalized MRI metrics between DCM and healthy subjects were made using Welch's T tests. These tests were also repeated against an age-matched group (by excluding healthy subjects age<40) to confirm findings. Diagnostic accuracy was assessed with area under the receiver-operating characteristic curve (AUC) and logistic regression with backward stepwise variable selection. Relationships between normalized MRI metrics and clinical measures were assessed using Pearson correlation coefficients and backward stepwise multiple linear regression. CSA of the SC and other metrics extracted from total WM were analyzed against mJOA, while metrics from each LCST and FC were analyzed against ipsilateral UE Motor and Sensory Scores, respectively. Two-way ANOVA with an interaction term was used to assess how T2*WI WM/GM and T2WI hyperintensity relate with mJOA.

Results were considered statistically significant at $p<0.05$, due to the exploratory nature of this study.

3.3 Results

3.3.1 Subject Characteristics

DCM subjects showed the following distribution of severity: 33 mild, 15 moderate, and 10 severe. Age differed significantly between healthy and DCM subjects (47.1 ± 15.3 vs. 57.0 ± 10.9, $p = 3x10^{-4}$; Table 3.1). When healthy subjects under age 40 were excluded, age became equivalent (N=26, age 56.3 ± 9.8, p=0.76). Other demographic variables (sex, height, weight, and neck length) did not vary between groups.

Characteristic	Healthy Subjects (N=40)	DCM Subjects (N=58)
Age	47.1 ± 15.3	57.0 ± 10.9*
Sex (M:F)	21:19	36:22
Height (cm)	171.4 ± 8.6	172.4 ± 10.4
Weight (kg)	74.6 ± 11.5	74.9 ± 9.9
Neck Length (mm)	106.1 ± 9.6	106.8 ± 9.4
mJOA	18.0 ± 0.0	14.2 ± 2.5*
R UE Motor	50.0 ± 0.0§	46.1 ± 5.2*
L UE Motor	50.0 ± 0.0§	46.5 ± 5.6*
R UE Sensation	12.0 ± 0.0§	10.5 ± 2.5*
L UE Sensation	12.0 ± 0.0§	10.6 ± 2.5*

Table 3.1: Subject Characteristics. Demographics and clinical measures are reported as mean ± SD. * denotes significant differences ($p < 0.05$) between DCM and healthy subjects. § denotes that motor and sensory scores for healthy subjects were assumed to be full, based on a screening examination. DCM: degenerative cervical myelopathy, L: left, R: right, SD: standard deviation, UE: upper extremity.

3.3.2 **Image Acquisition and Analysis**

Four T2WI datasets and 1 T2*WI dataset were excluded due to motion artefact. Individual slices were excluded due to artefacts as follows: DTI: 5.3%, MT: 0.8%, and T2*WI: 0.7%. 3 patients with metallic implants had images excluded at those levels and 2 axial slices above and below; remaining images and metrics appeared to be of acceptable quality. Analysis of DCM subjects required manual editing of segmentation masks in most cases due to deformation of the cord and a lack of contrast with surrounding tissues, requiring <5 minutes per dataset. Automatic registration to the SCT template/atlas was successful in all cases.

3.3.3 **MRI Metrics**

Significant differences between DCM and healthy subjects were found in 10/12 MRI metrics (Table 3.2), including decreased CSA (rostral: $p=9x10^{-5}$, MCL: $p=1x10^{-13}$), increased T2*WI WM/GM (rostral: $p=8x10^{-7}$, MCL: $p=1x10^{-11}$, caudal $p=1x10^{-4}$), decreased FA (rostral: $p=2x10^{-4}$, MCL: $p=2x10^{-9}$, caudal $p=2x10^{-4}$), and decreased MTR (rostral: p=0.01, MCL: p=0.001). DCM patients also showed a trend toward decreased caudal CSA (p=0.08). All differences remained significant when compared against age-matched healthy subjects, and caudal CSA became borderline significant (p=0.05). The strongest cross-correlations were found between the same metric at different levels (e.g. rostral and caudal CSA: r=0.77) (Figure 3.3). Cross-correlations were relatively strong between MCL metrics (0.44 to 0.57) but weaker at rostral and caudal levels.

Region	Metric	Healthy Subjects (N=40)	DCM Subjects (N=58)	P Value	Diagnostic Accuracy (AUC)
Rostral	CSA (mm^2)	78.5 ± 8.0	70.9 ± 10.4	$9x10^{-5}$	0.722
	FA	0.725 ± 0.036	0.687 ± 0.063	$2x10^{-4}$	0.692
	MTR	52.7 ± 2.4	51.2 ± 3.4	0.01	0.648
	T2*WI WM/GM	**0.848 ± 0.031**	**0.884 ± 0.034**	**$8x10^{-7}$**	**0.775**
MCL / C4-5	CSA (mm^2)	**76.2 ± 10.4**	**50.8 ± 18.1**	**$1x10^{-13}$**	**0.890**
	FA	0.652 ± 0.048	0.553 ± 0.094	$2x10^{-9}$	0.813
	MTR	49.9 ± 2.9	47.6 ± 3.8	0.001	0.698
	T2*WI WM/GM	0.850 ± 0.022	0.899 ± 0.038	$1x10^{-11}$	0.860
Caudal	CSA (mm^2)	63.7 ± 9.1	60.1 ± 10.9	0.08	0.585
	FA	0.599 ± 0.050	0.552 ± 0.060	$2x10^{-4}$	**0.724**
	MTR	46.2 ± 3.8	46.4 ± 5.1	0.85	0.515
	T2*WI WM/GM	**0.862 ± 0.047**	**0.903 ± 0.053**	**$1x10^{-4}$**	0.721

Table 3.2: Summary of MRI Metrics. Metrics (mean ± SD) are reported at uncompressed rostral levels (C1-C3), maximally compressed level (MCL) or C4-5 (healthy subjects), and uncompressed caudal levels (C6-C7). MCL data displayed are converted from Z scores to values at C4-5 for ease of interpretation. Diagnostic accuracy is reported as AUC. Strongest group differences for each region are highlighted in bold. AUC: area under the curve, CSA: cross-sectional area, FA: fractional anisotropy, MCL: maximally compressed level, MTR: magnetization transfer ratio, T2*WI: T2*-weighted imaging.

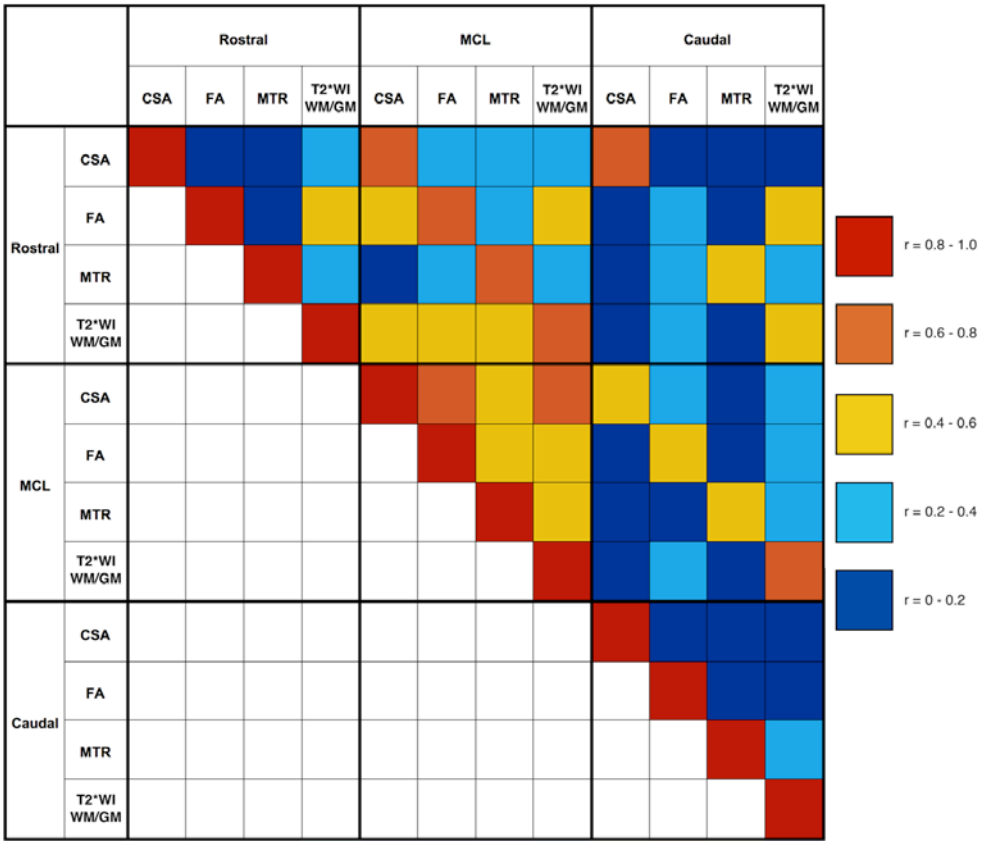

Figure 3.3: Correlation Matrix for MRI Metrics. Pearson correlation coefficients calculated between MRI metrics at rostral (C1-C3), MCL (or C4-5 in healthy subjects), and caudal (C6-7) levels are colour-coded to represent the degree of cross-correlation using data from all 98 subjects. CSA: cross-sectional area, FA: fractional anisotropy, MCL: maximally compressed level, MTR: magnetization transfer ratio, T2*WI: T2*-weighted imaging.

3.3.4 **Diagnostic Accuracy**

MCL CSA showed the highest diagnostic accuracy with AUC=0.890, outperforming other metrics at MCL: T2*WI WM/GM (0.860), FA (0.813) and MTR (0.698) (Table 3.2). At rostral and caudal levels, T2*WI WM/GM showed better discrimination than other metrics with

AUC=0.775 and 0.721, respectively. T2WI hyperintensity (T2WI+) was present in 37/58 (64%) of DCM subjects and 0/40 healthy subjects, with AUC=0.640. Multivariate analysis with logistic regression achieved AUC=0.954, retaining rostral T2*WI WM/GM (p=0.02), MCL FA (p=0.12), MCL CSA (p=0.14), and T2WI signal change (p=0.71).

3.3.5 **Correlation with Global and Focal Impairment**

The strongest univariate correlate with mJOA was MCL CSA (r=0.66) (Table 3.3). This was stronger than MCL T2*WI WM/GM (r=-0.59), FA (r=0.54), and MTR (r=0.43). At rostral and caudal levels, T2*WI WM/GM showed the strongest correlation with mJOA (r=-0.52, -0.36, respectively).. Multiple linear regression for mJOA found a good fit (R^2=0.59, adjusted R^2=0.55, $p=8x10^{-13}$), with rostral T2*WI WM/GM showing the strongest relationship (p=0.01), followed by rostral MTR (p=0.02), T2WI signal change (p=0.02), caudal CSA (p=0.05), caudal FA (p=0.27), MCL CSA (p=0.34), and MCL FA (p=0.44). The strongest correlate with UE motor and sensory scores was rostral T2*WI WM/GM, extracted from ipsilateral LCST (r=-0.45, $p=7x10^{-11}$) and FC (r=-0.49, $p = 4x10^{-13}$), respectively.

Region	MRI Metric	mJOA (N=98)	UE Motor Score (N=196)	UE Sensory Score (N=196)
Rostral	CSA	0.44 ($p=6x10^{-6}$)	-	-
	FA	0.37 ($p=2x10^{-4}$)	0.20 (p=0.006)	0.26 ($p=3x10^{-4}$)
	MTR	0.35 ($p=5x10^{-4}$)	0.22 (p=0.002)	0.11 (p=0.13)
	T2*WI WM/GM	**-0.52 ($p=5x10^{-8}$)**	**-0.45 ($p=7x10^{-11}$)**	**-0.49 ($p=4x10^{-13}$)**
MCL / C4-5	CSA	**0.66 ($p=2x10^{-13}$)**	-	-
	FA	0.54 ($p=2x10^{-8}$)	**0.36 ($p=5x10^{-7}$)**	0.40 ($p=1x10^{-8}$)
	MTR	0.43 ($p=1x10^{-5}$)	0.14 (p=0.04)	0.05 (p=0.48)
	T2*WI WM/GM	-0.59 ($p=7x10^{-10}$)	-0.33 ($p=3x10^{-6}$)	**-0.43 ($p=8x10^{-10}$)**
Caudal	CSA	0.27 (p=0.007)	-	-
	FA	0.35 (p=0.001)	0.09 (p=0.20)	0.05 (p=0.49)
	MTR	0.02 (p=0.83)	0.12 (p=0.11)	0.05 (p=0.51)
	T2*WI WM/GM	**-0.36 ($p=3x10^{-4}$)**	**-0.17 (p=0.01)**	**-0.25 ($p=6x10^{-4}$)**

Table 3.3: Correlation with Clinical Measures. Pearson coefficients are displayed with p values in parentheses. mJOA is analyzed against FA, MTR, and T2*WI WM/GM extracted from total WM and SC CSA. UE Motor Score and UE Sensory Score are analyzed with respect to non-CSA metrics extracted from the ipsilateral,LCST and FC, respectively. Strongest correlations with clinical measures for each region are highlighted in bold. CSA: cross-sectional area, FA: fractional anisotropy, FC: fasciculus cuneatus, LCST: lateral corticospinal tract, MCL: maximally compressed level, mJOA: modified Japanese Orthopedic Association score, MTR: magnetization transfer ratio, SC: spinal cord, T2*WI: T2*-weighted imaging, UE: upper extremity.

3.3.6 **Effects of T2WI Hyperintensity**

T2WI+ DCM subjects had lower mJOA than T2WI- DCM subjects (13.6 vs. 15.2, p=0.005) and higher MCL T2*WI WM/GM (0.905 vs. 0.886, p=0.07). Analyzing all 98 subjects, two-way ANOVA found significant independent relationships with mJOA for T2*WI WM/GM (p=0.01) and T2WI signal change (p=0.001), while the interaction term was non-significant (p=0.55), suggesting that T2WI hyperintensity does not impact the performance of T2*WI WM/GM. The within-group correlation between MCL T2*WI WM/GM and mJOA was slightly higher among T2*WI- subjects (r=-0.43) than among T2WI+ subjects (r=-0.36) (Table 3.4).

Measure	T2WI- (N=61)	T2WI+ (N=37)	P Value
mJOA	17.0 ± 1.6	13.6 ± 2.8	$7x10^{-9}$
MCL T2*WI WM/GM	0.862 ± 0.033	0.905 ± 0.037	$2x10^{-7}$
MCL T2*WI WM/GM ~ mJOA	-0.43 ($p=9x10^{-4}$)	-0.36 (p=0.03)	

Table 3.4: Analysis of T2*WI WM/GM and T2WI Signal Change. The entire cohort (including DCM and healthy) is divided into subjects with and without T2WI hyperintensity, denoted T2WI+ and T2WI-, respectively. Mean ± SD are reported. T2*WI WM/GM is extracted from MCL (DCM subjects) or C4-5 (healthy subjects), and Pearson correlation coefficients between mJOA and T2*WI WM/GM within each signal change group are displayed. DCM: degenerative cervical myelopathy, MCL: maximally compressed level, mJOA: modified Japaense Orthopedic Association score, SD: standard deviation, T2*WI: T2*-weighted imaging.

3.4 Discussion

3.4.1 Summary of Findings

All 4 qMRI metrics analyzed in this study demonstrated significant results in terms of group differences and clinical correlations, which was encouraging given the predominance of mild DCM subjects in our cohort. MCL CSA outperformed other measures in all univariate analyses, which is not surprising as this measure of spinal cord compression reflects the primary mechanism of tissue injury in DCM. Cord compression causes ischemia that often represents partially reversible neurological impairment (Tetreault et al., 2015b), whereas atrophy of the SC (rostral or caudal to compression) suggests axonal loss and/or demyelination, which are more likely to be permanent (Grabher et al., 2016). MCL CSA has previously been demonstrated to correlate well with severity in DCM (Nouri et al., 2015c), and atrophy measurement has also proven useful in DCM (Grabher et al., 2016) and MS (Kearney et al., 2014a, Oh et al., 2014, Kearney et al., 2015a). However, MCL CSA does not account for motion-related dynamic injury, which is also believed to be an important mechanism of tissue injury in DCM (Nouri et al., 2015c), suggesting that this metric may be better used in conjunction with other measures that directly interrogate microstructural changes. FA showed strong group differences and moderate correlations with impairment but diagnostic accuracy was modest, which are all consistent with previous literature (Martin et al., 2016)'(Uda et al., 2013a, Budzik et al., 2011, Ellingson et al., 2014, Grabher et al., 2016, Jones et al., 2013, Wen et al., 2014a). MTR results were relatively weak, which is consistent with prior studies in MS (Oh et al., 2013b, Oh et al., 2013a), but differs from results seen in chronic SCI (Cohen-Adad et al., 2011) We are not aware of published reports employing MTR in DCM patients. T2*WI WM/GM signal ratio showed the strongest results at rostral and caudal levels, and rostral T2*WI WM/GM was the strongest independent variable in multivariate models for diagnosis and correlation with mJOA. T2*WI WM/GM also demonstrated superior performance over FA and MTR in almost every comparison. The encouraging findings for T2*WI WM/GM indicate that this novel biomarker is a relatively accurate measure of WM injury, with particularly strong results in multivariate models. T2*WI WM/GM also shows better reliability compared with FA and MTR, using our techniques (Martin AR, 2017a). In comparison with DTI and MT techniques, T2*WI had fewer excluded slices, required less imaging time, and involved less post-processing, suggesting that this biomarker is well suited for clinical use.

Unfortunately, all qMRI metrics failed to show diagnostic accuracy (AUC) greater than 90% and provided only moderate clinical correlations, indicating somewhat limited utility when used individually. However, our protocol produced 10 measures of tissue injury that are relatively independent, enabling multivariate use to strengthen their accuracy. This was evident in the logistic regression model that achieved > 95% diagnostic accuracy, and the linear regression model for mJOA that had much higher adjusted R^2 than univariate measures. Overall, our results demonstrate that T2*WI WM/GM performs well in comparison with established biomarkers, and our multiparametric approach has the potential to overcome the limitations of individual qMRI measures.

3.4.2 **T2*WI WM/GM: A Novel Biomarker of WM Injury**

T2*WI is available on all major MRI vendors, including the GE MERGE, Siemens MEDIC, Philips M-FFE, and Hitachi ADAGE sequences, although differences may exist between implementations and cross-vendor validation is needed (White et al., 2011). Our investigation of T2*WI WM/GM signal intensity ratio follows from previous findings that T2*WI detects WM injury by exhibiting hyperintensity. In one study, a pattern consistent with Wallerian degeneration of fasciculus gracilis could be visualized rostrally following a cervical SC needle injury (Cohen-Adad et al., 2012). Another study found hyperintensity in bilateral LCSTs in a patient with amyotrophic lateral sclerosis (ALS), related to the degeneration of descending upper motor neurons (Cohen-Adad et al., 2013b). In our data, a small number of DCM subjects also exhibited focal T2*WI hyperintensity of the dorsal columns extending through all images rostral to compression, consistent with Wallerian degeneration (Figure 3.2). However, the majority of DCM patients only showed loss of grey-white contrast, which is somewhat akin to the diagnosis of acute ischemic stroke on brain CT. However, T2*WI signal intensity is a relative value that varies considerably between subjects, requiring normalization. Although GM may also experience injury in DCM, we found that using GM signal intensity as a reference produced more consistent results than cerebrospinal fluid (CSF) due to variable CSF signal (unpublished data). Furthermore, T2*WI WM/GM appears to be stable in the context of T2WI hyperintensity, which is commonly encountered in DCM, showing no significant interaction (effect modification) and minimal impact on clinical correlations. The calculation of WM/GM signal intensity ratio is easily and accurately performed using automated template-based analysis (Cohen-Adad J, 2014). The pathophysiological processes that underlie T2*WI hyperintensity

include demyelination, gliosis, increased calcium concentration, and non-heme iron stored in ferritin, but signal intensity also depends on water content and local concentration of deoxyhemoglobin (used in BOLD fMRI) (Cohen-Adad, 2014, Lee et al., 2012, Fukunaga et al., 2010, Haacke et al., 2005, Marques et al., 2009). Thus, T2*WI WM/GM is somewhat non-specific, reflecting several microstructural features. The moderate cross-correlations observed between T2*WI WM/GM and other metrics did not reveal a clear pattern, as these findings may simply be explained by multiple pathological processes occurring simultaneously. Histopathological studies are necessary to fully understand exactly what SC microstructural changes are detected by T2*WI WM/GM compared to other measures, and further research is needed to determine its performance in other pathologies. However, its simplicity, sensitivity, and excellent reliability suggest that it could be a highly useful imaging biomarker.

3.4.3 **Regions of Interest**

The strongest results for each metric were found at MCL in this study, with the exception of rostral T2*WI WM/GM for multivariate analyses and tract-specific correlations. This highlights a major challenge to employ quantitative MRI in DCM, as the compressed region suffers from potential bias related to distorted anatomy (leading to inaccurate registration to the template) and increased susceptibility artefact. This was partially mitigated by averaging MCL metrics over 3 slices, with slices above and below MCL often showing no compression. However, results from our reliability study showed a trend toward diminished reliability for FA, MTR, and T2*WI WM/GM at MCL (Martin AR, 2017a). It was encouraging to also find strong results rostrally for T2*WI WM/GM, which has been previously reported for FA (Vedantam et al., 2015, Wen et al., 2014a) This has important clinical implications as this region avoids the aforementioned issues and can be used for post-operative assessments rostral to metallic implants in most DCM patients. This region is also potentially useful for prediction of outcomes in acute SCI, using a post-operative scan in the days to weeks following early surgical decompression (Vedantam et al., 2015). The caudal region consistently showed weakest results, likely due to respiratory motion, susceptibility artifact from the lungs, and increased partial volume effects due to the angle between slices and the SC (in subjects with irreducible cervical lordosis). In spite of these issues, T2*WI WM/GM and FA showed some utility in this region. Metrics extracted from individual WM tracts showed significant correlations with focal neurological deficits, particularly at rostral and MCL levels, indicating that our quantitative analysis identifies focal

tissue injury. However, correlations with motor/sensory scores were modest, potentially because of the small number of voxels included in metric calculations, but also because clinical impairment can also result from GM injury, nerve root compression (radiculopathy), and pain.

3.4.4 Future Directions: Clinical Translation of Quantitative Spinal Cord MRI

At present, SC qMRI has yet to achieve clinical adoption due to challenges with the portability of acquisitions, cumbersome analysis, and modest results in terms of diagnostic accuracy and clinical correlations. However, our multiparametric approach using simple methods and automated analysis is designed to address each of these issues and be suitable for clinical use. We anticipate that the first clinical application of these techniques could be the development of more sensitive diagnostic tools. A diagnostic tool that can directly detect tissue injury could have a major impact in DCM, in which patients sometimes show minimal symptoms that cannot be definitely attributed to the SC by clinical and electrophysiological examinations. Furthermore, a large number of older individuals have spinal cord compression without neurological dysfunction (Wilson et al., 2013), indicating that anatomical imaging alone is insufficient. Our approach may also prove useful for monitoring DCM patients for progression of tissue injury using serial qMRI examinations. Mild DCM patients are often managed non-operatively with periodic clinical assessments, but symptoms are highly subjective and mechanisms of behavioural adaptation and neuroplasticity may mask subtle deterioration. Finally, several efforts have been made to predict outcomes using qMRI in DCM and other clinical populations(Martin et al., 2016, Wen et al., 2014a), but these have yet to show strong success, possibly because outcomes depend on factors that extend beyond the current state of tissue injury. However, if qMRI techniques can differentiate between reversible and permanent injury by quantifying specific microstructural changes (e.g. demyelination vs. axonal loss), enhanced outcome prediction may also be possible. Future studies should be directed at investigating each of these exciting potential applications.

3.4.5 Limitations

Clinical assessments utilized in this study are somewhat coarse (mJOA, sensory score) and subjective (mJOA, motor score), potentially limiting the strength of correlations. T1-weighted (T1w) imaging was not performed in this study, and the effect of T1w hypointensity on T2*WI

WM/GM has not been characterized. We aimed to minimize bias by using automated analysis, but almost all DCM datasets required manual correction of segmentations. Other DTI metrics were not analyzed due to an *a priori* decision to focus on FA, due to its consistent results in previous studies (Martin et al., 2016). The validity of MRI metrics for 3 patients with metallic implants is unknown, but quantitative results distant from the hardware appeared to be consistent with other subjects.

3.4.6 **Conclusions**

T2*WI WM/GM is a novel biomarker of SC WM degeneration that shows good diagnostic accuracy and correlation with clinical features of DCM, warranting further investigation. This biomarker has strong potential for clinical translation, particularly in multivariate approaches that combine quantitative measures of SC injury. Such measures have potential to provide more sensitive diagnosis of mild cord injury, monitoring of disease progression or recovery, and prediction of outcomes in DCM and other spinal pathologies.

Chapter 4
Rethinking the Definition of Myelopathy: Multiparametric Quantitative MRI Detects Subclinical Tissue Injury in Asymptomatic Cervical Spinal Cord Compression

*This chapter is based upon an article currently under review for the journal Annals of Neurology. Permission to reproduce this article will be requested following publication.

Degenerative cervical myelopathy (DCM) involves extrinsic spinal cord (SC) compression causing tissue injury and neurological dysfunction. Asymptomatic SC compression (ASCC) is more common but inadequately researched. This study investigates if: 1) ASCC can be diagnosed using SC shape analysis; 2) multiparametric quantitative MRI (qMRI) can detect similar SC tissue injury as previously observed in DCM. Forty neurologically intact subjects underwent 3T MRI to calculate cross-sectional area (CSA), diffusion fractional anisotropy (FA), magnetization transfer ratio (MTR), and T2*-weighted imaging white to grey matter signal intensity ratio (T2*WI WM/GM). qMRI data were extracted from rostral (C1-3), caudal (C6-7), and maximally compressed levels (MCL). Diagnosis of SC compression combined expert ratings with automated shape analysis of flattening, indentation, and torsion. Ten qMRI measures were analyzed individually and as a composite (averaged z scores). ASCC was present in 20/40 subjects and 15/21 over age 50. Shape analysis provided excellent diagnostic accuracy. Five qMRI metrics demonstrated evidence of tissue injury in ASCC, while the composite score showed stronger differences (p=0.002). At follow-up (median 21 months), two ASCC subjects developed DCM. Myelopathy begins prior to the onset of neurological symptoms and signs, with SC compression causing subclinical tissue injury. ASCC is a highly prevalent age-related preclinical state with an increased risk of symptomatic myelopathy development, and can be objectively diagnosed with shape analysis. These findings have far-reaching clinical implications, including the need to educate and monitor ASCC subjects, while offering the intriguing possibility of presymptomatic diagnosis and treatment of other spinal pathologies.

4.1 BACKGROUND

Degenerative cervical myelopathy (DCM) involves age-related degeneration of the discs, ligaments, and vertebrae leading to extrinsic spinal cord (SC) compression and neurological dysfunction (Nouri et al., 2015b). The prevalence of DCM is difficult to estimate, but it has been suggested that it is probably the most common cause of SC dysfunction (Nouri et al., 2015b, Kalsi-Ryan et al., 2013a). However, asymptomatic SC compression (ASCC) is far more frequent, with prevalence estimates ranging from 8% to 59% (Teresi et al., 1987, Boden et al., 1990, Matsumoto et al., 1998, Lee et al., 2007, Kato et al., 2012, Kovalova et al., 2016). Furthermore, SC compression may be underestimated using supine MRI, which misses dynamic compression that is visible with flexion/extension MRI (Bartlett et al., 2012). ASCC has received little research attention, but one study found that it confers an increased risk of myelopathy development (Bednarik et al., 2008).

Emerging quantitative MRI (qMRI) techniques offer in vivo measurement of SC microstructural features and tissue injury.(Martin et al., 2016, Stroman et al., 2014, Wheeler-Kingshott et al., 2014) Cross-sectional area (CSA) measures SC compression and atrophy, the diffusion tensor imaging (DTI) metric fractional anisotropy (FA) measures axonal integrity, magnetization transfer ratio (MTR) reflects myelin quantity, and T2*-weighted imaging (T2*WI) white matter to grey matter signal intensity ratio (T2*WI WM/GM) is a novel biomarker that we recently introduced that correlates with demyelination, gliosis, calcium, and iron concentrations (Martin et al., 2017b, Stroman et al., 2014, Martin et al., 2017c). These measures hold potential for earlier diagnosis of various conditions, but results to date have been modest and insufficient to drive clinical adoption (Martin et al., 2016, Wheeler-Kingshott et al., 2014).

Our group previously reported a clinically feasible multiparametric qMRI protocol that measures CSA, FA, MTR, and T2*WI WM/GM across the cervical SC (Martin et al., 2017b, Martin et al., 2017c). In DCM patients, these metrics reveal macro- and microstructural changes at the maximally compressed level (MCL) and in the uncompressed SC above and below; significant clinical correlations and group differences compared with healthy subjects were found at rostral, MCL, and caudal levels for FA and T2*WI WM/GM, while CSA and MTR showed significant results at rostral and MCL levels (Martin et al., 2017c). In the current study, we test the hypothesis that subjects with ASCC experience tissue injury compared with uncompressed

subjects, based on the same ten qMRI measures. We establish an objective definition of SC compression and assess newly developed automated SC shape analysis for diagnostic accuracy. Finally, we investigate the rate of symptomatic myelopathy development at follow-up and associated risk factors.

4.2 METHODS

4.2.1 Study Design and Subjects

This prospective study received institutional approval from University Health Network (UHN, Toronto, Ontario, Canada). 42 subjects were recruited between October 2014 and December 2016 by convenience sampling and provided written informed consent (Martin et al., 2017b, Martin et al., 2017c). All clinical data collection and physical examinations were performed by a physician member of the UHN Spine Program. Subjects were examined to rule out neurological symptoms (numbness, weakness, fine motor dysfunction, gait/balance difficulties, urinary urgency/incontinence) and signs (hyperreflexia, weakness, sensory deficits, Romberg sign, gait ataxia). Neck pain was not considered a neurological symptom. Subjects were also required to have 18/18 on the modified Japanese Orthopedic Association score. Two subjects were excluded during screening; one showed gait ataxia and both had sensory deficits, hyperreflexia, and MRI evidence of SC compression consistent with DCM. Follow-up assessments were performed by telephone, including mJOA administration. Subjects that reported any neurological symptoms underwent a complete neurological examination in person.

4.2.2 MRI Acquisitions

Subjects underwent T2-weighted imaging (T2WI), DTI, magetization transfer (MT), and T2*WI at 3T (GE Signa Excite HDxt) covering C1-C7, as previously described (Martin et al., 2017b). DTI, MT, and T2*WI images were acquired with 13 axial slices from C1 to C7. T2WI was performed with a FIESTA-C sequence with 0.8x0.8x0.8 mm^3 isotropic resolution. DTI used spin-echo single shot echo planar imaging (ssEPI) with 3 acquisitions averaged offline, b = 800 s/mm^2 in 25 directions, 5 images with b=0 s/mm^2, and resolution of 1.25x1.25x5 mm^3. MT used 2D spoiled gradient echo ± MT pre-pulse, with 1x1x5mm^3 voxels. T2*WI acquisition used multi-echo recombined gradient echo (MERGE) with 3 echoes at 5,10,15 ms and resolution

0.6x0.6x4 mm^3. Total imaging time was 30-35 minutes including patient positioning, slice prescription, and 2^{nd} order localized shimming (prior to DTI).

4.2.3 **Image Analysis**

Images were inspected and excluded from analysis if image quality was poor or artifacts were present. Quantitative imaging data were analyzed using Spinal Cord Toolbox (SCT) v3.0 (De Leener et al., 2017), including SC segmentation, registration to the probabilistic SCT template, and extraction of metrics with partial volume correction, as previously described (Martin et al., 2017b, Martin et al., 2017c). Segmentations and registered images were reviewed, and if necessary segmentations were manually edited to correct inaccuracies.

Diagnosis of SC compression followed a 3-step process. First, anatomical images (T2WI and T2*WI) were independently examined by 2 raters (ARM, AN) for indentation, flattening, torsion, or circumferential compression from extrinsic tissues (disc, ligament, or bone). Discrepancies were resolved by consensus. Effacement of the cerebrospinal fluid (CSF) was noted but not considered compression. Second, automated shape analysis was performed on each axial section of the T2*WI SC segmentation mask. 2D principle component analysis (PCA) identified the long and short axes, representing transverse and anterior-posterior (AP) directions, respectively (Figure 1). Flattening was measured with compression ratio (CR) = AP/transverse diameter (Kameyama et al., 1994). Indentation was measured using solidity = the percentage of area representing SC within the convex hull that subtends the SC. Torsion was measured with relative rotation, which was calculated as the angle between transverse axis and horizontal, relative to adjacent slices (difference from the average rotation of above and below slices). Circumferential compression was not specifically measured with a shape metric, as it typically coincides with flattening. Receiver operating characteristic (ROC) curves were plotted to determine diagnostic accuracy of shape metrics at each intervertebral level compared with consensus ratings. Third, discrepancies were discussed and diagnoses were revised if necessary. Normative values for shape parameters were calculated in uncompressed subjects. ROC curves were utilized to calculate revised diagnostic accuracy and optimal diagnostic thresholds (using Youden's Index). Analysis of variance (ANOVA) and Levene's test assessed if mean and variance of shape metrics varied among rostro-caudal levels, respectively. Pooled mean, SD, and diagnostic thresholds were calculated if levels showed no differences.

.

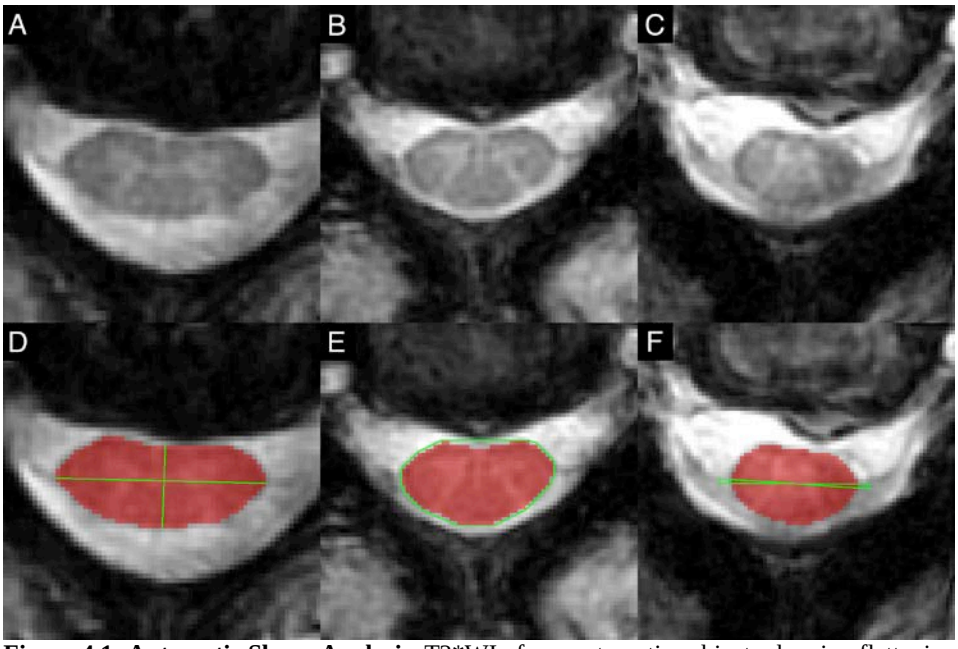

Figure 4.1: Automatic Shape Analysis. T2*WI of asymptomatic subjects showing flattening (A), indentation (B), and torsion (C) of the SC. D: the SC segmentation (red) is analyzed with 2D PCA to identify the long (transverse) and short (AP) axes (green) that intersect at the centre of mass, and CR is calculated as ratio of AP to transverse diameters to measure flattening. E: a convex hull (green) is computed that surrounds the segmentation (red), and solidity is calculated as the ratio of segmented area to subtended area. F: the angle between the transverse axis and horizontal is computed, and then relative rotation is calculated by subtracting the average rotation at all levels (in case the patient is not perfectly flat) and a 50% bias correction (to account for neck rotation).

Tissue injury was measured with CSA of the SC, and FA, MTR, and T2*WI WM/GM extracted from WM. Metrics were normalized for rostro-caudal level and averaged across rostral (C1-3), middle (C4-5 in uncompressed subjects or maximally compressed level, MCL, in ASCC

subjects), and caudal (C6-7) levels. The MCL for subjects with multilevel compression was determined by consensus ratings after considering automated shape results. For MCL measurements, data from a single level was used for CSA, whereas 3 slices centered at MCL were averaged for FA, MTR, and T2*WI WM/GM. Non-CSA metrics were also extracted from the ventral columns (VCs), lateral columns (LCs), dorsal columns (DCs) and GM averaged across C1-C7 to identify focal injury. Metrics were normalized for age, sex, height, weight, and cervical cord length, similar to our previous approach (Martin et al., 2017b), based on multiple linear regression with backward stepwise variable selection. However, the presence of SC compression was included to measure independent effects of other variables, and age was retained regardless of significance to mitigate the discrepancy between groups. Ratios of MCL/rostral metrics were also calculated (Kerkovsky et al., 2012).

4.2.4 **Statistical Analysis**

Statistical analysis was performed with R v3.3. Numerical data were summarized by mean ± standard deviation (SD). Binary variables were compared using Fisher exact tests, whereas numerical variables used two-tailed Welch's T tests (demographic data) or Wilcoxon tests (normalized qMRI metrics). 95% confidence intervals (CIs) for frequencies were calculated using the Wilson procedure with continuity correction. The z scores of individual qMRI metrics (using negative values for T2*WI WM/GM) were averaged to yield a composite score, following a t distribution with 10 degrees of freedom (t_{10}). A binomial test compared the pattern of differences in ASCC with that in DCM (Martin et al., 2017c). Logistic regression with backward stepwise elimination was used to develop a model for detecting tissue injury, retaining a maximum of 4 qMRI metrics as independent variables. Age, sex, and baseline qMRI metrics were analyzed for prediction of myelopathy development using Wilcoxon tests, Fisher exact tests, and logistic regression. Significance was set at $p < 0.05$, including individual measurements of $|z| > 1.96$, $|t_{10}| > 2.23$, and $|t_9| > 2.26$.

4.3 RESULTS

4.3.1 Subject Characteristics

Subject characteristics are listed in Table 4.1. Individuals with ASCC were older (54.9 vs. 39.4, p=0.0007) and weighed more (79.8 vs. 71.1, p=0.03) than subjects without cord compression, while other characteristics (sex, height, and neck length) did not differ.

Characteristic	Uncompressed Subjects (N=20)	Compressed Subjects (N=20)	P value
Age	39.4 ± 12.8	54.9 ± 13.8	0.0007**
Sex (M:F)	10:10	11:9	1.0
Height (cm)	172.7 ± 9.4	170.5 ± 8.0	0.43
Weight (kg)	71.1 ± 10.4	79.8 ± 13.3	0.03**
Neck Length (mm)	106.3 ± 9.6	107.0 ± 9.4	0.81

Table 4.1: Subject Characteristics. Demographics and clinical measures are tabulated for subjects with and without cervical spinal cord compression. ** denotes significant differences ($p < 0.05$) between groups.

4.3.2 Diagnosis of Spinal Cord Compression

Consensus ratings identified 19 subjects with SC compression at 41 levels (flattening: 20 levels, indentation: 30 levels, torsion: 8 levels, circumferential compression: 1 level). Relative to these ratings, automated shape analysis achieved AUC=99.2% for flattening, AUC=97.3% for indentation, and AUC=97.7% for torsion (Table 4.2). After reviewing shape analysis results, 3 levels were reclassified as flattened (total: 23 levels) and 1 level as indented (total: 31 levels). Remaining discrepancies were mostly at adjacent levels, which showed a transition between normal and abnormal shape. Using revised diagnoses and excluding adjacent levels, diagnostic accuracy of shape analysis improved to 99.8% for flattening, 99.3% for indentation, and 98.4% for torsion. CR differed across rostrocaudal levels, whereas solidity and relative rotation appeared to be invariant, yielding pooled normative values of 96.52 ± 0.56% and 0.3 ± 1.5 degrees, respectively.

Shape Parameter	Statistic	C2-3	C3-4	C4-5	C5-6	C6-7	Pooled Values
CR (%)	Normal Mean ± SD	67.2 ± 6.4	62.6 ± 5.1	59.3 ± 4.5	59.2 ± 4.2	58.7 ± 4.5	-
	Flattened Frequency	0/40	3/40	5/40	9/40	6/40	23/200
	AUC	-	1.00	0.989	1.0	0.977	0.992
	Diagnostic Threshold	-	53.1	52.0	49.9	50.5	-
Solidity (%)	Normal Mean ± SD	96.52 ± 0.47	96.25 ± 0.53	96.74 ± 0.59	96.64 ± 0.46	96.45 ± 0.76	96.52 ± 0.56
	Indented Frequency	0/40	6/40	11/40	9/40	5/40	31/200
	AUC	-	0.979	0.964	0.971	0.978	0.973
	Diagnostic Threshold	-	-	-	-	-	95.5
Relative Rotation (Degrees)	Normal Mean ± SD	0.0 ± 1.3	0.5 ± 1.6	0.5 ± 1.3	0.4 ± 1.4	0.3 ± 1.5	0.3 ± 1.5
	Rotated Frequency	0/40	1/40	0/40	3/40	4/40	8/200
	AUC	-	0.982	-	0.978	0.971	0.977
	Diagnostic Threshold	-	-	-	-	-	3.3

Table 4.2: Shape Metrics. Data for CR, solidity, and relative rotation are displayed for each intervertebral level from C2-C7. Normal data are derived from 20 subjects with no cord compression and reported as mean ± SD. Diagnostic accuracy is reported as AUC relative to consensus ratings (prior to revision incorporating these results). AUC: area under the curve, CR: compression ratio, ROC: receiver operating characteristic function, SD: standard deviation.

Final diagnostic ratings identified ASCC in 20/40 subjects (50%, 95% CI: 34.1-65.9%). Six additional subjects (15%) without compression had effacement of the CSF. The frequency of ASCC increased with age (Figure 4.2), including 15/21 (71.4%, 95% CI: 47.7-87.8%) among subjects aged ≥ 50.

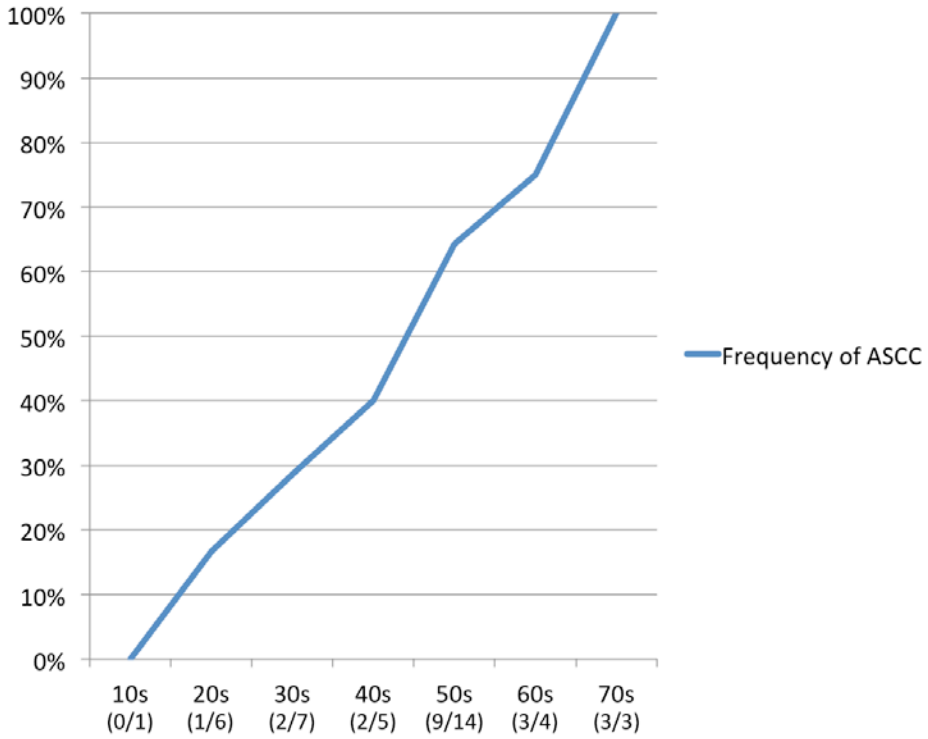

Figure 4.2: Frequency of ASCC by Decade. The frequency of ASCC is plotted against decade of life, with data for each decade provided in parentheses. ASCC: asymptomatic spinal cord compression.

Details of SC compression and shape metrics for each of the 20 ASCC subjects are provided in Table 4.3. SC compression was primarily anterior at all compressed levels, related to disc ± osteophyte complexes (DOCs), with an element of posterior compression due to ligamentum flavum (LF) hypertrophy at 9 levels. T2WI hyperintensity was not present in any subject, although 1 had a prominent central canal (1mm diameter, within normal limits).

#	Age, Sex	MCL	Comp. Levels	CR (%)	Sol. (%)	RR (°)	MRI Features

1	74M	C5-6	C4-5	51.5*	95.8	-1.4	Broad DOC flattening cord
			C5-6	49.3*	96.4	0.3	Broad DOC flattening cord
			C6-7	48.6*	95.2	-2.3	Lateral DOC flattening and rotating cord
2	55F	C3-4	C3-4	53.1*	93.9*	-1.0	Central DOC indenting and flattening cord, mild LF hypertrophy
			C4-5	51.7*	94.6*	-0.7	Central DOC indenting and flattening cord, mild LF hypertrophy
3	59F	C5-6	C3-4	47.8*	95.3*	1.3	Broad DOC flattening and indenting cord
			C4-5	48.5*	96.1	0.5	Broad DOC flattening cord
			C5-6	45.6*	98.2	0.5	Broad DOC flattening cord
4	28M	C4-5	C3-4	57.8	95.4*	-1.2	Central DOC indenting cord
			C4-5	53.4	94.4*	-1.0	Central DOC indenting cord
			C5-6	51.7	95.4*	-1.4	Central DOC indenting cord
5	30M	C5-6	C5-6	55.4	94.6*	2.1	Central DOC indenting cord
			C6-7	53.9	93.9*	2.1	Central DOC indenting cord
6	52F	C4-5	C3-4	56.4	94.3*	-1.8	Central DOC indenting cord, mild LF hypertrophy at C3-4, C4-5
			C4-5	60.8	92.7*	-2.9	Central DOC indenting cord, mild LF hypertrophy
			C5-6	61.1	95.4*	-7.0*	Lateral DOC indenting and rotating cord
			C6-7	48.6*	93.8*	1.0	Central DOC indenting and flattening cord
7	60F	C5-6	C5-6	50.4*	95.4*	0.7	Broad DOC flattening cord
8	69M	C5-6	C5-6	48.9*	97.5	-0.7	Broad DOC flattening cord
			C6-7	49.0*	95.8	2.5	Broad DOC flattening cord
9	66F	C4-5	C4-5	55.4	94.2*	0.0	Central DOC indenting cord, mild LF hypertrophy
10	51M	C6-7	C6-7	43.4*	91.6*	-0.9	Central DOC indenting and flattening cord
11	39M	C6-7	C6-7	55.4	94.7*	4.5*	Lateral DOC indenting and rotating cord
12	49M	C6-7	C4-5	55.2	93.7*	-0.2	Central DOC indenting cord
			C5-6	49.5*	95.8	2.1	Broad DOC flattening cord
			C6-7	46.1*	92.9*	-5.0*	Lateral DOC indenting, flattening, and rotating cord
13	50F	C5-6	C4-5	55.5	94.1*	0.5	Central DOC indenting cord
			C5-6	55.0	95.3*	-4.2*	Broad lateral DOC indenting and rotating cord
14	51F	C4-5	C3-4	55.8	95.4*	-0.8	Central DOC indenting cord
			C4-5	54.0	93.0*	1.9	Central DOC indenting cord
			C5-6	54.3	95.6	0.6	Central DOC indenting cord

15	55F	C4-5	C3-4	46.9*	96.2	0.8	Broad DOC flattening cord
			C4-5	41.3*	95.4*	0.6	Central DOC indenting cord
			C5-6	42.0*	96.0	-0.4	Broad DOC flattening cord
16	79F	C5-6	C4-5	52.3	95.5*	-1.3	Central DOC indenting cord
			C5-6	46.7*	93.3*	-2.0	Central DOC indenting and flattening cord
17	77M	C5-6	C3-4	53.2*	92.8*	-4.0*	Lateral DOC indenting and rotating cord
			C4-5	48.6*	95.8	-0.4	Broad central DOC flattening cord
			C5-6	48.3*	93.9*	-2.9*	Broad DOC indenting, flattening, and rotating cord
18	44M	C5-6	C3-4	55.6	94.9*	-0.7	Central DOC indenting cord
			C4-5	55.7	95.1*	1.4	Central DOC indenting cord
			C5-6	45.4*	93.4*	0.0	Central DOC indenting and flattening cord, mild LF hypertrophy
19	56M	C5-6	C5-6	53.6	94.8*	-1.3	Circumferential compression, flattening from broad DOC and LF hypertrophy
20	54M	C6-7	C4-5	51.5	95.3*	0.1	Central DOC indenting cord
			C6-7	46.6*	96.7	-2.4*	Broad DOC flattening and rotating cord

Table 4.3: Anatomical Features of Spinal Cord Compression and Quantitative Shape Metrics. MRI images were analyzed for degenerative changes causing cervical spinal cord compression, defined as indentation, flattening, or focal torsion. Levels with cord compression are listed with CR in parentheses, and a description of the degenerative changes and morphology of cord compression are provided. ASCC: asymptomatic spinal cord compresison, CR: compression ratio, DOC: disc ± osteophyte complex, LF: ligamentum flavum, MCL: maximally compressed level, RR: relative rotation, Sol.: solidity.

4.3.3 **Variation of MRI Metrics with Age and Other Characteristics**

CSA varied with cervical cord length and MTR varied with height at rostral and MCL levels, independent of the effect of cord compression (Table 4.4). None of the metrics varied significantly with age.

Region	MRI Metric	Age	Sex	Height	Weight	Cervical Cord Length
Rostral (C1-C3)	CSA	β=-0.168 (p=0.10)	-	-	-	β=4.81 (p=0.002)

	FA	$\beta=-6.06x10^{-4}$ ($p=0.19$)	-	-	-	-
	MTR	$\beta=-0.0472$ ($p=0.13$)	-	$\beta=-0.181$ ($p=0.0004$)	-	-
	T2*WI WM/GM	$\beta=2.34x10^{-4}$ ($p=0.53$)	-	-	-	-
MCL or C4-5	CSA	$\beta=-0.195$ ($p=0.17$)	-	-	-	$\beta=4.90$ ($p=0.02$)
	FA	$\beta=-7.16x10^{-4}$ ($p=0.22$)	-	-	-	-
	MTR	$\beta=-0.0545$ ($p=0.15$)	-	$\beta=-0.146$ ($p=0.01$)	-	-
	T2*WI WM/GM	$\beta=3.39x10^{-5}$ ($p=0.91$)	-	-	-	-
Caudal (C6-C7)	FA	$\beta=-0.00127$ ($p=0.12$)	-	-	-	-
	T2*WI WM/GM	$\beta=1.20x10^{-4}$ ($p=0.83$)	-	-	-	-

Table 4.4: Variations of MRI Measures with Subject Characteristics. The relationship between qMRI metrics and subject characteristics (age, sex, height, weight, and cervical cord length) were analyzed with backward stepwise multiple linear regression that also included a binary independent variable for the presence of cord compression. Age was retained in each model regardless of significance, and linear coefficients for age and any other significant relationships (CSA with cervical cord length and MTR with height) were subsequently used to normalize qMRI metrics.

4.3.4 **Quantitative MRI Measures of Tissue Injury**

Eight out of ten qMRI metrics showed the same direction of differences in ASCC as previously seen in DCM ($p=0.11$), including significant differences in five metrics: increased T2*WI WM/GM at all levels (rostral: $p=0.03$, MCL: $p=0.005$, caudal: $p=0.01$), decreased MCL FA ($p=0.04$), and decreased rostral MTR ($p=0.046$) (Table 4.5). CSA measures varied in the opposite direction from DCM, including significantly higher rostral CSA in ASCC ($p=0.02$).

Ratios of MCL:rostral qMRI metrics showed trends toward decreased FA ratio (p=0.06) and CSA ratio (p=0.09) in ASCC subjects (Table 4.6).

Region	MRI Metric	Uncompressed (N=20)	Compressed (N=20)	P Value	Direction Matches DCM
Rostral (C1-C3)	CSA	75.4 ± 4.7	81.7 ± 9.6	0.02**	N
	FA	0.731 ± 0.031	0.720 ± 0.037	0.48	Y
	MTR	53.6 ± 3.0	51.9 ± 1.8	0.046**	Y
	T2*WI WM/GM	0.838 ± 0.029	0.863 ± 0.031	0.03**	Y
Mid (MCL or C4-5)	CSA	79.2 ± 7.7	81.9 ± 12.8	0.34	N
	FA	0.670 ± 0.044	0.631 ± 0.043	0.04**	Y
	MTR	51.1 ± 3.3	49.8 ± 2.4	0.35	Y
	T2*WI WM/GM	0.842 ± 0.019	0.864 ± 0.026	0.005**	Y
Caudal (C6-C7)	FA	0.616 ± 0.046	0.595 ± 0.051	0.24	Y
	T2*WI WM/GM	0.845 ± 0.037	0.881 ± 0.050	0.01**	Y
Composite Score		0 ± 1	-0.984 ± 1.259	0.002**	Y

Table 4.5: Comparison of Normalized Quantitative MRI Metrics. Normalized MRI metrics were compared between subjects with and without cord compression. A composite Z score was used as an overall measure of tissue injury. Data extracted at the MCL were converted to Z scores to normalize for rostrocaudal variations prior to comparison and then converted back to values at C4-5 for convenience of interpretation. The direction of differences were compared to findings in DCM patients compared to asymptomatic subjects. Caudal CSA and MTR were not

analyzed because they did not show significant results in our prior DCM study.(Martin et al., 2017c) * denotes significance ($p<0.05$).

MCL: Rostral Ratio	Uncompressed (N=20)	Compressed (N=20)	P Value
CSA	1.050 ± 0.060	1.003 ± 0.106	0.09*
FA	0.917 ± 0.054	0.878 ± 0.056	0.06*
MTR	0.954 ± 0.042	0.960 ± 0.033	0.56
T2*WI WM/GM	1.005 ± 0.029	1.001 ± 0.025	0.67

Table 4.6: Comparison of Metric Ratios. Ratios were calculated by dividing MCL metric values by rostral values. * denotes trend ($p<0.10$) and ** denotes significance ($p<0.05$).

4.3.5 **Multivariate Results**

The qMRI composite score showed stronger differences than single metrics ($p=0.002$; Table 4.5), including abnormal results (t_{10} score < -2.23) in 6/20 compressed subjects (Figure 4.3). Replacing CSA measures with CSA ratio, a revised composite score showed even stronger results ($p=8x10^{-5}$), including 9/20 compressed subjects with abnormal results (t_9 score < -2.26; Figure 3). A logistic regression model retaining MCL T2*WI WM/GM ($p=0.006$), FA ratio ($p=0.06$), CSA ratio ($p=0.11$), and rostral MTR ($p=0.34$) yielded discrimination of 0.941 between compressed and uncompressed subjects ($p=2x10^{-5}$).

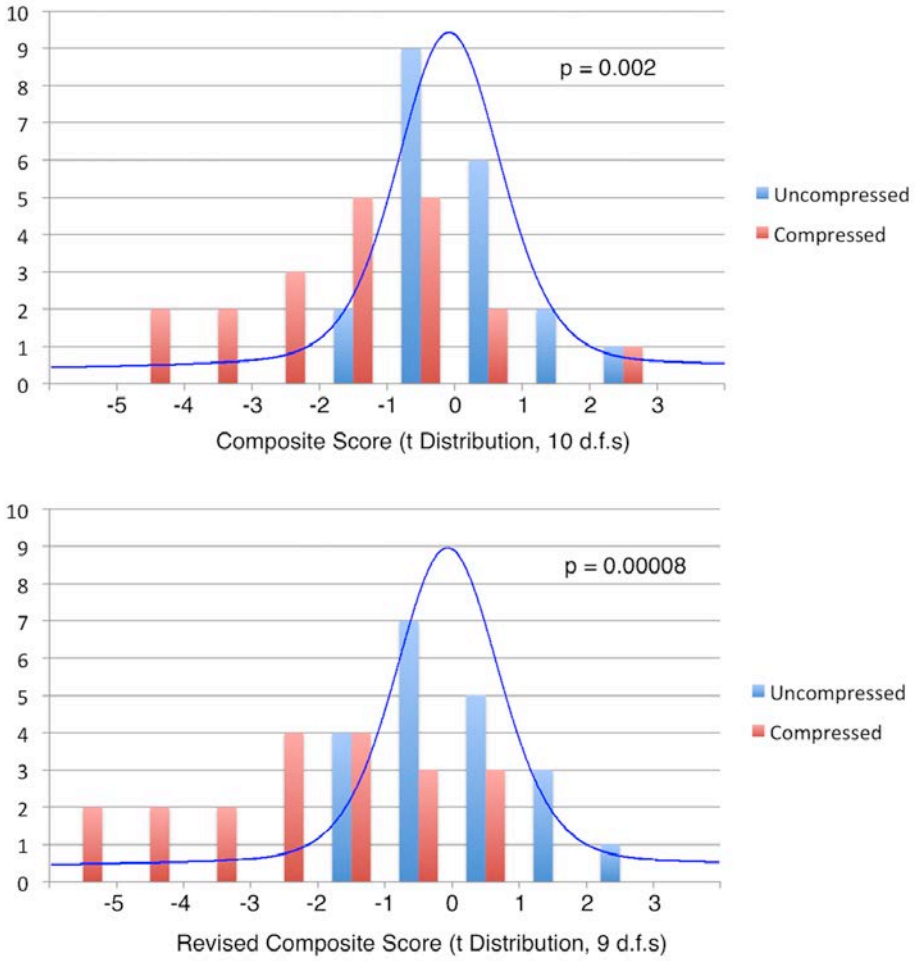

Figure 4.3: Distributions of Composite Scores. Top: histograms (bars) of composite scores (average of the z scores of 10 qMRI metrics) are displayed for subjects with ASCC (red) and no cord compression (blue). The expected distribution of results based on the null hypothesis (t distribution with ten d.f.s) is superimposed. Six ASCC subjects had abnormally low composite score ($t_{10} < -2.23$) and group differences were significant (Wilcoxon test: p=0.002). Bottom: the same plot is displayed for a revised composite score that replaces rostral and MCL CSA measures with CSA ratio (selected post hoc), and the corresponding t distribution with nine

degrees of freedom. Nine ASCC subjects had abnormal scores ($t_9 < -2.26$) and stronger group differences were found (p=0.00008).

4.3.6 **Tissue Injury by Anatomical Structure**

Compressed subjects had decreased FA and MTR in the VCs (p=0.01, 0.02, respectively), while the LCs, DCs, and GM did not show significant differences in these metrics (Figure 4.4). In contrast, T2*WI WM/GM was increased in the LCs and DCs (p=0.009, 0.0004, respectively) in compressed subjects, while the VCs showed no difference.

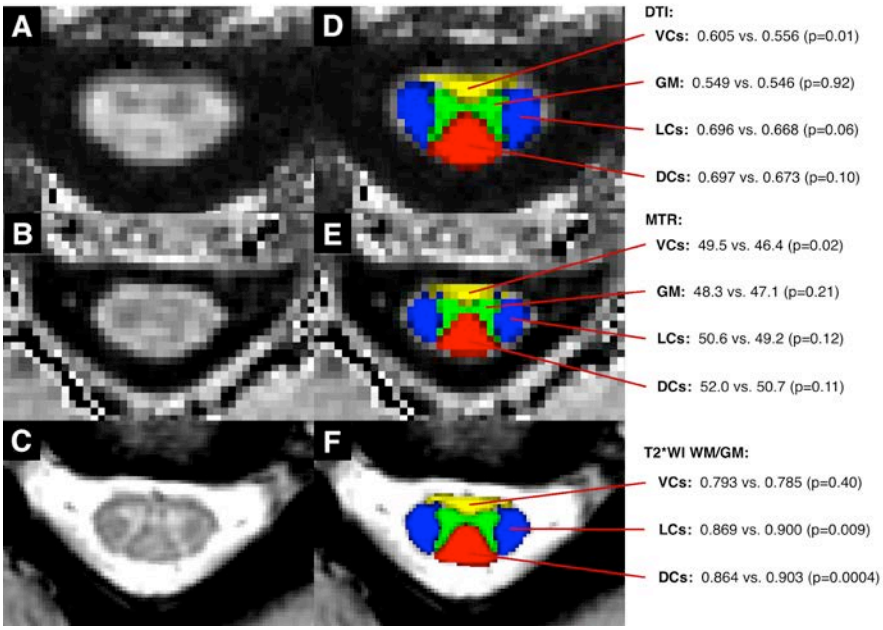

Figure 4.4: Quantitative MRI Metrics by Anatomical Structure. Images include a FA map (A), a MTR map (B), and a T2*-weighted image (C) of C3-4 in an uncompressed subject. Panels D-F show the SCT probabilistic maps of the VCs (yellow), LCs (blue), DCs (red), and GM (green) overlaid. DCs: dorsal columns, FA: fractional anisotropy, GM: grey matter, LCs: lateral columns, MTR: magnetization transfer ratio, SCT: Spinal Cord Toolbox, VCs: ventral columns.

4.3.7 Clinical Follow-up

All 20 ASCC subjects had follow-up assessments (median: 21 months, range: 3-27 months). Four subjects reported concerning new symptoms, and following physical examination two were diagnosed with DCM (10%, 95% CI: 1.8-33.1%) and referred for surgical consultation. One experienced neck pain, intermittent right hand numbness, and gait imbalance (mJOA=17), and examination showed marked gait ataxia, asymmetric hyperreflexia, and positive left Hoffman sign. The other had neck pain, left hand numbness, and mild gait instability (mJOA=16), and examination revealed symmetric hyperreflexia and mild gait ataxia. This individual sought medical attention with her family physician, but no diagnosis was made after a new MRI was reported as “normal degenerative changes”.

4.3.8 Prediction of Symptomatic Myelopathy Development

Demographic variables and baseline qMRI metrics were not predictive of myelopathy development in univariate or multivariate analyses.

4.4 DISCUSSION

4.4.1 Summary of Findings

This study establishes an objective definition of SC compression and finds that asymptomatic compression is common, affecting approximately half of healthy adults and increasing in frequency with age. Multiparametric quantitative MRI provides compelling evidence that ASCC involves a mild degree of SC tissue injury. Significant differences were found with five qMRI metrics (rostral, MCL, and caudal T2*WI WM/GM, rostral MTR, and MCL FA), with T2*WI WM/GM and MTR results suggesting that demyelination is the predominant pathophysiological mechanism in this preclinical state (Stroman et al., 2014, Wheeler-Kingshott et al., 2014, Cohen-Adad, 2014). The finding of decreased MCL FA confirms two previous reports (Kerkovsky et al., 2012, Lindberg et al., 2016), and may be indicative of axonal injury but could alternatively be related to demyelination (Cohen-Adad et al., 2011). However, this result could be artifactual, as DTI metrics can be biased in the compressed SC by increased susceptibility artefact (Cohen-Adad et al., 2011, Stroman et al., 2014), and thus it was reassuring that other measures showed changes away from the compressed region. Furthermore, the study by Lindberg et al. (2016) included only five ASCC subjects, who showed functional deficits, while the Kerkovsky et al.

(2012) study included subjects with radiculopathy, which can localize within the SC GM (i.e. myeloradiculopathy). In contrast, our cohort was carefully screened to ensure the absence of neurological symptoms and signs. Recently, a larger study was completed with 92 ASCC and 71 uncompressed subjects, but DTI differences between these groups were not reported (Kerkovsky et al., 2017). Our finding that rostral CSA was significantly greater among ASCC subjects suggests that atrophy does not occur in this condition, but rather, having a larger SC is a predisposing factor for compression, in keeping with a prior report that investigated SC occupation ratio (Kato et al., 2012). MCL CSA was also (non-significantly) larger in uncompressed subjects, but the ratio of MCL to rostral CSA showed a trend toward a decrease in ASCC, indicating that compression has a minor effect on CSA and normalization by rostral values helps to mitigate the high inter-subject variability of this measure (Kato et al., 2012, Martin et al., 2017b). Although the groups with and without cord compression differed significantly in age and weight, all qMRI metrics were corrected for age and none showed significant variation with weight. In fact, MTR and FA have previously been shown to vary with age (Martin et al., 2016, Martin et al., 2017b), but these relationships became non-significant when compression was included in the analysis, confirming a recent DTI study,(2017) suggesting that earlier studies overestimated the effect of age (Mamata et al., 2005, Martin et al., 2017b, Taso et al., 2016). SC compression was primarily anterior in all subjects, and this appeared to preferentially cause injury to the VCs, as measured by reduced FA and MTR. T2*WI WM/GM demonstrated conflicting results with significant changes in LCs and DCs and no significant effect in the VCs; we suspect that this is attributable to ventral artifacts on T2*WI, including chemical shift at the CSF-cord interface and blooming artefact from prominent anterior veins, but histopathological correlation is required. The GM did not show significant differences for FA or MTR, which is likely a limitation of these metrics as they are better at detecting WM pathology (Stroman et al., 2014). Follow-up clinical data showed development of clinical myelopathy in 10% of subjects, similar to a prior report (Bednarik et al., 2008), indicating that ASCC is a meaningful preclinical condition. Prediction of myelopathy development was not successful given the small ASCC sample and number of events, but further investigation is warranted to identify prognostic factors.

Our results highlight the value of multiparametric qMRI and multivariate analysis; the combination of multiple tissue injury measures into composite scores reduces the standard error

of effect estimation by approximately 1/ √n, revealing robust group differences. Post hoc analysis identified an even greater effect of compression, with the revised composite score finding abnormal results in nine ASCC subjects, and logistic regression results suggesting that the vast majority with ASCC experience tissue injury. However, such data-driven analysis may suffer from overfitting and must be interpreted with caution. In fact, without histopathological studies, the ground truth is unknown regarding microstructural changes that occur in ASCC, and to our knowledge no cadaver studies have investigated this topic. Overall, the results support our hypothesis at a group level, indicating that SC tissue injury occurs in subjects with only a mild degree of compression who lack any manifestation of clinical symptoms or signs. This offers the intriguing possibility of diagnosing SC tissue injury prior to the onset of neurological impairment in this condition and others, with far-reaching clinical implications.

4.4.2 **An Objective Definition of Spinal Cord Compression**

The prevalence estimates in our data are similar to the range of 51.5-66.2% (for age 40-80) reported by Kovalova et al. (2016), but far higher than earlier reports of 8-26% (Kato et al., 2012, Teresi et al., 1987, Boden et al., 1990, Matsumoto et al., 1998, Lee et al., 2007). These differences are primarily due to vague and subjective definitions of SC compression in prior studies, which used the terms impingement, encroachment, and compression without strict criteria (Teresi et al., 1987, Boden et al., 1990, Matsumoto et al., 1998, Lee et al., 2007, Kato et al., 2012). Kerkovsky et al. (2012) provided a more precise definition of SC compression: a concave defect adjacent to a bulging disc or osteophyte and/or CR < 0.4; however, their threshold for CR was very low, at 4.5 SDs below the mean (based on our normative data at C5-6) and did not account for normal variations of CR across levels. Furthermore, the error associated with manual CR measurement has not been characterized, and visual assessment of concavity is subjective. Kovalova et al. (2016) provided detailed descriptions of indentation, flattening, and circumferential compression, but did not establish quantitative criteria. Instead, we use automated analysis to reduce bias and define SC compression as deviation from normal SC morphology in 3 quantitative parameters that reflect flattening, indentation, and torsion (due to lateral bulging discs). This approach identified four levels of subtle compression missed by two expert raters and achieved diagnostic accuracy approaching 100%. 2D PCA readily detects the transverse axis of the SC, allowing calculation of CR and relative rotation, while indentation is robustly calculated using convex hulls. Several additional shape parameters are also under

investigation including asymmetry indices to detect lateral compression and relative CSA to detect circumferential compression, but these were not necessary in this cohort. Automatic analysis is fast and straightforward using the free open-source Spinal Cord Toolbox (De Leener et al., 2017), and the only manual step is reviewing and editing the segmentation. Our results define normative data for each shape parameter across cervical intervertebral levels, and ROC analysis identified diagnostic thresholds that were close to 2 SDs from the mean of each metric. Many of our ASCC cases showed CSF intervening between the compressive process (e.g. disc osteophyte complex) and the ventral spinal cord surface, as the SC shifts posteriorly when the subject is supine. This indicates that the cord deformity is observed in the absence of visible compression, suggesting that shape analysis can detect dynamic SC compression, which has previously only been possible with flexion/extension MRI (Nouri et al., 2016).

4.4.3 **Contemplating the Definition of Myelopathy**

Dictionaries typically define myelopathy as “a disease or disorder of the spinal cord”, and our results suggest that individuals with ASCC meet this description. In contrast, clinicians have historically favoured functional criteria: the presence of neurological symptoms and signs that localize to the SC (Seidenwurm and Expert Panel on Neurologic, 2008). This clinical definition most likely originated due to the lack of diagnostic investigations that can accurately detect early pathological changes within the cord. It appears that symptoms and signs of myelopathy only emerge once a considerable degree of tissue injury occurs, and homeostatic mechanisms of neuroplasticity and behavioural adaptation may mask early changes. Technological advances have led to the emergence of *in vivo* diagnostic tools, including qMRI, that have the potential to surpass clinical assessments by taking direct measurements from the SC. Similar progress has been made in electrophysiology with the development of contact heat evoked potentials (CHEPs) (Jutzeler et al., 2017), which appear to be more sensitive than motor and sensory evoked potentials for myelopathy (Kerkovsky et al., 2012). As these tools become more sophisticated and refined, they will allow progressively earlier detection of tissue injury in this condition, in which the ground truth likely constitutes a continuum between normal and abnormal without a clear division, similar to degenerative processes in the aging brain.

4.4.4 **Clinical Implications**

Our results suggest that the widely held paradigm – that mild SC indentation and flattening represent "normal degenerative changes" – is incorrect. Rather, ASCC represents a highly prevalent preclinical diagnosis with microstructural tissue changes, akin to the pre-diabetic state of insulin resistance, and these patients are at risk for progression to clinical myelopathy. A prior study found that 8% of individuals with ASCC experience progression to symptomatic myelopathy at 1 year and 22.6% at 4 years, with risk factors including presence of radiculopathy, T2WI hyperintensity, or prolonged conduction on electrophysiology studies (Bednarik et al., 2008). Thus, individuals with ASCC should be educated about myelopathy symptoms periodically examined by a clinician. Unfortunately, patients often ignore early neurological symptoms, as was evident in two excluded subjects with evidence of mild DCM, of which they were not aware. Furthermore, primary care clinicians sometimes miss the diagnosis of DCM, as in one of our ASCC subjects that developed myelopathy, or diagnose it only after debilitating symptoms have developed, at which point surgical treatment rarely restores normal ambulation and hand function. Earlier diagnosis of DCM would allow earlier treatment, and surgery is associated with reduced morbidity in all severity categories including mild DCM (Fehlings et al., 2013). Preliminary results suggest that serial qMRI assessments may also be helpful in detecting progression of tissue injury (Martin et al., 2017d), and long-term clinical and qMRI monitoring of this cohort of ASCC subjects is planned. Multiparametric qMRI may also hold potential for earlier diagnosis of other spinal conditions, which share pathophysiological mechanisms of demyelination, axonal injury, gliosis, and atrophy (Wheeler-Kingshott et al., 2014).

4.4.5 **Limitations**

Quantitative shape analysis is dependent on an accurate SC segmentation, and manual editing of segmentations was necessary in most subjects. Automatic segmentation of the compressed SC is challenging due to anatomical distortion and reduced contrast with surrounding tissues, and alternative approaches are under investigation by the SCT developers. Shape analysis would be enhanced by using an optimized high-resolution T2WI acquisition, but our T2WI had only moderate resolution and frequently showed motion artifacts. Our recruitment of subjects by convenience sampling has potential for selection bias. Validation of our findings in a larger cohort would be beneficial to allow more accurate characterization of prevalence and rate of myelopathy development.

4.4.6 **Conclusions**

ASCC is a common age-related preclinical state that can be accurately and objectively diagnosed with automated analysis of SC morphology. This condition involves a similar pattern of macro- and microstructural changes as symptomatic DCM, representing subclinical tissue injury, and individuals with ASCC at an increased risk of myelopathy development. These results have important clinical implications, including the need to educate and monitor ASCC subjects for symptoms and signs of myelopathy, while offering the possibility of presymptomatic diagnosis and treatment of other spinal pathologies.

Chapter 5
Serial Monitoring of Disease Progression*

*This chapter is based upon a manuscript that is currently under review in Journal of Neurology, Neurosurgery, and Psychiatry. Permission will be sought once it is accepted for publication.

Patients with mild degenerative cervical myelopathy (DCM) are often managed non-operatively, and surgery is recommended if neurological progression occurs. However, detection of progression is often subjective. Quantitative MRI (qMRI) directly measures spinal cord (SC) tissue changes, detecting axonal injury, demyelination, and atrophy. This longitudinal study compares multiparametric qMRI with clinical measures of progression in non-operative DCM patients. 26 DCM patients were followed. Clinical data included modified Japanese Orthopedic Association (mJOA) and additional assessments. 3T qMRI data included cross sectional area, diffusion fractional anisotropy, magnetization transfer ratio, and T2*-weighted white/grey matter signal ratio, extracted from the compressed SC and above/below. Progression was defined as 1) patients' subjective impression, 2) 2-point mJOA decrease, 3) ≥3 clinical measures worsening ≥5%, 4) increased compression on MRI, or 5) ≥1 of 10 qMRI measures or composite score worsening ($p < 0.004$, corrected). Follow-up (13.5 ± 4.9 months) included mJOA in all 26 patients, MRI in 25, and clinical/qMRI in 22. 42.3% reported subjective worsening, compared with mJOA (11.5%), MRI (20%), comprehensive assessments (54.6%), and qMRI (68.2%). Relative to subjective worsening, qMRI showed 100% sensitivity and 53.3% specificity compared with comprehensive assessments (75%, 60%), mJOA (27.3%, 100%), and MRI (18.2%, 81.3%). A decision-making algorithm incorporating qMRI identified progression and recommended surgery for 11 subjects (42.3%). Quantitative MRI detected myelopathic progression more sensitively and congruently with patients' perceptions than other assessments. Neuroplasticity and behavioural adaptation may mask incremental tissue injury. qMRI was implemented to inform decision-making for individual patients, representing a major advance toward clinical translation.

5.1 INTRODUCTION

5.1.1 Degenerative Cervical Myelopathy

Degenerative cervical myelopathy (DCM) is among the most common causes of spinal cord (SC) dysfunction, involving age-related degeneration of the discs, ligaments, and vertebrae leading to extrinsic compression and dynamic injury (Nouri et al., 2015b, Benzel et al., 1991). Low quality evidence suggests that 20-62% of DCM subjects will deteriorate over 3-7 years (Matz et al., 2009, Karadimas et al., 2013, Rhee et al., 2013). Non-operative treatments such as cervical collars and physiotherapy are sometimes employed, but no evidence exists to support their benefit (Rhee et al., 2013). Decompressive surgery not only halts neurological deterioration, it improves outcomes and is the recommended treatment for moderate/severe DCM in recent clinical practice guidelines (CPGs) (Fehlings et al., 2013, Fehlings et al., 2017). However, optimal management of mild DCM is controversial; surgery is a treatment option, but many patients are managed non-operatively and monitored periodically, in which case surgery is recommended if neurological deterioration occurs (Fehlings et al., 2017).

5.1.2 A Novel Approach to Monitoring for Progression

An array of MRI techniques have emerged that measure aspects of SC microstructure and tissue injury (Stroman et al., 2014). Cross-sectional area (CSA) measures the degree of SC compression in DCM, and atrophy in uncompressed regions. The diffusion tensor imaging (DTI) metric fractional anisotropy (FA) reflects axonal injury and demyelination. Magnetization transfer ratio (MTR) is a more specific measure of myelin quantity. T2*-weighted imaging (T2*WI) shows strong contrast between white and grey matter, and the white matter to grey matter signal intensity ratio (T2*WI WM/GM) reflects demyelination, gliosis, calcium, and iron changes (Martin et al., 2017c, Cohen-Adad, 2014). We developed a clinically feasible multiparametric quantitative MRI (qMRI) protocol that collects these data across the cervical SC, producing 10 measures of tissue injury that correlate with myelopathic impairment in DCM (Martin et al., 2017b, Martin et al., 2017c).

In the current study, we compare several methods of detecting myelopathic progression, including 1) patients' subjective impression of worsening, 2) mJOA, 3) comprehensive clinical assessments, 4) anatomical MRI, 5) multiparametric qMRI. We hypothesize that qMRI will

show a higher rate of progression than other measures due to the effects of neuroplasticity and behavioural adaption, which we suspect compensate for progressive tissue injury. Finally, we develop a practical framework for monitoring DCM patients and describe its initial implementation.

5.2 MATERIALS AND METHODS

5.2.1 Study Design and Subjects

This prospective longitudinal study received institutional approval from the University Health Network (Toronto, Ontario, Canada) and all participants provided written informed consent. Fifty-eight DCM patients were enrolled, as previously described.(Martin et al., 2017c) Among this cohort, 26 patients were initially managed non-operatively and reassessed approximately 12 months later, depending on subject availability.

5.2.2 Clinical Assessments

A battery of clinical assessments were administered by a clinician-scientist (Allan R. Martin, Sukhvinder Kalsi-Ryan; Table 5.1). To reduce inter-observer variability, scripts and agreed-upon criteria to interpret answers were used. This included a modified version of mJOA (Table 5.2) to simplify language and allow substitute findings, such as worsened handwriting for mild upper extremity motor impairment. The percent change in clinical measures was calculated using the maximum score as the denominator for finite scales (e.g. 18 for mJOA) or the baseline score for infinite scales (e.g. grip strength).

Clinical Measure	Description
mJOA Score (Benzel et al., 1991)	18-point ordinal scale of neurological impairment including subscores for upper extremity motor function, lower extremity motor function (gait), upper extremity sensory function, and urinary function
QuickDASH (Beaton et al., 2005)	44-point interval scale for upper limb function, pain, and effects on quality of life
ISNCSCI UEMS	50-point interval scale for neurological function of the upper limb

(Kirshblum et al., 2011)	(power in 10 myotomes), administered separately for each upper limb
JAMAR Grip Dynamometer (Hamilton et al., 1992)	Measures maximal grip force in each hand; calculated as average of 3 measurements
GRASSP-M (Kalsi-Ryan et al., 2012)	Dexterity testing of each hand to place four metallic nuts on screws, scored for precision, grasp, number of drops, and completeness (9 points), and time to completion
Monofilament Sensory Testing (Ellaway and Catley, 2013)	Semmes Weinstein monofilaments applied to C6, C7, and C8 dermatomes of each hand to measure sensation
Berg Balance Scale (Berg et al., 1992)	56-point interval scale to measure balance while standing, transferring, and performing simple tasks
GaitRITE (Webster et al., 2005)	Quantitative analysis of gait using an electronic pressure mat, measured with gait stability ratio (single stance time / double stance time)

Table 5.1: Battery of Clinical Assessments for Degenerative Cervical Myelopathy. Various clinical assessments were selected to comprehensively assess common neurological and functional impairments that occur in cervical myelopathy, including fine motor dysfunction of the hands, weakness, numbness, gait imbalance, and urinary difficulties.

Category	**Score**	**Description**
Upper Extremity Motor Subscore (/5)	0	Unable to move hands
	1	Unable to eat with a spoon but able to move hands
	2	Unable to button a shirt but able to eat with a spoon

	3	Able to button a shirt with great difficulty
	4	Able to button a shirt with mild difficult OR other mild fine motor dysfunction (marked handwriting change, frequent dropping of objects, difficult clasping jewelry, etc.)
	5	Normal hand coordination
Lower Extremity Subscore (/7)	0	Complete loss of movement and sensation
	1	Complete loss of movement, some sensation present
	2	Inability to walk but some movement
	3	Able to walk on flat ground with walking aid
	4	Able to walk without walking aid, but must hold a handrail on stairs
	5	Moderate to severe walking imbalance but able to perform stairs without handrail
	6	Mild imbalance when standing OR walking
	7	Normal walking
Upper Extremity Sensory Subscore (/3)	0	Complete loss of hand sensation
	1	Severe loss of hand sensation OR pain
	2	Mild loss of hand sensation
	3	Normal hand sensation

Urinary Function Subscore (/3)	0	Inability to urinate voluntarily (requiring catheterization)
	1	Frequent urinary incontinence (more than once per month)
	2	Urinary urgency OR occasional stress incontinence (less than once per month)
	3	Normal urinary function

Table 5.2: Modified Japanese Orthopedic Association (mJOA) Score. The mJOA is an 18 point score of functional disability specific to cervical myelopathy, including upper extremity motor subscore, lower extremity subscore, upper extremity sensory subscore, and sphincter function. The descriptions of each score are modified slightly from Benzel et al. (1991).

5.2.3 **MRI Acquisitions**

All imaging was performed on the same clinical scanner (3T GE), including T2-weighted imaging (T2WI), DTI, magnetization transfer (MT), and T2*WI in 30-35 minutes, as previously described (Martin et al., 2017b).

5.2.4 **Image Analysis**

Images were reviewed by 2 raters (ARM, AN) and excluded if they showed motion or other artifacts, along with corresponding images from the comparison examination. T2WI and T2*WI images were reviewed to identify T2WI hyperintensity and record levels with extrinsic SC compression, defined as indentation, flattening, torsion, or circumferential compression. The maximally compressed level (MCL) was subjectively determined, with discrepancies resolved by consensus. When the MCL changed between baseline and follow-up, the new level was used for comparisons.

Quantitative image analysis was performed with the Spinal Cord Toolbox (SCT) v3.0 (De Leener et al., 2017). Automatic SC segmentation was performed, and segmentation masks were reviewed and manually corrected if necessary (Figure 5.1). Segmentation editing was blinded by

anonymizing and randomizing baseline and follow-up scans. CSA was calculated from the T2*WI segmentation (or T2WI segmentation if T2*WI was excluded). Registration to the SCT template was performed for each dataset and FA, MTR, and T2*WI WM/GM were extracted from WM in each slice. Metrics were age-corrected based on linear regression in 40 healthy subjects (CSA: β=-0.0867 mm^2/year, FA: β =-0.00121/year, MTR: β=-0.0815 %/year, T2*WI WM/GM: β=0.000740/year) (Martin et al., 2017b). Corrected metrics were averaged across rostral (C1-C3) and caudal (C6-C7) levels, excluding compressed slices, and at MCL using a single slice for CSA or 3 slices for FA, MTR, and T2*WI WM/GM (Martin et al., 2017c). This approach produces 12 metrics, of which 10 previously demonstrated significant clinical correlations in DCM (Martin et al., 2017c), leading to exclusion of caudal CSA and MTR from this study.

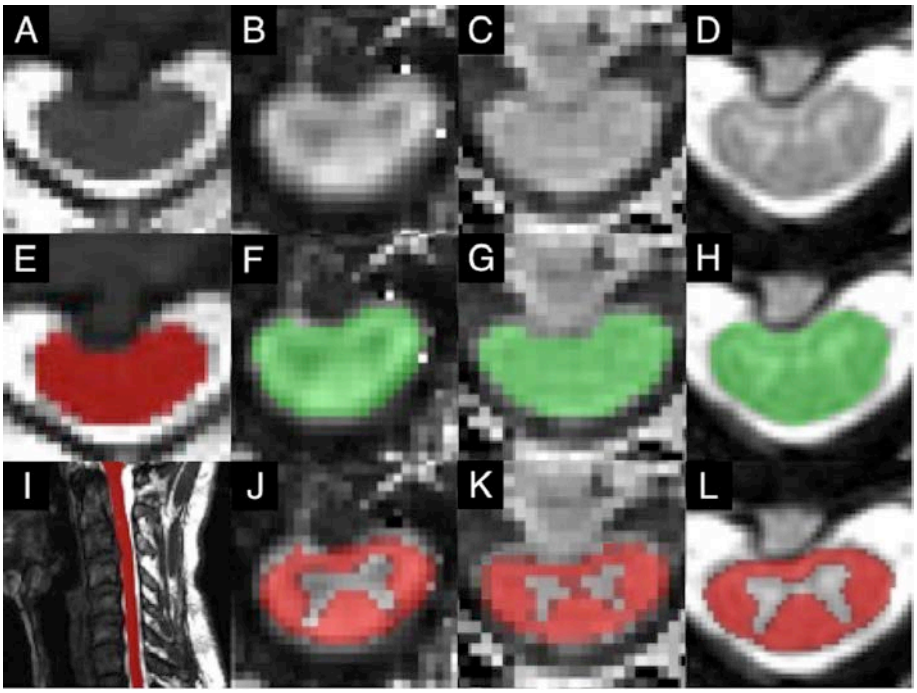

Figure 5.1: Representative Images. T2-weighted image (A) of C3-4 disc herniation indenting the spinal cord with corresponding DTI FA map (B), MTR map (C), and T_2*-weighted image (D). Spinal cord segmentations are displayed (E-I) and the registered SCT white matter template is shown for FA, MTR, and T2*w images (J-L).

5.2.5 **Statistical Analysis**

Overall α was set to 0.05. Continuous data were summarized by mean ± standard deviation (SD). Group deterioration at follow-up was analyzed with single-tailed paired t tests. 95% confidence intervals (CIs) of proportions were calculated using the Wilson method (continuity corrected). qMRI progression was tested against the null hypothesis that changes were due to measurement error (assuming normal distribution and SD = $\sqrt{2}$ * standard error of measurement, SEM), using z scores (Bland and Altman, 1999). SEM of FA, MTR, and T2*WI WM/GM were derived from our previous reliability study, and SEM of CSA was calculated using T2*WI data from 5 healthy and 11 DCM subjects (Martin et al., 2017b). For rostral and caudal measures, pooled estimates of SEM were derived from healthy and DCM subjects, whereas MCL SEM values were derived from DCM subjects only (Table 5.3). Z scores were also averaged to yield an unweighted composite score (null hypothesis: *t* distribution, 10 degrees of freedom, d.f.s, standard error = 1/ $\sqrt{10}$).

5.2.6 **Myelopathic Progression**

Patients were asked if their neurological symptoms were better, the same, maybe worse (defining borderline progression), or worse (defining progression) than at the initial assessment. For mJOA, progression was defined as a decrease of ≥ 2 points and borderline progression as a 1-point decline (Bartels et al., 2010). For comprehensive clinical assessments, progression was defined as ≥ 3 measures worsening by ≥ 5%, and borderline progression as 1-2 measures worsening. qMRI progression was defined as z score < -2.65 for any single metric or composite score: t_{10} < - 3.30 (p=0.004, single-tailed, Bonferroni corrected). Patients' subjective impression was used as the clinical case definition of myelopathic progression, and sensitivity, specificity, and Youden's Index (YI) were calculated for other measures (based on available follow-up events for each measure).

qMRI Metric	Level	Mean Difference	P Value	SEM	Individuals with Progression
CSA	Rostral	-0.34 ± 1.08	0.07	0.95	0

(mm^2)	MCL	-3.5 ± 5.4	0.003	2.94	3
FA	Rostral	-0.027 ± 0.037	0.001	0.018	6
	MCL	-0.038 ± 0.050	0.0007	0.029	4
	Caudal	-0.016 ± 0.049	0.06	0.025	4
T2*WI WM/GM	Rostral	+0.006 ± 0.018	0.09	0.008	4
	MCL	+0.005 ± 0.039	0.21	0.034	0
	Caudal	+0.012 ± 0.033	0.03	0.022	3
MTR (%)	Rostral	-0.80 ± 3.2	0.12	1.26	2
	MCL	-1.1 ± 2.8	0.03	3.10	0
Composite Score (t_{10})		-2.2 ± 2.2	0.00004	0.316	7

Table 5.3: Summary of Age-Corrected Quantitative MRI Metrics. Group results are displayed for the qMRI metric differences between baseline and follow-up, reported as mean ± SD. P values are reported for single-tailed paired t tests. SEM values are derived from our previous reliability study, and the SEM of CSA was measured in 5 healthy subjects and 11 DCM patients (Martin et al., 2017b). The composite score is calculated as an average of z scores for each metric, which is expected to follow a t distribution with 10 d.f.s under the null hypothesis. The number of individuals with progression detected by each measure is displayed ($z < -2.65$ or $t_{10} < -3.30$, $p<0.004$, one-tailed, corrected for multiple comparisons). CSA: cross-sectional area; d.f.s: degrees of freedome; FA: fractional anisotropy; MCL: maximally compressed level; MTR: magnetization transfer ratio; SEM: standard error of measurement

5.3 RESULTS:

5.3.1 Subjects

The cohort was aged 57.6 ± 9.1, included 15 men and 11 women, and baseline mJOA score was 15.7 ± 1.3 (21 mild, 5 moderate severity). Follow-up data included subjective impression and mJOA score for all 26 subjects (100%), anatomical MRI for 25 subjects (96.2%), and comprehensive clinical and qMRI data for 22 subjects (84.6%) (Table 5.4). One subject had two complete follow-up assessments due to interim subjective deterioration. Among four subjects without complete follow-up, three (11.5%) experienced rapid progression (subjectively worse, mJOA declined ≥ 2 points) requiring urgent surgery and the remaining subject reported stable symptoms and mJOA but declined follow-up.

#	Age, Sex	mJOA	FU (m)	Subjective	FU mJOA	Comprehensive Clinical Assessment; Confounding Factors	Anatomical MRI	Quantitative MRI Assessment
1	56, M	15	2	Worse	Declined (-3)	N/A	Stable	N/A
2	52, F	16	10	Worse	Declined (-2)	N/A	Stable	N/A
3	60, F	15	10	Worse	Declined (-2)	N/A	Stable	N/A
4	47, M	15	15	Worse	Borderline	Declined: mJOA (-1), R grip (-9%), L grip (-5%), L arm power (-8%)	Declined: increased compression at C5-6	Declined: CSA_{MCL} (-13mm^2), FA_{MCL} (-0.089), FA_{Caudal} (-0.084)
5	50, M	17	13	Better	Stable	Borderline: L grip (-18%), L arm power (-6%); L elbow injury**	Stable	Declined: $MTR_{Rostral}$ (-3.7%)
6	60, M	17	13	Maybe worse	Borderline	Declined: mJOA (-1), R grip (-9%), L grip (-7%), L hand sensation (-25%)	Declined: increased compression at C5-6	Declined: Composite (z=-3.9), FA_{Caudal} (-0.086), T2* WM/GM_{Caudal} (+0.078)
7	60, M	16	12	Same	Stable	Stable	Stable	Stable

8	69, F	16	13	Maybe worse	Stable	Declined: L grip (-18%), Berg Balance (-9%), R hand dexterity (-23%); lumbar radiculopathy, psoriatic arthritis (hands) and knee replacement**	Stable	Stable
9	59, F	17	14	Same (worse but recovered)	Stable	Declined: R grip (-6%), L arm power (-6%), R hand dexterity (-29%), L hand dexterity (-16%), gait stability (-11%)	Stable	Declined: T2* WM/GM_{Caudal} (+0.060)
10	55, F	15	17	Worse	Stable	Declined: R grip (-30%), L hand dexterity (-43%), gait stability (-6%); rheumatoid arthritis**	Declined: increased compression at C5-6	Declined: CSA_{MCL} (-12mm^2),
11	54, F	17	14	Same	Borderline	Borderline: mJOA (-1)	Stable	Stable
12	56, F	16	12	Same	Stable	Borderline: QuickDASH (-10%), gait stability (-23%)	Stable	Stable
2nd Follow-up			26	Worse	Borderline	Declined: mJOA (-1), QuickDASH (-10%), R grip (-15%), L grip (-26%), gait stability (-25%)	Stable	Declined: T2*WI WM/$GM_{Rostral}$ (+0.022)
13	59, F	13	13	Worse	Borderline	Declined: mJOA (-1), R grip (-10%), L grip (-12%)	Stable	Declined: Composite (z=-6.4), $FA_{Rostral}$ (-0.058), FA_{MCL} (-0.090), FA_{Caudal} (-0.136), $MTR_{Rostral}$ (-3.5%)
14	81, M	17	12	Same	Stable	Declined: R grip (-27%), L grip (-22%), L hand dexterity (-18%)	Declined: increased compression at C5-6	Declined: Composite (z=-5.0), $FA_{Rostral}$ (-0.066), FA_{MCL} (-0.106)
15	69, M	17	13	Worse	Stable	Borderline: L grip (-7%), L hand dexterity (-11%)	Stable	Declined: Composite (z=-5.0), CSA_{MCL} (-11mm^2), $FA_{Rostral}$ (-0.111), FA_{MCL} (-0.181)
16	69, M	17	13	Same	Stable	Declined: L grip (-13%), L arm power (-6%), L hand dexterity (-6%); L hand fasciitis**	Stable	Stable
17	48, M	14	12	Worse	Stable	Borderline: L grip (-12%), R hand sensation (-8%)	Stable	Declined: $FA_{Rostral}$ (-0.059)
18	49,	17	17	Maybe worse	Borderline	Declined: mJOA (-1), QuickDASH (-5%), R grip (-5%),	Stable	Stable

	F					L grip (-8%); severe back pain**		
19	61, M	14	13	Worse	Stable	Declined: QuickDASH (-10%), L grip (-6%), R sensation (-8%), L sensation (-8%)	Stable	Declined: Composite (z=-4.1), $MTR_{Rostral}$ (-3.8%), T2* $WM/GM_{Rostral}$ (+0.031)
20	61, M	16	12	Same	Stable	Borderline: QuickDASH (-10%)	Stable	Declined: Composite (z=-4.7), $FA_{Rostral}$ (-0.072), T2* $WM/GM_{Rostral}$ (+0.024)
21	58, M	14	15	Same	Stable	Stable; mild TBI with post-concussion symptoms**	Stable	Declined: FA_{Caudal} (-0.078)
22	49, M	14	11	Worse	Borderline	Declined: mJOA (-1), QuickDASH (-10%), Berg Balance (-7%)	Stable	Declined: Composite (z=-3.7), T2* $WM/GM_{Rostral}$ (+0.041)
23	54, M	17	6	Same	Stable	Borderline: L hand dexterity (-5%), gait stability (-5%)	Stable	Declined: $FA_{Rostral}$ (-0.049), T2* WM/GM_{Caudal} (+0.069)
24	54, F	15	27	Better	Improved (+3)	Borderline: R grip (-23%), L grip (-10%); MVA with shoulder and neck injury**	Stable	Stable
25	45, F	17	15	Better	Stable	Stable	Declined: new compression at C4-5	Stable
26	76, M	15	6	Same	Stable	N/A	N/A	N/A

Table 5.4: Summary of DCM Patient Characteristics, Clinical Changes, and Quantitative MRI Changes at Follow-up. Subject demographics include baseline age, sex, mJOA, and time to follow-up (in months). Patients subjectively rated their neurological symptoms as same/better (green), maybe worse (yellow), or worse (red). Change in mJOA was categorized as stable/improved (green), borderline declined (1-point decrease, yellow), or declined (≥2-point decrease, red). Comprehensive clinical assessments were rated as stable (green) if no measures declined, borderline declined (yellow) if 1 or 2 clinical measures worsened by ≥5%, or declined (red) if ≥3 clinical measures worsened. Anatomical MRI was rated as declined (red) new/worsened SC compression was present at any level, and stable (green) otherwise. Quantitative MRI was rated as stable (green) if no measures showed statistically significant worsening, borderline declined if 1 measure worsened, and declined if ≥2 measures worsened.

Subject 12 had 2 follow-up assessments, experiencing subjective deterioration after the 1st follow-up.

5.3.2 **Clinical Measures of Myelopathy**

Follow-up duration was 13.5 ± 4.9 months (range 6-27). Eleven patients (42.3%, 95% CI: 24.0-62.8%) reported subjective neurological worsening, 3 (11.5%) reported being “maybe worse”, and 12 (46.2%) reported feeling the same or better (Figure 5.2, Table 5.4). Based on mJOA, 3 subjects (11.5%, 95% CI: 3.0-31.3%) showed clinical progression and 9 (34.6%) had borderline progression. mJOA detected deterioration in 3/11 follow-up events with subjective worsening (sensitivity=27.3%, specificity=100%, YI=27.3%).

Among 22 subjects with complete follow-up data, comprehensive clinical assessments identified progression in 12 subjects (54.6%, 95% CI: 32.7-74.9%), including 6/8 follow-ups with subjective deterioration (sensitivity=75%, specificity=60%, YI=35%). Abnormal results included grip strength (15 subjects, 7 bilateral), hand dexterity (7 subjects, 1 bilateral), mJOA (7), QuickDASH (6), gait stability ratio (5), arm power (4 subjects), sensation (3 subjects, 1 bilateral), and Berg Balance scale (2). Seven subjects had physical injuries/conditions that potentially affected follow-up clinical assessments.

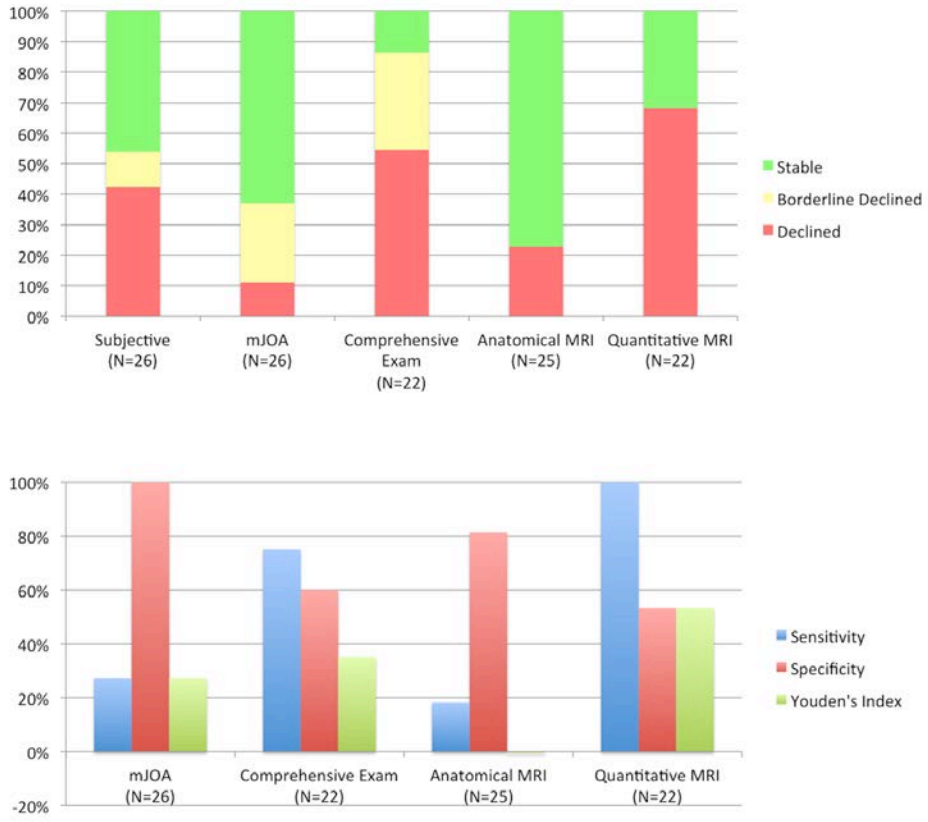

Figure 5.2: Comparison of Methods to Monitor for Myelopathic Progression in DCM. Top panel: The bar graphs display the fraction of subjects that are deemed to be stable (green), borderline declined (yellow), or declined (red) for each clinical and MRI method of monitoring. For mJOA, a 1-point decreases are considered borderline and ≥ 2-point decreases are considered declined. For comprehensive examinations, subjects that have 1 or 2 measures that worsen ≥ 5% are considered borderline and worsening of ≥ 3 measures is considered declined. For anatomical MRI, any new or increased compression that can be visually appreciated is considered declined. For qMRI, deterioration of ≥ 1 measure is considered declined. DCM: degenerative cervical myelopathy; mJOA: modified Japanese Orthopedic Association. Bottom panel: diagnostic accuracy of each measure was measured as sensitivity, specificity, and Youden's Index relative to patients' subjective impression, which was selected as the clinical case definition.

5.3.3 **Anatomical Imaging**

Baseline anatomical images showed spinal cord compression at a total of 79 intervertebral levels (3.0 levels/subject), with 21/26 subjects having multilevel SC compression. T2WI hyperintensity was present in 14/26 subjects. At follow-up, two subjects had new SC compression (total: 3 levels) and compression resolved at one level in another subject. The degree of cord compression also increased three subjects (total: 4 levels). No changes in T2WI hyperintensity were observed. Overall, five subjects had progression on anatomical imaging (20%, 95% CI: 7.6-41.3%), including 2/11 events with subjective progression (sensitivity=18.2%, specificity=81.3%, YI=-0.5%).

5.3.4 **Quantitative MRI**

All DTI and MT datasets were of acceptable quality, but two T2*WI datasets were degraded by motion artifact and excluded. Individual slices were excluded 24/585 DTI, 17/585 MT, and 11/533 T2*WI images. Analysis was successful for all remaining data, including accurate registration to the SCT atlas.

At the group level, all age-corrected qMRI metrics deviated pathologically at follow-up, including significant changes in five measures (CSA_{MCL}, $FA_{Rostral}$, FA_{MCL}, T2*WI WM/GM_{Caudal}, and MTR_{MCL}) and trends in three ($CSA_{Rostral}$, FA_{Caudal}, T2*WI $WM/GM_{Rostral}$(Table 5.3). Composite score showed the strongest group change (p=0.00004).

In individual patients, qMRI progression occurred in 15/22 (68.2%, 95% CI: 45.1-85.3%) (Table 5.4; Figure 5.3). $FA_{Rostral}$ was the most sensitive single qMRI measure, identifying progression in six subjects, while seven subjects deteriorated on composite score. All eight cases of subjective worsening were detected by qMRI (sensitivity=100%, specificity=53.3%). qMRI results showed statistical improvements (potential outliers) in 2/247 comparisons (0.8%).

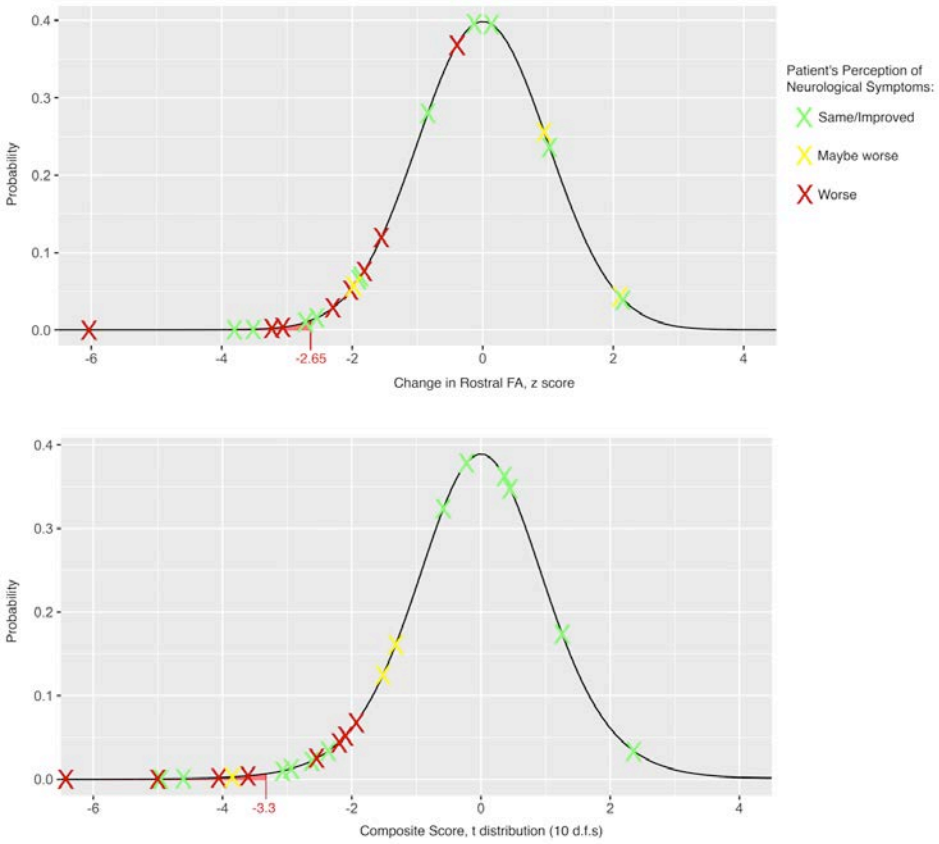

Figure 5.3: Distribution of Observed Changes in Quantitative MRI (qMRI) Metrics at Follow-up. The observed changes in age-corrected qMRI metrics for individual subjects (displayed as Xs) are plotted in relation to the expected distribution based on the null hypothesis of no change, using test-retest reliability data to characterize the SEM and calculate z scores. The results for $FA_{Rostral}$ (top panel) are overlaid on a normal distribution. The composite score is calculated as an average of z scores for each metric, which is overlaid on a t distribution with 10 d.f.s (bottom panel). Each result is colour-coded based on the patient's subjective impression of neurological worsening (red: worse, yellow: maybe worse, and green: the same or better). CSA: cross-sectional area; d.f.s: degrees of freedom; FA: fractional anisotropy; MCL: maximally compressed level; PDF: probability density function, SEM: standard error of measurement.

5.3.5 **Clinical Implementation**

Based on the results, a practical definition of myelopathic progression was developed: subjective progression of neurological symptoms and any objective sign of progression, with the latter including mJOA, comprehensive clinical assessments, anatomical MRI, or qMRI. (Figure 5.4). Possible myelopathic progression was defined as either subjective or objective worsening. Using these definitions, 11 subjects had progression (42.3%, 95% CI: 24.0-62.8%), seven (30.8%) had possible progression, and nine were stable (including three with clinical deterioration that was attributed to another cause). Fifteen subjects were invited for reassessment in clinic, with the decision-making algorithm being used to guide surgical recommendations, in addition to patient-specific factors such as preferences and goals. The remaining seven subjects were educated about myelopathy symptoms and encouraged to contact their surgeon if subjective progression occurred. To date, two patients have been reassessed in clinic and are planned for operative treatment, seven have pending visits, and six declined, stating they are comfortable monitoring their symptoms.

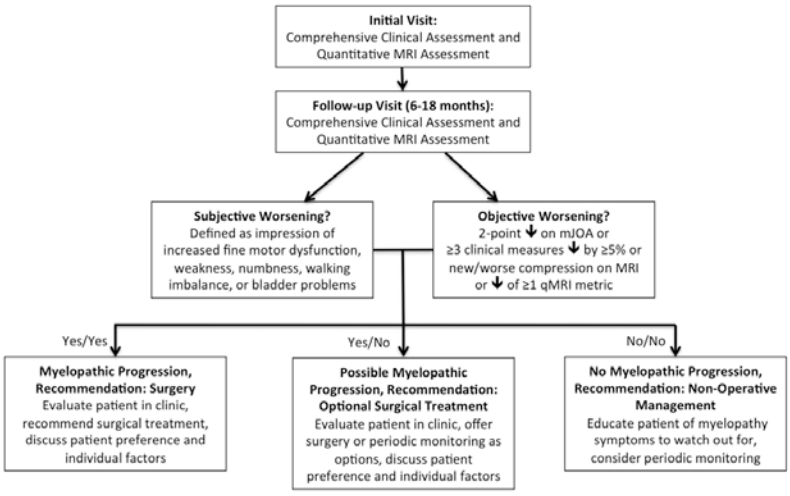

Figure 5.4: Decision-Making Algorithm for Degenerative Cervical Myelopathy Patients Initially Managed Non-operatively. The decision-making algorithm requires clinical and

quantitative MRI data collection at 2 time-points, and takes into account the patient's subjective impression of worsening and objective measures of progression, including mJOA, a battery of clinical assessments, anatomical MRI, or quantitative MRI.

5.4 DISCUSSION

5.4.1 Interpretation of Results

Myelopathic progression was more frequently detected with multiparametric qMRI than by subjective impression, clinical assessments, or anatomical imaging. Furthermore, qMRI progression was more congruent (via Youden's Index) with subjective progression than other measures, indicating that macro- and microstructural changes captured by qMRI are clinically meaningful. Eight qMRI metrics demonstrated significant deterioration in either group or individual analyses. The composite score showed increased statistical power, which could be further strengthened using weightings (e.g. logistic regression), but this was not performed to avoid overfitting, given our small sample. Other groups have developed similar multiparametric protocols (Oh et al., 2013b, Samson et al., 2013, Taso et al., 2016), and our data suggest that this approach overcomes the limitations of single qMRI techniques, such as modest reliability. Two potential outliers (improvements of $z > 2.65$) were observed, close to the expected value of 1.1, validating our statistical approach. These changes may represent tissue regeneration (e.g. remyelination), or alternatively these and some qMRI decreases could be spurious due to sampling error, artifacts, analysis errors, or inaccurate estimation of SEM. The ground truth regarding progression is unknown, but qMRI correlated well with other measures and multiple qMRI metrics showed progression in 9/15 subjects. Patients' subjective impression was used as the clinical case definition, in the absence of a gold standard. However, this method is affected by recall bias, and one subject clearly had worsened gait and hand dexterity but reported feeling "the same", highlighting that patients are often unaware of neurological changes. Two-point mJOA changes were specific but not sensitive for progression, whereas comprehensive clinical assessments were far more sensitive but less specific, primary due to confounding physical ailments (7 subjects) that commonly affect older individuals. Anatomical MRI was not sensitive for progression, but new/worsened compression was specific. Visual assessment of compression on anatomical MRI overlaps with CSA_{MCL} measurement, which in our previous study showed stronger correlation with clinical impairment than any other qMRI measure (Martin et al.,

2017c); thus, we suggest that new/worsened compression should be considered evidence of progression (Figure 5.4).

Overall, qMRI results were sufficiently convincing to incorporate into surgical decision-making, in addition to comprehensive clinical data and anatomical MRI. The proposed algorithm builds upon recent CPGs that recommend surgery when myelopathic progression occurs, combining patients' perceptions with objective assessments. However, the final decision regarding surgery depends on patient preference and other factors, requiring a fulsome discussion to balance risks and benefits and select the optimal treatment. The initial implementation of this algorithm has led to surgical treatment in two patients; both showed only 1-point decreases in mJOA and minimal neurological worsening, which many surgeons would manage conservatively, but qMRI helped to confirm progression. qMRI also provided evidence against myelopathy in two subjects that felt "maybe worse" and declined clinically, but had confounding physical ailments. This study represents, to the authors' knowledge, the first instance in which qMRI measurement of SC integrity has informed decision-making in individual patients, constituting an important step toward clinical translation. Longitudinal monitoring for progression is an attractive first use of qMRI because it circumvents the normal inter-subject variability of these data, which limit qMRI's utility for diagnosis and prognostication (Martin et al., 2016, Martin et al., 2017b).

5.4.2 **Natural History**

Our results suggest that DCM is less benign than previously thought (Karadimas et al., 2013). mJOA showed a rate of progression of 3.0-31.3%, consistent with previous reports (adjusting for follow-up duration) (Matsumoto et al., 2000, Matsumoto et al., 2001, Shimomura et al., 2007, Sumi et al., 2012, Yoshimatsu et al., 2001, Kadanka et al., 2000, Kadanka et al., 2011). In contrast, progression with our clinical battery was 32.7-74.9%, in spite of missing follow-up data in three subjects that deteriorated badly. This difference was expected, as our clinical instruments were selected to detect subtle myelopathic changes (Kalsi-Ryan et al., 2013b). Quantitative MRI showed even higher frequency of progression (40.8-82.0%). These results cast doubt that the natural history of myelopathy has been accurately characterized, and larger prospective studies are needed with clear definitions of progression and comprehensive assessments. If the natural history is, in fact, as aggressive as our estimates suggest, early surgery would be indicated in mild DCM. However, further research is needed to determine the impact of subtle progression on

1) quality of life and 2) the risk of more substantial deterioration. Long-term monitoring of non-operative subjects will determine if isolated qMRI progression is a precursor to physical deterioration.

5.4.3 **The Art and Science of Clinical Assessment**

The neurological examination is among the most elegant skills in medicine, but it includes subjective elements and varies between practitioners, making it an art rather than a science. In contrast, clinical research is becoming increasingly quantitative and standardized, driven by the fields of epidemiology, biostatistics, and clinical measurement (Altman, 2009). Myelopathy can present variably, and the design of valid, reliable, and responsive instruments is challenging. mJOA is easy to administer and provides a useful summary measure, but lacks sensitivity to detect subtle changes (Fehlings et al., 2013). Furthermore, one-point changes in mJOA are probably not trustworthy, based on one small reliability study (Bartels et al., 2010). Thus, mJOA is not adequate as a standalone measure for detecting progression, and broader clinical data are needed. The neurological impairments in cervical myelopathy include gait imbalance, hand incoordination, sensory dysfunction, weakness (e.g. hand intrinsics), and bladder dysfunction, which are all captured in our comprehensive clinical assessments. Grip strength was the most sensitive measure of progression, which has high inter-subject variability but excellent within-subject reliability, making it ideal for longitudinal monitoring (Hamilton et al., 1992). Decreases in hand dexterity were also often encountered, which involved judging subjects' precision, grasp, and speed of tightening metallic nuts on screws (Kalsi-Ryan et al., 2012). QuickDASH, a questionnaire of upper limb function (Beaton et al., 2005), frequently showed progression, but it is not specific to myelopathic impairment. Gait impairment in DCM primarily involves imbalance, which is difficult to measure, and quantitative analysis with GAITRite may offer greater sensitivity than the 30-meter walk test (Webster et al., 2005). However, quantitative gait analysis produces dozens of parameters, and further investigation is needed to determine if gait stability ratio is the optimal measure. Quantitative standardized clinical assessments are needed to enable precise quantification of myelopathic impairment (i.e. "personalized medicine"), which will allow more informed treatment decisions and greater standardization of care.

5.4.4 Neuroplasticity and Behavioural Adaption May Mask Progressive Tissue Injury

Direct measurement of spinal cord integrity with qMRI is appealing because it avoids the challenges of clinical measurement, which assess injury to the SC indirectly. qMRI showed a higher rate of progression than clinical measures, suggesting that homeostatic mechanisms act to preserve normal function in the context of progressive tissue injury. Physical assessments (strength, dexterity) showed higher rates of progression than self-reported functional measures (mJOA, QuickDASH), which may be related to behavioural adaption, recall bias, and psychological denial. DCM patients typically alter their grasp and gait, often unconsciously, to maintain function despite incoordination and hyperactive reflexes. Furthermore, deterioration of low-level physical functions (e.g. grip strength) occurred more often than higher-level functions (gait, dexterity) that involve more complex neurological systems, potentially due to neuroplasticity (Pascual-Leone et al., 2005, Cadotte et al., 2012a). Complex neural circuits show more plasticity than simple circuits, such as spinal reflexes, due to the number of neurons and synapses involved (Pascual-Leone et al., 2005). However, our data are only suggestive of this concept; histopathological studies that correlate qMRI measurements with actual tissue changes are needed to fully elucidate these mechanisms. However, other qMRI techniques such as functional MRI have provided similar evidence of neuroplasticity in spinal cord injury (SCI) and may yield further insights as they become more refined (Cadotte et al., 2012a).

5.4.5 Clinical Translation of Quantitative Spinal Cord MRI

The field of SC qMRI has produced numerous technical advances and encouraging results, but research to date has mostly involved preliminary investigations and group analyses (Martin et al., 2016). However, notable exceptions have recently emerged. Li *et al.* (2014) applied DTI to diagnose the symptomatic level in patients with multilevel DCM, which showed high diagnostic accuracy when combined with compression ratio and could help target surgical treatment to a single level, along with clinical and electrophysiology methods. Egger *et al.* (2016) applied DTI tractography to differentiate between inflammatory and neoplastic intramedullary SC lesions, which could help avoid unnecessary biopsies. However, further research is necessary to determine if these approaches can be successfully implemented in clinical practice. Furthermore, many qMRI studies have employed acquisition techniques that are not suitable for clinical translation, due to their complexity, lack of portability, and lengthy scan times. To address these

issues, we developed a DTI, MT, and T2*WI protocol that requires approximately 20 minutes and employs standard pulse sequences and hardware (Martin et al., 2017b). At this point, the major barrier to clinical translation may have shifted to qMRI analysis, as busy clinicians are unlikely to adopt cumbersome methods. In response, tools such as the free, open-source SCT can automate analysis and extract metrics from the SC, WM, GM, and individual tracts (De Leener et al., 2017). However, automatic SC segmentation is a difficult task when compression distorts SC anatomy and reduces contrast with surrounding tissues, and further work is needed to address this challenge. Overall, this study represents an important step toward clinical translation, but additional well-designed studies are needed with low risk of bias, clinically feasible methods, and applications for individual patients. Then, finally, knowledge translation efforts will be necessary to disseminate information, promote uptake, and implement these techniques into widespread clinical use.

5.4.6 **Limitations**

This study involved a relatively small sample, and larger studies would be beneficial to validate our results and more accurately characterize test-retest reliability, relationships with age, and the natural history of DCM. The accuracy of CSA measurement could likely be improved with high-resolution T2WI using a different sequence that is less affected by motion. DTI with cardiac triggering may slightly improve reliability, based on previous data (Martin et al., 2017b). We assumed that qMRI measurement errors were normally distributed, but this is potentially incorrect. The methods to detect myelopathic progression used in this study require considerable resources (MRI, clinical tools, expertise) that may not be feasible to implement in some clinical settings, highlighting the importance of developing simple accurate clinical assessments for myelopathy. Finally, our decision-making algorithm is an initial attempt at rational use of these novel assessments, but should be refined as greater experience is obtained, while taking into account additional patient-specific factors.

5.4.7 **Conclusions**

Multiparametric qMRI sensitively detects subtle myelopathic progression in individual DCM patients, while correlating well with patients' perceptions. The natural history of DCM appears to be more progressive than previously thought, in part because neuroplasticity and behavioural adaption act to mask progressive tissue injury. Our pilot implementation of qMRI into a

decision-making algorithm represents one of the first clinical uses of SC qMRI to inform management of individual patients.

Chapter 6
General Discussion, Future Directions, and Conclusions

6.1 General Discussion

6.1.1 Interpretation of Results and Contributions to the Field

Viewing the results of the original research described in this dissertation (Chapters 2-5) in the context of the prior body of literature (reviewed in Chapter 1), several knowledge gaps were addressed.

A clinically feasible multiparametric quantitative MRI protocol was developed and validated (Chapter 2). This protocol was implemented on a 3T clinical scanner and used generic pulse sequences that are widely available from all MRI hardware vendors, a standard spine coil, and requires only 20 minutes of acquisition time (in addition to anatomical imaging). The protocol produced 4 quantitative metrics that reflect aspects of SC macrostructure (CSA) and microstructure, including axonal integrity (FA), myelination (FA, MTR, and our novel biomarker T2*WI WM/GM), gliosis, iron, and calcium concentrations (T2*WI WM/GM). Normative data and variations of these metrics with rostrocaudal level, age, sex, height, weight, and cervical cord length were characterized in 40 healthy subjects, 2 of which have not been previously described (CSA with cervical cord length, MTR with height). Normalization procedures were developed that reduce the inter-subject variability within the normal population, which is helpful so that abnormal results in individuals can more easily be detected with statistical tests. A comprehensive semi-automated workflow was developed using state-of-the-art template-based probabilistic analysis with the Spinal Cord Toolbox, providing high-fidelity readouts from numerous ROIs (SC, WM, GM, and individual WM tracts). The test-retest reliability of FA, MTR, and T2*WI WM/GM the metrics from various ROIs was measured for healthy subjects and DCM patients, and our results for FA and MTR were similar to previous reports from other groups (some using more complex techniques such as rFOV DTI). The reliability of our novel biomarker T2*WI WM/GM compared favourably with FA and MTR. A comparison of DTI with and without cardiac triggering (with outlier rejection) in 10 subjects showed roughly equivalent performance, validating our simplified approach.

The novel biomarker of WM tissue injury, T2*WI WM/GM, showed good performance in comparison with CSA, FA, and MTR in terms of group differences, diagnostic accuracy, and clinical correlations with global and focal impairment (Chapter 3). The performance of this qMRI metric was also found to be stable in the context of T2WI signal hyperintensity. This study also found that CSA of the maximally compressed level showed slightly stronger results than any other measure. Unfortunately, all of the metrics showed only moderate diagnostic accuracy and strength of clinical correlations, closely matching previous literature and highlighting that individual qMRI metrics have limited performance. However, the strength of correlation with mJOA improved greatly when the qMRI measures were combined using linear regression, and similarly the diagnostic accuracy was far higher in multivariate analysis with logistic regression. These results underscore the value of the multiparametric approach, which provides far more accurate measurement of tissue injury than any univariate qMRI measure.

In Chapter 4, the qMRI multiparametric protocol was applied to investigate the effect of asymptomatic SC compression (ASCC). To perform this analysis, a novel methods of automated morphological analysis of the SC was developed, in collaboration with the group at Ecole Polytechnique de Montreal. This shape analysis established normative values for compression ratio (CR), solidity (measured as the percent area of the cord segmentation within a subtending convex hull), and relative rotation. It was discovered that half of the 40 subjects recruited for the earlier studies as healthy controls had minor indentation or flattening, and these subjects had strong evidence of tissue injury with 5 univariate qMRI measures showing significant pathological changes ($p<0.05$), 8/10 measures varying in the same direction as in DCM ($p=0.055$), and a composite score showing even greater differences ($p=0.002$). The only measures that did not differ in the same direction as seen in DCM were CSA measures, with significantly higher rostral CSA in compressed subjects suggesting that a larger spinal cord is a predisposing factor for compression. In addition, 2 of the 20 subjects subsequently developed mild myelopathy at follow-up (median 21 months). The results of this study have far reaching clinical implications, arguably redefining what consitutues myelopathy from a clinical diagnosis (based on the presence of neurological symptoms/signs) to a pathological diagnosis (as measured by qMRI). Furthermore, this study also provides a new objective definition of cord compression, based on abnormal SC shape, which appears to detect both static and dynamic SC compression, with the latter only being previously possible with flexion/extension MRI studies. The rate of

ASCC was much higher at 50% than previous reports that estimated a prevalence of 8-26%, due to the new defining criteria. Most importantly, longitudinal data confirmed that even the mild cord compression present in this group was a predisposing factor for myelopathy development.

The longitudinal study in which spinal cord qMRI was used to monitor non-operative DCM patients for disease progression (Chapter 5) demonstrated one of the first-ever applications of quantitative spinal cord MRI to alter clinical decision-making in individual patients. The results with qMRI were largely congruent with detailed clinical examinations, but qMRI detected progression of tissue injury slightly more often than clinical measures showed decreased function. Furthermore, detailed clinical examinations showed progression more often than the simple self-reported measure mJOA, suggesting that DCM patients are sometimes unaware of subtle clinical worsening. These results were consistent with our hypothesis that neuroplasticity and behavioural adaption act to mask progressive tissue injury in DCM, contributing to the perception of clinical stability when, in reality, most patients experience a slowly progressive injury to their spinal cord. This also calls into question the existing (low quality) body of evidence regarding the natural history of DCM, which includes only a small number of studies that are mostly retrospective, as it seems the natural history involves slow and subtle disease progression in a majority of cases. Furthermore, controversy exists about the optimal management of mild DCM patients, and this study provides a practical methodology for monitoring these patients for progression, based on the combination of detailed physical testing and qMRI. This study represents several major advances, including a better understanding of the pathophysiology and chronological course of DCM, and clinical implications that could transform practice, including the knowledge that most DCM patients tend to decline (adding support for earlier surgery) and the development of a practical method of monitoring patients that are managed non-operative.

6.1.2 **Novelty and Contributions to the Field**

The original research described in this dissertation and summarized in the preceding section includes numerous contributions that are likely to move the field of quantitative spinal cord MRI closer to clinical adoption. The novelty and success of our approach are closely linked to several decisions that were made early in the design of this research that set it apart from previous studies. Several of these were technical decisions that allowed us to achieve highly accurate

qMRI readouts while using simple, portable, and clinically relevant methods. In large part, this was only possible due to the contributions of our technical collaborator, Dr. Julien Cohen-Adad, who provided the technical expertise to set up all of our acquisition sequences, in addition to the tools upon which our analysis methods were built. The remainder of critical design decisions were at a high-level, that pertained to clinical data collection and reduction of bias, which enhanced the potential impact of this research.

First, we decided to employ an array of qMRI acquisition techniques, collecting multiparametric data, rather than focusing on just a single technical method (e.g. DTI). This generates a range of quantitative measures of tissue injury that measure similar but slightly different microstructural features of the tissue, with the beneficial effects of increasing statistical power, cross-validating each other, and detecting minor tissue changes with individual measures (e.g. demyelination). The increased statistical power with multiparametric data also overcomes the limitations of individual techniques, such as high inter-subject variability and noisy image acquisition. Furthermore, the added statistical benefits of the multiparametric approach offset the slightly reduced accuracy and precision of our simplistic DTI acquisition protocol, in comparison to more complex rFOV or cardiac triggered DTI, thus permitting the creation of highly portable acquisitions. Second, our approach to analysis provided high fidelity readouts from numerous ROIs using template-based probabilistic averages, while reducing the burden of analysis to only a few simple steps. This analysis pipeline is far more suited to a clinical workflow than the manual analysis techniques that have been used in the vast majority of prior studies, and I contributed several novel ideas to improve these tools. Third, our normalization scheme for qMRI data allows for unbiased comparisons across different rostrocaudal levels, which is essential for analysis in individual patients that have SC compression are different levels, but has been overlooked in many previous DCM qMRI studies. The normalization procedures also corrected for subject characteristics, reducing the inter-subject variability among healthy subjects and increasing the statistical power to make meaningful assertions in individual patients. Fourth, multivariate analysis using multiple linear regression, logistic regression, and composite scores took full advantage of the multiparametric data, strengthening clinical correlations, diagnostic accuracy, detection of subtle tissue injury in ASCC, and detection of subtle disease progression. Fifth, we collected comprehensive clinical data to accurately characterize the various aspects of neurological and functional deficits that occur due to cervical myelopathy. This provided a rich

set of data to compare qMRI results against, and also a complimentary assessment that could be used in addition to qMRI to more accurately measure myelopathic progression. Finally, each of the specific studies was designed to minimize sources of bias, using consecutive enrollment, testing a priori hypotheses, correcting for multiple comparisons, using automated analysis tools, and achieving high follow-up rates. As a result, the research was conducted with a low risk of bias (according to our own rating), in contrast to the majority of prior clinical studies that were rated to have high or moderately high risk of bias in our systematic review (Martin et al., 2016).

The novelty of this research also includes the creation of a novel biomarker of WM injury, T2*WI WM/GM signal intensity ratio, as discussed above. This is an exciting development, as it seems to be highly reliable, sensitive to mild pathology (e.g. ASCC), and responsive to subtle worsening in monitoring DCM patients for progression. However, much work remains to understand exactly what this measure represents in the spinal cord, as this may differ from its pathological correlates in the brain of demyelination, gliosis, calcium, and iron changes (Cohen-Adad, 2014). Validation of this measure in larger samples of patients and across different MRI vendors (e.g. Siemens, Philips) is also needed to determine if similar results can be achieved. Application of T2*WI WM/GM to other pathologies such as SCI, MS, and ALS would also be valuable to determine if it is a useful biomarker in these conditions.

Another innovation produced by this research was the automated shape analysis of the SC to detect deformation, thereby inferring the presence of static and/or dynamic compression. The overall concept came from myself, while the implementation of the methods and further innovations came from members of Dr. Cohen-Adad's laboratory. This approach to automatically detect abnormal spinal cord shape has already proven useful at identifying subtle indentation, flattening, and torsion in individuals with ASCC. However, SC shape analysis has numerous other potential clinical applications, including characterizing the degree of compression in symptomatic DCM, and also in a range of other pathological conditions (e.g. tumours, inflammation, SCI) to detect deviation from normal SC morphology. The development of this shape analysis is ongoing, and is currently being extended to include metrics of SC asymmetry (e.g. comparing left and right hemi-cord CSA or computing left-right fold-over overlap).

Several other opportunities for innovation of analysis tools arose during this research, and I was able to contribute ideas that were subsequently implemented within the Spinal Cord Toolbox. For example, early efforts to analyze qMRI data with the SCT frequently showed inaccurate registration between the images and the SCT template. In response, I suggested a new registration algorithm based purely on the 2 SC segmentation masks, which follows the following simple steps:

1. Translate the template segmentation to the anatomical space (to align both centers of mass).
2. Perform 2-dimensional principal component analysis (2D-PCA) to identify the long axis of the cord in the anatomical segmentation, assumed to be the transverse axis.
3. Rotate the template segmentation to align with the rotation of the transverse axis of the anatomical segmentation, from step 2.
4. Dilate (i.e. scale) the template segmentation in the left-right direction to match the width of the anatomical segmentation.
5. Divide both segmentations into columns that are perpendicular to the transverse axis.
6. Translate each column of the template segmentation to match the column-wise center of mass of the anatomical segmentation.
7. Dilate each column of the template segmentation to match the AP length of the anatomical columns.

This algorithm is particularly useful in the context of extrinsic SC compression because the cord is almost always flattened in the A-P direction, and the resulting registrations appear highly realistic in terms of expected deformation of internal cord structure (Figure 6.1). Following implementation of this algorithm in the SCT by Dr. Cohen-Adad, I re-analyzed all of the data and found greater grey-white contrast for all 3 metrics (T2*WI WM/GM ratio, FA, and MTR) slightly stronger clinical correlations, indicating that registrations were more accurate. It is expected that the development and validation of this registration algorithm will be included in a future journal publication.

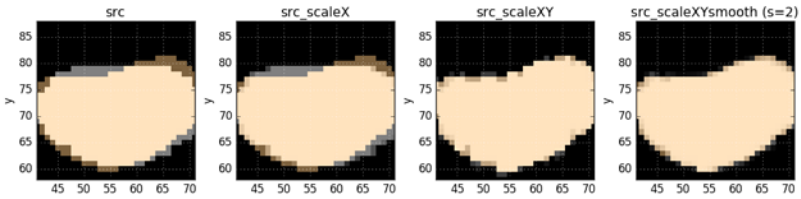

Figure 6.1: Novel Registration Algorithm. First panel: demonstrates the initial segmentation of the anatomical data (brown) and SCT template (grey) with overlap shown in beige. Second panel: the template segmentation is scaled laterally to match the width of the anatomical segmentation. Third panel: vertical columns of the template segmentation are translated and scaled to match the anatomical segmentation. Fourth panel: the transformed template segmentation is spatially smoothed. Following these steps, a warping field is calculated in both directions (anatomical to template space and vice versa).

Overall, this research included numerous contributions, including interesting new findings, incremental improvements to previously published methods, and technical innovations. However, most importantly, our multiparametric qMRI approach produced sufficiently accurate results that they can be used to make assertions about individual patients, which is an achievement within the field.

6.1.3 **Weaknesses and Limitations**

6.1.3.1 *Study Design and Implementation*

This research was conceived of and designed by me, in conjunction with my supervisor Dr, Michael Fehlings, my technical collaborator Dr. Julien Cohen-Adad, and my thesis Program Advisory Committee (PAC) over a 6 months period at the beginning of my PhD studies, while I concurrently was completing the large systematic review detailed in Chapter 1. With the benefit of hindsight, there are certain changes to the overall study design that could have enhanced this work. Sample size is always a critical consideration in clinical research, with a larger number of subjects allowing more accurate characterization of normative data, normalization coefficients, clinical correlations, etc. We also performed a post hoc subgroup analysis of our “healthy” population to examine the effects of ASCC, which would have benefited from greater numbers

to more accurately estimate its prevalence and the rate of progression to symptomatic myelopathy. It would have been beneficial to expand the test-retest reliability study to include more DCM and healthy subjects to better characterize differences in reliability of metric calculation, particularly at the level of maximal compression in DCM. It would also have been useful to determine the reliability of CSA measurement, particularly of the compressed cord for intra- and inter-rater reliability when manual correction of the segmentation is needed. The clinical data that were acquired are very good at representing the major neurological and functional impairments that subjects experience, but in retrospect ISNCSCI sensory scores with light touch and pin prick testing would be useful, as the latter may be more sensitive than monofilaments in DCM and would allow correlation with measures of WM injury extracted from the spinothalamic tract. Detailed calculation of the reliability of all of the clinical measures that were employed (particularly mJOA) would also be useful, but is a major undertaking as well. It would also have been useful to perform the comprehensive clinical assessments on healthy subjects, so that differences between ASCC and uncompressed healthy subjects could have been understood. Finally, this research included an initial implementation of qMRI to inform clinical decision-making for individual DCM patients that show disease progression. However, this was only in the context of a single institution, and members of the research team performed all assessments (clinical and qMRI), which does not constitute complete implementation. The next step is to begin the process of knowledge translation and clinical integration, which includes the development of training materials (e.g. standard operating procedures, SOPs) and the transfer of skills and knowledge to hospital personnel (clinicians and MRI technologists).

6.1.3.2 *Quantitative MRI Acquisition Techniques*

Quantitative MRI is a rapidly evolving field, consisting of an ever-changing landscape of new techniques and incremental refinements. This phenomenon is well recognized across all technological fields, reflected by the term “the bleeding edge” that cautions against early adoption of technology until more practical (and mundane) implementation problems have been solved. This concept is highly pertinent to medical integration of technology, and we had this in mind during the design of the technical methods used in this research. There is also a need to “freeze” on a certain technology or set of methods for the duration of a longitudinal study, which can be problematic if a certain method does not work well (requiring abandonment or a major change) or if it becomes outdated by the study’s conclusion. This occurred with our T2WI

acquisition, which produced good results in pilot testing but proved to be sensitive to motion (likely swallowing), producing artifacts that propogated throughout the volume in a number of subjects. It was fortunate that we could also calculate CSA from T2*WI data, which were much less affected by motion. However, future studies would benefit from optimization of T2WI for the purpose of CSA calculation, which would ideally have high isotropic resolution to represent the 3D contour of the SC accurately (Kearney et al., 2014). It could also be argued that the DTI acquisition that we performed is not state-of-the-art, with rFOV methods showing higher SNR and decreased distortions, and our own data demonstrating that cardiac gating may also provide a small advantage. However, a recent study by Samson et al. (2016) indicated that rFOV DTI showed nearly equivalent reliability compared with a generic ssEPI sequence with saturation bands used for outer volume suppression. Thus, the minor improvements available from rFOV and cardiac triggering do not invalidate our simpler DTI approach. For measurement of myelin, we employed a standard gradient echo sequence with and without MT pre-pulse, which has been available from the major MRI vendors for more than 2 decades. However, during the course of this study the use of MTsat and inhomogenous MT (ihMT) techniques have been introduced. Again, the preliminary results with these methods to date do not suggest that our approach is invalid, but future studies need to determine if these techniques are superior to standard MT, and if they are feasible to implement in a clinical context.

Several additional qMRI techniques were explored during the course of this research to determine if they could add value to our multiparametric data acquisition, but they did not yield strong results. These included fMRI, MRS, and spinal cord perfusion using arterial spin labeling (ASL), which are discussed below in the context of future directions. Other members of Dr. Fehlings lab previously had found success using Flow Alternating Inversion Recovery (FAIR) to study spinal cord perfusion in rat models of DCM, but we were not able to obtain this sequence on our current GE scanner (related to the software level and contract issues). Similarly, we were not able to obtain rFOV or ihMT sequences for the purpose of comparing these with our techniques.

6.1.3.3 *Analysis Techniques*

Although we used automated analysis for most steps of image processing, visual inspection was performed for each step and manual intervention was frequently required to ensure that

segmentations of the SC were accurate. This is a limitation of the available tools, as it is very difficult to determine the edge of the spinal cord when CSF is effaced and/or the normal spinal cord anatomy is distorted. Our study design involved only a single rater (myself), due to the time and effort required to master the tools and analyze the data, but the use of multiple raters would have reduced potential bias and allowed for calculation of inter-rater reliability. It was also observed that registration to the SCT template often showed minor inaccuracies, in spite of the improved algorithm that was created for this step. The result is that template-based analysis with the SCT involves a certain amount of measurement, as is the case with any complex technique, which we did not measure directly but is included in the variability that we quantified in our test-retest reliability study. In particular, T2*WI WM/GM is particularly sensitive to the registration step because of its definition as a ratio between internal SC structures (WM and GM). However, the overall error of measurement was deemed acceptable for all techniques (and was surprisingly the lowest for T2*WI WM/GM), but ongoing efforts to improve the SCT are very likely to reduce this error and produce more accurate qMRI results. Specific areas for these improvements include automatic detection of the spinal cord, segmentation, registration, grey-white segmentation, and the user interface (i.e. ease of use). The latter area is of critical importance for clinical translation, as the analysis workflow that I used in this study included writing numerous command-shell scripts, which was only possible due to my background as a software engineer. The SCT was the primary analysis tool selected for this research, but several others exist that were not explored (e.g. ACID toolbox). Our overall approach of ROI-based analysis using the probabilistic SCT template has not been directly compared against alternative methodologies such as voxel-wise group analysis (Liu et al., 2009), and further research in this area is needed.

6.1.4 **Impact of this Research**

Quantitative MRI provides a wealth of information about macro- and microstructure of the spinal cord, but we are only beginning to understand how to use this in meaningful ways. This research demonstrated that SC qMRI using clinically feasible methods can inform decision-making for individual patients, which is likely to have a substantial impact in both research and clinical domains.

The strong results obtained with our multiparametric protocol and composite measures of tissue injury are likely to lead to an increased interest in this approach among qMRI researchers,

particularly among the large number of groups that have previously only focused on diffusion MRI techniques. As discussed above, using a single imaging technique such as DTI limits statistical power and the range of different microstructural changes that can be detected, while increasing the risk of spurious values (e.g. due to artifact). Our focus on straightforward acquisitions that are easily portable between vendors will hopefully inspire further research to optimize qMRI methods for clinical use and validate them in multi-center and multi-vendor studies. The variations of qMRI metrics with subject characteristics that were identified are important for future studies to take into account, and our suggested normalization procedures are likely to be adopted by other groups to reduce inter-subject variability and make qMRI metrics better measures of tissue injury. Furthermore, this research highlighted knowledge gaps in the clinical research body of evidence, including the natural history of DCM and the psychometric properties of various tools (e.g. mJOA) to monitor DCM for progression.

This research is also likely to have a major clinical impact in several ways. Our systematic review identified 3 likely uses of qMRI: diagnosis, correlation with disease severity, and prediction of outcomes, and our results have shown substantial utility for the first 2 of these. In terms of diagnosis, we demonstrate that univariate qMRI metrics show modest performance, but a multivariate approach with logistic regression shows greater diagnostic accuracy (area under the curve of >95%). The automated spinal cord shape analysis that was developed also has strong clinical potential for diagnosis and characterization of cord compression (in ASCC and DCM), as this highly accurate quantitative approach fits well with the current movement toward standardizing radiological assessments that is occurring. At some point in the future, it may be possible that aspects of radiological assessment and reporting are completely automated, and quantitative image analysis algorithms such as our SC shape analysis are a step in that direction. Furthermore, our results provided evidence that even minor SC compression in asymptomatic subjects causes tissue injury, which arguably represents a new definition of myelopathy. This is likely to change the perception and clinical management of subjects with mild SC compression, which is currently viewed by radiologists, surgeons, and other clinicians as unimportant. For example, one of the ASCC subjects that subsequently developed early myelopathy had an MRI that showed very mild compression, but was dismissed by the radiologist as “normal degenerative changes.” Thus, a paradigm shift is needed to recognize ASCC as a highly prevalent preclinical state that has an increased risk of myelopathy development, and these

subjects should be monitored by primary care physicians for neurological symptoms and signs. Perhaps more importantly, we demonstrated what we believe to be the first-ever use of spinal cord qMRI to inform decision-making in individual patients, which is a major step forward for this field. The monitoring of non-operative DCM patients for disease progression addresses an important clinical problem, as there exist a large number of mild DCM patients and it is not entirely clear if surgical treatment is justified in this group. Thus, widespread monitoring of these individuals with comprehensive clinical assessments and qMRI could provide important health benefits by detecting deterioration earlier and reducing morbidity. This work also suggested that the natural history is worse than previously reported, which also implies that early surgery should be strongly considered. Finally, the data were suggestive that neuroplasticity and behavioural adaptation play a role in masking progressive tissue injury in DCM, which should be further studied to determine if there are modifiable factors or rehabilitation strategies that can augment this effect, possibly obviating or delaying surgery.

Overall, the clinically feasible multiparametric qMRI techniques that have been developed and many of the specific results are likely to have a positive impact on patients with DCM and other pathologies. Our systematic review of previous studies identified numerous barriers to clinical translation in terms of study design, acquisition techniques, and analysis methods, and our it appears that our clinically-minded approach overcomes these. The next section explores the next steps of how to bring quantitative spinal cord MRI into regular clinical use.

6.2 Future Directions

There are a large number of exciting avenues for future research using quantitative spinal cord MRI. Several of these were introduced above in the limitations section (6.1.3), many of which are active areas of research in Dr. Cohen-Adad's laboratory and in other research groups. We have also begun to investigate several additional research directions, which are described in the next section. Looking beyond these current areas of study, a broad range of additional directions are contemplated and explored, including the study of new technical methods and the application of qMRI to additional clinical areas. Finally, the steps required to successfully translate current knowledge into future clinical use are outlined.

6.2.1 **Works in Progress**

6.2.1.1 *Quantitative MRI as a Diagnostic Tool*

The use of our multiparametric qMRI protocol for the purpose of diagnosis of DCM and ASCC was explored in Chapters 3 and 4, respectively. As discussed above, the clinical diagnosis of myelopathy is sometimes challenging as symptoms (e.g. fine motor dysfunction, numbness, and gait impairment) are highly subjective and often transient in nature. Diagnosis is usually made by an experienced neurologist or neurosurgeon based on clinical examination, but this is also subjective (e.g. hyperreflexia, gait ataxia) and cases with diagnostic uncertainty are relatively common. Anatomical MRI showing cord compression has poor specificity, as this is present in up to 50% of healthy subjects (Chapter 4). Several groups have investigated the use of DTI for diagnosis of DCM (Wang et al., 2015, Facon et al., 2005, Uda et al., 2013a)Lee et al. (2015), Li et al. (2014), sometimes comparing it with the performance of T2WI hyperintensity, although the latter is not a good diagnostic tool as it is only present in 50-70% of cases (Nouri et al., 2016). We investigated the use of our multiparametric quantitative MRI approach for the purpose of diagnosis, comparing 5 statistical approaches for classification between healthy subjects and those with DCM. Preliminary analysis was performed in a subset of our cohort (35 healthy subjects and 56 DCM patients). The 5 diagnostic models that were compared included: 1) logistic regression (LR) with backwards stepwise variable selection; 2) linear discriminant analysis (LDA); 3) principal~~le~~ component analysis followed by logistic regression (PCA-LR); 4) k-nearest neighbors (kNN) with various k values (3,5,7); and 5) a support vector machine (SVM) model using a radial basis function kernel and various values for cost=(1,10,100,1000), and gamma=1. Logistic regression models were limited to 4 degrees of freedom due to the limited sample size. Validation was performed using bootstrap (LR, PCA-LR) with 500 iterations or leave-one out cross-validation (LDA, kNN, SVM), based on available R functions for each statistical method, to yield estimates of diagnostic accuracy reported as corrected area under receiver operating characteristic curves (AUC). All 5 models showed good diagnostic accuracy, with the SVM model showing the highest performance (AUC=95.6%), outperforming LR (AUC=93.6%), PCA-LR (AUC=89.0%), LDA (AUC=87.9%), and kNN (k=5, AUC=84.6%). The SVM model with cost=100 outperformed other SVM models, which showed AUC ranging from 91.2% to 94.3%. The LR model retained CSA_{MCL} (p=0.0007), T2*WI $WM/GM_{Rostral}$ (p=0.04), $CSA_{Rostral}$ (p=0.08), and $MTR_{Rostral}$ (p=0.39). The results showed that supervised

machine learning algorithms such as SVM can achieve greater diagnostic accuracy than conventional statistical approaches such as LR or LDA. SVM classification works by finding a hyperplane that optimally separates 2 classes of multivariate data, and it is not surprising that this approach yielded superior results given the complexity of the multi-parametric input data. These results warrant further investigation in a large series of cases with diagnostic uncertainty of myelopathy to determine the clinical utility of this approach.

6.2.1.2 *Prediction of Outcomes in DCM*

The use of qMRI measures to improve prognostication is an appealing potential clinical use of qMRI techniques, offering the possibility of identifying which patients will improve with surgery, which could be used to affect treatment decisions. This has already been investigated by several groups in DCM patients treated with surgery (Jones et al., 2013, Wen et al., 2014b, (Holly et al., 2016), Wang et al. (2016), Rajasekaran et al. (2017)), all of which used DTI for the prediction of outcome except for 1, which used MRS (Holly et al., 2016). The results have been modest, with 3 DTI studies (Wen et al., 2014b, Wang et al., 2016, Vedantam et al., 2017) and the MRS study showing weak relationships with outcome, while DTI was unable to predict neurological outcome in 2 studies (Jones et al., 2013, Rajasekaran et al., 2017). The use of qMRI to predict outcomes in patients managed non-operatively could also be useful, but this has yet to be reported.

Our longitudinal study in DCM subjects was also designed to investigate prediction of outcomes in DCM, both in operative and non-operative cohorts. This work is still in progress and results are not reported in this dissertation, but follow-up data collection is nearing completion and preliminary analyses are promising. Our approach is based on multivariate analysis that includes previously established predictors of outcome as covariates, so that the utility of qMRI data can be weighed appropriately. As discussed above, a new prognostic factor is not useful if it provides purely redundant information from an established factor, and baseline neurological status is a very strong predictor of outcome that must be included in these analyses. We also plan to use age, duration of symptoms, smoking status, and conventional MRI measures (T1WI and T2WI signal change) as covariates in the analyses. We expect that this work will help advance the knowledge regarding outcome prediction, as it could be the first to employ multiparametric

qMRI data for outcome prediction, and also the first to perform such an analysis in non-operative DCM patients.

6.2.1.3 *The Role of Cardiac Gating in Spinal Cord DTI*

The importance of cardiac gating or triggering in the acquisition of spinal cord DTI has yet to be clearly established, as discussed in section 2.5.4. Cardiac-related motion of the spinal cord has a large amplitude relative its small size, and thus it makes intuitive sense that confining data acquisition to the quiescent phase of the cardiac cycle could improve its quality. This was demonstrated by Summers et al. (2006) in a study of 4 healthy subjects. However, DTI data is inherently redundant, as numerous directions of data are acquired and then averaged to fit an elliptical model (described with a 3x3 tensor). Thus, data post-processing can be used to reject individual measurements that do not fit well with the remainder of the data, known as outlier rejection. Furthermore, ungated acquisition can acquire almost twice as much data in the same period of time, and DTI is also affected by respiratory motion that is not accounted for by cardiac gating.

We previously explored differences between cardiac-gated and un-gated DTI acquisitions in 10 subjects (Chapter 2), finding a trend toward improved reliability of FA measurement with gating of about 1%. Gating also showed a trend toward slightly higher mean FA values. However, this study did not have sufficient sample size to show significant differences, so a larger study is needed. We have now collected comparative data in more than 30 subjects, and analysis is in progress. If reliability is significantly better with cardiac gating, even by as little as 1%, it would be beneficial for future studies to employ this approach for DTI because the effects of interest are on the same order of magnitude, in the range of approximately 3-10% for diagnosis and monitoring of disease progression.

6.2.2 **Emerging Quantitative MRI Acquisition Techniques**

The future of quantitative spinal cord MRI research is extremely bright, as many new techniques and innovations are becoming available. As discussed extensively throughout this dissertation, it is essential that new technological advances are viewed critically and vetted thoroughly for their potential as clinical tools. Conversely, it is also important to remain open and agnostic to new methods, and those that are proven effective should be investigated for their clinical potential.

During this research, I investigated several MRI techniques outside of those described above, but a lack of strong findings led to their exclusion from the studies that were performed. However, these and many other emerging quantitative MRI techniques show promise and deserve further investigation for potential clinical translation.

6.2.2.1 *Functional MRI of the Brainstem and Spinal Cord*

Investigation of the functional activation, connectivity, and plasticity of the spinal cord has previously been reported by only a small number of groups (Table 1.8), most of them including Dr. Patrick Stroman as a co-author and using the acquisition techniques that he developed. This work has showed great promise, including a study from members of our own research group that revealed increased functional activation of the dorsal horn in zones of normal sensation in patients with incomplete injury, but decreased proportional to the degree of sensory loss at the level of diminished sensation (Cadotte et al., 2012a). The same study also revealed increased intra-spinal connectivity in patients with incomplete injury, suggestive of neuroplasticity. However, the fMRI techniques employed in this study and others yield low spatial resolution, temporal resolution, and SNR, greatly limiting the extent to which this approach can be used in a clinical setting. An alternative to spinal cord fMRI is to investigate brain structures, which are relatively larger and have been studied more extensively. However, study of the cerebral cortex with fMRI is complicated by the fact that it is a highly plastic structure that shows evidence of widespread changes following injury or damage to the spinal cord (Mikulis et al., 2002). Instead, investigation of subcortical structures such as nucleus cuneatus, nucleus gracilis, and the thalamus might allow measurement of low-level sensory processing more directly, although fMRI acquisition in this region is more affected by magnetic field inhomogeneity, and reports of successful brainstem fMRI were rare until recently (Karachi et al., 2010, Bosma et al., 2016).

During the initial stages of this research, we investigated brainstem fMRI for its potential to add to the multiparametric protocol that was under development. We hypothesized that the degree of activation of sensory nuclei in the brainstem and thalamus would be proportional to the functional integrity of the dorsal column sensory pathways, providing a direct measure of their functional integrity. We investigated brainstem fMRI in 22 subjects in a blocked sensory stimulus paradigm using a non-painful electrical stimulus of the ulnar nerve. This used an EPI sequence for T2*WI with BOLD contrast, which detects the level of neural activity through

changes in the levels of oxygenated and de-oxygenated hemoglobin that alter the T2*WI signal by approximately 2-4% (Stroman et al., 2014). Our fMRI data were acquired in the coronal plane parallel to the rostrocaudal axis through the brainstem. Unfortunately, the fMRI data showed severe distortions around the air sinuses located in the skull base (e.g. mastoid sinus, sphenoid sinus), and the SNR appeared to be too low to detect the BOLD response. Analysis of these data with FSL found no useful activations in the sensory areas of the brainstem or thalamus, and further use of fMRI was abandoned to focus more on microstructural techniques.

However, brainstem and spinal cord fMRI remain promising techniques, and further research is warranted. The difficulties that were experienced in our fMRI approach were likely related to the acquisition sequence (T2*-weighted EPI), and better results may be possible with fast spin echo (FSE), which mitigates magnetic field inhomogeneity through 180° refocusing pulses and has been utilized successfully by Dr. Stroman and his collaborators. The study of the low-level circuits of the brainstem and spinal cord are appealing because they are likely to directly correspond with the degree of functional impairment of the spinal cord. This does not need to be limited to the study of sensory processing, as motor paradigms for blocked fMRI studies, such as finger tapping, hand grasp, or walking, have been described (Cadotte et al., 2012b)(Stroman et al., 2014). However, greater experience and more granular data are needed to determine the clinical utility of spinal cord or brainstem fMRI approaches, including characterization of the variability in the healthy population, variations of fMRI metrics with age and other subject characteristics, and test-retest reliability. Unfortunately, none of the previous spinal fMRI studies have reported these data, suggesting that this technique is relatively far from clinical readiness compared to microstructural MRI approaches such as those in our multiparametric protocol.

In parallel to the investigation of spinal cord fMRI, further research into cortical fMRI may elucidate widespread cortical changes, the detection of which may have useful clinical applications (Kaushal et al., 2017). This research has previously demonstrated altered sensorimotor cortical representations and connectivity (Mikulis et al., 2002, Kaushal et al., 2017). Ways in which this information can be applied to solve clinical problems have not yet been clearly elucidated, but one possibility is for prognostication in DCM and SCI (Cadotte et al., 2012b, Kaushal et al., 2017). Resting-state fMRI (rs-fMRI) studies have also been reported in DCM and SCI (Oni-Orisan et al., 2016) (Kaushal et al., 2017). The resting-state approach to fMRI has the ability to examine changes in connectivity and activity of specific functional

networks independent of any task, which likely provides unique information from that derived from the more traditional motor-task or sensory stimulation block-design fMRI studies. Moving forward, carefully designed studies are needed that investigate these exciting fMRI approaches for specific clinical applications.

6.2.2.2 *Metabolic Imaging with MR Spectroscopy*

This research also included a preliminary investigation of MR spectroscopy, which was not included in this dissertation. MRS allows *in vivo* measurement of the concentration of key molecules within neural tissue. This has been previously applied to DCM in several studies, showing decreased N-acetylaspartate (NAA, a marker of neuronal density), increased choline (Cho, a marker of cell membrane turnover and demyelination), increased myo-inositol (MyoI, a marker of gliosis), and increased lactate (Lac, a marker of hypoxia). The measurement of each of these metabolites is typically performed as a ratio to that of creatine (Cr), which is an abundant molecule and relatively invariant in pathological states. Spinal cord MRS studies have typically used a single voxel in the C1-C3 region, as the spinal canal is wider at this level and the magnetic field less affected by magnetic susceptibility artifacts (that occur at interfaces between bone, disc, CSF, and cord) than the compressed region, typically between C3 and C7.

Holly et al. (2009) promisingly applied MRS to demonstrate significantly altered levels of lactate and an altered ratio of NAA/creatine in CSM patients compared to healthy controls. In a follow-up longitudinal study, they reported significant correlations between the NAA/creatine ratios and change in clinical scores suggesting metabolite ratios are predictive of neurological outcome in DCM, although multivariate analysis was not performed, as discussed above (Holly et al., 2016). These studies were completed 1.5T field strength, whereas the field of advanced MRI has largely moved to 3T for clinical studies (Martin et al., 2016). The use of higher magnetic field (3T) has two important advantages compared to using conventional 1.5T scanners during MRS data acquisition. First, the MR signal to noise ratio scales roughly linearly with field strength and the 3T scanner is capable of providing twice the signal-to-noise ratio for equivalent scans done at 1.5 Tesla (Bartha *et al.*, 2000). Second, MRS at 3T doubles the spectral dispersion, which increase metabolite measurement precision and allow the acquisition of data from smaller volumes of tissue (Bartha *et al.*, 2000).

We obtained a grant from Cervical Spine Research Society (CSRS) to investigate MRS in DCM patients. The goals of this study were to 1) establish a 3 Tesla (3T) MRS protocol that can be performed on standard clinical hardware and using standard MRI pulse sequences to examine local metabolite changes in the rostral cervical spinal cord (C1-C3) above the level of stenosis; 2) compare MRS measures beteween DCM patients with healthy controls; 3) assess the ability of each metabolite ratio to correlate with severity in DCM; 4) determine the feasibility of performing MRS studies in post-operative DCM patients with metallic implants; 5) determine the responsiveness of metabolite ratios to correlate with recovery following surgery; and 6) determine if pre-operative metabolite ratios are predictive of recovery. We also planned to compare the performance of MRS with other qMRI techniques in our multiparametric protocol. 7 DCM patients and 6 healthy subjects underwent MRS acquisitions using point-resolved spectroscopy (PRESS) on a 3T GE clinical scanner. The MRS acquisition was based on a literature review and optimized over several sessions, resulting in the following parameters: PROBE-P sequence, chemical shift selective (CHESS) water suppression using 256 samples, single 8x8x30mm^3 voxel placed over the spinal cord behind the C2 body (which showed better results than a smaller voxel, Figure 6.2), TR=3000ms, TE=135ms, 128 signal averages, 6 saturation bands placed immediately adjacent to the voxel to surround it completely, and 2nd order localized shimming using a box volume of interest. Total acquisition time for patient positioning, anatomical imaging (T2WI), localized shimming, pre-scan, and MRS acquisition was approximately 30 minutes. MRS data were analyzed with LCModel, and when this software failed to fit a metabolite model to the data a manual method of peak measurement was employed.

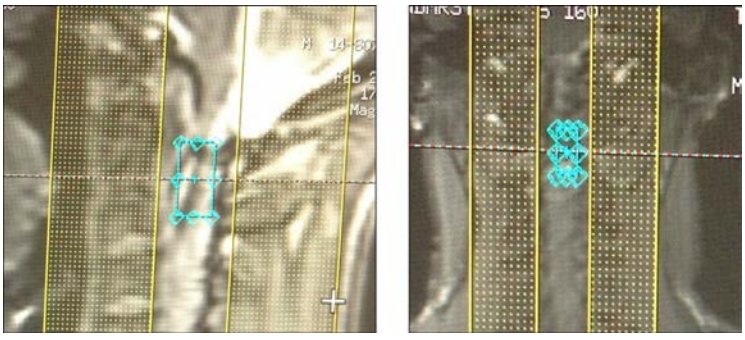

Figure 6.2: MRS Voxel Placement. Placement of a 8x8x15mm voxel (blue) on the C2 level of the spinal cord surrounded by saturation bands (yellow) in sagittal (left) and coronal (right) view.

Subsequent optimization found that a larger 8x8x30mm voxel produced better signal to noise ratio (SNR).

Unfortunately, several technical challenges were encountered with sequence optimization, including a limitation of the GE scanner software that would not allow the MRS voxel to be rotated into an oblique angle to fit the spinal cord. This issue could not be resolved due to the research contract between UHN and GE that would not permit the needed scanner software upgrade.

The protocol was then applied to 6 additional healthy subjects, 7 pre-operative DCM patients, and 5 post-operative DCM patients with metallic implants. MRS acquisition was successful in 11/13 of the subjects without implants. Unfortunately, the MRS pre-scan failed in all 5 post-operative DCM patients due to broad line width (related to the effect of metallic implants), and the subsequent MRS scan could not be performed (Figure 6.3). The analysis of the 11 MRS datasets with LCModel was successful in fitting a model in 8 subjects, with the remaining 3 analyzed manually. On visual inspection, the MRS data were noisy and peaks were challenging to identify, suggesting low signal to noise ratio (SNR). The healthy subject data (N=6) analyzed with LCModel showed a value of NAA/Cr of 2.43 ± 1.37, which was considerably higher and had much greater inter-subject variability than previous studies (Table 6.1). No significant relationships were identified between the metabolite ratios and subject characteristics. Group analysis found similar mean values for healthy subjects compared with previous studies, but the inter-subject variability was greater than previous reports, most likely due to the error of measurement stemming from low SNR. Although the sample size was too low to expect significant differences, an interim analysis of this preliminary data found no trends toward differences between healthy and DCM subjects were present, nor were any significant correlations with clinical measures identified.

Subjects	Study	NAA/Cr	Cho/Cr	MyoI/Cr	Lac

Healthy	Holly (2009)	1.83 ± 0.18	0.93 ± 0.18	N/A	0/13
	Salamon (2013)	1.37 ± 0.32	0.31 ± 0.08	1.42 ± 0.57	0.19 ± 0.13
	Taha Ali (2013)	1.82 ± 0.08	0.75 ± 0.14	N/A	0/11
	Pilot data (LCModel: N=6)	2.43 ± 1.37	0.74 ± 0.43	3.43 ± 1.96	0/6
DCM	Holly (2009)	1.27 ± 0.52*	0.96 ± 0.18	N/A	7/21
	Salamon (2013)	T2W+: 1.17 ± 0.42 T2W-: 1.27 ± 0.27	T2W+: 0.49 ± 0.17* T2W-: 0.41 ± 0.09	T2W+: 1.31 ± 0.67 T2W-: 1.49 ± 0.58	T2W+: 0.36 ± 0.38 T2W-: 0.27 ± 0.21
	Taha Ali (2013)	1.34 ± 0.09*	0.82 ± 0.12	N/A	9/24
	Pilot data (LCModel: N=2, manual: N=3)	LCModel: 2.49 ± 0.95 Manual: 1.11 ± 0.82	LCModel: 0.38 ± 0.22 Manual: 0.72 ± 0.47	LCModel: 0.30 (1 dataset could not identify MyoI peak) Manual: 0.62 ± 0.22	0/5

Table 6.1: Comparison of MRS Results with Previous Studies. Metabolite ratios and the frequency of a lactate peak are compared between the current study pilot data and 3 previous studies comparing healthy and DCM subjects. Metrics are reported as mean ± SD.

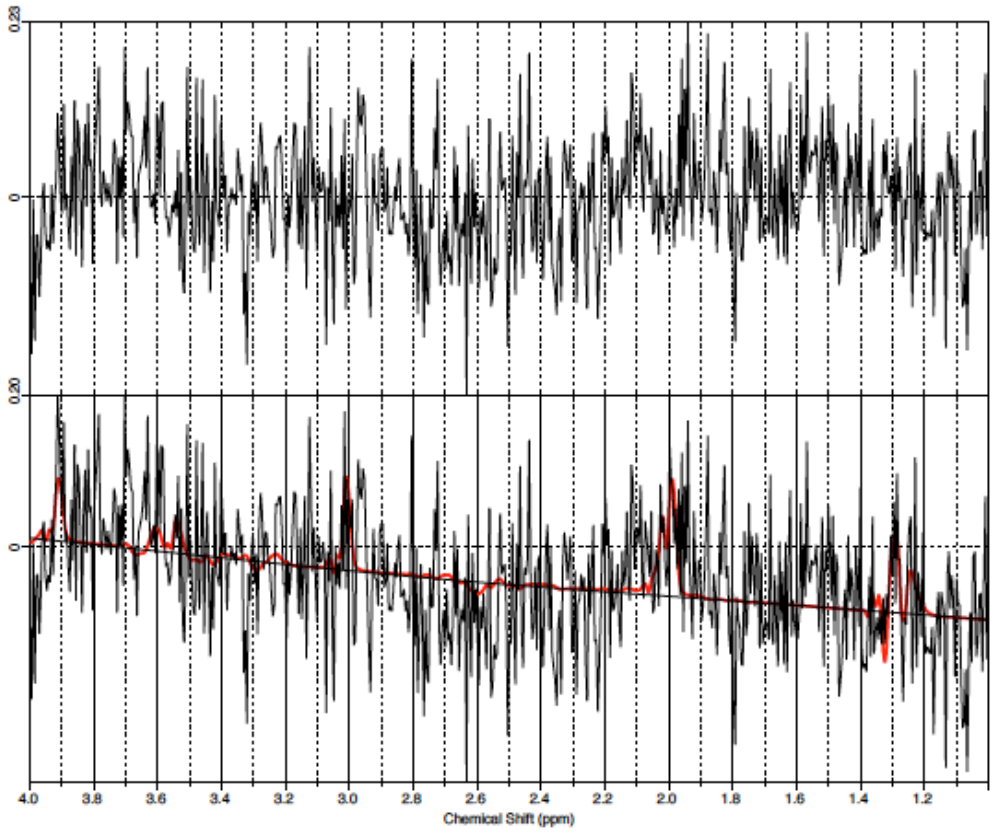

Figure 6.3: Representive MRS Data from a Healthy Subject. The image shows the raw spectroscopy signal (top) and the fitted model (bottom, red line) produced by LCModel with NAA, Cho, MyoI, Lac, and Cr peaks. The peaks are difficult to identify, related to low signal to noise ratio (SNR).

Following this interim analysis, we felt that the quality of the MRS data was insufficient to permit the planned analyses of the longitudinal study, and we are now in the process of exploring further changes to the acquisition protocol to improve the quality of the data prior to moving forward with the clinical study. The results of this pilot feasibility study illustrate that it is challenging to obtain high quality MRS data in the cervical spinal cord using standard clinical

MRI hardware and pulse sequences. However, the results indicate that without further technical refinements, MRS of the rostral cervical spinal cord may not be feasible in post-operative DCM patients with metallic implants, and may also be unreliable in subjects with metallic dental implants. These are important findings to guide future spinal cord MRS studies. In subjects without implants, the MRS acquisitions had slightly too low SNR to reliably measure the biochemical profile of subjects, which explains why inter-subject variability was higher than previous published reports. Our inability to rotate the voxel to lie directly over the spinal cord also contributed to poor results. Our data also suggest that shimming to correct minor magnetic field inhomogeneity is extremely important, and previous studies have acquired B0 field maps and/or had an MR physicist perform more complex manual shimming procedures for this purpose, which suggest that advances in shimming technology are needed to enable clinically feasible MRS with short acquisition times and minimal resource requirements. One possible solution that is currently under investigation by our technical collaborator (Dr. Julien Cohen-Adad) is automated active shimming based on real-time feedback from probes placed within the scanner, feeding into external shim coils that manipulate the magnetic field to be more homogenous. We plan to investigate this exciting technological strategy and others to move spinal cord MRS closer toward clinical utilization.

In summary, MRS of the spinal cord is particularly technically challenging and only a small number of research groups have previously demonstrated successful results, while it is unknown how many other groups have attempted this technique without success. This pilot study provided numerous learning points that have already led to improvements in our MRS protocol, and several others that we will carry forward for future studies. Furthermore, the use of ultra-high field MRI, at 7T or higher, may demonstrate sufficiently higher SNR with MRS that it can move forward into more focused clinical investigations.

6.2.2.3 *Spinal Cord Perfusion*

Ischemia is believed to be one of the predominant mechanisms of tissue injury in DCM (Kalsi-Ryan et al., 2013a, Karadimas et al., 2013, Nouri et al., 2015b). Previous work has demonstrated that spinal cord tissue perfusion is inversely correlated with functional disability, in rodent models of DCM (Karadimas et al., 2015). Tissue perfusion can be measured with MRI using

various forms of arterial spin labelling (ASL), which labels water protons and then detects their diffusion into the extra-vascular tissue compartment (Deibler et al., 2008). This labelling of protons is often called “tagging”, and is performed by inverting the spins of protons in one of several ways. The most popular ASL techniques for cerebral perfusion measurement have been continuous ASL (CASL) or pseudocontinuous pCASL (pcASL), which continuously tag protons moving through a narrow slab (plane) that is oriented perpendicular to the blood flow. An alternative to this is pulsed ASL (PASL), which tags protons in a thick slab in a single pulse. Unfortunately, the blood supply to the cervical spinal cord is much more complex than that of the brain, including contributions from above (vertebral arteries), below (anterior spinal artery and thoracic radicular arteries), and within the cervical region (cervical radicular arteries). Thus, the definition of a suitable perpendicular tagging plane is not possible for cervical SC perfusion measurement. We made a brief attempt at investigating human SC perfusion with pCASL in a single session (with the help of Dr. Adrian Crawley), but this experiment found no useful signal and this technique was not pursued further. Previous success in rodents was achieved using PASL techniques, specifically with the flow alternating inversion recovery (FAIR) sequence (Duhamel et al., 2008, Karadimas et al., 2015), as this method appears to be better suited to the SC blood supply. We were unable to obtain the FAIR sequence on our GE scanner, related to the aforementioned contract issues. However, future research of this promising technique could have a major impact in DCM, as it may be useful for outcome prediction by differentiating between reversible changes due to ischemia from more permanent microstructural changes detected with other techniques.

6.2.2.4 *Emerging Approaches to Diffusion MRI*

Diffusion MRI is, in itself, a rapidly growing field due to its potential to characterize aspects of tissue microstructure. These techniques are based on measuring the diffusion of water in various directions. This is typically performed by applying a diffusion sensitizing gradient that causes the magnetic field to vary linearly and causes protons to water protons to precess at different rates and dephase, followed by an opposite refocusing gradient that causes protons to rephase; signal is reduced proportional to movement of protons during this process, and this approximately reflects the diffusion of water parallel to the applied gradient (Stroman et al., 2014). This process can be used to model water diffusion within tissues in a various levels of complexity, ranging from the scalar measure of apparent diffusion coefficient (ADC) or mean diffusivity (MD),

which requires measurement in only 3 directions, to highly complex models of diffusion that can detect crossing WM pathways. DTI has been a popular choice, as it is a relatively simple model of diffusion, representing diffusion as an ellipsoid described by 3 eigenvectors/eigenvalues in each voxel, that appears to capture useful information about axonal integrity and myelination. DTI requires acquisition in only 6 directions to compute tensors, and moderate evidence suggests that axial diffusivity (AD) reflects axonal injury or loss, while radial diffusivity (RD) is a measure of myelin changes (Wheeler-Kingshott et al., 2002). Our systematic review, however, found that fractional anisotropy (FA) showed more consistent correlations with clinical impairment in various pathologies, possibly because it combines the information represented by AD and RD (Martin et al., 2016). In our studies, we employed FA as our only DTI metric, which proved to be a good measure of WM injury and useful for clinical applications. Our DTI data, however, included frequent artifacts, distortions, and moderately high inter-subject variability, which are limitations of this technique that can only be partially mitigated by post-processing strategies. As discussed above, rFOV DTI and cardiac gating may help to reduce some of these issues, and these should be investigated further. However, a range of other diffusion MRI approaches have been proposed, and future research is needed to determine if these exciting advances can surpass DTI or provide complimentary information for clinical purposes.

Diffusion kurtosis imaging (DKI, discussed briefly in Chapter 1), offers additional information about the non-Gaussian diffusion behavior (reflecting the complex interactions between tissue structures) by varying the strength of the diffusion-sensitizing gradients (b-values). This has shown promising early results in DCM (Hori et al., 2012), but the clinical value of this information needs to be further elucidated and additional acquisition time is required. Another technique has been described that can accurately measure axon diameter and density, called AxCaliber, although this has only been implemented on the Human Connectome research scanner that uses much higher strength gradients 300mT/m than are currently available on clinical hardware (Duval et al., 2015). Neurite orientation and dispersion density imaging (NODDI) has also been recently implemented in the spinal cord (Grussu et al., 2015), having been previously demonstrated in the brain. This diffusion-based approach provides several tissue parameters, including intra-neurite tissue volume fraction, orientation dispersion index, and the isotropic volume fraction. However, it has yet to be applied in clinical studies to my knowledge. An alternative approach has been proposed that may be considerably easier to implement than

the aforementioned techniques, called double diffusion encoding, applies a diffusion-weighted filter orthogonal to the spinal cord prior to diffusion-weighted encoding parallel to the cord (Skinner et al., 2016). The output of this technique is a value similar to the DTI metric axial diffusivity, but that mitigates the confounding effects of edema and has been reported to show stronger correlations with behavioural measures in a rat model of SCI.

All of these exciting innovations in diffusion MRI warrant further study regarding their potential for clinical use. Overall, diffusion is among the most powerful and promising of all MRI methods, and it will undoubtedly continue to garner much research focus in the years to come.

6.2.2.5 *Myelin Imaging Techniques*

Several different methods of quantifying myelin using MRI are available, including MTR, MTCSF, MWF, and MTsat, reviewed in Chapter 1, and it is unclear at present which of these is best suited for clinical use. Our results with MTR were modest, showing smaller differences between DCM and healthy subjects and weaker correlations with clinical measures. MTR was, however, useful in detecting early tissue injury in asymptomatic cord compression and monitoring DCM patients for progression. Improvements in the accuracy of myelin measurement with more complex qMRI acquisitions have been suggested by preliminary studies using inhomogenous MT (ihMT) (Girard et al., 2017, Girard et al., 2015, Taso et al., 2016), MTsat (Grabher et al., 2015, Lema et al., 2016), and quantitative MT (Levesque et al., 2010), which yields several parameters of magnetization exchange between the free and restricted proton pools. Finally, myelin g-ratio, which is the ratio of outer to inner myelin diameter, can be computed using a combination of MT and diffusion imaging techniques (Stikov et al., 2015). Once again, however, it is unclear if the improved accuracy and/or anatomical specificity that is possible with these methods is sufficient to justify their added complexity and acquisition time, and additional comparative studies are needed that explore their value for specific clinical purposes.

6.2.2.6 *Spinal Cord MRI at Ultra-High Field Strength*

The field of MRI research extends far beyond what is possible with standard 1.5T and 3T clinical scanners, through the use of ultra-high magnetic field (UHF) strength at 7T and beyond. There has been a recent proliferation of 7T research systems worldwide, and it can be expected that a

surge of 7T clinical studies will soon arise. Furthermore, Siemens has begun marketing 7T clinical scanners, which will make this technology more affordable and widely available (Siemens). Higher field strength offers it is inevitable that new clinical studies at ultra-high field strength are coming soon and these could potentially show substantial improvements that strengthen the case for clinical utility.

The general principles governing MRI involve an inherent trade-off between SNR, image resolution, and acquisition time, for a given main magnetic field strength (B_0). However, as mentioned previously, SNR shows a nearly linear increase with field strength for most MRI sequences (Bartha *et al.*, 2000). Thus, the higher SNR that can be achieved at 7T is a type of capital that can be used to acquire more accurate images, or exchanged for higher resolution or, shorter scan time. However, UHF imaging also involves numerous technical challenges, the most important of which are increased magnetic susceptibility artefact, increased distortions, and increased specific absorption rate (SAR), the latter of which can cause dangerous heating if not controlled. Susceptibility artefact and distortions are most likely to affect DTI acquisitions, and specialized approaches may be necessary to mitigate their effects. For this reason, some have argued that diffusion MRI at 1.5T produces better results than 3T or higher, but this remains a subject of debate (Stroman et al., 2014). In contrast, T2*WI benefits greatly from the increase in SNR and has been used to produce detailed images of the spinal cord showing Wallerian degeneration in specific tracts (Cohen-Adad et al., 2013b). Similarly, myelin imaging techniques are also likely to benefit from an increase in B_0 field strength.

In fact, many of the technical challenges of obtaining high quality images at 7T (including diffusion MRI) have already been addressed, and preliminary results have been reported showing success with DTI and mapping of R1 and R2* parameters, including findings of excellent grey-white contrast and significant differences between individual WM tracts (Massire et al., 2016). As greater experience is obtained at 7T, the potential clinical uses will be more clearly revealed. However, it is important to keep in mind that 1.5T and 3T MRI systems will continue to be the most commonly available for years (if not decades) to come, so clinically-minded research should not solely focus on 7T.

6.2.2.7 *Other Acquisition Techniques*

A wide array of additional MRI techniques exist that could have useful applications to the spinal cord. Phase-contrast MRI can image the velocity of CSF flow, which has been studied in DCM showing high flow rates that correlated with FA and functional measures (Kim et al., 2015). This measure of CSF flow velocity may relate closely with the degree of static pressure and tissue ischemia in DCM, but further data is needed. MR elastography can measure the stiffness of tissues (Young's Modulus), and feasibility in the spinal cord has been demonstrated in a pilot study (Kruse et al., 2009). This could be potentially useful in DCM to determine structural changes that occur in the compressed spinal cord, which might correlate with the degree of gliosis, fibrosis, and tissue ischemia. Susceptibility-weighted imaging (SWI) is a method that combines magnitude and phase data from a fully flow-compensated gradient echo sequence, producing images that are highly sensitive to venous blood and hemorrhage (Wang et al., 2011). SWI might be useful to investigate the degree of vascular recruitment in DCM, as this compensatory response to tissue ischemia may contribute to the varying degree functional impairment experienced by individual patients for a given amount of cord compression. These and many other emerging MRI techniques could be potentially useful in DCM and other clinical pathologies (e.g. SCI), and should be explored further.

6.2.3 **The Evolution of Analysis Methods**

In parallel with ongoing developments in quantitative MRI acquisition techniques, a similar evolution of analysis methods is occurring. The post-processing of SC qMRI data is highly complex, including motion and eddy-current correction, SC segmentation, non-linear registration between imaging types or to a group template, tensor calculation (DTI), outlier rejection, data extraction from individual ROIs, correction for partial volume effects, and normalization to account for rostrocaudal level and subject characteristics. Each of these steps has the potential to improve accuracy of the processed data to reflect underlying tissue properties, but conversely, each step also has the potential to introduce error.

The quality and complexity of various analysis tools dedicated to analysis of SC qMRI data have increased dramatically over the past few years, beginning to match that available from brain image processing tools (e.g. FSL, AFNI, SPM, BrainVoyager) that have a much longer history. Our experience with the Spinal Cord Toolbox (SCT) has been overwhelmingly positive, but many of its current features were not available 2 years ago when we began using it. Many of the numerous features available in the SCT appear to improve the quality of the processed data, such as probabilistic extraction from ROIs, outlier rejection (using RESTORE method for diffusion tensor calculation), grey-white segmentation, and correction for partial volume effects. However, the effects of each of these features should be further investigated in the context of clinical studies to determine their positive and negative effects on clinical outputs (e.g. correlations and diagnostic accuracy). This type of validation with clinical data should also be directed towards comparisons of different tools (e.g. SCT vs. ACID toolbox), and different analysis approaches (e.g. template-based analysis vs. voxel-wise group analysis) to determine which are superior.

The possibility of performing analyses on numerous ROIs also brings with it the problem of multiple comparisons, and it is unclear which ROIs are best suited for specific applications. For example, we assumed that FA extracted from WM would provide a better measure of tissue injury than extraction from the whole SC, which was confirmed by preliminary data, but we have not compared all of our analyses between these ROIs. Ideally clinical studies should limit themselves to test a small number of hypotheses with an a priori data analysis plan, which means

that ROIs should be selected beforehand. Thus, comparative studies that investigate the relationship of various ROIs with clinical outputs would also be helpful to direct the design of future studies.

The majority of qMRI metrics have focused on microstructural changes in WM (e.g. diffusion, myelin), whereas measures that are more specific to GM changes are lacking. This is unfortunate for applications in DCM, because GM injury may be a greater cause of deficits than WM, which has been suggested by post-mortem studies (Ito et al., 1996, Ohshio et al., 1993, Mizuno et al., 2003). One possibility is CSA measurement of the GM, based on T2*WI or PSIR sequences that have strong grey-white contrast and high resolution. More specifically, each anatomical region of the GM (ventral horns, dorsal horns, intermediate zone) could be measured for atrophy at each level, which may correlate with focal weakness/numbness in DCM. Alternatively, MRS may some potential to reveal GM-specific pathology through the measurement of NAA, but advances are needed to provide spatially localized measurement of this neuronal marker. Functional MRI of the spinal cord may also hold potential to reveal focal injury to the GM, but the methods used to date have low spatial resolution and firm conclusions cannot be drawn.

The normalization of qMRI data was an important area of focus in this research, and further characterization of the variation of metrics with subject characteristics could be highly beneficial. For example, a recent study found that DTI metrics vary considerably depending on the subject's position in the scanner, demonstrated decreased FA with greater neck extension (Kuhn et al., 2016). This requires further study to determine if cord curvature explains some of the inter-subject variability in the healthy population, which could be used as a factor for normalization of DTI metrics. Similarly, other potential sources of variability in qMRI metrics could be explored, such as ethnicity, smoking status, blood pressure, and nutritional status (iron, calcium, albumin, etc.). However, accurate characterization of numerous factors will require large datasets with a large number of healthy controls, which is costly to perform and difficult to ensure uniformity of the data collection.

Finally, the statistical methods used to analyze qMRI data need to evolve to keep pace with the complex data that are generated from these techniques. Simple univariate analyses are not sufficient to understand the complex relationships between qMRI metrics and clinical measures, largely because all of these are inter-correlated. Multivariate analyses such as multiple linear

regression, logistic regression, and the use of composite scores are useful methods of combining data to show independent associations and make inferences. However, the assumptions of these methods need to be checked, such as normal distribution of residuals and equal variances (homoscedasticity). In many cases of prior studies, it is unclear if these assumptions were checked or violated, but future clinical studies that attempt to prove the clinical utility of these methods need to be statistically rigorous and explicit. Furthermore, the use of linear models may be inappropriate and lead to inaccuracy, such as may be the case with the complex effect of age on qMRI metrics and other clinical measures. For example, one can imagine the effect of age on gait stability might be negligible between the ages of 18 and 50, but then become increasingly stronger as individuals enter their golden years. Our research also made extensive use of composite scores, which were all unweighted averages of qMRI metrics because we did not have prior knowledge to guide a weighting scheme. However, more refined composite scores can be developed for various purposes that assign stronger weights to the most accurate and reliable measures. This does not need to be confined to qMRI measures, as these can potentially be combined with clinical measures, anatomical MRI measurements, and electrophysiology data to provide more potent composite measures.

All qMRI analysis techniques that are contemplated for clinical use, however, must be subjected to the same critical question as was posed for qMRI acquisition techniques: “Is the improvement from this method worth the increased complexity?” Clinical application of quantitative methods needs to be as simple as possible, for the purpose of feasibility and reliability. For example, if a complex normalization procedure to qMRI data is applied that results in spurious values, this could lead to medical errors. Therefore, a tension exists between accuracy and simplicity, and each new innovation or must be considered in this context.

As it stands, it may be the case that the current quality of qMRI acquisition techniques is “good enough” for clinical use, and the major barrier to clinical translation lies with analysis methods. The greatest of these barriers almost certainly lies with automation. As discussed above, busy clinicians are not going to adopt quantitative MRI, which is unfamiliar and highly complex, if it makes their typical workflow more difficult. The possibility that radiologists or surgeons might perform manual analysis, such as ROI selection across a number of slices, is highly unlikely. Thus, qMRI analysis needs to be made almost completely automatic for it to be widely adopted. In template-based analysis, this includes automatic detection of the spinal cord, SC

segmentation, and registration to a template, in addition to many other possible data processing steps. This may ultimately prove impracticable, and an alternative approach may be to outsource qMRI data to a 3rd-party analysis firm, as is the case with specialty lab tests such as genomic analysis. This approach would allow highly specialized experts to perform this analysis, rather than inexperienced clinicians, while also automatically blinding the 3rd party analyst from clinical information, as the data would have to be anonymized. In either case, advances in the automation of spinal cord quantitative MRI are useful to move the field forward.

6.2.4 **Expanding the Clinical Focus**

The field of SC qMRI has now reached a level of maturity to justify larger and more focused clinical studies. As stated earlier, these studies need to be carefully designed and conducted with a low risk of bias so that their results can provide justification for clinical use. These results will also need to be strong enough to offset the costs associated with implementing qMRI, which will need to be subsequently assessed via cost-utility analysis. To move this field closer to clinical uptake, greater involvement of clinicians and clinical researchers (e.g. methodology experts) is needed to identify specific problems and design appropriate studies. Greater investment by physicians, surgeons, radiologists, and other clinical personnel in this research will also help to promote the collection of more comprehensive clinical data, while increasing awareness of qMRI and its clinical potential. There exist numerous potential clinical applications of qMRI, and several of these are discussed below.

6.2.4.1 *Longitudinal Monitoring of Asymptomatic Spinal Cord Compression*

In Chapter 5, a method of monitoring DCM patients for progression of tissue injury using our multiparametric qMRI protocol was proposed. A similar approach for individuals with ASCC could also be helpful. One difference in ASCC that was reported in Chapter 4 is that these subjects do not appear to experience significant atrophy in terms of rostral CSA, so it is preferable to use a ratio of MCL to rostral CSA instead of these individual measures, as was proposed in the refined composite score. Our group plans to follow the 20 ASCC patients that were identified in a longitudinal study, but it would also be advantageous to increase the sample size of this study so that the prevalence and rate of myelopathic progression can be more accurately determined.

6.2.4.2 *DTI Tractography for Intramedullary Spinal Cord Tumours*

The use of DTI tractography for quantitative analysis of SC tissue injury does not appear to be as robust as ROI-based analysis, as it is based on several loose assumptions of what constitutes a "fiber". However, DTI tractography has been used fairly frequently in the brain to visualize the displacement of WM pathways around tumours. This approach has also been applied to the spinal cord, showing excellent results at diffentiating between inflammatory lesions and neoplasms (Egger et al., 2016). This exciting potential clinical use should be further explored, warranting a pilot study of its use in a decision-making algorithm to further explore its value.

The use of tractography in intramedullary tumours could also be highly beneficial for surgical planning, as these cases are highly challenging and pose a serious risk of injury to the WM. Typically, the surgeon attempts to identify the midline of the dorsal columns, which are separated by a thin septum, but this is often distorted and displaced to one side by an underlying tumour. A midline myelotomy (longitudinal cut into the spinal cord) is then made, which has a high risk of injury the neighboring fasciculi gracilis if it is off by even a millimeter. Therefore, accurate imaging that can display these pathways might help to identify where the natural division lies, and reduce surgical morbidity of this operation. This could also be integrated into a navigation system, although the accuracy would have to be very high for this to be useful in this delicate procedure.

6.2.4.3 *Prognostication in Acute SCI*

The use of MRI to improve prediction of outcomes in acute SCI (aSCI) has long been a subject of interest. I was recently involved in a systematic review on this topic, which identified 7 studies with moderate quality evidence suggesting that conventional MRI has some utility in prognostication in acute SCI beyond that of baseline neurological status (Kurpad et al., 2017). These studies identified that greater rostrocaudal length of hemorrhage, smaller canal diameter at level of maximal compression, and presence of cord swelling were all predictive of a worse neurological outcome, after adjusting for baseline neurological status in multivariate analysis. However, qMRI techniques may have the potential to surpass these coarse measures by quantifying the integrity of WM pathways and interrogating specific microstructural changes at, or away from, the lesion site. If these measures can discriminate between reversible (e.g. ischemia) and irreversible (e.g. axonal loss) components of damage, then more accurate

prognostication should be possible. To date, only a small number of qMRI studies have investigated the aSCI population, probably because it is difficult to study due to the short time window before surgical treatment (that usually involves metallic implants), the rarity of the condition (with an incidence that is falling in developed countries), the severity of illness, and the co-occurrence of other injuries such as traumatic brain injury, that make it difficult to perform accurate clinical assessments. However, our results in DCM and the research performed by numerous other groups have demonstrated sufficient evidence that SC qMRI in aSCI studies are now warranted. These would preferably be implemented across multiple institutions to ensure adequate enrolment, and use multiple measures of tissue injury to assess their value as prognostic factors.

6.2.4.4 *The Use of Quantitative MRI in Clinical Trials*

Quantitative MRI may also prove useful in therapeutic clinical trials, as a short-term surrogate end-point for more meaningful long-term recovery. This could include investigation of acute therapies such as the neuroprotective agent riluzole in acute SCI, following a similar strategy as described for prognostication in acute SCI. Alternatively, therapeutic interventions such as stem cell transplantation in the chronic phase of SCI could be monitored with myelin imaging or diffusion MRI for specific features of remyelination or axonal sprouting, respectively, as has been used in animal studies (Jirjis et al., 2017). This type of investigation has already begun, including an MRI sub-study embedded within the riluzole in spinal cord injury study (RISCIS-MRI), which we are actively engaged in. However, further study of the correlation between qMRI changes and underlying physiological (or histopathological) changes are needed, as it is important that studies do not make unwarranted assertions based on qMRI data without definite knowledge of what they actually represent.

6.2.5 **Multi-Centre Quantitative MRI Studies**

One of the critical next steps in the field of SC qMRI is a transition from small studies at a single institution to large multi-center studies across different vendors. This effort is now well underway, including several multi-center and multi-vendor studies.

Samson et al. (2016) performed a validation study of DTI across 3 sites and 2 MRI manufacturers, showing nearly equivalent results. However, the same subjects were not studied

at each site, meaning that the variability included inter-subject differences. Future validation studies should include the same subjects so that the contribution of different sequences and manufacturer to the overall variance can be discerned. This preliminary study has led to a larger study (led by Dr. Cohen-Adad, in which I am a contributor) involving a group of SC DTI experts worldwide to develop a consensus DTI protocol, which will then be subjected to validation across multiple sites and MRI manufacturers.

As mentioned above, the RISCIS-MRI study is now underway to investigate the utility of DTI to predict outcomes in acute SCI, which is funded by a grant from Rick Hansen Institute. My personal involvement has included contributing to the study design, grant writing, and data collection. In this study, DTI is performed of the high cervical cord (C1-2) level at 72 hours following cervical injury. In most cases, it is expected that surgery will have been performed, and thus DTI may be affected by the presence of nearby hardware. The inclusion criteria for this study are a C4 to C8 neurological level, and ASIA Impairment Scale of grade A, B, or C, indicating severe injuries. The DTI protocol was developed at Medical College of Wisconsin, but we have been involved in the overall study design, and are 1 of 3 active recruiting sites. In addition to DTI, a conventional MRI measure of lesion length expansion (between an initial MRI and the MRI performed at 72 hours) will be collected, which has previously shown promise as a prognostic factor in aSCI (Aarabi et al., 2012). This exciting study has created a close collaboration between 3 MRI research groups, which is an important side-effect of multi-center studies that promotes idea-sharing and future collaborations. Studies such as RISCIS-MRI are important to investigate qMRI techniques in the setting of a clinical trial, which includes severe time constraints on data collection and available resources. In the future, implementation of our multiparametric data acquisition in similar trials would be beneficial to determine its utility for aSCI outcome prediction.

Our group is also involved in the INSPIRED multi-center study, which is funded by Wings for Life, Craig H. Neilsen Foundation, and International Spinal Research Trust. My involvement in this study has been contributing to design of the MRI and clinical data, grant writing, and data collection. The MRI techniques involved in this study are based on the multi-parametric mapping approach described above (Samson et al., 2013, Freund et al., 2013, Grabher et al., 2015), in addition to brain and cervical SC DTI acquisition. This approach has potential to characterize a host of brain and spinal cord structural changes, and it was decided to begin this study with a

focus on the DCM population, for the purpose of validating the approach in comparison with healthy subjects. The ultimate goal of this research, however, is also to develop prognostic tools for acute SCI (traumatic SCI is the primary interest of the funding bodies). This effort has also fostered co-operation between 4 of the leading SC qMRI groups worldwide, again providing an opportunity to share knowledge and pave the way for future collaborations.

In addition to the multi-center studies described above, there is potential going forward to perform multi-center and multi-vendor SC qMRI studies within the University of Toronto hospitals, as these are linked by a common Research Ethics Board and the University of Toronto Spine Program. All 3 of the major MRI vendors are represented across the hospitals (University Health Network, Sunnybrook Health Sciences Centre, and St. Michael's Hospital), and each of these institutions has a busy spine surgery practice that includes access to DCM and SCI patients. Therefore, the next steps of qMRI within our own group may also include small to medium sized multi-center studies, given that all of the infrastructure for this is already in place.

Overall, the field is moving toward greater collaboration and large-scale multi-center studies, which will bring about greater standardization and more rigorously designed trials. The collaborations that have been fostered as a result of this trend also present a possibility to share and pool previously collected data, which might be valuable to analyze retrospectively. For example, a broader analysis of ASCC could help to determine the prevalence of this condition and the effects it has on tissue injury. Furthermore, this pooled analysis might also provide hints at which qMRI techniques and parameter settings provide the best results, potentially solving hotly debated topics such as the optimal b-value for diffusion MRI. In conclusion, the recent proliferation of multi-center studies is an achievement for this field, providing numerous opportunities for collaboration, and offering a sign that successful clinical translation is close at hand.

6.2.6 **Knowledge Translation**

The final act of bringing quantitative spinal cord MRI into clinical use will be knowledge translation (KT). The field of KT is itself rapidly evolving in an effort to fill the critical gap between the development of breakthroughs and their implementation. Knowledge and skills need to be disseminated to the end users of a specific technology, so that they can make use of it optimally. For SC qMRI, this will mean the development of standard operating procedures

(SOPs) and training seminars for MRI technologists, who will eventually have to be able to perform acquisitions without any assistance, clinicians such as radiologists, who may be involved in qMRI data analysis, and other interested parties such as engineers and scientists that may further refine the methods. KT is not a trivial exercise, as the process of dissemination and implementation of complex technologies such as qMRI often reveal problems that are not apparent in a research setting. Furthermore, this process is also an opportunity for scientific inquiry, which might take the form of a satisfaction survey of MRI technicians regarding the clarity of the SOPs, or of radiologists regarding their willingness to perform certain manual components of qMRI analysis as part of their clinical duties. Training seminars for analysis techniques may also be an opportunity to get valuable feedback from clinicians on how qMRI will best be integrated into clinical workflows. Other study designs are also possible, such as a comparison of the quality of qMRI data collection (e.g. correct placement of slices and saturation bands) with and without research personnel supervising the MRI technologist during acquisition. Furthermore, it would be ideal to move the use of our qMRI protocol outside of a research protocol into standard clinical care, such every DCM patient would undergo this protocol automatically (without research consent). This would bring longitudinal monitoring of DCM patients using qMRI into immediate use, and offer a large sample size to examine the clinical utility of this scheme in more detail. However, the logistics of such a transition are complex and require discussions with the radiologists and hospital administrators.

6.3 Conclusions

It is an exciting time in the field of quantitative spinal cord MRI, as the array of powerful techniques are rapidly developing and transitioning into initial clinical utilization. The research described in this dissertation explored a wide array of MRI techniques, with many failures along the way, but found success with the simple set of qMRI measures: CSA, FA, MTR, and T2*WI WM/GM. The strengths of our approach were the multiparametric acquisition, use of simple and clinically feasible sequences, template-based analysis that provided high-fidelity readouts from various ROIs, normalization for nuisance variables, and multivariate analysis that combines qMRI measures. This work made various contributions to technical aspects of the field, including the development of a novel biomarker of WM injury (T2*WI WM/GM), a comparison of DTI with and without cardiac gating, identification of the variation of MTR with height and CSA with cervical cord length, a robust normalization scheme, the development of automated

SC shape analysis, a novel algorithm for registration (based on the segmentation), and several other improvements to the SCT analysis tools. Several key clinical results also were found, including strong correlations between multivariate qMRI data and clinical measures, diagnostic accuracy using multivariate qMRI data exceeding 95% between DCM and healthy subjects, diagnostic accuracy of >98% for spinal cord compression using automated shape analysis, a predicted prevalence of ASCC (based on a new definition) far exceeding previous reports, the discovery of subclinical tissue injury in asymptomatic subjects with mild cord compression, data suggestive of neuroplasticity and behavioural adaptation masking progressive tissue injury in DCM, data indicating that mJOA alone is not sufficient to detect myelopathic progression, and a practical method of monitoring for myelopathic progression using a combination of qMRI and clinical measures. The field has transitioned into large multi-center studies, and this research has allowed our group to be at the center of many of these, while fostering numerous collaborations and close relationships. Much work lies ahead to successfully bring qMRI into routine clinical use, but this research has undoubtedly contributed to advancing this effort.

References

AARABI, B., SIMARD, J. M., KUFERA, J. A., ALEXANDER, M., ZACHERL, K. M., MIRVIS, S. E., SHANMUGANATHAN, K., SCHWARTZBAUER, G., MAULUCCI, C. M., SLAVIN, J., ALI, K., MASSETTI, J. & EISENBERG, H. M. 2012. Intramedullary lesion expansion on magnetic resonance imaging in patients with motor complete cervical spinal cord injury. *J Neurosurg Spine,* 17**,** 243-50.

ABBAS, S., JAIN, A. K., SAINI, N. S., KUMAR, S., MUKUNTH, R., KUMAR, J., KUMAR, P. & KAUR, P. 2015. Diffusion tensor imaging observation in Pott's spine with or without neurological deficit. *Indian J Orthop,* 49**,** 289-99.

AGOSTA, F., ABSINTA, M., SORMANI, M. P., GHEZZI, A., BERTOLOTTO, A., MONTANARI, E., COMI, G. & FILIPPI, M. 2007. In vivo assessment of cervical cord damage in MS patients: a longitudinal diffusion tensor MRI study. *Brain,* 130**,** 2211-9.

AGOSTA, F., BENEDETTI, B., ROCCA, M. A., VALSASINA, P., ROVARIS, M., COMI, G. & FILIPPI, M. 2005. Quantification of cervical cord pathology in primary progressive MS using diffusion tensor MRI. *Neurology,* 64**,** 631-5.

AGOSTA, F., ROCCA, M. A., BENEDETTI, B., CAPRA, R., CORDIOLI, C. & FILIPPI, M. 2006. MR imaging assessment of brain and cervical cord damage in patients with neuroborreliosis. *AJNR Am J Neuroradiol,* 27**,** 892-4.

AGOSTA, F., ROCCA, M. A., VALSASINA, P., SALA, S., CAPUTO, D., PERINI, M., SALVI, F., PRELLE, A. & FILIPPI, M. 2009a. A longitudinal diffusion tensor MRI study of the cervical cord and brain in amyotrophic lateral sclerosis patients. *J Neurol Neurosurg Psychiatry,* 80**,** 53-5.

AGOSTA, F., VALSASINA, P., ABSINTA, M., SALA, S., CAPUTO, D. & FILIPPI, M. 2009b. Primary progressive multiple sclerosis: tactile-associated functional MR activity in the cervical spinal cord. *Radiology,* 253**,** 209-15.

AGOSTA, F., VALSASINA, P., CAPUTO, D., STROMAN, P. W. & FILIPPI, M. 2008a. Tactile-associated recruitment of the cervical cord is altered in patients with multiple sclerosis. *Neuroimage,* 39**,** 1542-8.

AGOSTA, F., VALSASINA, P., ROCCA, M. A., CAPUTO, D., SALA, S., JUDICA, E., STROMAN, P. W. & FILIPPI, M. 2008b. Evidence for enhanced functional activity of cervical cord in relapsing multiple sclerosis. *Magn Reson Med,* 59**,** 1035-42.

AHUJA, C. S., MARTIN, A. R. & FEHLINGS, M. 2016. Recent advances in managing a spinal cord injury secondary to trauma. *F1000Res,* 5.

ALTMAN, D. G. 2009. Assessing new methods of clinical measurement. *Br J Gen Pract,* 59**,** 399-400.

ASMAN, A. J., BRYAN, F. W., SMITH, S. A., REICH, D. S. & LANDMAN, B. A. 2014. Groupwise multi-atlas segmentation of the spinal cord's internal structure. *Med Image Anal,* 18**,** 460-71.

BANASZEK, A., BLADOWSKA, J., SZEWCZYK, P., PODGORSKI, P. & SASIADEK, M. 2014. Usefulness of diffusion tensor MR imaging in the assessment of intramedullary changes of the cervical spinal cord in different stages of degenerative spine disease. *Eur Spine J,* 23**,** 1523-30.

BARTELS, R. H., VERBEEK, A. L., BENZEL, E. C., FEHLINGS, M. G. & GUIOT, B. H. 2010. Validation of a translated version of the modified Japanese orthopaedic association score to assess outcomes in cervical spondylotic myelopathy: an approach to globalize outcomes assessment tools. *Neurosurgery,* 66**,** 1013-6.

BARTLETT, R. J., HILL, C. A., RIGBY, A. S., CHANDRASEKARAN, S. & NARAYANAMURTHY, H. 2012. MRI of the cervical spine with neck extension: is it useful? *Br J Radiol,* 85**,** 1044-51.

BEATON, D. E., WRIGHT, J. G., KATZ, J. N. & UPPER EXTREMITY COLLABORATIVE, G. 2005. Development of the QuickDASH: comparison of three item-reduction approaches. *J Bone Joint Surg Am,* 87**,** 1038-46.

BEDNARIK, J., KADANKA, Z., DUSEK, L., KERKOVSKY, M., VOHANKA, S., NOVOTNY, O., URBANEK, I. & KRATOCHVILOVA, D. 2008. Presymptomatic spondylotic cervical myelopathy: an updated predictive model. *Eur Spine J,* 17**,** 421-31.

BEDNARIK, J., KADANKA, Z., VOHANKA, S., STEJSKAL, L., VLACH, O. & SCHRODER, R. 1999. The value of somatosensory- and motor-evoked potentials in predicting and monitoring the effect of therapy in spondylotic cervical myelopathy. Prospective randomized study. *Spine (Phila Pa 1976),* 24**,** 1593-8.

BELLENBERG, B., BUSCH, M., TRAMPE, N., GOLD, R., CHAN, A. & LUKAS, C. 2013. 1H-magnetic resonance spectroscopy in diffuse and focal cervical cord lesions in multiple sclerosis. *Eur Radiol,* 23**,** 3379-92.

BENEDETTI, B., ROCCA, M. A., ROVARIS, M., CAPUTO, D., ZAFFARONI, M., CAPRA, R., BERTOLOTTO, A., MARTINELLI, V., COMI, G. & FILIPPI, M. 2010. A diffusion tensor MRI study of cervical cord damage in benign and secondary progressive multiple sclerosis patients. *J Neurol Neurosurg Psychiatry,* 81**,** 26-30.

BENZEL, E. C., LANCON, J., KESTERSON, L. & HADDEN, T. 1991. Cervical laminectomy and dentate ligament section for cervical spondylotic myelopathy. *J Spinal Disord,* 4**,** 286-95.

BERG, K. O., WOOD-DAUPHINEE, S. L., WILLIAMS, J. I. & MAKI, B. 1992. Measuring balance in the elderly: validation of an instrument. *Can J Public Health,* 83 Suppl 2**,** S7-11.

BLAND, J. M. & ALTMAN, D. G. 1999. Measuring agreement in method comparison studies. *Stat Methods Med Res,* 8**,** 135-60.

BODEN, S. D., MCCOWIN, P. R., DAVIS, D. O., DINA, T. S., MARK, A. S. & WIESEL, S. 1990. Abnormal magnetic-resonance scans of the cervical spine in asymptomatic subjects. A prospective investigation. *J Bone Joint Surg Am,* 72**,** 1178-84.

BOSMA, R. L., MOJARAD, E. A., LEUNG, L., PUKALL, C., STAUD, R. & STROMAN, P. W. 2016. FMRI of spinal and supra-spinal correlates of temporal pain summation in fibromyalgia patients. *Hum Brain Mapp,* 37**,** 1349-60.

BOZZALI, M., ROCCA, M. A., IANNUCCI, G., PEREIRA, C., COMI, G. & FILIPPI, M. 1999. Magnetization-transfer histogram analysis of the cervical cord in patients with multiple sclerosis. *AJNR Am J Neuroradiol,* 20**,** 1803-8.

BUDREWICZ, S., SZEWCZYK, P., BLADOWSKA, J., PODEMSKI, R., KOZIOROWSKA-GAWRON, E., EJMA, M., SLOTWINSKI, K. & KOSZEWICZ, M. 2016. The possible meaning of fractional anisotropy measurement of the cervical spinal cord in correct diagnosis of amyotrophic lateral sclerosis. *Neurol Sci,* 37**,** 417-21.

BUDZIK, J. F., BALBI, V., LE THUC, V., DUHAMEL, A., ASSAKER, R. & COTTEN, A. 2011. Diffusion tensor imaging and fibre tracking in cervical spondylotic myelopathy. *European Radiology,* 21**,** 426-433.

CADOTTE, D. W., BOSMA, R., MIKULIS, D., NUGAEVA, N., SMITH, K., POKRUPA, R., ISLAM, O., STROMAN, P. W. & FEHLINGS, M. G. 2012a. Plasticity of the injured human spinal cord: insights revealed by spinal cord functional MRI. *PLoS One,* 7**,** e45560.

CADOTTE, D. W., CADOTTE, A., COHEN-ADAD, J., FLEET, D., LIVNE, M., WILSON, J. R., MIKULIS, D., NUGAEVA, N. & FEHLINGS, M. G. 2015. Characterizing the location of spinal and vertebral levels in the human cervical spinal cord. *AJNR Am J Neuroradiol,* 36**,** 803-10.

CADOTTE, D. W. & FEHLINGS, M. G. 2013. Will imaging biomarkers transform spinal cord injury trials? *Lancet Neurol,* 12**,** 843-4.

CADOTTE, D. W., STROMAN, P. W., MIKULIS, D. & FEHLINGS, M. G. 2012b. A systematic review of spinal fMRI research: outlining the elements of experimental design. *J Neurosurg Spine,* 17**,** 102-18.

CAREW, J. D., NAIR, G., ANDERSEN, P. M., WUU, J., GRONKA, S., HU, X. & BENATAR, M. 2011a. Presymptomatic spinal cord neurometabolic findings in SOD1-positive people at risk for familial ALS. *Neurology,* 77**,** 1370-5.

CAREW, J. D., NAIR, G., PINEDA-ALONSO, N., USHER, S., HU, X. & BENATAR, M. 2011b. Magnetic resonance spectroscopy of the cervical cord in amyotrophic lateral sclerosis. *Amyotroph Lateral Scler,* 12**,** 185-91.

CASSEB, R. F., DE PAIVA, J. L., BRANCO, L. M., MARTINEZ, A. R., REIS, F., DE LIMA-JUNIOR, J. C., CASTELLANO, G. & JUNIOR, M. C. 2016. Spinal cord diffusion tensor imaging in patients with sensory neuronopathy. *Neuroradiology,* 58**,** 1103-1108.

CASTELLANO, A., PAPINUTTO, N., CADIOLI, M., BRUGNARA, G., IADANZA, A., SCIGLIUOLO, G., PAREYSON, D., UZIEL, G., KOHLER, W., AUBOURG, P., FALINI, A., HENRY, R. G., POLITI, L. S. & SALSANO, E. 2016. Quantitative MRI of the spinal cord and brain in adrenomyeloneuropathy: in vivo assessment of structural changes. *Brain,* 139**,** 1735-46.

CHANG, L. C., JONES, D. K. & PIERPAOLI, C. 2005. RESTORE: robust estimation of tensors by outlier rejection. *Magn Reson Med,* 53**,** 1088-95.

CHEN, C. J., LYU, R. K., LEE, S. T., WONG, Y. C. & WANG, L. J. 2001. Intramedullary high signal intensity on T2-weighted MR images in cervical spondylotic myelopathy: prediction of prognosis with type of intensity. *Radiology,* 221**,** 789-94.

CHERAN, S., SHANMUGANATHAN, K., ZHUO, J., MIRVIS, S. E., AARABI, B., ALEXANDER, M. T. & GULLAPALLI, R. P. 2011. Correlation of MR diffusion tensor imaging parameters with ASIA motor scores in hemorrhagic and nonhemorrhagic acute spinal cord injury. *J Neurotrauma,* 28**,** 1881-92.

CICCARELLI, O., ALTMANN, D. R., MCLEAN, M. A., WHEELER-KINGSHOTT, C. A., WIMPEY, K., MILLER, D. H. & THOMPSON, A. J. 2010a. Spinal cord repair in MS: does mitochondrial metabolism play a role? *Neurology,* 74**,** 721-7.

CICCARELLI, O., TOOSY, A. T., DE STEFANO, N., WHEELER-KINGSHOTT, C. A., MILLER, D. H. & THOMPSON, A. J. 2010b. Assessing neuronal metabolism in vivo by modeling imaging measures. *J Neurosci,* 30**,** 15030-3.

CICCARELLI, O., WHEELER-KINGSHOTT, C. A., MCLEAN, M. A., CERCIGNANI, M., WIMPEY, K., MILLER, D. H. & THOMPSON, A. J. 2007. Spinal cord spectroscopy and diffusion-based tractography to assess acute disability in multiple sclerosis. *Brain,* 130**,** 2220-31.

COHEN-ADAD, J. 2014. What can we learn from T2* maps of the cortex? *Neuroimage,* 93 Pt 2**,** 189-200.

COHEN-ADAD, J., BUCHBINDER, B. & OAKLANDER, A. L. 2012. Cervical spinal cord injection of epidural corticosteroids: Comprehensive longitudinal study including multiparametric magnetic resonance imaging. *Pain,* 153**,** 2292-2299.

COHEN-ADAD J, D. L. B., BENHAMOU M, CADOTTE D, FLEET D, CADOTTE A, FEHLINGS MG, PELLETIER PAQUETTE JP, THONG W, TASO M, COLLINS DL, CALLOT V, FONOV V 2014. Spinal Cord Toolbox: an open-source framework for processing spinal cord MRI data. *Proceedings of the 20th Annual Meeting of OHBM.* Hamburg, Germany

COHEN-ADAD, J., EL MENDILI, M. M., LEHERICY, S., PRADAT, P. F., BLANCHO, S., ROSSIGNOL, S. & BENALI, H. 2011. Demyelination and degeneration in the injured human spinal cord detected with diffusion and magnetization transfer MRI. *Neuroimage,* 55**,** 1024-1033.

COHEN-ADAD, J., EL MENDILI, M. M., MORIZOT-KOUTLIDIS, R., LEHERICY, S., MEININGER, V., BLANCHO, S., ROSSIGNOL, S., BENALI, H. & PRADAT, P. F. 2013a. Involvement of spinal sensory pathway in ALS and specificity of cord atrophy to lower motor neuron degeneration. *Amyotroph Lateral Scler Frontotemporal Degener,* 14**,** 30-8.

COHEN-ADAD, J., ZHAO, W., KEIL, B., RATAI, E. M., TRIANTAFYLLOU, C., LAWSON, R., DHEEL, C., WALD, L. L., ROSEN, B. R., CUDKOWICZ, M. & ATASSI, N. 2013b. 7-T MRI of the spinal cord can detect lateral corticospinal tract abnormality in amyotrophic lateral sclerosis. *Muscle & Nerve,* 47**,** 760-762.

CRUZ, L. C., JR., DOMINGUES, R. C. & GASPARETTO, E. L. 2009. Diffusion tensor imaging of the cervical spinal cord of patients with relapsing-remising multiple sclerosis: a study of 41 cases. *Arq Neuropsiquiatr,* 67**,** 391-5.

CUI, J. L., LI, X., CHAN, T. Y., MAK, K. C., LUK, K. D. & HU, Y. 2015. Quantitative assessment of column-specific degeneration in cervical spondylotic myelopathy based on diffusion tensor tractography. *Eur Spine J,* 24**,** 41-7.

DATTA, E., PAPINUTTO, N., SCHLAEGER, R., ZHU, A., CARBALLIDO-GAMIO, J. & HENRY, R. G. 2016. Gray Matter Segmentation of the Spinal Cord with Active Contours in MR Images. *Neuroimage.*

DE LEENER, B., LEVY, S., DUPONT, S. M., FONOV, V. S., STIKOV, N., LOUIS COLLINS, D., CALLOT, V. & COHEN-ADAD, J. 2017. SCT: Spinal Cord Toolbox, an open-source software for processing spinal cord MRI data. *Neuroimage,* 145**,** 24-43.

DEIBLER, A. R., POLLOCK, J. M., KRAFT, R. A., TAN, H., BURDETTE, J. H. & MALDJIAN, J. A. 2008. Arterial spin-labeling in routine clinical practice, part 1: technique and artifacts. *AJNR Am J Neuroradiol,* 29**,** 1228-34.

DEMIR, A., RIES, M., MOONEN, C. T., VITAL, J. M., DEHAIS, J., ARNE, P., CAILLE, J. M. & DOUSSET, V. 2003. Diffusion-weighted MR imaging with apparent diffusion coefficient and apparent diffusion tensor maps in cervical spondylotic myelopathy. *Radiology,* 229**,** 37-43.

DOWELL, N. G., JENKINS, T. M., CICCARELLI, O., MILLER, D. H. & WHEELER-KINGSHOTT, C. A. 2009. Contiguous-slice zonally oblique multislice (CO-ZOOM) diffusion tensor imaging: examples of in vivo spinal cord and optic nerve applications. *J Magn Reson Imaging,* 29**,** 454-60.

DUHAMEL, G., CALLOT, V., COZZONE, P. J. & KOBER, F. 2008. Spinal cord blood flow measurement by arterial spin labeling. *Magn Reson Med,* 59**,** 846-54.

DUVAL, T., MCNAB, J. A., SETSOMPOP, K., WITZEL, T., SCHNEIDER, T., HUANG, S. Y., KEIL, B., KLAWITER, E. C., WALD, L. L. & COHEN-ADAD, J. 2015. In vivo mapping of human spinal cord microstructure at 300 mT/m. *Neuroimage,* 118**,** 494-507.

EGGER, K., HOHENHAUS, M., VAN VELTHOVEN, V., HEIL, S. & URBACH, H. 2016. Spinal diffusion tensor tractography for differentiation of intramedullary tumor-suspected lesions. *Eur J Radiol,* 85**,** 2275-2280.

EL MENDILI, M. M., COHEN-ADAD, J., PELEGRINI-ISSAC, M., ROSSIGNOL, S., MORIZOT-KOUTLIDIS, R., MARCHAND-PAUVERT, V., IGLESIAS, C., SANGARI, S., KATZ, R., LEHERICY, S., BENALI, H. & PRADAT, P. F. 2014. Multi-parametric spinal cord MRI as potential progression marker in amyotrophic lateral sclerosis. *PLoS One,* 9**,** e95516.

ELLAWAY, P. H. & CATLEY, M. 2013. Reliability of the electrical perceptual threshold and Semmes-Weinstein monofilament tests of cutaneous sensibility. *Spinal Cord,* 51**,** 120-5.

ELLINGSON, B. M., SALAMON, N., GRINSTEAD, J. W. & HOLLY, L. T. 2014. Diffusion tensor imaging predicts functional impairment in mild-to-moderate cervical spondylotic myelopathy. *Spine Journal,* 14**,** 2589-2597.

ELLINGSON, B. M., SALAMON, N., HARDY, A. J. & HOLLY, L. T. 2015a. Prediction of Neurological Impairment in Cervical Spondylotic Myelopathy using a Combination of Diffusion MRI and Proton MR Spectroscopy. *PLoS One,* 10**,** e0139451.

ELLINGSON, B. M., SALAMON, N., WOODWORTH, D. C. & HOLLY, L. T. 2015b. Correlation between degree of subvoxel spinal cord compression measured with super-resolution tract density imaging and neurological impairment in cervical spondylotic myelopathy. *J Neurosurg Spine,* 22**,** 631-8.

FACON, D., OZANNE, A., FILLARD, P., LEPEINTRE, J. F., TOURNOUX-FACON, C. & DUCREUX, D. 2005. MR diffusion tensor imaging and fiber tracking in spinal cord compression. *AJNR Am J Neuroradiol,* 26**,** 1587-94.

FATEMI, A., SMITH, S. A., DUBEY, P., ZACKOWSKI, K. M., BASTIAN, A. J., VAN ZIJL, P. C., MOSER, H. W., RAYMOND, G. V. & GOLAY, X. 2005. Magnetization transfer MRI demonstrates spinal cord abnormalities in adrenomyeloneuropathy. *Neurology,* 64**,** 1739-45.

FEHLINGS, M. G., IBRAHIM, A., TETREAULT, L., ALBANESE, V., ALVARADO, M., ARNOLD, P., BARBAGALLO, G., BARTELS, R., BOLGER, C., DEFINO, H., KALE, S., MASSICOTTE, E., MORAES, O., SCERRATI, M., TAN, G., TANAKA, M., TOYONE, T., YUKAWA, Y., ZHOU, Q., ZILELI, M. & KOPJAR, B. 2015. A global perspective on the outcomes of surgical decompression in patients with cervical spondylotic myelopathy: results from the prospective multicenter AOSpine international study on 479 patients. *Spine (Phila Pa 1976),* 40**,** 1322-8.

FEHLINGS, M. G., TETREAULT, L., AARABI, B., ARNOLD, P., BRODKE, D. S., BURNS, A., CARETTE, S., CHEN, R., CHIBA, K., DETTORI, J. R., FURLAN, J. C., HARROP,

J., HOLLY, L. T., KALSI-RYAN, S., KOTTER, M., KWON, B., MARTIN, A. R., MIDDLETON, J., MILLIGAN, J., NAKASHIMA, H., NAGOSHI, N., RHEE, J. M., RIEW, D., SINGH, A., SKELLY, A. C., SODHI, S., WILSON, J. R. & YEE, A. 2017. A Clinical Practice Guideline for the Management of Patients with Degenerative Cervical Myelopathy: Recommendations for Patients with Mild, Moderate and Severe Disease and Non-myelopathic Patients with Evidence of Cord Compression. *Global Spine J,* In press.

FEHLINGS, M. G., WILSON, J. R., KOPJAR, B., YOON, S. T., ARNOLD, P. M., MASSICOTTE, E. M., VACCARO, A. R., BRODKE, D. S., SHAFFREY, C. I., SMITH, J. S., WOODARD, E. J., BANCO, R. J., CHAPMAN, J. R., JANSSEN, M. E., BONO, C. M., SASSO, R. C., DEKUTOSKI, M. B. & GOKASLAN, Z. L. 2013. Efficacy and safety of surgical decompression in patients with cervical spondylotic myelopathy: results of the AOSpine North America prospective multi-center study. *J Bone Joint Surg Am,* 95**,** 1651-8.

FILIPPI, M., BOZZALI, M., HORSFIELD, M. A., ROCCA, M. A., SORMANI, M. P., IANNUCCI, G., COLOMBO, B. & COMI, G. 2000. A conventional and magnetization transfer MRI study of the cervical cord in patients with MS. *Neurology,* 54**,** 207-13.

FILIPPI, M., ROCCA, M. A., FALINI, A., CAPUTO, D., GHEZZI, A., COLOMBO, B., SCOTTI, G. & COMI, G. 2002. Correlations between structural CNS damage and functional MRI changes in primary progressive MS. *Neuroimage,* 15**,** 537-46.

FINSTERBUSCH, J. 2009. High-resolution diffusion tensor imaging with inner field-of-view EPI. *J Magn Reson Imaging,* 29**,** 987-93.

FONOV, V. S., LE TROTER, A., TASO, M., DE LEENER, B., LEVEQUE, G., BENHAMOU, M., SDIKA, M., BENALI, H., PRADAT, P. F., COLLINS, D. L., CALLOT, V. & COHEN-ADAD, J. 2014. Framework for integrated MRI average of the spinal cord white and gray matter: The MNI-Poly-AMU template. *Neuroimage,* 102**,** 817-827.

FREUND, P., WEISKOPF, N., ASHBURNER, J., WOLF, K., SUTTER, R., ALTMANN, D. R., FRISTON, K., THOMPSON, A. & CURT, A. 2013. MRI investigation of the sensorimotor cortex and the corticospinal tract after acute spinal cord injury: a prospective longitudinal study. *Lancet Neurol,* 12**,** 873-81.

FREUND, P., WHEELER-KINGSHOTT, C., JACKSON, J., MILLER, D., THOMPSON, A. & CICCARELLI, O. 2010. Recovery after spinal cord relapse in multiple sclerosis is predicted by radial diffusivity. *Mult Scler,* 16**,** 1193-202.

FUKUNAGA, M., LI, T. Q., VAN GELDEREN, P., DE ZWART, J. A., SHMUELI, K., YAO, B., LEE, J., MARIC, D., ARONOVA, M. A., ZHANG, G., LEAPMAN, R. D., SCHENCK, J. F., MERKLE, H. & DUYN, J. H. 2010. Layer-specific variation of iron content in cerebral cortex as a source of MRI contrast. *Proc Natl Acad Sci U S A,* 107**,** 3834-9.

GAO, S. J., YUAN, X., JIANG, X. Y., LIU, X. X., LIU, X. P., WANG, Y. F., CAO, J. B., BAI, L. N. & XU, K. 2013. Correlation study of 3T-MR-DTI measurements and clinical symptoms of cervical spondylotic myelopathy. *Eur J Radiol,* 82**,** 1940-5.

GHOBRIAL, G. M. & HARROP, J. S. 2015. Surgery vs Conservative Care for Cervical Spondylotic Myelopathy: Nonoperative Operative Management. *Neurosurgery,* 62 Suppl 1**,** 62-5.

GIRARD, O. M., CALLOT, V., PREVOST, V. H., ROBERT, B., TASO, M., RIBEIRO, G., VARMA, G., RANGWALA, N., ALSOP, D. C. & DUHAMEL, G. 2017. Magnetization transfer from inhomogeneously broadened lines (ihMT): Improved imaging strategy for spinal cord applications. *Magn Reson Med,* 77**,** 581-591.

GIRARD, O. M., PREVOST, V. H., VARMA, G., COZZONE, P. J., ALSOP, D. C. & DUHAMEL, G. 2015. Magnetization transfer from inhomogeneously broadened lines (ihMT): Experimental optimization of saturation parameters for human brain imaging at 1.5 Tesla. *Magn Reson Med,* 73**,** 2111-21.

GOMEZ-ANSON, B., MACMANUS, D. G., PARKER, G. J., DAVIE, C. A., BARKER, G. J., MOSELEY, I. F., MCDONALD, W. I. & MILLER, D. H. 2000. In vivo 1H-magnetic resonance spectroscopy of the spinal cord in humans. *Neuroradiology,* 42**,** 515-7.

GRABHER, P., CALLAGHAN, M. F., ASHBURNER, J., WEISKOPF, N., THOMPSON, A. J., CURT, A. & FREUND, P. 2015. Tracking sensory system atrophy and outcome prediction in spinal cord injury. *Ann Neurol,* 78**,** 751-61.

GRABHER, P., MOHAMMADI, S., TRACHSLER, A., FRIEDL, S., DAVID, G., SUTTER, R., WEISKOPF, N., THOMPSON, A. J., CURT, A. & FREUND, P. 2016. Voxel-based analysis of grey and white matter degeneration in cervical spondylotic myelopathy. *Sci Rep,* 6**,** 24636.

GRAHAM, S. J. & HENKELMAN, R. M. 1997. Understanding pulsed magnetization transfer. *Jmri-Journal of Magnetic Resonance Imaging,* 7**,** 903-912.

GRUSSU, F., SCHNEIDER, T., ZHANG, H., ALEXANDER, D. C. & WHEELER-KINGSHOTT, C. A. 2015. Neurite orientation dispersion and density imaging of the healthy cervical spinal cord in vivo. *Neuroimage,* 111**,** 590-601.

HAACKE, E. M., CHENG, N. Y., HOUSE, M. J., LIU, Q., NEELAVALLI, J., OGG, R. J., KHAN, A., AYAZ, M., KIRSCH, W. & OBENAUS, A. 2005. Imaging iron stores in the brain using magnetic resonance imaging. *Magn Reson Imaging,* 23**,** 1-25.

HAMILTON, G. F., MCDONALD, C. & CHENIER, T. C. 1992. Measurement of grip strength: validity and reliability of the sphygmomanometer and jamar grip dynamometer. *J Orthop Sports Phys Ther,* 16**,** 215-9.

HARRISON, N. A., COOPER, E., DOWELL, N. G., KERAMIDA, G., VOON, V., CRITCHLEY, H. D. & CERCIGNANI, M. 2015. Quantitative Magnetization Transfer Imaging as a Biomarker for Effects of Systemic Inflammation on the Brain. *Biol Psychiatry,* 78**,** 49-57.

HASHEMI, R. H., BRADLEY, W. G. & LISANTI, C. J. 2010. *MRI: The Basics,* Lippincott Williams & Wilkins.

HATEM, S. M., ATTAL, N., DUCREUX, D., GAUTRON, M., PARKER, F., PLAGHKI, L. & BOUHASSIRA, D. 2009. Assessment of spinal somatosensory systems with diffusion tensor imaging in syringomyelia. *J Neurol Neurosurg Psychiatry,* 80**,** 1350-6.

HATEM, S. M., ATTAL, N., DUCREUX, D., GAUTRON, M., PARKER, F., PLAGHKI, L. & BOUHASSIRA, D. 2010. Clinical, functional and structural determinants of central pain in syringomyelia. *Brain,* 133**,** 3409-22.

HESSELTINE, S. M., LAW, M., BABB, J., RAD, M., LOPEZ, S., GE, Y., JOHNSON, G. & GROSSMAN, R. I. 2006. Diffusion tensor imaging in multiple sclerosis: assessment of regional differences in the axial plane within normal-appearing cervical spinal cord. *AJNR Am J Neuroradiol,* 27**,** 1189-93.

HODEL, J., BESSON, P., OUTTERYCK, O., ZEPHIR, H., DUCREUX, D., MONNET, A., CHECHIN, D., ZINS, M., RODALLEC, M., PRUVO, J. P., VERMERSCH, P. & LECLERC, X. 2013. Pulse-triggered DTI sequence with reduced FOV and coronal acquisition at 3T for the assessment of the cervical spinal cord in patients with myelitis. *AJNR Am J Neuroradiol,* 34**,** 676-82.

HOLLY, L. T., ELLINGSON, B. M. & SALAMON, N. 2016. Metabolic Imaging Using Proton Magnetic Spectroscopy as a Predictor of Outcome Following Surgery for Cervical Spondylotic Myelopathy. *Clin Spine Surg*.

HOLLY, L. T., FREITAS, B., MCARTHUR, D. L. & SALAMON, N. 2009. Proton magnetic resonance spectroscopy to evaluate spinal cord axonal injury in cervical spondylotic myelopathy. *J Neurosurg Spine,* 10**,** 194-200.

HORI, M., FUKUNAGA, I., MASUTANI, Y., NAKANISHI, A., SHIMOJI, K., KAMAGATA, K., ASAHI, K., HAMASAKI, N., SUZUKI, Y. & AOKI, S. 2012. New diffusion metrics for spondylotic myelopathy at an early clinical stage. *Eur Radiol,* 22**,** 1797-802.

IGLESIAS, C., SANGARI, S., EL MENDILI, M. M., BENALI, H., MARCHAND-PAUVERT, V. & PRADAT, P. F. 2015. Electrophysiological and spinal imaging evidences for sensory dysfunction in amyotrophic lateral sclerosis. *BMJ Open,* 5**,** e007659.

IKEDA, K., MURATA, K., KAWASE, Y., KAWABE, K., KANO, O., YOSHII, Y., TAKAZAWA, T., HIRAYAMA, T. & IWASAKI, Y. 2013. Relationship between cervical cord 1H-magnetic resonance spectroscopy and clinoco-electromyographic profile in amyotrophic lateral sclerosis. *Muscle Nerve,* 47**,** 61-7.

INGLESE, M., ROVARIS, M., BIANCHI, S., LA MANTIA, L., MANCARDI, G. L., GHEZZI, A., MONTAGNA, P., SALVI, F. & FILIPPI, M. 2001. Magnetic resonance imaging, magnetisation transfer imaging, and diffusion weighted imaging correlates of optic nerve, brain, and cervical cord damage in Leber's hereditary optic neuropathy. *J Neurol Neurosurg Psychiatry,* 70**,** 444-9.

ITO, T., OYANAGI, K., TAKAHASHI, H., TAKAHASHI, H. E. & IKUTA, F. 1996. Cervical spondylotic myelopathy. Clinicopathologic study on the progression pattern and thin

myelinated fibers of the lesions of seven patients examined during complete autopsy. *Spine (Phila Pa 1976),* 21**,** 827-33.

JAIN, N., SAINI, N. S., KUMAR, S., RAJAGOPALAN, M., CHAKRABORTI, K. L. & JAIN, A. K. 2016. Correlation of diffusion tensor imaging parameters with neural status in Pott's spine. *SICOT J,* 2**,** 21.

JEANTROUX, J., KREMER, S., LIN, X. Z., COLLONGUES, N., CHANSON, J. B., BOURRE, B., FLEURY, M., BLANC, F., DIETEMANN, J. L. & DE SEZE, J. 2012. Diffusion tensor imaging of normal-appearing white matter in neuromyelitis optica. *J Neuroradiol,* 39**,** 295-300.

JIRJIS, M. B., VALDEZ, C., VEDANTAM, A., SCHMIT, B. D. & KURPAD, S. N. 2017. Diffusion tensor imaging as a biomarker for assessing neuronal stem cell treatments affecting areas distal to the site of spinal cord injury. *J Neurosurg Spine,* 26**,** 243-251.

JONES, J. G., CEN, S. Y., LEBEL, R. M., HSIEH, P. C. & LAW, M. 2013. Diffusion tensor imaging correlates with the clinical assessment of disease severity in cervical spondylotic myelopathy and predicts outcome following surgery. *AJNR Am J Neuroradiol,* 34**,** 471-8.

JUTZELER, C., ULRICH, A., HUBER, B., ROSNER, J., KRAMER, J. & CURT, A. 2017. Improved diagnosis of cervical spondylotic myelopathy with contact heat evoked potentials. *J Neurotrauma*.

KADANKA, Z., BEDNARIK, J., NOVOTNY, O., URBANEK, I. & DUSEK, L. 2011. Cervical spondylotic myelopathy: conservative versus surgical treatment after 10 years. *Eur Spine J,* 20**,** 1533-8.

KADANKA, Z., BEDNARIK, J., VOHANKA, S., VLACH, O., STEJSKAL, L., CHALOUPKA, R., FILIPOVICOVA, D., SURELOVA, D., ADAMOVA, B., NOVOTNY, O., NEMEC, M., SMRCKA, V. & URBANEK, I. 2000. Conservative treatment versus surgery in spondylotic cervical myelopathy: a prospective randomised study. *Eur Spine J,* 9**,** 538-44.

KADANKA, Z., MARES, M., BEDNARIK, J., SMRCKA, V., KRBEC, M., CHALOUPKA, R. & DUSEK, L. 2005. Predictive factors for spondylotic cervical myelopathy treated conservatively or surgically. *Eur J Neurol,* 12**,** 55-63.

KALSI-RYAN, S., BEATON, D., CURT, A., DUFF, S., POPOVIC, M. R., RUDHE, C., FEHLINGS, M. G. & VERRIER, M. C. 2012. The Graded Redefined Assessment of Strength Sensibility and Prehension: reliability and validity. *J Neurotrauma,* 29**,** 905-14.

KALSI-RYAN, S., KARADIMAS, S. K. & FEHLINGS, M. G. 2013a. Cervical spondylotic myelopathy: the clinical phenomenon and the current pathobiology of an increasingly prevalent and devastating disorder. *Neuroscientist,* 19**,** 409-21.

KALSI-RYAN, S., SINGH, A., MASSICOTTE, E. M., ARNOLD, P. M., BRODKE, D. S., NORVELL, D. C., HERMSMEYER, J. T. & FEHLINGS, M. G. 2013b. Ancillary

outcome measures for assessment of individuals with cervical spondylotic myelopathy. *Spine (Phila Pa 1976),* 38**,** S111-22.

KAMBLE, R. B., VENKATARAMANA, N. K., NAIK, A. L. & RAO, S. V. 2011. Diffusion tensor imaging in spinal cord injury. *Indian J Radiol Imaging,* 21**,** 221-4.

KAMEYAMA, T., HASHIZUME, Y., ANDO, T. & TAKAHASHI, A. 1994. Morphometry of the normal cadaveric cervical spinal cord. *Spine (Phila Pa 1976),* 19**,** 2077-81.

KARACHI, C., GRABLI, D., BERNARD, F. A., TANDE, D., WATTIEZ, N., BELAID, H., BARDINET, E., PRIGENT, A., NOTHACKER, H. P., HUNOT, S., HARTMANN, A., LEHERICY, S., HIRSCH, E. C. & FRANCOIS, C. 2010. Cholinergic mesencephalic neurons are involved in gait and postural disorders in Parkinson disease. *J Clin Invest,* 120**,** 2745-54.

KARADIMAS, S. K., ERWIN, W. M., ELY, C. G., DETTORI, J. R. & FEHLINGS, M. G. 2013. Pathophysiology and Natural History of Cervical Spondylotic Myelopathy. *Spine,* 38**,** S21-S36.

KARADIMAS, S. K., LALIBERTE, A. M., TETREAULT, L., CHUNG, Y. S., ARNOLD, P., FOLTZ, W. D. & FEHLINGS, M. G. 2015. Riluzole blocks perioperative ischemia-reperfusion injury and enhances postdecompression outcomes in cervical spondylotic myelopathy. *Sci Transl Med,* 7**,** 316ra194.

KATO, F., YUKAWA, Y., SUDA, K., YAMAGATA, M. & UETA, T. 2012. Normal morphology, age-related changes and abnormal findings of the cervical spine. Part II: Magnetic resonance imaging of over 1,200 asymptomatic subjects. *Eur Spine J,* 21**,** 1499-507.

KAUSHAL, M., ONI-ORISAN, A., CHEN, G., LI, W., LESCHKE, J., WARD, B. D., KALINOSKY, B., BUDDE, M. D., SCHMIT, B. D., LI, S. J., MUQEET, V. & KURPAD, S. N. 2017. Evaluation of Whole-Brain Resting-State Functional Connectivity in Spinal Cord Injury: A Large-Scale Network Analysis Using Network-Based Statistic. *J Neurotrauma*.

KEARNEY, H., ALTMANN, D. R., SAMSON, R. S., YIANNAKAS, M. C., WHEELER-KINGSHOTT, C. A., CICCARELLI, O. & MILLER, D. H. 2015a. Cervical cord lesion load is associated with disability independently from atrophy in MS. *Neurology,* 84**,** 367-73.

KEARNEY, H., SCHNEIDER, T., YIANNAKAS, M. C., ALTMANN, D. R., WHEELER-KINGSHOTT, C. A., CICCARELLI, O. & MILLER, D. H. 2015b. Spinal cord grey matter abnormalities are associated with secondary progression and physical disability in multiple sclerosis. *J Neurol Neurosurg Psychiatry,* 86**,** 608-14.

KEARNEY, H., YIANNAKAS, M. C., ABDEL-AZIZ, K., WHEELER-KINGSHOTT, C. A., ALTMANN, D. R., CICCARELLI, O. & MILLER, D. H. 2014a. Improved MRI quantification of spinal cord atrophy in multiple sclerosis. *J Magn Reson Imaging,* 39**,** 617-23.

KEARNEY, H., YIANNAKAS, M. C., SAMSON, R. S., WHEELER-KINGSHOTT, C. A., CICCARELLI, O. & MILLER, D. H. 2014b. Investigation of magnetization transfer ratio-derived pial and subpial abnormalities in the multiple sclerosis spinal cord. *Brain,* 137**,** 2456-68.

KERKOVSKY, M., BEDNARIK, J., DUSEK, L., SPRLAKOVA-PUKOVA, A., URBANEK, I., MECHL, M., VALEK, V. & KADANKA, Z. 2012. Magnetic resonance diffusion tensor imaging in patients with cervical spondylotic spinal cord compression: correlations between clinical and electrophysiological findings. *Spine (Phila Pa 1976),* 37**,** 48-56.

KERKOVSKY, M., BEDNARIK, J., JUROVA, B., DUSEK, L., KADANKA, Z., KADANKA, Z., JR., NEMEC, M., KOVALOVA, I., SPRLAKOVA-PUKOVA, A. & MECHL, M. 2017. Spinal Cord MR Diffusion Properties in Patients with Degenerative Cervical Cord Compression. *J Neuroimaging,* 27**,** 149-157.

KIM, S. Y., SHIN, M. J., CHANG, J. H., LEE, C. H., SHIN, Y. I., SHIN, Y. B. & KO, H. Y. 2015. Correlation of diffusion tensor imaging and phase-contrast MR with clinical parameters of cervical spinal cord injuries. *Spinal Cord,* 53**,** 608-14.

KIRSHBLUM, S. C., BURNS, S. P., BIERING-SORENSEN, F., DONOVAN, W., GRAVES, D. E., JHA, A., JOHANSEN, M., JONES, L., KRASSIOUKOV, A., MULCAHEY, M. J., SCHMIDT-READ, M. & WARING, W. 2011. International standards for neurological classification of spinal cord injury (revised 2011). *J Spinal Cord Med,* 34**,** 535-46.

KOSKINEN, E., BRANDER, A., HAKULINEN, U., LUOTO, T., HELMINEN, M., YLINEN, A. & OHMAN, J. 2013. Assessing the state of chronic spinal cord injury using diffusion tensor imaging. *J Neurotrauma,* 30**,** 1587-95.

KOVALOVA, I., KERKOVSKY, M., KADANKA, Z., KADANKA, Z., JR., NEMEC, M., JUROVA, B., DUSEK, L., JARKOVSKY, J. & BEDNARIK, J. 2016. Prevalence and Imaging Characteristics of Nonmyelopathic and Myelopathic Spondylotic Cervical Cord Compression. *Spine (Phila Pa 1976),* 41**,** 1908-1916.

KOWALCZYK, I., DUGGAL, N. & BARTHA, R. 2012. Proton magnetic resonance spectroscopy of the motor cortex in cervical myelopathy. *Brain,* 135**,** 461-8.

KRUSE, S. A., KOLIPAKA, A., MANDUCA, A. & EHMAN, R. L. 2009. Feasibility of Evaluating the Spinal Cord with MR Elastography. *ISMRM*.

KUHN, F. P., FEYDY, A., LAUNAY, N., LEFEVRE-COLAU, M. M., POIRAUDEAU, S., LAPORTE, S., MAIER, M. A. & LINDBERG, P. 2016. Kinetic DTI of the cervical spine: diffusivity changes in healthy subjects. *Neuroradiology,* 58**,** 929-35.

KURPAD, S. N., MARTIN, A. R., TETREAULT, L., FISCHER, D. J., SKELLY, A. C., MIKULIS, D., FLANDERS, A. E., AARABI, B., MROZ, T., C., T. E. & FEHLINGS, M. G. 2017. Impact of baseline magnetic resonance imaging on neurologic, functional, and safety outcomes in patients with acute traumatic spinal cord injury. *Global Spine J,* In press.

LAULE, C., VAVASOUR, I. M., ZHAO, Y., TRABOULSEE, A. L., OGER, J., VAVASOUR, J. D., MACKAY, A. L. & LI, D. K. 2010. Two-year study of cervical cord volume and myelin water in primary progressive multiple sclerosis. *Mult Scler,* 16**,** 670-7.

LEE, J., SHMUELI, K., KANG, B. T., YAO, B., FUKUNAGA, M., VAN GELDEREN, P., PALUMBO, S., BOSETTI, F., SILVA, A. C. & DUYN, J. H. 2012. The contribution of myelin to magnetic susceptibility-weighted contrasts in high-field MRI of the brain. *Neuroimage,* 59**,** 3967-75.

LEE, J. W., KIM, J. H., PARK, J. B., PARK, K. W., YEOM, J. S., LEE, G. Y. & KANG, H. S. 2011. Diffusion tensor imaging and fiber tractography in cervical compressive myelopathy: preliminary results. *Skeletal Radiol,* 40**,** 1543-51.

LEE, M. J., CASSINELLI, E. H. & RIEW, K. D. 2007. Prevalence of cervical spine stenosis. Anatomic study in cadavers. *J Bone Joint Surg Am,* 89**,** 376-80.

LEE, S., LEE, Y. H., CHUNG, T. S., JEONG, E. K., KIM, S., YOO, Y. H., KIM, I. S., YOON, C. S., SUH, J. S. & PARK, J. H. 2015. Accuracy of Diffusion Tensor Imaging for Diagnosing Cervical Spondylotic Myelopathy in Patients Showing Spinal Cord Compression. *Korean J Radiol,* 16**,** 1303-12.

LEMA, A., BISHOP, C., MALIK, O., MATTOSCIO, M., ALI, R., NICHOLAS, R., MURARO, P. A., MATTHEWS, P. M., WALDMAN, A. D. & NEWBOULD, R. D. 2016. A Comparison of Magnetization Transfer Methods to Assess Brain and Cervical Cord Microstructure in Multiple Sclerosis. *J Neuroimaging*.

LEVESQUE, I. R., GIACOMINI, P. S., NARAYANAN, S., RIBEIRO, L. T., SLED, J. G., ARNOLD, D. L. & PIKE, G. B. 2010. Quantitative magnetization transfer and myelin water imaging of the evolution of acute multiple sclerosis lesions. *Magn Reson Med,* 63**,** 633-40.

LEVITT, M. H. 2008. *Spin Dynamics: Basics of Nuclear Magnetic Resonance,* New York, John Wiley & Sons.

LEVY, S., BENHAMOU, M., NAAMAN, C., RAINVILLE, P., CALLOT, V. & COHEN-ADAD, J. 2015. White matter atlas of the human spinal cord with estimation of partial volume effect. *Neuroimage,* 119**,** 262-271.

LI, X., CUI, J. L., MAK, K. C., LUK, K. D. & HU, Y. 2014. Potential use of diffusion tensor imaging in level diagnosis of multilevel cervical spondylotic myelopathy. *Spine (Phila Pa 1976),* 39**,** E615-22.

LIBERATI, A., ALTMAN, D. G., TETZLAFF, J., MULROW, C., GOTZSCHE, P. C., IOANNIDIS, J. P., CLARKE, M., DEVEREAUX, P. J., KLEIJNEN, J. & MOHER, D. 2009. The PRISMA statement for reporting systematic reviews and meta-analyses of studies that evaluate health care interventions: explanation and elaboration. *J Clin Epidemiol,* 62**,** e1-34.

LINDBERG, P. G., FEYDY, A., SANCHEZ, K., RANNOU, F. & MAIER, M. A. 2012. Measures of spinal canal stenosis and relationship to spinal cord structure in patients with cervical spondylosis. *J Neuroradiol,* 39**,** 236-42.

LINDBERG, P. G., SANCHEZ, K., OZCAN, F., RANNOU, F., POIRAUDEAU, S., FEYDY, A. & MAIER, M. A. 2016. Correlation of force control with regional spinal DTI in patients with cervical spondylosis without signs of spinal cord injury on conventional MRI. *Eur Radiol,* 26**,** 733-42.

LINDEMANN, K., MULLER, H. P., LUDOLPH, A. C., HORNYAK, M. & KASSUBEK, J. 2016. Microstructure of the Midbrain and Cervical Spinal Cord in Idiopathic Restless Legs Syndrome: A Diffusion Tensor Imaging Study. *Sleep,* 39**,** 423-8.

LIU, X., QIAN, W., JIN, R., LI, X., LUK, K. D., WU, E. X. & HU, Y. 2016. Amplitude of Low Frequency Fluctuation (ALFF) in the Cervical Spinal Cord with Stenosis: A Resting State fMRI Study. *PLoS One,* 11**,** e0167279.

LIU, Z., ZHU, H., MARKS, B. L., KATZ, L. M., GOODLETT, C. B., GERIG, G. & STYNER, M. 2009. Voxel-Wise Group Analysis of Dti. *Proc IEEE Int Symp Biomed Imaging***,** 807-810.

LYCKLAMA A NIJEHOLT, G. J., CASTELIJNS, J. A., LAZERON, R. H., VAN WAESBERGHE, J. H., POLMAN, C. H., UITDEHAAG, B. M. & BARKHOF, F. 2000. Magnetization transfer ratio of the spinal cord in multiple sclerosis: relationship to atrophy and neurologic disability. *J Neuroimaging,* 10**,** 67-72.

MAKI, S., KODA, M., OTA, M., OIKAWA, Y., KAMIYA, K., INADA, T., FURUYA, T., TAKAHASHI, K., MASUDA, Y., MATSUMOTO, K., KOJIMA, M., OBATA, T. & YAMAZAKI, M. 2015. Reduced Field-of-View Diffusion Tensor Imaging of the Spinal Cord Shows Motor Dysfunction of the Lower Extremities in Patients with Cervical Compression Myelopathy. *Spine (Phila Pa 1976).*

MAKI, S., KODA, M., SAITO, J., TAKAHASHI, S., INADA, T., KAMIYA, K., OTA, M., IIJIMA, Y., MASUDA, Y., MATSUMOTO, K., KOJIMA, M., TAKAHASHI, K., OBATA, T., YAMAZAKI, M. & FURUYA, T. 2016. Tract-Specific Diffusion Tensor Imaging Reveals Laterality of Neurological Symptoms in Patients with Cervical Compression Myelopathy. *World Neurosurg,* 96**,** 184-190.

MAMATA, H., JOLESZ, F. A. & MAIER, S. E. 2005. Apparent diffusion coefficient and fractional anisotropy in spinal cord: Age and cervical spondylosis-related changes. *Journal of Magnetic Resonance Imaging,* 22**,** 38-43.

MANCONI, M., ROCCA, M. A., FERINI-STRAMBI, L., TORTORELLA, P., AGOSTA, F., COMI, G. & FILIPPI, M. 2008. Restless legs syndrome is a common finding in multiple sclerosis and correlates with cervical cord damage. *Mult Scler,* 14**,** 86-93.

MARLIANI, A. F., CLEMENTI, V., ALBINI RICCIOLI, L., AGATI, R., CARPENZANO, M., SALVI, F. & LEONARDI, M. 2010. Quantitative cervical spinal cord 3T proton MR spectroscopy in multiple sclerosis. *AJNR Am J Neuroradiol,* 31**,** 180-4.

MARQUES, J. P., MADDAGE, R., MLYNARIK, V. & GRUETTER, R. 2009. On the origin of the MR image phase contrast: an in vivo MR microscopy study of the rat brain at 14.1 T. *Neuroimage,* 46**,** 345-52.

MARTIN, A. R., ALEKSANDEREK, I., COHEN-ADAD, J., TARMOHAMED, Z., TETREAULT, L., SMITH, N., CADOTTE, D. W., CRAWLEY, A., GINSBERG, H., MIKULIS, D. J. & FEHLINGS, M. G. 2016. Translating state-of-the-art spinal cord MRI techniques to clinical use: A systematic review of clinical studies utilizing DTI, MT, MWF, MRS, and fMRI. *Neuroimage Clin,* 10**,** 192-238.

MARTIN, A. R., COHEN-ADAD, J. & FEHLINGS, M. G. 2017a. Magnetic Resonance Imaging of the Injured Spinal Cord: The Present and the Future. *In:* VIALLE, L. R. (ed.) *AOSpine Masters Series: Spinal Cord Injury and Regeneration.*

MARTIN, A. R., DE LEENER, B., COHEN-ADAD, J., CADOTTE, D. W., CRAWLEY, A., GINSBERG, H., MIKULIS, D. J. & FEHLINGS, M. G. 2017b. Clinically feasible microstructural MRI to quantify cervical spinal cord tissue injury using DTI, MT, and T2*-weighted imaging: assessment of normative data and reliability. *AJNR,* In press.

MARTIN, A. R., DE LEENER, B., COHEN-ADAD, J., CADOTTE, D. W., KALSI-RYAN, S., LANGE, S. F., TETREAULT, L., NOURI, A., CRAWLEY, A., MIKULIS, D. J., GINSBERG, H. & FEHLINGS, M. G. 2017c. A Novel MRI Biomarker of Spinal Cord White Matter Injury: T2*-weighted White Matter to Grey Matter Signal Intensity Ratio. *AJNR,* In press.

MARTIN, A. R., DE LEENER, B., COHEN-ADAD, J., CADOTTE, D. W., WILSON, J. R., TETREAULT, L., LANGE, S. F., NOURI, A., CRAWLEY, A., MIKULIS, D. J., GINSBERG, H. & FEHLINGS, M. G. 2017d. Toward Clinical Translation of Quantitative Spinal Cord MRI: Serial Monitoring to Identify Disease Progression in Patients with Degenerative Cervical Myelopathy. *International Society for Magnetic Resonance in Medicine.* Honolulu, Hawaii, USA.

MARTIN AR, D. L. B., COHEN-ADAD J, CADOTTE DW, CRAWLEY A, GINSBERG H, MIKULIS DJ, FEHLINGS MG. 2017a. Clinically feasible microstructural MRI to quantify cervical spinal cord tissue injury using DTI, MT, and T2*-weighted imaging: assessment of normative data and reliability. *AJNR,* In press.

MARTIN AR, D. L. B., COHEN-ADAD J, CADOTTE DW, KALSI-RYAN S, LANGE SF, TETREAULT L, NOURI A, CRAWLEY A, MIKULIS DJ, GINSBERG H, FEHLINGS MG 2017b. A Novel MRI Biomarker of Spinal Cord White Matter Injury: T2*-weighted White Matter to Grey Matter Signal Intensity Ratio. *AJNR,* In press.

MASSIRE, A., TASO, M., BESSON, P., GUYE, M., RANJEVA, J. P. & CALLOT, V. 2016. High-resolution multi-parametric quantitative magnetic resonance imaging of the human cervical spinal cord at 7T. *Neuroimage,* 143**,** 58-69.

MATSUDA, Y., SHIBATA, T., OKI, S., KAWATANI, Y., MASHIMA, N. & OISHI, H. 1999. Outcomes of surgical treatment for cervical myelopathy in patients more than 75 years of age. *Spine (Phila Pa 1976),* 24**,** 529-34.

MATSUMOTO, M., CHIBA, K., ISHIKAWA, M., MARUIWA, H., FUJIMURA, Y. & TOYAMA, Y. 2001. Relationships between outcomes of conservative treatment and magnetic resonance imaging findings in patients with mild cervical myelopathy caused by soft disc herniations. *Spine (Phila Pa 1976)*, 26**,** 1592-8.

MATSUMOTO, M., FUJIMURA, Y., SUZUKI, N., NISHI, Y., NAKAMURA, M., YABE, Y. & SHIGA, H. 1998. MRI of cervical intervertebral discs in asymptomatic subjects. *J Bone Joint Surg Br*, 80**,** 19-24.

MATSUMOTO, M., TOYAMA, Y., ISHIKAWA, M., CHIBA, K., SUZUKI, N. & FUJIMURA, Y. 2000. Increased signal intensity of the spinal cord on magnetic resonance images in cervical compressive myelopathy. Does it predict the outcome of conservative treatment? *Spine (Phila Pa 1976)*, 25**,** 677-82.

MATZ, P. G., ANDERSON, P. A., HOLLY, L. T., GROFF, M. W., HEARY, R. F., KAISER, M. G., MUMMANENI, P. V., RYKEN, T. C., CHOUDHRI, T. F., VRESILOVIC, E. J., RESNICK, D. K., JOINT SECTION ON DISORDERS OF THE, S., PERIPHERAL NERVES OF THE AMERICAN ASSOCIATION OF NEUROLOGICAL, S. & CONGRESS OF NEUROLOGICAL, S. 2009. The natural history of cervical spondylotic myelopathy. *J Neurosurg Spine*, 11**,** 104-11.

MIKULIS, D. J., JURKIEWICZ, M. T., MCILROY, W. E., STAINES, W. R., RICKARDS, L., KALSI-RYAN, S., CRAWLEY, A. P., FEHLINGS, M. G. & VERRIER, M. C. 2002. Adaptation in the motor cortex following cervical spinal cord injury. *Neurology*, 58**,** 794-801.

MIRALDI, F., LOPES, F. C., COSTA, J. V., ALVES-LEON, S. V. & GASPARETTO, E. L. 2013. Diffusion tensor magnetic resonance imaging may show abnormalities in the normal-appearing cervical spinal cord from patients with multiple sclerosis. *Arq Neuropsiquiatr*, 71**,** 580-3.

MIZUNO, J., NAKAGAWA, H., INOUE, T. & HASHIZUME, Y. 2003. Clinicopathological study of "snake-eye appearance" in compressive myelopathy of the cervical spinal cord. *J Neurosurg*, 99**,** 162-8.

MUELLER-MANG, C., LAW, M., MANG, T., FRUEHWALD-PALLAMAR, J., WEBER, M. & THURNHER, M. M. 2011. Diffusion tensor MR imaging (DTI) metrics in the cervical spinal cord in asymptomatic HIV-positive patients. *Neuroradiology*, 53**,** 585-92.

NAIR, G., CAREW, J. D., USHER, S., LU, D., HU, X. P. & BENATAR, M. 2010. Diffusion tensor imaging reveals regional differences in the cervical spinal cord in amyotrophic lateral sclerosis. *Neuroimage*, 53**,** 576-83.

NAISMITH, R. T., XU, J., KLAWITER, E. C., LANCIA, S., TUTLAM, N. T., WAGNER, J. M., QIAN, P., TRINKAUS, K., SONG, S. K. & CROSS, A. H. 2013. Spinal cord tract diffusion tensor imaging reveals disability substrate in demyelinating disease. *Neurology*, 80**,** 2201-9.

NOURI, A., MARTIN, A. R., MIKULIS, D. J. & FEHLINGS, M. G. 2016. Magnetic resonance imaging assessment of degenerative cervical myelopathy: A review of structural changes and measurement techniques. *Neurosurgical Focus,* 40**,** E5.

NOURI, A., TETREAULT, L., COTE, P., ZAMORANO, J. J., DALZELL, K. & FEHLINGS, M. G. 2015a. Does Magnetic Resonance Imaging Improve the Predictive Performance of a Validated Clinical Prediction Rule Developed to Evaluate Surgical Outcome in Patients With Degenerative Cervical Myelopathy? *Spine (Phila Pa 1976),* 40**,** 1092-100.

NOURI, A., TETREAULT, L., SINGH, A., KARADIMAS, S. K. & FEHLINGS, M. G. 2015b. Degenerative Cervical Myelopathy: Epidemiology, Genetics, and Pathogenesis. *Spine (Phila Pa 1976),* 40**,** E675-93.

NOURI, A., TETREAULT, L., ZAMORANO, J. J., DALZELL, K., DAVIS, A. M., MIKULIS, D., YEE, A. & FEHLINGS, M. G. 2015c. Role of Magnetic Resonance Imaging in Predicting Surgical Outcome in Patients With Cervical Spondylotic Myelopathy. *Spine,* 40**,** 171-178.

OH, J., SAIDHA, S., CHEN, M., SMITH, S. A., PRINCE, J., JONES, C., DIENER-WEST, M., VAN ZIJL, P. C., REICH, D. S. & CALABRESI, P. A. 2013a. Spinal cord quantitative MRI discriminates between disability levels in multiple sclerosis. *Neurology,* 80**,** 540-7.

OH, J., SEIGO, M., SAIDHA, S., SOTIRCHOS, E., ZACKOWSKI, K., CHEN, M., PRINCE, J., DIENER-WEST, M., CALABRESI, P. A. & REICH, D. S. 2014. Spinal Cord Normalization in Multiple Sclerosis. *Journal of Neuroimaging,* 24**,** 577-584.

OH, J., SOTIRCHOS, E. S., SAIDHA, S., WHETSTONE, A., CHEN, M., NEWSOME, S. D., ZACKOWSKI, K., BALCER, L. J., FROHMAN, E., PRINCE, J., DIENER-WEST, M., REICH, D. S. & CALABRESI, P. A. 2015. Relationships between quantitative spinal cord MRI and retinal layers in multiple sclerosis. *Neurology,* 84**,** 720-8.

OH, J., ZACKOWSKI, K., CHEN, M., NEWSOME, S., SAIDHA, S., SMITH, S. A., DIENER-WEST, M., PRINCE, J., JONES, C. K., VAN ZIJL, P. C., CALABRESI, P. A. & REICH, D. S. 2013b. Multiparametric MRI correlates of sensorimotor function in the spinal cord in multiple sclerosis. *Mult Scler,* 19**,** 427-35.

OHGIYA, Y., OKA, M., HIWATASHI, A., LIU, X., KAKIMOTO, N., WESTESSON, P. L. & EKHOLM, S. E. 2007. Diffusion tensor MR imaging of the cervical spinal cord in patients with multiple sclerosis. *Eur Radiol,* 17**,** 2499-504.

OHSHIO, I., HATAYAMA, A., KANEDA, K., TAKAHARA, M. & NAGASHIMA, K. 1993. Correlation between histopathologic features and magnetic resonance images of spinal cord lesions. *Spine (Phila Pa 1976),* 18**,** 1140-9.

ONI-ORISAN, A., KAUSHAL, M., LI, W., LESCHKE, J., WARD, B. D., VEDANTAM, A., KALINOSKY, B., BUDDE, M. D., SCHMIT, B. D., LI, S. J., MUQEET, V. & KURPAD, S. N. 2016. Alterations in Cortical Sensorimotor Connectivity following Complete Cervical Spinal Cord Injury: A Prospective Resting-State fMRI Study. *PLoS One,* 11**,** e0150351.

PASCUAL-LEONE, A., AMEDI, A., FREGNI, F. & MERABET, L. B. 2005. The plastic human brain cortex. *Annu Rev Neurosci,* 28**,** 377-401.

PESSOA, F. M., LOPES, F. C., COSTA, J. V., LEON, S. V., DOMINGUES, R. C. & GASPARETTO, E. L. 2012. The cervical spinal cord in neuromyelitis optica patients: a comparative study with multiple sclerosis using diffusion tensor imaging. *Eur J Radiol,* 81**,** 2697-701.

PETERSEN, J. A., WILM, B. J., VON MEYENBURG, J., SCHUBERT, M., SEIFERT, B., NAJAFI, Y., DIETZ, V. & KOLLIAS, S. 2012. Chronic cervical spinal cord injury: DTI correlates with clinical and electrophysiological measures. *J Neurotrauma,* 29**,** 1556-66.

RAJASEKARAN, S., KANNA, R. M., CHITTODE, V. S., MAHESWARAN, A., AIYER, S. N. & SHETTY, A. P. 2017. Efficacy of Diffusion Tensor Imaging Indices in Assessing Postoperative Neural Recovery in Cervical Spondylotic Myelopathy. *Spine (Phila Pa 1976),* 42**,** 8-13.

RAJASEKARAN, S., YERRAMSHETTY, J. S., CHITTODE, V. S., KANNA, R. M., BALAMURALI, G. & SHETTY, A. P. 2014. The assessment of neuronal status in normal and cervical spondylotic myelopathy using diffusion tensor imaging. *Spine (Phila Pa 1976),* 39**,** 1183-9.

RAZ, E., BESTER, M., SIGMUND, E. E., TABESH, A., BABB, J. S., JAGGI, H., HELPERN, J., MITNICK, R. J. & INGLESE, M. 2013. A better characterization of spinal cord damage in multiple sclerosis: a diffusional kurtosis imaging study. *AJNR Am J Neuroradiol,* 34**,** 1846-52.

RENOUX, J., FACON, D., FILLARD, P., HUYNH, I., LASJAUNIAS, P. & DUCREUX, D. 2006. MR diffusion tensor imaging and fiber tracking in inflammatory diseases of the spinal cord. *AJNR Am J Neuroradiol,* 27**,** 1947-51.

RHEE, J. M., SHAMJI, M. F., ERWIN, W. M., BRANSFORD, R. J., YOON, S. T., SMITH, J. S., KIM, H. J., ELY, C. G., DETTORI, J. R., PATEL, A. A. & KALSI-RYAN, S. 2013. Nonoperative management of cervical myelopathy: a systematic review. *Spine (Phila Pa 1976),* 38**,** S55-67.

ROCCA, M. A., ABSINTA, M., VALSASINA, P., COPETTI, M., CAPUTO, D., COMI, G. & FILIPPI, M. 2012. Abnormal cervical cord function contributes to fatigue in multiple sclerosis. *Mult Scler,* 18**,** 1552-9.

ROCCA, M. A., AGOSTA, F., MARTINELLI, V., FALINI, A., COMI, G. & FILIPPI, M. 2006. The level of spinal cord involvement influences the pattern of movement-associated cortical recruitment in patients with isolated myelitis. *Neuroimage,* 30**,** 879-84.

ROCCA, M. A., FILIPPI, M., HERZOG, J., SORMANI, M. P., DICHGANS, M. & YOUSRY, T. A. 2001. A magnetic resonance imaging study of the cervical cord of patients with CADASIL. *Neurology,* 56**,** 1392-4.

ROVARIS, M., BOZZALI, M., ROCCA, M. A., COLOMBO, B. & FILIPPI, M. 2001a. An MR study of tissue damage in the cervical cord of patients with migraine. *J Neurol Sci,* 183**,** 43-6.

ROVARIS, M., BOZZALI, M., SANTUCCIO, G., GHEZZI, A., CAPUTO, D., MONTANARI, E., BERTOLOTTO, A., BERGAMASCHI, R., CAPRA, R., MANCARDI, G., MARTINELLI, V., COMI, G. & FILIPPI, M. 2001b. In vivo assessment of the brain and cervical cord pathology of patients with primary progressive multiple sclerosis. *Brain,* 124**,** 2540-9.

ROVARIS, M., BOZZALI, M., SANTUCCIO, G., IANNUCCI, G., SORMANI, M. P., COLOMBO, B., COMI, G. & FILIPPI, M. 2000. Relative contributions of brain and cervical cord pathology to multiple sclerosis disability: a study with magnetisation transfer ratio histogram analysis. *J Neurol Neurosurg Psychiatry,* 69**,** 723-7.

ROVARIS, M., GALLO, A., RIVA, R., GHEZZI, A., BOZZALI, M., BENEDETTI, B., MARTINELLI, V., FALINI, A., COMI, G. & FILIPPI, M. 2004. An MT MRI study of the cervical cord in clinically isolated syndromes suggestive of MS. *Neurology,* 63**,** 584-5.

ROVARIS, M., JUDICA, E., CECCARELLI, A., GHEZZI, A., MARTINELLI, V., COMI, G. & FILIPPI, M. 2008. Absence of diffuse cervical cord tissue damage in early, non-disabling relapsing-remitting MS: a preliminary study. *Mult Scler,* 14**,** 853-6.

SALAMON, N., ELLINGSON, B. M., NAGARAJAN, R., GEBARA, N., THOMAS, A. & HOLLY, L. T. 2013. Proton magnetic resonance spectroscopy of human cervical spondylosis at 3T. *Spinal Cord,* 51**,** 558-63.

SAMSON, R. S., CICCARELLI, O., KACHRAMANOGLOU, C., BRIGHTMAN, L., LUTTI, A., THOMAS, D. L., WEISKOPF, N. & WHEELER-KINGSHOTT, C. A. 2013. Tissue- and column-specific measurements from multi-parameter mapping of the human cervical spinal cord at 3 T. *NMR Biomed,* 26**,** 1823-30.

SAMSON, R. S., LEVY, S., SCHNEIDER, T., SMITH, A. K., SMITH, S. A., COHEN-ADAD, J. & GANDINI WHEELER-KINGSHOTT, C. A. 2016. ZOOM or Non-ZOOM? Assessing Spinal Cord Diffusion Tensor Imaging Protocols for Multi-Centre Studies. *PLoS One,* 11**,** e0155557.

SARITAS, E. U., CUNNINGHAM, C. H., LEE, J. H., HAN, E. T. & NISHIMURA, D. G. 2008. DWI of the spinal cord with reduced FOV single-shot EPI. *Magn Reson Med,* 60**,** 468-73.

SCHUNEMANN, H. J., OXMAN, A. D., BROZEK, J., GLASZIOU, P., JAESCHKE, R., VIST, G. E., WILLIAMS, J. W., JR., KUNZ, R., CRAIG, J., MONTORI, V. M., BOSSUYT, P., GUYATT, G. H. & GROUP, G. W. 2008. Grading quality of evidence and strength of recommendations for diagnostic tests and strategies. *BMJ,* 336**,** 1106-10.

SEIDENWURM, D. J. & EXPERT PANEL ON NEUROLOGIC, I. 2008. Myelopathy. *AJNR Am J Neuroradiol,* 29**,** 1032-4.

SHANMUGANATHAN, K., GULLAPALLI, R. P., ZHUO, J. & MIRVIS, S. E. 2008. Diffusion tensor MR imaging in cervical spine trauma. *AJNR Am J Neuroradiol,* 29**,** 655-9.

SHIMOMURA, T., SUMI, M., NISHIDA, K., MAENO, K., TADOKORO, K., MIYAMOTO, H., KUROSAKA, M. & DOITA, M. 2007. Prognostic factors for deterioration of patients with cervical spondylotic myelopathy after nonsurgical treatment. *Spine (Phila Pa 1976),* 32**,** 2474-9.

SIEMENS. *7T Magnetom Terra* [Online]. Available: https://www.healthcare.siemens.com/magnetic-resonance-imaging/7t-mri-scanner [Accessed].

SILVER, N. C., BARKER, G. J., LOSSEFF, N. A., GAWNE-CAIN, M. L., MACMANUS, D. G., THOMPSON, A. J. & MILLER, D. H. 1997. Magnetisation transfer ratio measurement in the cervical spinal cord: a preliminary study in multiple sclerosis. *Neuroradiology,* 39**,** 441-5.

SKELLY, A. C., HASHIMOTO, R. E., NORVELL, D. C., DETTORI, J. R., FISCHER, D. J., WILSON, J. R., TETREAULT, L. A. & FEHLINGS, M. G. 2013. Cervical spondylotic myelopathy: methodological approaches to evaluate the literature and establish best evidence. *Spine (Phila Pa 1976),* 38**,** S9-18.

SKINNER, N. P., KURPAD, S. N., SCHMIT, B. D., TUGAN MUFTULER, L. & BUDDE, M. D. 2016. Rapid in vivo detection of rat spinal cord injury with double-diffusion-encoded magnetic resonance spectroscopy. *Magn Reson Med*.

SMITH, S. A., JONES, C. K., GIFFORD, A., BELEGU, V., CHODKOWSKI, B., FARRELL, J. A. D., LANDMAN, B. A., REICH, D. S., CALABRESI, P. A., MCDONALD, J. W. & VAN ZIJL, P. C. M. 2010. Reproducibility of tract-specific magnetization transfer and diffusion tensor imaging in the cervical spinal cord at 3 tesla. *Nmr in Biomedicine,* 23**,** 207-217.

SONG, T., CHEN, W. J., YANG, B., ZHAO, H. P., HUANG, J. W., CAI, M. J., DONG, T. F. & LI, T. S. 2011. Diffusion tensor imaging in the cervical spinal cord. *Eur Spine J,* 20**,** 422-8.

STEVENSON, V. L., LEARY, S. M., LOSSEFF, N. A., PARKER, G. J., BARKER, G. J., HUSMANI, Y., MILLER, D. H. & THOMPSON, A. J. 1998. Spinal cord atrophy and disability in MS: a longitudinal study. *Neurology,* 51**,** 234-8.

STIKOV, N., CAMPBELL, J. S., STROH, T., LAVELEE, M., FREY, S., NOVEK, J., NUARA, S., HO, M. K., BEDELL, B. J., DOUGHERTY, R. F., LEPPERT, I. R., BOUDREAU, M., NARAYANAN, S., DUVAL, T., COHEN-ADAD, J., PICARD, P. A., GASECKA, A., COTE, D. & PIKE, G. B. 2015. In vivo histology of the myelin g-ratio with magnetic resonance imaging. *Neuroimage,* 118**,** 397-405.

STROMAN, P. W., KORNELSEN, J., BERGMAN, A., KRAUSE, V., ETHANS, K., MALISZA, K. L. & TOMANEK, B. 2004. Noninvasive assessment of the injured human spinal cord by means of functional magnetic resonance imaging. *Spinal Cord,* 42**,** 59-66.

STROMAN, P. W., KRAUSE, V., MALISZA, K. L., FRANKENSTEIN, U. N. & TOMANEK, B. 2001. Characterization of contrast changes in functional MRI of the human spinal cord at 1.5 T. *Magn Reson Imaging,* 19**,** 833-8.

STROMAN, P. W., WHEELER-KINGSHOTT, C., BACON, M., SCHWAB, J. M., BOSMA, R., BROOKS, J., CADOTTE, D., CARLSTEDT, T., CICCARELLI, O., COHEN-ADAD, J., CURT, A., EVANGELOU, N., FEHLINGS, M. G., FILIPPI, M., KELLEY, B. J., KOLLIAS, S., MACKAY, A., PORRO, C. A., SMITH, S., STRITTMATTER, S. M., SUMMERS, P. & TRACEY, I. 2014. The current state-of-the-art of spinal cord imaging: Methods. *Neuroimage,* 84**,** 1070-1081.

SUMI, M., MIYAMOTO, H., SUZUKI, T., KANEYAMA, S., KANATANI, T. & UNO, K. 2012. Prospective cohort study of mild cervical spondylotic myelopathy without surgical treatment. *J Neurosurg Spine,* 16**,** 8-14.

SUMMERS, P., STAEMPFLI, P., JAERMANN, T., KWIECINSKI, S. & KOLLIAS, S. 2006. A preliminary study of the effects of trigger timing on diffusion tensor imaging of the human spinal cord. *AJNR Am J Neuroradiol,* 27**,** 1952-61.

TAHA ALI TF, B. A. 2013. Feasibility of 1H-MR Spectroscopy in evaluation of cervical

spondylotic myelopathy. *Egypt. J. Radiol. Nucl. Med.,* 44**,** 93-99.

TASO, M., GIRARD, O. M., DUHAMEL, G., LE TROTER, A., FEIWEIER, T., GUYE, M., RANJEVA, J. P. & CALLOT, V. 2016. Tract-specific and age-related variations of the spinal cord microstructure: a multi-parametric MRI study using diffusion tensor imaging (DTI) and inhomogeneous magnetization transfer (ihMT). *NMR Biomed,* 29**,** 817-32.

TASO, M., LE TROTER, A., SDIKA, M., COHEN-ADAD, J., ARNOUX, P. J., GUYE, M., RANJEVA, J. P. & CALLOT, V. 2015. A reliable spatially normalized template of the human spinal cord--Applications to automated white matter/gray matter segmentation and tensor-based morphometry (TBM) mapping of gray matter alterations occurring with age. *Neuroimage,* 117**,** 20-8.

TERESI, L. M., LUFKIN, R. B., REICHER, M. A., MOFFIT, B. J., VINUELA, F. V., WILSON, G. M., BENTSON, J. R. & HANAFEE, W. N. 1987. Asymptomatic degenerative disk disease and spondylosis of the cervical spine: MR imaging. *Radiology,* 164**,** 83-8.

TETREAULT, L., NOURI, A., SINGH, A., FAWCETT, M., NATER, A. & FEHLINGS, M. G. 2015a. An Assessment of the Key Predictors of Perioperative Complications in Patients with Cervical Spondylotic Myelopathy Undergoing Surgical Treatment: Results from a Survey of 916 AOSpine International Members. *World Neurosurg,* 83**,** 679-90.

TETREAULT, L. A., DETTORI, J. R., WILSON, J. R., SINGH, A., NOURI, A., FEHLINGS, M. G., BRODT, E. D. & JACOBS, W. B. 2013. Systematic review of magnetic resonance imaging characteristics that affect treatment decision making and predict clinical outcome in patients with cervical spondylotic myelopathy. *Spine (Phila Pa 1976),* 38**,** S89-110.

TETREAULT, L. A., KARPOVA, A. & FEHLINGS, M. G. 2015b. Predictors of outcome in patients with degenerative cervical spondylotic myelopathy undergoing surgical treatment: results of a systematic review. *Eur Spine J,* 24 Suppl 2**,** 236-51.

TOOSY, A. T., KOU, N., ALTMANN, D., WHEELER-KINGSHOTT, C. A., THOMPSON, A. J. & CICCARELLI, O. 2014. Voxel-based cervical spinal cord mapping of diffusion abnormalities in MS-related myelitis. *Neurology,* 83**,** 1321-5.

UDA, T., TAKAMI, T., TSUYUGUCHI, N., SAKAMOTO, S., YAMAGATA, T., IKEDA, H., NAGATA, T. & OHATA, K. 2013a. Assessment of cervical spondylotic myelopathy using diffusion tensor magnetic resonance imaging parameter at 3.0 tesla. *Spine (Phila Pa 1976),* 38**,** 407-14.

UDA, T., TAKAMI, T., TSUYUGUCHI, N., SAKAMOTO, S., YAMAGATA, T., IKEDA, H., NAGATA, T. & OHATA, K. 2013b. Assessment of cervical spondylotic myelopathy using diffusion tensor magnetic resonance imaging parameter at 3.0 tesla. *Spine,* 38**,** 407-14.

UKMAR, M., MONTALBANO, A., MAKUC, E., SPECOGNA, I., BRATINA, A., LONGO, R. & COVA, M. A. 2012. Fiber density index in the evaluation of the spinal cord in patients with multiple sclerosis. *Radiol Med,* 117**,** 1215-24.

VALSASINA, P., AGOSTA, F., ABSINTA, M., SALA, S., CAPUTO, D. & FILIPPI, M. 2010. Cervical cord functional MRI changes in relapse-onset MS patients. *J Neurol Neurosurg Psychiatry,* 81**,** 405-8.

VALSASINA, P., AGOSTA, F., BENEDETTI, B., CAPUTO, D., PERINI, M., SALVI, F., PRELLE, A. & FILIPPI, M. 2007. Diffusion anisotropy of the cervical cord is strictly associated with disability in amyotrophic lateral sclerosis. *J Neurol Neurosurg Psychiatry,* 78**,** 480-4.

VALSASINA, P., ROCCA, M. A., ABSINTA, M., AGOSTA, F., CAPUTO, D., COMI, G. & FILIPPI, M. 2012. Cervical cord FMRI abnormalities differ between the progressive forms of multiple sclerosis. *Hum Brain Mapp,* 33**,** 2072-80.

VALSASINA, P., ROCCA, M. A., AGOSTA, F., BENEDETTI, B., HORSFIELD, M. A., GALLO, A., ROVARIS, M., COMI, G. & FILIPPI, M. 2005. Mean diffusivity and fractional anisotropy histogram analysis of the cervical cord in MS patients. *Neuroimage,* 26**,** 822-8.

VAN HECKE, W., NAGELS, G., EMONDS, G., LEEMANS, A., SIJBERS, J., VAN GOETHEM, J. & PARIZEL, P. M. 2009. A diffusion tensor imaging group study of the spinal cord in multiple sclerosis patients with and without T2 spinal cord lesions. *J Magn Reson Imaging,* 30**,** 25-34.

VARGAS, M. I., DELAVELLE, J., JLASSI, H., RILLIET, B., VIALLON, M., BECKER, C. D. & LOVBLAD, K. O. 2008. Clinical applications of diffusion tensor tractography of the spinal cord. *Neuroradiology,* 50**,** 25-9.

VAVASOUR, I. M., LAULE, C., LI, D. K., TRABOULSEE, A. L. & MACKAY, A. L. 2011. Is the magnetization transfer ratio a marker for myelin in multiple sclerosis? *J Magn Reson Imaging,* 33**,** 713-8.

VEDANTAM, A., ECKARDT, G., WANG, M. C., SCHMIT, B. D. & KURPAD, S. N. 2015. Clinical Correlates of High Cervical Fractional Anisotropy in Acute Cervical Spinal Cord Injury. *World Neurosurgery,* 83**,** 824-828.

VEDANTAM, A., RAO, A., KURPAD, S. N., JIRJIS, M. B., ECKARDT, G., SCHMIT, B. D. & WANG, M. C. 2017. Diffusion Tensor Imaging Correlates with Short-Term Myelopathy Outcome in Patients with Cervical Spondylotic Myelopathy. *World Neurosurg,* 97**,** 489-494.

VON MEYENBURG, J., WILM, B. J., WECK, A., PETERSEN, J., GALLUS, E., MATHYS, J., SCHAETZLE, E., SCHUBERT, M., BOESIGER, P., VON MEYENBURG, K., GOEBELS, N. & KOLLIAS, S. 2013. Spinal Cord Diffusion-Tensor Imaging and Motor-evoked Potentials in Multiple Sclerosis Patients: Microstructural and Functional Asymmetry. *Radiology,* 267**,** 869-879.

WADA, E., OHMURA, M. & YONENOBU, K. 1995. Intramedullary changes of the spinal cord in cervical spondylotic myelopathy. *Spine (Phila Pa 1976),* 20**,** 2226-32.

WANG, K., CHEN, Z., ZHANG, F., SONG, Q., HOU, C., TANG, Y., WANG, J., CHEN, S., BIAN, Y., HAO, Q. & SHEN, H. 2016. Evaluation of DTI Parameter Ratios and Diffusion Tensor Tractography Grading in the Diagnosis and Prognosis Prediction of Cervical Spondylotic Myelopathy. *Spine (Phila Pa 1976)*.

WANG, M., DAI, Y., HAN, Y., HAACKE, E. M., DAI, J. & SHI, D. 2011. Susceptibility weighted imaging in detecting hemorrhage in acute cervical spinal cord injury. *Magn Reson Imaging,* 29**,** 365-73.

WANG, S. Q., LI, X., CUI, J. L., LI, H. X., LUK, K. D. & HU, Y. 2015. Prediction of myelopathic level in cervical spondylotic myelopathy using diffusion tensor imaging. *J Magn Reson Imaging,* 41**,** 1682-8.

WANG, W., QIN, W., HAO, N., WANG, Y. & ZONG, G. 2012. Diffusion tensor imaging in spinal cord compression. *Acta Radiol,* 53**,** 921-8.

WANG, Y., LIU, L., MA, L., HUANG, X., LOU, X., WANG, Y., WU, N., LIU, T. & GUO, X. 2014. Preliminary study on cervical spinal cord in patients with amyotrophic lateral sclerosis using MR diffusion tensor imaging. *Acad Radiol,* 21**,** 590-6.

WEBSTER, K. E., WITTWER, J. E. & FELLER, J. A. 2005. Validity of the GAITRite walkway system for the measurement of averaged and individual step parameters of gait. *Gait Posture,* 22**,** 317-21.

WEN, C. Y., CUI, J. L., LIU, H. S., MAK, K. C., CHEUNG, W. Y., LUK, K. D. & HU, Y. 2014a. Is diffusion anisotropy a biomarker for disease severity and surgical prognosis of cervical spondylotic myelopathy? *Radiology,* 270**,** 197-204.

WEN, C. Y., CUI, J. L., MAK, K. C., LUK, K. D. & HU, Y. 2014b. Diffusion tensor imaging of somatosensory tract in cervical spondylotic myelopathy and its link with electrophysiological evaluation. *Spine J,* 14**,** 1493-500.

WHEELER-KINGSHOTT, C. A., STROMAN, P. W., SCHWAB, J. M., BACON, M., BOSMA, R., BROOKS, J., CADOTTE, D. W., CARLSTEDT, T., CICCARELLI, O., COHEN-ADAD, J., CURT, A., EVANGELOU, N., FEHLINGS, M. G., FILIPPI, M., KELLEY, B. J., KOLLIAS, S., MACKAY, A., PORRO, C. A., SMITH, S., STRITTMATTER, S. M., SUMMERS, P., THOMPSON, A. J. & TRACEY, I. 2014. The current state-of-the-art of spinal cord imaging: Applications. *Neuroimage,* 84**,** 1082-1093.

WHEELER-KINGSHOTT, C. A. M., HICKMAN, S. J., PARKER, G. J. M., CICCARELLI, O., SYMMS, M. R., MILLER, D. H. & BARKER, G. J. 2002. Investigating cervical spinal cord structure using axial diffusion tensor imaging. *Neuroimage,* 16**,** 93-102.

WHITE, M. L., ZHANG, Y. & HEALEY, K. 2011. Cervical spinal cord multiple sclerosis: evaluation with 2D multi-echo recombined gradient echo MR imaging. *J Spinal Cord Med,* 34**,** 93-8.

WILM, B. J., GAMPER, U., HENNING, A., PRUESSMANN, K. P., KOLLIAS, S. S. & BOESIGER, P. 2009. Diffusion-weighted imaging of the entire spinal cord. *NMR Biomed,* 22**,** 174-81.

WILSON, J. R., BARRY, S., FISCHER, D. J., SKELLY, A. C., ARNOLD, P. M., RIEW, K. D., SHAFFREY, C. I., TRAYNELIS, V. C. & FEHLINGS, M. G. 2013. Frequency, Timing, and Predictors of Neurological Dysfunction in the Nonmyelopathic Patient With Cervical Spinal Cord Compression, Canal Stenosis, and/or Ossification of the Posterior Longitudinal Ligament. *Spine,* 38**,** S37-S54.

WILSON, J. R., GROSSMAN, R. G., FRANKOWSKI, R. F., KISS, A., DAVIS, A. M., KULKARNI, A. V., HARROP, J. S., AARABI, B., VACCARO, A., TATOR, C. H., DVORAK, M., SHAFFREY, C. I., HARKEMA, S., GUEST, J. D. & FEHLINGS, M. G. 2012. A Clinical Prediction Model for Long-Term Functional Outcome after Traumatic Spinal Cord Injury Based on Acute Clinical and Imaging Factors. *Journal of Neurotrauma,* 29**,** 2263-2271.

WRIGHT, J. G., SWIONTKOWSKI, M. F. & HECKMAN, J. D. 2003. Introducing levels of evidence to the journal. *J Bone Joint Surg Am,* 85-A**,** 1-3.

WU, J. C., KO, C. C., YEN, Y. S., HUANG, W. C., CHEN, Y. C., LIU, L., TU, T. H., LO, S. S. & CHENG, H. 2013. Epidemiology of cervical spondylotic myelopathy and its risk of causing spinal cord injury: a national cohort study. *Neurosurg Focus,* 35**,** E10.

WU, Y., ALEXANDER, A. L., FLEMING, J. O., DUNCAN, I. D. & FIELD, A. S. 2006. Myelin water fraction in human cervical spinal cord in vivo. *J Comput Assist Tomogr,* 30**,** 304-6.

XIANGSHUI, M., XIANGJUN, C., XIAOMING, Z., QINGSHI, Z., YI, C., CHUANQIANG, Q., XIANGXING, M., CHUANFU, L. & JINWEN, H. 2010. 3 T magnetic resonance

diffusion tensor imaging and fibre tracking in cervical myelopathy. *Clin Radiol,* 65**,** 465-73.

YAN, H., ZHU, Z., LIU, Z., ZHANG, X., SUN, X., SHA, S., HAN, X., QIAN, B. & QIU, Y. 2015. Diffusion tensor imaging in cervical syringomyelia secondary to Chiari I malformation: preliminary results. *Spine (Phila Pa 1976),* 40**,** E381-7.

YIANNAKAS, M. C., KEARNEY, H., SAMSON, R. S., CHARD, D. T., CICCARELLI, O., MILLER, D. H. & WHEELER-KINGSHOTT, C. A. M. 2012. Feasibility of grey matter and white matter segmentation of the upper cervical cord in vivo: A pilot study with application to magnetisation transfer measurements. *Neuroimage,* 63**,** 1054-1059.

YING, J., ZHOU, X., ZHU, M., ZHOU, Y., HUANG, K., ZHOU, B. & TENG, H. 2016. The Contribution of Diffusion Tensor Imaging to Quantitative Assessment on Multilevel Cervical Spondylotic Myelopathy. *Eur Neurol,* 75**,** 67-74.

YOSHIMATSU, H., NAGATA, K., GOTO, H., SONODA, K., ANDO, N., IMOTO, H., MASHIMA, T. & TAKAMIYA, Y. 2001. Conservative treatment for cervical spondylotic myelopathy. prediction of treatment effects by multivariate analysis. *Spine J,* 1**,** 269-73.

ZACKOWSKI, K. M., SMITH, S. A., REICH, D. S., GORDON-LIPKIN, E., CHODKOWSKI, B. A., SAMBANDAN, D. R., SHTEYMAN, M., BASTIAN, A. J., VAN ZIJL, P. C. & CALABRESI, P. A. 2009. Sensorimotor dysfunction in multiple sclerosis and column-specific magnetization transfer-imaging abnormalities in the spinal cord. *Brain,* 132**,** 1200-1209.

ZHOU, F., GONG, H., LIU, X., WU, L., LUK, K. D. & HU, Y. 2014. Increased low-frequency oscillation amplitude of sensorimotor cortex associated with the severity of structural impairment in cervical myelopathy. *PLoS One,* 9**,** e104442.

7.1 APPENDIX A – Additional Tables

Table 1.3: Summary of ROI-Based Quantitative DTI Studies.

Authors (Year); Design	Subjects	B_0; Vendor; Coil; Gradients	Anatomical Region/ Position	DTI Acquisition	FOV; Matrix; Voxel size; TR/TE (ms); Cardiac Gating; AT	DTI Metrics	ROI	Clinical Measures	Key Results	Risk of Bias; Key Barriers to Translation
Demir et al. (2003); prospective, cross-sectional	CSM (36 total, 21 with myelopathy) vs. HCs (8)	1.5T; Philips; surface coil; 23mT/m	• C1-C7 • 3 sagittal slices, 1mm gap	• SE Multishot EPI, 13 echoes • 6 directions • b=300,600s/mm^2	240mm^2; 256x195; 0.9x1.2x5mm^3; 3 beats/36; yes; 13m	FA, MD	Manual, whole cord at MCL and NASC	• Presence of myelopathy • SSEPs	• To detect clinical/SSEP myelopathy, MD had SE=92%, SP=50%, PPV=80%, NPV=75%, and FA had SE=90%, SP=50%, PPV=76%, NPV=75% • MD, FA had higher SE but lower SP than T2w changes	High; minimal clinical data, several subjects excluded due to low SNR
Agosta et al. (2005); prospective, cross-sectional	PPMS (24) vs. HCs (13)	1.5T; Siemens; Phased-array spine coil	• C1-C7 • 5 sagittal slices, contiguous	• ssEPI, SENSE=2 • 3 sat bands • Repeated x 4 • 14 directions • b=900 s/mm^2	240x90mm^2; 128x48; 1.9x1.9x4mm^3; 7000/100; No; AT NR	FA, MD (corrected with CSA)	Manual ROI, mid-sagittal slice, excluding edge voxels	• EDSS	• Reduced mean FA: 0.38 vs. 0.42, P=0.007 • Increased MD: 1.20 vs. 1.28 (P=0.024) • No correlations of DTI metrics found with EDSS	High; coarse clinical data, large voxels increase partial volume effect
Facon et al. (2005); prospective, cross-sectional	CM (15 total, 6 CSM, 5 abscess, 4 tumour) vs. HCs (11)	1.5T; NR; NR; NR	• Cervical, thoracic • 12 sagittal slices, contiguous	• ssEPI, GRAPPA=2 • 6 directions • b=500 s/mm^2	179mm^2; 128x128; 1.4x1.4x3mm^3; 4600/73; no; 7m (3 acquisitions)	FA, MD	Manual, at MCL (CM) or averaged over all levels (HCs)	• Presence of pain, motor or sensory impairment	• No effect of rostrocaudal level seen on FA, MD • FA lower at compressed levels (0.67) than normal appearing cord (0.74, P=0.01) and controls (0.75, P=0.01) • FA had better SE (73%) and SP (100%) than T2w-HI or ADC	High; heterogeneous population, metrics at MCL potentially biased
Mamata et al. (2005); prospective, cross-sectional	CSM (79) vs. HCs (11)	1.5T; GE; spine PAC; 22mT/m or 40mT/m	• C1-C7 • 1 sagittal slice	• Sagittal line scan • b=5 s/mm^2 taken in 2 directions • 6 directions • b=1000 s/mm^2	220x110mm^2; 128x128; 1.7x1.7x4mm^3; 2733/86; no; 31s per slice	FA, MD	Manual, 2 ROIs drawn at C2-3 and at MCL (or C4-C7 in HCs)	• None	• 54% of spondylosis subjects have low FA, high MD • Age correlates with FA (r=-0.24) and MD (r=0.24) • FA is decreased, MD increased within T2 hyper-intensity (P<0.05)	High; no clinical data, single mid-sagittal slice misses key WM tracts
Valsasina et al. (2005); prospective, cross-sectional	MS (44 total, 21 RRMS, 23 SPMS) vs. HCs (17)	Same as Agosta et al. (2005)					Manual, drawn on mid-sagittal slice	• EDSS	• Reduced mean FA: 0.36 vs. 0.43, P=0.008 • FA not different in SPMS vs. RRMS • FA correlates with EDSS: r=-0.48, P=0.001 • MD correlates with EDSS: r=0.37, P=0.02	High; coarse clinical data, single mid-sagittal slice misses key WM tracts
Hesseltine et al. (2006); prospective, cross-sectional	RRMS (24) vs. HCs (24)	1.5T; NR; NR; NR	• C2-C3 • 10 axial slices, contiguous	• SE EPI • 6 directions • b=1000 s/mm^2	140mm^2; 128x128; 1.1x1.1x4mm^3; 2000/74; no; 2m20s	FA, MD	Manual, 7 ROIs at C2-3: bilateral STTs, LCSTs, DCs, and central cord	• None	• FA decreased in LCSTs (P<0.0001) and DCs (P=0.001) • Model using spatial FA data has SE=87%, SP=92%	High; no clinical data
Renoux et al. (2006); prospective, cross-sectional	Myelitis (15 total, 9 MS, 6 other) vs. HCs (11)	1.5T; Philips; NR; 23mT/m	• C2-C5, T1-T6, T7-T12 • 3 sagittal slices, 1mm gap	• Multi-shot EPI • 25 directions • b=300, 600 s/mm^2	240mm^2; 256x195; 0.9x1.2x5mm^3; 3 beats/80; yes; NR	FA, MD (calculated as z-statistics)	Manual, whole-cord (avoiding edge voxels)	• None	• All T2 hyperintense lesions had significantly decreased FA • 9 subjects showed significant FA decrease in normal-appearing SC, and 5 had areas of increased FA	High; no clinical data, no correction for multiple comparisons

Agosta et al. (2007); prospective, longitudinal	MS (42 total, 13 RRMS, 14 SPMS, 15 PPMS) vs. HCs (9)	Same as Agosta et al. (2005)						• EDSS • FU at 1.5-3 years (mean 2.4)	• At FU, FA decreased: 0.36 vs. 0.37, P=0.01 • At FU, MD increased: 1.26 vs. 1.37, P<0.001 • Cord FA correlates with EDSS: r=-0.51, P=0.001 • Cord FA decrease was greatest in PPMS: P=0.05 • Baseline FA predicts EDSS at FU: r=-0.40, P=0.03	High; coarse clinical data
Ohgiya et al. (2007); prospective, cross-sectional	MS (21 total, 16 RRMS, 4 SPMS, 1 PPMS) vs. HCs (21)	1.5T; GE; 8-channel neuro-vascular PAC	• C2-C5 • Axial slices, number NR, contiguous	• ssEPI • 25 directions • b=900 s/mm^2	170mm^2; 128x128; 1.3x1.3x4mm^3; 12000/107; No; 6m	FA, MD	Manual, ROIs drawn on plaques and NAWM (DCs and R/L LCs), matched in HCs	• None	• FA decreased in all ROIs vs. HCs (all P<0.001) • MD increased in 6/9 ROIs (P<0.05) • FA decreased in plaques vs. NAWM vs. HCs (0.44 vs. 0.54 vs. 0.74, P<0.01)	High; no clinical data
Valsasina et al. (2007); prospective, cross-sectional	ALS (28) vs. HCs (20)	1.5T; Siemens; spine PAC; 33 mT/m, 125 mT/m/ms	• C1-C7 • 5 sagittal slices, 1.2mm gap	• ssEPI • 12 directions • 3 sat bands • Repeated x 2 • b=900 s/mm^2	240x90mm^2; 128x48; 1.9x1.9x4mm^3; 2900/84; No; NR	FA, MD (with and without correction for CSA)	Semi-automated segmentation, manual ROI of cord excluding edge voxels	• ALSFRS • FU at 6-12 months (mean 9)	• Decreased mean FA: 0.48 vs. 0.52, P=0.002 • MD not different than controls: 0.88 vs. 0.85, NS • Mean FA correlates with ALSFRS, r=0.74, P<0.001	High (diagnostic), moderately high (correlation); gaps in sagittal acquisition exclude some WM
Agosta et al. (2008a); prospective, cross-sectional	RRMS (25) vs. HCs (12)	1.5T; Siemens; spine PAC; 33 mT/m, 125 mT/m/ms	• C1-C7 • 5 sagittal slices, contiguous	• ssEPI • 12 directions • 3 sat bands • Repeated x 4 • b=900 s/mm^2	240x180mm^2; 192x144; 1.3x1.3x4mm^3; 2700/71; No; NR	FA, MD (with and without correction for CSA)	Semi-automated segmentation, manual ROI of cord excluding edge voxels	• EDSS	• Decreased mean FA: 0.48 vs. 0.58, P<0.001	High; FA higher than in previous similar studies, correlation with EDSS NR
Manconi et al. (2008); prospective, cross-sectional	MS (82 total, 30 with restless leg syndrome), no HCs	Same as Agosta et al. (2005)					Semi-automated segmentation, manual ROI in mid-sagittal slice from C1-C5	• EDSS • Qualitative RLS and sleep data	• Mean FA decreased in RLS subjects vs. non-RLS (P=0.02) • FA histogram peak higher in RLS (P=0.004) • No correlations between spinal cord DTI metrics and brain DTI or number of cord lesions (on STIR)	High; coarse clinical data, single mid-sagittal slice misses key WM tracts
Shanmuganathan et al. (2008); retrospective, cross-sectional	aSCI (20 total, 16 with neurological injury) vs. HCs (8)	1.5T; Siemens; 12-channel head/neck PAC	• Medulla-T1 • 67 axial slices, contiguous	• ssEPI • Partial Fourier • 6 direcctions • b=1000 s/mm^2	200mm^2; 128x128; 1.6x1.6x3mm^3; 8000/76; No; 3m40s	FA, MD, RA, VR, λ_1, λ_2, λ_3	Manual, 3 ROIs drawn to include GM and WM, medulla-C2, C3-C5, and C6-T1	• None	• Decreased MD vs. HCs in all 3 ROIs: P<=0.01 • Decreased λ_1 vs. HCs in all 3 ROIs: P<=0.002	High; retrospective, 4/20 subjects excluded due to image quality, no clinical data
Agosta et al. (2009a); prospective, longitudinal	ALS (17) vs. HCs (20)	Same as Valsasina et al. (2007)						• ALSFRS • FU at 6-12 months (mean 9)	• At FU, FA decreased: 0.45 vs. 0.48, P=0.01 • At FU, MD increased: 0.95 vs. 0.89, P=0.01 • FA, MD changes did not correlate with ALSFRS changes	High; only 61% had FU MRI, prediction of FU EDSS NR
Agosta et al. (2009b); prospective, cross-sectional	PPMS (23) vs. HCs (18)	Same as Agosta et al. (2008)b						• EDSS	• Decreased FA: 0.45 vs. 0.57, P<0.001 • Increased MD: 0.99 vs. 0.85, P<0.001 • FA correlates with mean cord fMRI signal change: r=-0.58	High; coarse clinical data, correlation with EDSS NR
Cruz et al. (2009); retrospective, cross-sectional	RRMS (41) vs. HCs (37)	1.5T; Siemens; 8 channel head coil; NR	• C2-C3 • Axial slices: 30% gap; sagittal slices: contiguous, number NR	• DTI sequence NR • 12 directions • b value NR	Axial: 225mm^2; 128x128; 1.8x1.8x 3mm^3; 3200/80; No; AT NR; sagittal: 280mm^2 192x192; 1.5x1.5x 3mm^3, 2800/90; No; NR	FA	Manual, on plaque, peri-plaque, NASC, vs. whole-cord (HCs)	• None	• FA in plaques (0.44) is lower than periplaque (0.57), NASC (0.63), or HCs (0.74): P<0.001 • FA lower in NASC vs. controls: P<0.05	High; retrospective, no clinical data
van Hecke et al. (2009); prospective, cross-sectional	MS (21) vs. HCs (21)	1.5T; Siemens; spine, neck coils; 40mT/m	• C1-C5 • 30 axial slices, contiguous	• ssEPI • Parallel (factor NR) • 60 directions • b=700 s/mm^2	256mm^2; 128x128; 1.4x1.4x3mm^3; 10400/100; No; 12m18s	FA, MD, AD, RD, ψ (from FT)	Manual, whole cord	• None	• Decreased FA, ψ in MS with lesions (P<0.01) and without (P<0.02)	High; no clinical data, diagnostic accuracy NR
Benedetti et al. (2010); prospective,	MS (68 total, 40 BMS, 28 SPMS) vs. HCs (18)	Same as Agosta et al. (2005)						• EDSS	• Total MS: increased MD (P=0.001), decreased FA: (P<0.001) • SPMS: lower mean cord FA than BMS: 0.33 vs. 0.37, P=0.01 • Mean FA correlates with EDSS: r=-0.37, P=0.002	High (diagnostic), moderately high (correlation); coarse

cross-sectional									• Multivariate model (brain, cord) correlates with EDSS: r=0.58	clinical data
Freund et al. (2010); prospective, longitudinal	MS with acute lesion (14) vs. HCs (13)	1.5T; GE; NR; 33mT/m	• C1-C5 • 30 axial slices, contiguous	• CO-ZOOM-EPI rFOV • 60 directions • b=1000 s/mm^2	70x47mm^2; 48x32; 1.5x1.5x5mm^3; 15 beats/96; yes; NR	FA, MD, AD, RD, FU MRI at 1m, 3m, 6m	Manual, 4 ROIs in ACs, DCs, L/R LCs	• EDSS • 9 hole peg • 25-foot TWT • MSWS-12 • FU at 1m, 3m, 6m	• FA decreased and RD increased vs. HCs in all ROIs (P<0.05) • Baseline RD predicted EDSS, 9 hole peg, and TWT at 6m (P<0.05) • Baseline FA of the LCs predicted EDSS recovery at 6m (P=0.02)	Moderately high; several datasets excluded due to artefact
Nair et al. (2010); prospective, cross-sectional	ALS (14) vs. HCs (15)	3T; Siemens; 12-channel head and 2-channel neck PACs	• C1-C6 • 19 coronal slices, contiguous	• ssEPI • NEX=2 • 2 acquisitions • 30 directions • b=1000 s/mm^2	160mm^2; 128x128; 1.3x1.3x2.5mm^3; 3200/105; no; 7m (for 2 acquisitions)	FA, MD, AD, RD	Semi-automatic, FA skeleton used to define WM	• ALSFRS-R • FVC • Finger/foot tapping speed	• FA decreased (P=0.003), RD increased (P=0.03) • Multiple correlations: FA with tapping: r=0.61, P=0.02; RD with ALSFRS-R (r=-0.55, P=0.04), FVC (r=-0.69, P=0.01), and tapping (r=-0.59, P=0.03); MD with ALSFRS-R (r=-0.56, P=0.04) and FVC (r=-0.54, P=0.01)	High (diagnostic), moderately high (correlation); complex analysis likely requires expert
Xiangshui et al. (2010); prospective, cross-sectional	CSM (84) vs. HCs (21)	3T; GE; neck PAC; 40mT/m	• C1-C7 • 28 axial slices, contiguous	• SENSE EPI • 15 directions • b=1000 s/mm^2	270mm^2; 96x96; 2.8x2.8x4mm^3; 6000/83; no; 5m	FA, MD, λ_1, λ_2, λ_3	Manual, whole-cord	• None	• CSM divided into group A-D by T2w changes • All metrics altered vs. HCs in groups B-D (P<0.01) • Only λ_2, λ_3 differed between group A and HCs (P<0.05)	High, no clinical data, large voxels
Cheran et al. (2011); prospective, longitudinal	aSCI (25 total, 13 HC, 12 NHC) vs. HCs (11)	1.5T; Siemens; 12-channel head/neck PAC	• Caudal medulla and C1-T1 • 67 axial slices, contiguous	• ssEPI, partial Fourier, GRAPPA=2 • 6 directions • b=1000 s/mm^2	200mm^2; 128x128; 1.6x1.6x3mm^3; 8000/76; no; 3m40s	FA, MD, AD, RD	Manual, mid-sagittal slice: C1-C2, C3-C5, C6-T1, avoiding hemorrhage	• ASIA motor score • FU data in 12 subjects (at 1-29 months)	• FA reduced at C3-C5, C6-T1 (NHC: P<0.001, HC: P<0.05) and at injury site (P<0.001) • MD, AD reduced in all regions (P<0.001) • All metrics correlated with motor score in NHC (R=0.78-0.92)	High (diagnostic), moderately high (correlation); 7 subjects excluded, ROI misses key WM, prediction of outcomes NR
Cohen-Adad et al. (2011); prospective, cross-sectional	cSCI (14) vs. HCs (14)	3T; Siemens; head/neck/spine PACs; NR	• C2-T2 • 8 axial slices, mid-VB (gap adjusted to fit)	• ssEPI, GRAPPA=2 • 2 sat bands • Repeated x 4 • Manual shim • 64 directions • b=1000 s/mm^2	128mm^2; 128x128; 1x1x5mm^3; 1 heartbeat/76; yes (delay NR); NR	FA, MD, AD, RD, GFA	Manual, 4 ROIs: ACs, DCs, L/R LCSTs; lesion levels skipped	• ASIA motor and sensory scores	• Decreased FA,GFA (P<0.0001) and AD, RD (P=0.01) • FA, GFA, RD correlate with total ASIA (abs r=0.66-0.74, P<0.01) • Tract-specific metrics: weak specificity with motor vs. sensory scores	High (diagnostic), moderately high (correlation); manual ROI
Kamble et al. (2011); prospective, cross-sectional	cSCI (18) vs. HCs (11)	1.5T; GE; spine coil; NR	• Cervical or lumbar • Axial slices, contiguous, number NR	• EPI • 25 directions • b=1000 s/mm^2	260mm^2; 128x128; 2x2x5mm^3; 8500/98; no; NR	FA	Manual, 3 ROIs placed randomly	• None	• FA in areas above/below lesion decreased vs. HCs: 0.37 vs. 0.55, P=0.001	High; no clinical data, random ROI placement could miss key WM
Lee et al.(2011); prospective, longitudinal	CM (20) vs. HCs (20)	3T; Philips; head/neck PAC; 40 mT/m	• C1-T1 • Sagittal slices, number, gap NR	• ssEPI, SENSE=2 • NEX=4 • 15 directions • b=600 s/mm^2	250x224mm^2; 128x128; 2x2x2mm^3; 3380/56; no; 3m43s	FA, MD	Manual, whole-cord	• JOA • FU JOA at 3 months	• FA decreased at MCL: 0.50 vs. 0.60, P=0.001 • MD increased at MCL: 1.44 vs. 1.17, P=0.001 • FA, MD not correlated with JOA and not predictive of outcome	High; heterogeneous subjects, correlation coefficients not calculated
Mueller-Mang et al. (2011); prospective, cross-sectional	HIV (20) vs. HCs (20)	3T; Siemens; standard neck coil; NR	• C2-C3 • 10 axial slices, contiguous	• SE double shot EPI, parallel=2 • 6 directions • b=1000 s/mm^2	180mm^2; 256x256; 0.7x0.7x3mm^3; 3700/98; no; 2m	FA, MD, λ_1, λ_2, λ_3	Manual, 7 ROIs at C2-3: central GM, L/R ACs, DCs, LCSTs	• None	• No difference in metrics between HIV and HCs	High; negative study results, small voxels likely have very low SNR
Song et al. (2011); prospective, cross-sectional	CSM (53) vs. HCs (20)	1.5T; Philips; spine PAC; 23 mT/m, 150 mT/m/ms	• C2-C6 • Sagittal slices, contiguous, number NR	• ssEPI • NEX=4 • 6 directions • b=400 s/mm^2	230mm^2; 128x128; 1.8x1.8x3mm^3; NR; no;	FA, MD	Manual, ROIs drawn at MCL (CSM), at disc levels (HCs)	• None	• FA decreases at descending cervical levels: P<0.01 • MD increased (837 vs. 733, P<0.01) and FA decreased (736 vs. 776, P<0.01)	High; no clinical data, patients followed for 6 months but outcomes NR
Hori et al. (2012); prospective, cross-sectional	CSM (50 total, 18 with cord compression), no HCs	3T; Philips; NR; NR	• C3-C6 • 30 axial slices, contiguous	• Sequence NR • 6 directions • b=400, 800, 1200, 1600, 2000 s/mm^2	80mm^2; 64x64; 1.3x1.3x3mm^3; 6996/73; no; 7m	FA, MD, MK, RMSD	Manual, whole-cord at C3-4, C4-5, C5-6	• None	• Compressed cords (N=18) had lower FA (0.61 vs. 0.66, P=0.006), lower MK (0.80 vs. 0.91, P=0.002), and higher RMSD (8.4 vs. 8.3, P=0.006)	High; 15/50 subjects excluded due to artefacts, no clinical data, no HCs
Jeantroux et al. (2012); prospective,	NMO (25) vs. HCs (20)	1.5T; Siemens; head, spine	• C1-C7 • 30 axial slices, contiguous	• SE EPI • 12 directions • b=800 s/mm^2	230mm^2; 104x104; 2.2x2.2x5mm^3; 2700/71; no; 7m	FA, MD	Manual, NAWM and intralesional (based on T2)	• None	• Decreased FA in lesions (0.48, P<0.001) and NAWM (0.58, P<0.05) vs. HCs (0.61) • Increased MD in lesions (1.29, P<0.001) and NAWM (1.11, P<0.05)	High; no clinical data, large voxels

cross-sectional		PACs; NR							vs. HCs (1.03)	
Kerkovsky et al. (2012); prospective, cross-sectional	CSM (52 total, 20 with myelopathy) vs. HCs (13)	1.5T; Philips; 16-channel head/neck PAC; NR	• Axial slices (number, gap NR)	• ssEPI, SENSE=2 • 15 directions • FA=25° • b=900 s/mm^2	NR; NR; 4mm thick; 3549/83; no; NR	FA, MD	Manual, whole-cord at C2-3 and max. compression	• SSEPs • MEPs	• FA decreased at MCL in myelopathic subgroup (P=0.001) and non-myelopathic subgroup (P=0.04) • No difference in FA, MD at C2-3 between groups • EP measures only 67% sensitive in myelopathy	High; no clinical data (only EP), MRI details NR
Lindberg et al. (2012); prospective, cross-sectional	CSM (15) vs. HCs (10)	1.5T; Siemens; NR; NR	• C2-C7 • 12 sagittal slices, contiguous	• ssEPI, SENSE=2 • NEX=4 • 2 sat bands • 25 directions • b=900 s/mm^2	180mm^2; 128x128; 1.4x1.4x3mm^3; 2000/95; no; 4m26s	FA, MD, AD, RD	Manual, whole-cord	• Presence/ absence of gait change or hyperreflexia	• FA decreased (C2-C7): 0.50 vs. 0.54, P=0.02 • RD increased (C2-C7): 0.56 vs. 0.52, P=0.03 • FA decreased with descending vertebral level (P value NR)	High; minimal clinical data
Pessoa et al. (2012); prospective, cross-sectional	MS (32) vs. NMO (8) vs. HCs (17)	1.5T; Siemens; 8-channel head and neck PACs; NR	• C2-C7 • 16 sagittal slices, 0.3mm gap	• ssEPI • 20 directions • b=400,800 s/mm^2	260mm^2; 128x128; 2x2x3mm^3; 2800/88; no; NR	FA, MD, AD, RD	Manual, 4 ROIs at C2 and C7: ACs, DCs, and R/L LCs	• EDSS (NMO subjects only)	• FA decreased, RD increased (only in AC at C2) in NMO vs. MS (P<0.05) and NMO vs. HC (P<0.05) • In NMO, FA in DC at C2 correlates with EDSS (r=-0.80, P=0.02)	High; coarse clinical data (NMO only), large voxels
Peterson et al. (2012); prospective, cross-sectional	cSCI (19) vs. HCs (28)	3T; Philips; 6-element spine coil; NR	• C2, C5, T5, T12 • 6 axial slices per region, gap NR	• ssEPI, partial Fourier • NEX=12 • Directions NR • b=750 s/mm^2	120x30mm^2; 176x44; 0.7x0.7x5mm^3; 4000/49; no; 30m (for 3 regions)	FA, MD	Manual, 5 ROIs: whole-cord, L/R LCSTs and DCs; slices with SNR<20 excluded	• AIS • SSEPs • MEPs	• FA (C2) decreased in whole-cord, LCSTs, and DCs (P<0.005) • FA (C2) correlates with AIS in each ROI: whole-cord (r=0.64, P=0.001), LCSTs (r=0.50, P=0.002), and DCs (r=0.41, P=0.01) • Mean FA of DCs correlates with tibial SSEP amplitude (r=0.46, P<0.001)	High (diagnostic), moderately high (correlation); coarse clinical data, long acquisition time
Rocca et al. (2012); prospective, cross-sectional	MS (35 total, 20 with fatigue, 15 without) vs. HCs (20)	Same as Agosta et al. (2008)b;						• EDSS • Fatigue Severity Scale	• FA decreased, MD increased in all MS vs. HCs (P<0.001) • No difference in FA, MD between MS groups • DTI metrics do not correlate with clinical measures	High (diagnostic), moderately high (correlation); no correlations found
Wang et al. (2012); prospective, cross-sectional	CM (42) vs. HCs (49)	3T; Philips; CTL coil; 80mT/m, 200mT/m/s	• C1-C7 or T6-T12 • Sagittal slices, number NR, contiguous	• SE ssEPI • 6 directions • b=700 s/mm^2	170x136mm^2; 96x61; 1.6x1.9x2mm^3; 5000/64; no; 30m (for 3 regions)	FA, MD	Manual, rectangular ROIs placed at MCL (in CM) or mid-disc levels in HCs	• None	• FA decreased, MD increased in CM with T2w-HI vs. HCs (P<0.05) • Metrics not different in CM without T2w-HI vs. HCs	High; heterogeneous subjects, no clinical data
Cohen-Adad et al. (2013a); prospective, cross-sectional	ALS (29) vs. HCs (21)	Same as Cohen-Adad et al. (2011)				FA, MD, AD, RD	Same as Cohen-Adad et al. (2011)	• ALSFRC-R • TMS motor threshold	• FA decreased in LCST: 0.51 vs. 0.60, P<0.0005 • FA correlates with ALSFRC-R (R=0.38, P=0.04) and motor threshold (R=-0.47, P=0.02) • Reduction in FA greatest at caudal levels	High; manual ROI
Gao et al. (2013); prospective, cross-sectional	CSM (104), no HCs	3T; GE; 8-channel head/neck PAC	• C2-C7 • 27 axial slices, contiguous	• ssEPI • 2 sat bands • High order shim • 15 directions • b=1000 s/mm^2	27mm^2; 96x96; 0.3x0.3x4mm^3; 6000/83; no; NR	FA, MD, λ_1, λ_2, λ_3	Manual, 3 regions of 10 voxels per slice	• JOA	• FA, MD, λ_2, λ_3 differ between JOA severity groups: P<0.001 • FA, MD, λ_2, λ_3 differ with T1w/T2w signal change • FA correlates with JOA: r=0.88, P<0.05	High; no HCs, small voxels with low SNR, small FOV likely to have aliasing
Jones et al. (2013); prospective, longitudinal	CSM (30), no HCs	3T; GE; cervical spine coil	• C2-T1 • 24 axial slices, contiguous	• ssEPI • 6 directions • b=1000 s/mm^2	180mm^2; 128x128; 1.4x1.4x4mm^3; 8100/94; no; 3m55s	FA	Manual, 3 ROIs: DCs, L/R LCs at C2-3, MCL, C7-T1	• mJOA, Nurick, NDI, SF-36 • FU at 2-12 months (N=15)	• FA correlates with mJOA (r=0.62, P<0.01) and Nurick (r=-0.46, P=0.01) • Higher FA predicts post-op improvement on NDI (r=-0.61, P=0.04)	Moderately high (correlation), high (prognostic); short FU times, multiple comparisons not corrected
Koskinen et al. (2013); prospective, cross-sectional	cSCI (28 total, 13 with surgical fixation hardware) vs. HCs (40)	3T; Siemens; 12-channel head and 4-channel neck PACs; NR	• C2-C6 • Axial slices, number NR, 1.2mm gap	• EPI • 20 directions • NEX=4 • b=1000 s/mm^2	152mm^2; 128x128; 1.2x1.2x4mm^3; 4000/103; no; 5m50s	FA, MD, AD, RD	Manual, whole-cord at C2-3, lesion (rostral edge), and C3-4, C4-5, C5-6 (HCs)	• ASIA motor and sensory scores • FIM	• Decreased FA at C2-3: 0.58 vs. 0.69, P<0.001 • Increased MD and RD at C2-3: P<0.001 • FA, MD significantly altered at lesion level (P<0.001) • FA at lesion correlates with ASIA motor: r=0.67, P<0.01	High (diagnostic), moderately high (correlation); subjects not age-matched with HCs, 6 subjects excluded
Miraldi et al. (2013); prospective,	RRMS (32) vs. HCs (17)	1.5T; Siemens; 8-channel	• C2-C7 • 16 axial slices, 0.3mm gap	• ssEPI • 20 directions • b=800 s/mm^2	260mm^2; 128x128; 2x2x3mm^3; 2800/88; no; 15m	FA, MD, AD, RD (from FT)	Manual, 4 ROIs in ACs, DCs, L/R LCs, at C2 and C7	• EDSS	• Most metrics showed no difference with controls • No significant correlation with EDSS	High; negative results, high variance of metrics

cross-sectional		head/neck PAC; NR								
Naismith et al. (2013); prospective, cross-sectional	Myelitis (37 total, 26 MS, 11 NMO) vs. HCs (15)	3T; Siemens; 2 or 4-channel neck PAC; NR	• C1-2, C3-4, C5-6 • 6 axial slices /region, contiguous	• rFOV ssEPI • 25 directions • Repeated x 4 • Shim: field-map • b=600 s/mm^2	72x29mm^2; 80x32; 0.9x0.9x5mm^3; 5 beats/99; yes; 45m (4 acquisitions)	FA, MD, AD, RD	Manual, whole-cord and L/R DCs and LCSTs drawn on each slice	• EDSS • Vibration threshold • 25-foot TWT • 9 hole peg	• FA, RD of DCs (but not LCSTs) correlate with vibration (P<0.01) • FA, RD of DCs and LCSTs correlate with 9 hole peg (all P<0.0001) • FA, RD of whole cord (or tracts) correlate with EDSS categories (P<0.0001)	High; heterogeneous subjects, 4 subjects and 33% of ROIs excluded due to artefacts/SNR
Oh et al. (2013a); prospective, cross-sectional	MS (124 total, 69 RRMS, 36 SPMS, 19 PPMS), no HCs	3T; Philips; 2 element surface PAC;	• C2-C6 • 30 axial slices, contiguous	• Multi-slice SE ssEPI, parallel=2 • 16 directions • b=500 s/mm^2	NR; NR; 1.5x1.5x3mm^3; 4727/63; No; NR	FA, MD, AD, RD	Automatic segmentation, whole-cord at C3-4 (11 slices)	• EDSS • MSFC	• FA, MD, AD, RD more abnormal with high vs. low EDSS in low or high lesion count subjects (all P<0.05 except AD in high lesion count)	Moderately high; convenience sampling enrollment
Oh et al. (2013b); prospective, cross-sectional	MS (129 total, 74 RRMS, 36 SPMS, 19 PPMS) vs. HCs (14)	Same as Oh et al. (2013)a						• EDSS • Hip flexion power • Vibration	• FA, MD, AD, RD differed vs. HCs (P<0.05) • FA, MD, RD differed from progressive MS vs. RRMS (P<0.05) • FA, MD, RD correlate with EDSS (P<0.05) • FA, RD correlate with vibration (P<0.05) • MD, AD, RD correlate with hip flexion power (P<0.05)	Moderately high (diagnostic), moderately low (correlation); diagnostic accuracy NR
Raz et al. (2013); prospective, cross-sectional	RRMS (19) vs. HCs (16)	3T; Siemens; 4-channel neck PAC	• C1-C4 • 20 axial slices, contiguous	• SE (twice-refocused) EPI • NEX=2 • 30 directions • b=500, 1000, 1500, 2000, 2500 s/mm^2	160mm^2; 128x128; 1.3x1.3x3mm^3; 3100/110; no; 15m7s	FA, MD, MK	Manual, whole-cord from C1-C4, and NAGM, NAWM (DCs) at C2	• EDSS • Disease duration	• WM at C2: decreased FA vs. HCs: 0.52 vs. 0.62, P=0.01 • GM at C2: decreased MK vs. HCs: 1.11 vs. 1.16, P=0.01 • Lesions: decreased FA, MK, increased MD vs. NASC (P<0.0001) • Metrics in whole-cord and GM (but not WM) differ between high EDSS vs. low (P<=0.01) • No correlation between FA, MD, MK and EDSS	Moderately high (diagnostic), moderately low (correlation); no correlations found
Uda et al. (2013a); prospective, cross-sectional	CSM (26) vs. HCs (30)	3T; Philips; 16-element PAC; NR	• C2-T1 • 30 axial slices, contiguous	• SS FSE • NEX=1 • 15 directions • b=1000 s/mm^2	240mm^2; 160x160; 1.5x1.5x3mm^3; 8000/80; no; 4m54s	FA, MD, z-statistics calculated per level	Manual, whole-cord at discs, C2-T1	• None	• FA varied with cervical level (P<0.0001) but increased at C7-T1 • MD had ROC AUC=0.90, with SE=100%, SP=75%, PPV=90%, and NPV=100% • FA had ROC AUC=0.76, with SE=95%, SP=50%	High; groups not age-matched, no clinical data
Von Meyenburg et al. (2013); prospective, cross-sectional	MS (38 total, 15 RRMS, 13 SPMS, 10 PPMS), 28 HCs	3T; Philips; 6-element spine PAC	• C5 • 6 axial slices, contiguous	• rFOV ssEPI • Partial Fourier=0.6 • 6 directions • b=750 s/mm^2	120x30mm^2; 176x44; 0.7x0.7x5mm^3; 4000/49; no; 10m	FA, MD	Manual, 4 ROIs: L/R LCs and DCs	• EDSS • MEPs	• Decreased FA in all ROIs (all P<=0.001) • No differences in MD • FA correlates with age (P<0.05) • Tract-specific FA correlates with corresponding MEPs: r=-0.93-0.94, P<0.01	High; groups not age-matched, correlation with EDSS NR
Banaszek et al. (2014); prospective, cross-sectional	CSM (132) vs. HCs (25)	1.5T; GE; 16-channel head/spine PAC; 33mT/m	• C2-C7 • Axial slices, variable number, contiguous	• SE ssEPI • 2 acquisitions • 14 directions • b=1000 s/mm^2	160mm^2; 96x96; 1.6x1.6x4mm^3; 10000/99; no; 5-7m	FA, MD	Manual, whole-cord; images divided into 5 groups based on cord compression	• None	• FA decreased at all levels (C2-C6) vs. HCs (P<0.0001) • FA correlated with measures of cord compression (P<0.01) • MD increased in most levels/subgroups vs. HCs (P<0.05)	High; no clinical data, images at C6-7 excluded due to artefacts
El Mendili et al. (2014); prospective, longitudinal	ALS (29), no HCs	3T; Siemens; neck/spine coil; NR	• C2-T2 • 8 axial slices, mid-VB, variable gap	• ssEPI, GRAPPA=2 • Repeated x 4 • 64 directions • b=1000 s/mm^2	128mm^2; 128x128; 1x1x5mm^3; 700/60; yes; 15m	FA, MD, AD, RD; FU MRI at 1y	Manual, 4 ROIs: ACs, DCs, L/R LCSTs	• ALSFRS-R • Muscle power • FU at 1y	• FA of LCSTs correlates with ALSFRS-R leg (P<0.001) and total (P=0.04) scores • Baseline FA predicts ALSFRS-R leg (P=0.002) and total (P=0.001) scores at 1y FU • No change in DTI metrics at 1y FU vs. baseline	Moderately high; manual ROI
Ellingson et al. (2014); prospective, cross-sectional	CSM (48 total, 16 mJOA=18,) vs. HCs (9)	3T; Siemens; CTL spine PAC (2 elements); NR	• Upper cervical cord (HCs) • MCL (CSM) • Axial slices, number NR	• rFOV ZOOMED-EPI • 6 directions • NEX=15 • b=500 s/mm^2	NR; NR; NR; 5000/67; no; NR	FA, MD, AD, RD, ψ, SD(θ)	Manual, whole-cord at MCL or upper cord (HCs)	• mJOA	• FA diagnostic of mJOA<18 vs. mJOA=18 with SE=72%, SP=75% (AUC=0.77) • FA diagnostic of mJOA<15 with SE=81%, SP=92% (AUC=0.95) • FA correlates with mJOA: R^2=0.41, P<0.0001 • SD(θ) correlates with mJOA: R^2=0.41, P<0.0001	High; MRI details NR, age/gender of HCs NR, metrics at MCL potentially biased
Li et al. (2014); prospective, cross-sectional	CSM (14) vs. HCs (14)	3T; Philips; NR; NR	• C3-C7 • Axial slices, number/gap NR	• SE EPI • 15 directions • b=600 s/mm^2	NR; NR; 1x1.3x7mm^3; 5 beats/60; yes; NR	OE, wOE	Manual, whole-cord	• Muscle power • Reflexes • Sensory testing	• Diagnosis of symptomatic level with OE had SE=81%, SP=67%, wOE had SE=81%, SP=100%	High; groups not age-matched, OE not compared with standard metrics
Rajasekaran et al. (2014);	CSM (35) vs. HCs (40)	1.5T; Siemens; NR;	• C1-T1 • 40 axial slices,	• SE ssEPI • 12 directions	220mm^2; 256x256; 0.9x0.9x4mm^3;	FA, MD, λ_1, λ_2, λ_3	Manual, whole-cord, at C1 and	• Nurick	• All metrics differed between CSM vs. HCs at MCL: P<0.01 • DTI metrics not different between high and low Nurick grades	High; coarse clinical data, comparison vs. HCs not at

prospective, cross-sectional		NR	gap NR	• b=500 s/mm^2	6000/85; no; NR		discs: C2-T1		• No correlation between DTI metrics and Nurick grades	same level (C1-T1) as MCL
Toosy et al. (2014); prospective, cross-sectional	MS (14) vs. HCs (11)	1.5T; GE; NR; 33mT/m	• C1-C5 • 30 axial slices, contiguous	• CO-ZOOM-EPI rFOV • 60 directions • b=1000 s/mm^2	70x47mm^2; 48x32; 1.5x1.5x5mm^3; 15 beats/96; yes; NR	FA, MD, AD, RD	Automatic (registered to template), whole-cord and lesions using TFCE, P<0.01	• EDSS • 9 hole peg • 25-foot TWT • MSWS	• FA decreased, RD increased (P<0.01) • FA correlates with EDSS (R=-0.6, P=0.05) and TWT (R=0.7, P=0.02) • RD correlates with EDSS (R=0.7, P=0.01) and TWT (R=-0.6, P=0.05)	High (diagnostic), moderately high (correlation); 4 subjects excluded (image processing)
Wang et al. (2014); prospective, cross-sectional	ALS (24) vs. HCs (16)	1.5T; GE; 8-channel spine coil; NR	• C2-C4 • 24 axial slices, contiguous	• SE ssEPI, NEX=4 • 6 directions • b=400 s/mm^2	240mm^2; 128x128; 1.9x1.9x4mm^3; 6000/min; no; NR	FA, MD	Manual, 5 ROIs: DCs, L/R STs, LCSTs at mid-VB C2-C4	• ALSFRS-R • mNorris • EMG	• FA decreased in LCSTs at all levels (P<0.01), not DCs, STs • MD increased in LCSTs at all levels (P<0.05), not DCs, STs • DTI metrics not correlated with clinical measures	High; large voxels (difficult to assess individual tracts), manual ROI
Wen et al. (2014b); prospective, cross-sectional	CSM (15) vs. HCs (25)	3T; Philips; head/neck PAC; NR	• C1-C7 • 12 axial slices mid-VB or mid-disc	• ssEPI with spatial presaturation • 15 directions • b=600 s/mm^2	80mm^2; 80x64; 1x1.3x4mm^3; 5 beats/60; yes; 24m	FA, MD, AD, RD	Manual, ACs, LCs, DCs at MCL	• mJOA • SSEPs	• FA in HCs higher in DCs and LCs than ACs (P<0.05) • FA decreased selectively in LCs and DCs at MCL, but not in ACs (P<0.05)	High; groups not age-matched, only severe CSM subjects included
Wen et al. (2014a); prospective, longitudinal	CSM (45) vs. HCs (20)	Same as Wen et al. (2014)a					Manual, whole-cord	• mJOA • SSEPs • Recovery Ratio (6m-2y FU)	• Reduced mean FA: 0.65 vs. 0.52, P<0.001 • FA correlates with mJOA: R^2 = 0.33, P=0.02 • FA predicts good mJOA Recovery Ratio: P=0.03	High; groups not age-matched, coarse clinical data, 2 inconsistent definitions of mJOA recovery rate
Zhou et al. (2014); prospective, cross-sectional	CSM (19) vs. HCs (19)	3T; Siemens; NR; NR	• C1-C7 • 16 axial slices, gap NR	• SE ssEPI, NEX=2 • 20 directions • b=600 s/mm^2	128x124mm^2; 128x124; 1x1x5mm^3; 5000/106; yes; 24m	FA	Manual, whole-cord at C2, MCL	• JOA	• FA decreased at C2 (0.60 vs. 0.67, P=0.01) and MCL (0.51 vs. 0.66, P<0.001 • Amplitude of right pre-central and post-central gyri oscillations correlate weakly with FA at C2 (P<0.05)	High; primarily brain fMRI study, with cord DTI as secondary measure
Abbas et al. (2015); prospective, cross-sectional	Pott Disease (30 total, 15 with paraplegia, 15 without), no HCs	3T; Siemens; NR; NR	• 1 VB above to 1VB below lesion • 25 axial slices, 2mm gap	• SPAIR, NEX=4 • 20 directions • b=700 s/mm^2	280mm^2; 128x128; 2.2x2.2x5mm^3; 4100/66; no; NR	FA, MD	Manual, central GM/WM at 3 levels: 1 VB above, at lesion, and 1 VB below	• Jain and Sinha score • Presence of paraplegia	• FA higher above vs. below lesion in all subjects (P<0.05) • No difference between metrics with or without paraplegia	High; non-standard/coarse clinical data, large voxels
Iglesias et al. (2015); prospective, cross-sectional	ALS (21) vs. HCs (21)	3T; Siemens; neck/spine coil; NR	• C2-T2 • 8 axial slices, mid-VB, variable gap	• ssEPI, GRAPPA=2 • Repeated x 2 • 64 directions • b=1000 s/mm^2	128mm^2; 128x128; 1x1x5mm^3; 700/60; yes; 10m	FA, MD, AD, RD	Manual, 4 ROIs: ACs, DCs, L/R LCSTs	• SSEPs • ALSFRS-R • 9 hole peg • Muscle power	• 58% of ALS group had abnormal MD, RD values (outside 95% CI) in DCs • DTI metrics only correlated with N9 amplitude, not N20 • DTI metrics not correlated with clinical measures	High; 3 subjects excluded due to artefacts, no correlation with clinical scores
Maki et al. (2015); prospective, cross-sectional	CSM (20) vs. HCs (10)	3T; GE; 8 channel neck PAC; NR	• C1-T1 • 15 axial slices, mid-VB/mid-disc, variable gap	• rFOV SE ssEPI, NEX=16 • 6 directions • b=700 s/mm^2	140x30mm^2; 176x44; 0.7x0.7x5mm^3; 3000/75; no; NR	FA	Manual, 2 ROIs: DCs, LCs one slice above MCL	• JOA	• FA decreased in LCs (0.59 vs. 0.71, P=0.01) and DCs (0.58 vs. 0.72, P<0.01) but ranges overlap • FA correlates with JOA: r=0.48, P=0.03 for both LCs, DCs • FA correlates with JOA lower extremity subscore in LCs (r=0.76, P<0.01) and DCs (r=0.74, P<0.01) • ICC for ROI selection: 0.72-0.80	High; groups not age-matched, manual tract-specific ROIs had only moderate reliability
Oh et al. (2015); prospective, cross-sectional	MS (102 total, 66 RRMS, 24 SPMS, 12 PPMS) vs. HCs (11)	Same as Oh et al. (2013)a				FA, RD	Same as Oh et al. (2013)a	• EDSS • MSFC • Vibration • Hip flexion • OCT retinal measures	• RD (but not FA) decreased in progressive MS vs. RRMS (P=0.03) • FA, RD correlate with several measures of retinal layers (P<0.01) • DTI metrics do not independently correlate with clinical measures in multivariate regression	Moderately high (diagnostic), moderately low (correlation); no correlation found
Vedantam et al. (2015); retrospective, cross-sectional	aSCI (12) vs. HCs (12)	1.5T; GE; CTL spine coil; NR	• C1-T1	• Sequence NR • 15/25 directions (19/5 subjects) • b=500/600 s/mm^2	190mm^2; 128x128; 1.5x1.5mm^2 (thickness NR); 5000/98; no; NR	FA	Manual, whole-cord and LCSTs, C1-C2	• ASIA motor and sensory scores • AIS	• FA decreased at C1-2 in whole-cord (0.61 vs. 0.67, P<0.01) and LCSTs (0.66 vs. 0.70, P=0.04) • FA of LCSTs correlates with AIS (r=0.71, P=0.01), and upper limb motor score (r=0.67, P=0.01) • DTI metrics did not correlate with sensory scores	High; MR pulse sequence NR, manual ROIs
Yan et al. (2015); prospective,	Chiari I with Syringomyelia (23) vs. HCs (8)	1.5T; Philips; 16-channel NC coil;	• C2-T1 • Axial slices,	• EPI • 15 directions	224mm^2; 112x109; 2x2x2mm^3; 2170/59; no; 10m	FA	Manual, whole-cord at syrinx and above/below	• None	• No difference in FA above/below syrinx vs. HCs • FA at syrinx decreased vs. HCs: 0.43 vs. 0.53, P<0.05	High; large voxels (and thinly stretched cord), definition of symptomatic

cross-sectional			number/gap NR	• b=400 s/mm^2					• FA decreased at syrinx in symptomatic patients vs. asymptomatic: 0.37 vs. 0.45, P<0.05	NR

Table 1.4: Summary of DTI Fiber Tractography (FT) Studies.

Authors (Year); Design	Subjects	B_0; Vendor; Coil; Gradients	Anatomical Region/ Position	DTI Acquisition	FOV; Matrix; Voxel size; TR/TE (ms); Cardiac Gating; AT	FT Metrics	FT Method; ROI	Clinical Measures	Key Results	Risk of Bias; Key Barriers to Translation
Facon et al. (2005); prospective, cross-sectional	See Table 1.3					None	Vector-based tracing; none	See Table 1.3	• FT only used in 3 subjects to assist with ROI	High; Detailed FT method NR, no quantitative analysis using FT
Renoux et al. (2006); prospective, cross-sectional	See Table 1.3					None	DPTools using FA>0.17, angle<45°; none	See Table 1.3	• Areas of myelitis with T2 hyper-intensity (and low FA) tended to show 'spreading fibers' or 'broken fibers' • FT had optimal results with b=500 s/mm^2	High; no quantitative analysis using FT
Ciccarelli et al. (2007); prospective, longitudinal	MS (14 acute, lesion at C1-C3) vs. HCs (13)	1.5T; GE; NR; 33mT/m	• C1-C7 • 30 axial slices, contiguous	• CO-ZOOM-EPI rFOV • 31 directions • b=1000 s/mm^2	70x47mm^2; 48x32; 1.5x1.5x5mm^3; 15 heartbeats/90; yes; AT NR	Connecti-vity index, FA, MD, AD, RD (from FT)	4 seed points (ACs, DCs, L/R LCSTs), FT with FA>0.1; C1-C3 for each FT bundle	• EDSS • 9-hole peg • 25-foot TWT • MSWS-12 • FU: 3-6m EDSS	• Decreased connectivity in LCSTs and DCs (P=0.03) • Decreased FA in LCSTs (P=0.006) and DCs (P=0.02) • MD, AD, RD not different than HCs • Connectivity and FA of DCs correlates with 9-hole peg test (P<0.05, r value NR)	High (diagnostic), moderately high (correlation); min FA, max angle NR, no prediction of EDSS
Hatem et al. (2009); prospective, cross-sectional	Syringomyelia (28) vs. HCs (19)	1.5T; Siemens; NR; 40 mT/m	• C1-C7 • 12 sagittal slices, contiguous	• ssEPI • GRAPPA parallel factor=2 • 25 directions • b=1000 s/mm^2	179mm^2; 128x128; 1.4x1.4x3mm^3; 2100/97; No; 4m37s	FA, MD (from FT)	MedINRIA, with FA>0.2; manual, 5 ROIs: whole-cord, L/R/A/P hemi-cords at C3-4, C6-7	• Thermal sensory tests • Laser EPs	• FA reduced in all ROIs: P<0.05 • MD not different than HCs • FA at C3-4 (but not C6-7) correlates with thermal: r=-0.63, P<0.01	High; 9 subjects excluded due to artefacts, only sensory clinical data
van Hecke et al. (2009); prospective, cross-sectional	See Table 1.3					FA, MD, AD, RD, ψ (from FT)	Streamline-based FT, manual seed points, FA>0.3, angle<20°; whole-cord based on FT	• None	• FT segmentation had improved ICC vs. manual ROI: 0.96 vs. 0.79 (for FA) • Decreased FA, ψ in MS with lesions (P<0.01) and without (P<0.02)	High; no clinical data, diagnostic accuracy NR
Hatem et al. (2010); prospective, cross-sectional	Syringomyelia (37) vs. HCs (21)	Same as Hatem et al. (2009)				FA, MD (from FT), number of FT fibers	MedINRIA, with FA>0.2; whole-cord based on FT, A/P hemi-cords	• Pain scores • Mechanical, vibration, thermal • Laser EPs • SSEPs	• FA (r=-0.64, P=0.02) and number of FT fibers (r=-0.75, P=0.02) correlate with average daily pain scores	High; correlation with sensory testing NR, only sensory clinical data
Xiangshui et al. (2010); prospective, cross-sectional	See Table 1.3					None	GE Functool, FA>0.18, angle< 45°; none	• None	• Subjects with only dural indentation on T2w had normal FT • FT appeared distorted in subjects with cord compression on T2w	High; no quantitative analysis using FT
Budzik et al. (2011); prospective, cross-sectional	CSM (20) vs. HCs (15)	1.5T; Philips; Sense spine coil; NR	• C1-C7 • 12 sagittal slices, contiguous	• ssEPI with SPIR, partial Fourier • 25 directions • b=900 s/mm^2	200mm^2; 128x128; 1.6x1.6x3mm^3; 2010/94; no; 3m33s	FA, MD (from FT > 10mm)	Semi-automated, no seed points; whole-cord based on FT at C2-3, MCL or C4-C7 (HCs)	• JOACMEQ	• FA decreased at compressed level vs. C4-C7 in HCs: 0.40 vs. 0.50, P=0.0003 • FA at compressed level correlates with detailed UE (P<0.001) and LE (P<0.001) scores • FA negatively correlated with age: P=0.04	High; FT parameters (min FA, max angle) NR
Lee et al. (2011); prospective, longitudinal	See Table 1.3					FT: intact, waist, partial, or broken	PRIDE, FA>0.1, angle<27°; whole-cord at MCL based on FT	See Table 1.3	• Tractography patterns not correlated with JOA	High; heterogeneous subjects, FT analysis uses subjective categories
Ukmar et al. (2012);	MS (27 total, 9 RRMS, 9 SPMS,	1.5T; Philips; NR; 33mT/m,	• C1-C7, 40 axial slices,	• Sequence NR, fat sat, SENSE=2	224mm^2; 112x112; 2x2x2mm^3; 6731/91;	FA (manual ROI), FDI	DTI Studio, FA> 0.25, angle<70°;	• EDSS	• No difference in FA vs. HCs • FDi decreased in MS: 12 vs. 16, P<0.01	High; large voxels, groups not age-matched, no

prospective, cross-sectional	9 PPMS) vs. HCs (18)	slew=150mT/m/s	contiguous	• 32 directions • b=1000 s/mm^2	no; 4m2s		manual, whole-cord, C1-C7		• No correlation of metrics with EDSS	correlation found
Wang et al. (2012); prospective, cross-sectional	See Table 1.3					FT: amount of compression	PRIDE, FA>0.2; none	See Table 1.3	• FT normal in all 49 HCs • FT slightly compressed in 25/27 without T2w-HI • FT showed various degrees of severe compression in CM with T2w-HI	High; subjective analysis of FT, large voxels
Gao et al. (2013); prospective, cross-sectional	See Table 1.3					FT: deformed, thinning, or broken	NR; no ROI, qualitative impression of MCL	See Table 1.3	• FT deformed in 28/31 mild (JOA 13-16) subjects, thinning in 10/27 moderate (JOA 9-12) and 19/25 severe (JOA 5-8) subjects, broken in 18/21 serious (JOA 0-4)	High; DTT method NR, subjective FT categorization
Hodel et al. (2013); prospective, cross-sectional	Myelitis (40 total, 25 MS, 11 NMO, 4 other) vs. HCs (12)	3T; Philips; 16-channel head/neck PAC; NR	• C1-C7 • 11 coronal slices	• rFOV ZOOMED-EPI, fat sat, partial Fourier, NEX=3 • 15 directions • b=600 s/mm^2	42x170mm^2; 23x96; 1.8x1.8x2.5mm^3; 3 beats/39; yes; 7m30s	FA, MD, AD, RD, Ψ (from FT)	Manual seed and termination points at C1, C7, using FMRIB; whole-cord based on FT	• EDSS • Pyramidal score • Sensory score	• FA and Ψ significantly decreased in overall cohort and all subgroups except MS with acute cervical lesions • Excluding active lesions, FA correlates with sensory score: r=-0.4, P=0.01	High; groups not age-matched, heterogeneous subjects, large voxels
Rajasekaran et al. (2014); prospective, cross-sectional	See Table 1.3					FT: intact, waist, partial, or broken	Method NR, manual seed points at C1-2, FA > 0.2; none	See Table 1.3	• FT results showed 4 waist, 21 partially broken, and 10 completely broken • No correlation between FT results and Nurick grade	High; FT method NR, no correlation found
Abbas et al. (2015); prospective, cross-sectional	See Table 1.3					None	Method NR; none	See Table 1.3	• 13/15 subjects without paraplegia had decreased FT thickness below lesion, and 14/15 had some disruption • 4/15 subjects with paraplegia had decreased FT thickness below lesion, 6/15 had some disruption, and 2/15 had complete cessation of FT	High; minimal clinical data, FT method NR, only qualitative assessment of FT
Cui et al. (2015); prospective, cross-sectional	CSM (23) vs. HCs (20)	3T; Philips; head/neck coil; NR	• C1-C7 • 12 axial slices, gap NR	• rFOV SE ssEPI, fat sat • 15 directions • b=600 s/mm^2	80x36mm^2; 80x28; 1x1.3x7mm^3; 5 beats/60; yes; 24m	FA, MD, AD, RD (from FT), FD	TrackVis, manual seed points at C2, angle<35°; 7 ROIs from FT: whole-cord, L/R ACs, LCs, DCs	• JOA • Hand 10 second test	• Decreased FA in LCs, DCs: P<0.001 • MD, AD, RD higher in all columns: P<0.05 • Decreased FD: 0.29 vs. 0.32, P<0.05	High; correlation with clinical measures NR

Table 1.5: Summary of MT Studies.

Authors (Year); Design	Subjects	B_0; Vendor; Coil	Anatomical Region/ Position	MT Acquisition	FOV; Matrix; Voxel size; TR/TE (ms); Cardiac Gating; AT	MT Metrics	ROI	Clinical Measures	Key Results	Risk of Bias; Key Barriers to Translation
Silver et al. (1997); prospective, cross-sectional	MS (12 total, 8 RRMS, 4 SPMS) vs. HCs (12)	1.5T; NR; neck PAC	• C1-C7 • 3 sagittal slices, contiguous	• FSE +/- MT pre-pulse (sinc, 1kHz offset, 20 ms, 1430°), NEX=8	NR; 256x192; 5mm thick; 1600/17; No; 17m40s	MTR	Manual, ellipse drawn on mid-sagittal image from C1-C3	• EDSS	• Decreased MTR: 18 vs. 19, P=0.0004 • No correlation between MTR and EDSS	High; no correlation with EDSS, mid-sagittal ROI misses key WM tracts
Bozzali et al. (1999); prospective, cross-sectional	MS (90) vs. HCs (20)	1.5T; NR; tailored cervical PAC	• C1-C7 • 20 axial slices (contiguous) • 17 sagittal slices (0.3mm gap)	• 2D GE +/- MT pre-pulse (Gaussian, 1.5kHz offset, 7.7ms, 500°), NEX=2, FA=20°	Axial: 250mm^2; 192x256; 1x1x3mm^3; 640/10; No; NR; sagittal: 280mm^2; 224x256; 1x1x5mm^3; 640/10; No; NR	MTR, histogram peak, location	Manual, whole-cord	• EDSS	• Axial data more sensitive to pathology • Decreased MTR (axial): 44 vs. 46, P=0.001 • Patients with EDSS >= 4.0 had lower MTR: P=0.02	High; correlation coefficient not calculated
Filippi et al. (2000); prospective, cross-sectional	MS (96 total, 52 RRMS, 33 SPMS, 11 PPMS) vs. HCs (21)	1.5T; Siemens; tailored cervical PAC	• C1-C7 • Slice orientation, number, gap NR	• 2D GE +/- MT pre-pulse (Gaussian, 1.5kHz offset, 7.7ms, 500°), FA=20°, NEX=2	192x250mm^2; 256x256; 1x1x5mm^3; 640/12; No; NR	MTR, histogram peak, location	Semi-automatic, whole-cord, excluding voxels with MTR<10%	• EDSS	• Decreased MTR in MS patients: 44% vs. 46% P=0.006 • Peak location and height were independent predictors of EDSS >= 4.0 in multivariate analysis	High; correlation coefficient not calculated
Lycklama et al. (2000); prospective, cross-sectional	MS (65 total, 14 RRMS, 34 SPMS, 17 PPMS) vs. HCs (9)	1.0T; Siemens; quadrature head coil	• Brain-C1 • 22 axial slices, 3mm gap	• 2D GE +/- MT pre-pulse (Gaussian, 1.5kHz offset, 7.6ms, 500°), FA=30°, NEX=2	NR; NR; 3mm thick; 700/10; no; NR	MTR	Manual, whole-cord excluding edge voxels at C1,	• EDSS	• Decreased MTR: 30 vs. 33, P<0.01 • MTR correlates weakly with EDSS: r=-0.25, P<0.05	High; coarse clinical data, weak correlation with EDSS
Rovaris et al. (2000); prospective, cross-sectional	MS (77 total, 40 RRMS, 28 SPMS, 9 PPMS), no HCs	1.5T; Siemens; tailored cervical PAC	• C1-C7 • 20 axial slices, contiguous	• 2D GE +/- MT pre-pulse (Gaussian, 1.5kHz offset, 7.7ms, 500°), FA=20°, NEX=2	250mm^2; 192x256; 1x1x3mm^3; 640/10; no; NR	MTR, histogram peak, location	Semi-automatic, whole-cord, excluding voxels with MTR<10%	• EDSS	• No difference in mean MTR, histogram height between RRMS, SPMS, and PPMS • Peak location significantly different for RRMS>SPMS>PPMS, P=0.01 • Peak location corresponds with EDSS >=3, P<0.001	High; correlation coefficients not calculated
Inglese et al. (2001); prospective, cross-sectional	LHON (14) vs. HCs (20)	1.5T; NR; standard cervical coil; NR	• C1-C4 • 20 axial slices, 0.3mm gap	• 2D GE +/- MT pre-pulse (Gaussian, 1.5kHz offset, 16ms, 850°), FA=20°	250mm^2; 256x256; 1x1x5mm^3; 640/10; no; NR	MTR, histogram peak, location	Manual, whole-cord	• None	• No significant differences in MTR or histogram metrics vs. HCs	High; no group differences found, no clinical data
Rocca et al. (2001); prospective, cross-sectional	CADASIL (25) vs. HCs (14)	1.5T; NR; tailored cervical PAC	• C1-C7 • 24 axial slices (contiguous)	• 2D GE +/- MT pre-pulse (Gaussian, 1.5kHz offset, 7.7ms, 500°), FA=20°	NR; NR; 5mm thick; 792/10; no; NR	MTR, histogram peak, location	Semi-automatic, whole-cord, excluding voxels with MTR<10%	• Rankin score	• No difference in MTR or histogram location • MTR peak height lower in CADASIL: P=0.02 • MTR correlates with Rankin disability: r=-0.4, P=0.05	High (diagnostic), moderately high (correlation); coarse clinical data, results are NS if corrected
Rovaris et al. (2001a); prospective, cross-sectional; high	Migraine (16) vs. HCs (17)	Same as Rovaris et al. (2000)						• Presence/ absence of aura	• No differences in mean MTR or histogram metrics	High; no group differences found, minimal clinical data
Rovaris et al. (2001b); prospective, cross-sectional	PPMS (91) vs. SPMS (36) vs. HCs (30)	Same as Rovaris et al. (2000)				MTR, histogram peak	Same as Rovaris et al. (2000)		• Mean MTR decreased vs. HCs: 42 vs. 46, P<0.001 • Peak height decreased vs. HCs: 61 vs. 72, P=0.001 • Peak height increased vs. SPMS: 61 vs. 57, P=0.003 • No metric had univariate correlation with EDSS	Moderately high (diagnostic), moderately low (correlation); coarse clinical data, no correlations found

Filippi et al. (2002); prospective, cross-sectional	PPMS (26) vs. HCs (15)	1.5T; Siemens; tailored cervical PAC	• C1-C7 • 24 axial slices (contiguous)	• 2D GE +/- MT pre-pulse (Gaussian, 1.5kHz offset, 7.7ms, 500°), FA=20°, NEX=2	250mm^2; 256x256; 1x1x5mm^3; 640/12; no; NR	MTR, histogram peak, location	Semi-automatic, whole-cord, excluding voxels with MTR<10%	• EDSS • fMRI brain activations	• Decreased MTR: 40 vs. 46, P<0.001 • Decreased peak height: 62 vs. 112, P<0.001 • Decreased peak location: 35 vs. 40, P=0.003 • MTR does not correlate with EDSS • MTR metrics correlate moderately with fMRI activation of several motor areas	High; no correlations with EDSS, utility of correlations with brain fMRI activation is unclear
Rovaris et al. (2004); prospective, cross-sectional	CIS (45) vs. HCs (27)	Same as Rovaris et al. (2000)							• No significant differences in metrics vs. HCs • 3/45 subjects had mean MTR 2 SDs below mean of HCs	High; no group differences found
Fatemi et al. (2005); prospective, cross-sectional	AMN (17 total, 9 full AMN, 8 X-ALD hetero-zygotes) vs. HCs (10)	1.5T; Philips; 2 element neck PAC	• C1-C3 • 32 axial slices (contiguous)	• 3D GE with MT pre-pulse (sinc, 15ms, 5 offsets 10-63kHz), FA=7°	225x 48mm^3; 256x256x32; 1x1x1.5mm^3; 50/13; no; NR	MTCSF	Manual, DCs	• EDSS • R, L 1st toe vibration • Standing balance test	• MTCSF increased in AMN (34) vs. X-ALD (30) vs. controls (27): P<0.0001 • DC MTCSF correlates with EDSS (r=0.62, P=0.01), vib. Sense (r=0.75, P=0.002), and balance sway (r=0.62, P=0.01)	High (diagnostic), moderately high (correlation); manual ROI, DCs only
Agosta et al. (2006); prospective, cross-sectional	Neuro-borreliosis (Lyme Disease) (20) vs. HCs (11)	1.5T; Siemens; tailored cervical PAC	• C1-C7 • 24 axial slices (contiguous)	• 2D GE +/- MT pre-pulse (Gaussian, 1.5kHz offset, 7.7ms, 500°), FA=20°	250mm^2; 256x256; 1x1x5mm^3; 640/12; no; NR	MTR	Semi-automatic, whole-cord, excluding voxels with MTR<10%	• None	• No difference in cervical cord MTR	Moderately high; no group difference found
Rocca et al. (2006); prospective, cross-sectional	Isolated myelitis (24) vs. HCs (15)	1.5T; Siemens; NR	• C1-C7 • 20 axial slices (gap NR)	• 2D GE +/- MT pre-pulse (Gaussian, 1.5kHz offset, 7.7ms, 500°), FA=20°	NR; NR; 5mm thick; 640/12; no; NR	MTR	Semi-automatic, whole-cord, excluding voxels with MTR<10%	• EDSS • 9 hole peg • Finger-tapping	• MTR decreased in myelitis vs. HCs: 36 vs. 41, P<0.0001 • MTR decreased in cervical vs. thoracic myelitis: 35 vs. 37, P=0.01 • No correlation between MTR and clinical measures • Various correlations between MTR and brain fMRI activations	High (diagnostic), moderately high (correlation); no correlations with clinical measures
Agosta et al. (2008b); prospective, cross-sectional	RRMS (18) vs. HCs (13)	1.5T; Siemens; tailored cervical PAC	• C1-C7 • 20 axial slices (contiguous)	• 2D GE +/- MT pre-pulse (Gaussian, 1.5kHz offset, 7.7ms, 500°), FA=20°	180mm^2; 128x128; 1.4x1.4x4mm^3; 600/25; no; NR	MTR	Manual, GM (avoiding edge voxels)	• EDSS	• Decreased GM MTR: 23.5 vs. 24.8, P=0.009 • GM MTR correlates with EDSS: r=-0.48, P=0.048	High (diagnostic), moderately high (correlation); coarse clinical data
Rovaris et al. (2008); prospective, cross-sectional	RRMS (23) vs. HCs (10)	Same as Rovaris et al. (2001)b						• EDSS	• No difference in metrics vs. HCs • No correlation in metrics with brain T2w lesions	High; no group differences found, correlation with EDSS NR
Zackowski et al. (2009); prospective, cross-sectional	MS (42) vs. HCs (18)	3T; Philips; 2-element surface PAC	• C2-C6 • 40 contiguous axial slices	• GE +/- MT pre-pulse (sinc-Gauss, 1.5kHz offset, 24ms), FA=9°, SENSE=2	NR; NR; 0.6x0.6x2.25^3; 110/13; no; NR	MTCSF	Manual, 3 ROIs in each slice: DCs and R/L LCs; GM ROI in 5 slices at C2-3	• EDSS • Vibration • Posture sway • Ankle power • Walk speed	• MTCSF of LC (but not DC, GM) increased in MS vs. HCs: 0.55 vs. 0.50, P=0.008 • MTCSF of DC correlates with vibration (r=0.58, P<0.001), sway (r=0.32, P=0.02), EDSS (r=0.41, P<0.05) • MTCSF of LC correlates with ankle strength (r=-0.45, P=0.003), walk speed (r=-0.51, P<0.001), and EDSS (r=0.59, P<0.05)	High; groups not age-matched, manual tract-specific ROIs
Cohen-Adad et al. (2011); prospective, cross-sectional	cSCI (14) vs. HCs (14)	3T; Siemens; multi-channel head, neck, spine PACs	• C2-T2 • 52 axial slices, 0.4mm gap	• 3D GE +/- MT pre-pulse (Gaussian, 1.2kHz offset, 10ms)	230mm^2; 256x256; 0.9x0.9x2mm^3; 28/3.2; no; 10m	MTR	Manual, 4 ROIs: ACs, DCs, L/R LCs; lesion levels skipped in cSCI	• ASIA motor and sensory scores	• Decreased MTR: 26 vs. 32, P<0.0001 • MTR correlates with total ASIA score: r=0.59, P=0.04 • MTR of ACs/LCs more specifically predicts motor score (P=0.03), dorsal region predicts sensory score (P=0.03)	High (diagnostic), moderately high (correlation); manual tract-specific ROIs
Cohen-Adad et al. (2013a); prospective, cross-sectional	ALS (29) vs. HCs (21)	Same as Cohen-Adad et al. (2011)						• ALSFRS-R • TMS motor threshold	• Reduction in MTR greatest at caudal levels • MTR not correlated with ALSFRS-R	High; manual tract-specific ROIs, groups not gender-matched
Oh et al. (2013a); prospective, cross-sectional	MS (124 total, 69 RRMS, 36 SPMS, 19 PPMS), no HCs	3T; Philips; 2 element surface PAC	• C2-C6 • 30 axial slices, contiguous	• 3D GE T2*w EPI +/- MT pre-pulse (1.5kHz offset, sinc-Gauss shape), FA=9°, SENSE=2	NR; NR; 0.6x0.6x3mm^3; 121/12.5; no; NR	MTR	Automatic segmentation, whole-cord at C3-4 (11 slices)	• EDSS • MSFC	• MTR decreased in high vs. low EDSS in high lesion count subjects (P=0.003) • No difference in MTR in high lesion count subjects	Moderately high; diagnostic accuracy NR

Oh et al. (2013b); prospective, cross-sectional	MS (129 total, 74 RRMS, 36 SPMS, 19 PPMS) vs. HCs (14)	Same as Oh et al. (2013)a						• EDSS • Hip flexion power • Vibration	• Decreased MTR in total MS vs. HCs: 30 vs. 31, P=0.04 • Decreased MTR in progressive MS vs. RRMS: 0.28 vs. 0.31, P<0.001 • MTR correlates with EDSS (P=0.02) and vibration (P=0.05) in multivariate regression	Moderately high (diagnostic), moderately low (correlation); no diagnostic accuracy
El Mendili et al. (2014); prospective, longitudinal	ALS (29), no HCs	3T; Siemens; neck/spine coil; NR	• C2-T2 • 52 axial slices, gap NR	• 3D GE +/- MT pre-pulse (Gaussian, 1.2kHz offset, 10ms)	230mm^2; 256x256; 0.9x0.9x2mm^3; 28/3.2; no; 5m	MTR	Manual, 4 ROIs: ACs, DCs, L/R LCSTs	• ALSFRS-R • Muscle power • FU at 1y	• MTR at 1y decreased from baseline: 30 vs. 33, P=0.003 • No correlation between change in MTR and change in clinical scores • Baseline MTR not predictive of 1y outcome	Moderately high; no correlation/ prediction found, manual ROIs
Kearney et al. (2014b); prospective, cross-sectional	MS (133 total, 22 CIS, 29 RRMS, 28 SPMS, 28 PPMS) vs. HCs (26)	3T; Philips; 16 channel neuro-vascular coil	• C1-C7 • 22 axial slices	• 3D spoiled GE +/- MT pre-pulse (Gaussian, 1kHz offset, 16ms), FA=20° NEX=2, SENSE=2	180x240mm^2; 240x320; 0.8x0.8x5mm^3; 36/3.5,5.9; no; NR	MTR	Semi-automatic, outer cord, WM, GM at C2-3 (3 slices)	• EDSS • 25-foot TWT • 9 hole peg • ASIA motor, sensory	• WM MTR decreased in all subgroups vs. controls (P<0.05) • MTR correlates with EDSS in GM (r=-0.34), WM (r=-0.32), outer cord (r=-0.41) • Cord CSA showed stronger correlations with all clinical measures (e.g. R=-0.60 with EDSS) than MTR	Moderately high (diagnostic), moderately low (correlation); CSA outperformed MTR
Kearney et al. (2015a); prospective, cross-sectional	MS (92 total, 34 RRMS, 29 SPMS, 29 PPMS) vs. HCs (28)	Same as Kearney et al. (2014)					Semi-automatic, whole-cord, lesions	• EDSS • MSFC • 9 hole peg • PASAT • TWT	• Whole-cord MTR decreased in SPMS (P=0.01) and PPMS (P=0.004) vs. HCs • No difference in whole-cord or lesion MTR between subgroups • MTR not independently associated with disability (CSA, lesion load were stronger multivariate factors)	Moderately high (diagnostic), moderately low (correlation); no correlations with disability found
Oh et al. (2015); prospective, cross-sectional	MS (102 total, 66 RRMS, 24 SPMS, 12 PPMS) vs. HCs (11)	Same as Oh et al. (2013)a					Same as Oh et al. (2013)a	• EDSS • MSFC • Vibration • Hip flexion • OCT of retina	• MTR not different between total MS vs. HCs • MTR decreased in progressive MS vs. RRMS: P<0.001 • MTR not correlated with retinal layer measures • MTR not correlated with clinical measures	Moderately high (diagnostic), moderately low (correlation); no group difference vs. HCs, no correlations found

Table 1.6: Summary of MWF Studies.

Authors (Year); Design	Subjects	B_0; Vendor; Coil	Anatomical Region/ Position	MWF Acquisition	FOV; Matrix; Voxel size; TR/TE (ms); Cardiac Gating; AT	MWF Metrics	ROI	Clinical Measures	Key Results	Risk of Bias; Key Barriers to Translation
Laule et al. (2010); prospective, longitudinal	PPMS (24) vs. HCs (24)	1.5T; GE; standard head coil	• C2-C3 • Single axial slice	• T2w 32-echo sequence (spacing 10ms) with IR (TI=1200ms), NEX=2	220mm^2; 256x128; 0.9x0.9x5mm^3; 3000/10 (32 echoes); no; 30m	MWF (ratio of 15-40ms signal to total); MRI repeated at 1y, 2y	Manual, whole-cord	• EDSS • FU EDSS at 1y, 2y	• NS difference in MWF vs HCs: 0.23 vs. 0.25, P=0.12 • 10% decrease in MWF in PPMS over 2 years (P=0.01) • Baseline MWF not correlated with EDSS, not predictive of decline • No effect of demyelination treatment on MWF	High; no group difference vs. HCs, coarse clinical data, no correlations or successful prediction found

Table 1.7: Summary of MRS Studies.

Authors (Year); Design	Subjects	B_0; Vendor; Coil	Anatomical Region/ Position	MRS Acquisition	Voxel size; TR/TE (ms); Cardiac Gating; AT	MRS Metrics	Clinical Measures	Key Results	Risk of Bias; Key Barriers to Translation
Ciccarelli et al. (2007); prospective, longitudinal	MS (14 acute, lesion at C1-C3) vs. HCs (13)	1.5T; GE; saddle coil	• Single voxel, C1-C3	• PRESS • Sat bands (NR) • NSA=192 (w CHESS) • Shim method: NR • Phantom scanned using same voxel	6x8x50mm^3 (variable to fit cord); 3 heartbeats/30; yes (delay NR); NR	Absolute values and ratios for: NAA, Cre, Cho, Myo	• EDSS • 9-hole peg • 25-foot TWT • MSWS-12 • FU: EDSS at 3-6 months	• Decreased NAA: 4.1 vs. 6.7, P<0.0001 • No difference in Myo, Cho, Cre • Correlations found with EDSS: Myo (r=0.64, P=0.02), Cho (r=0.65, P=0.01), Cre (r=0.75, P=0.003) • Cre correlates with upper limb metrics (P<0.05) and MSWS-12	High (diagnostic), moderately high (correlation); no prediction of FU EDSS, high variance of metrics
Holly et al. (2009); prospective, cross-sectional	CSM (21) vs. HCs (13)	1.5T; Siemens; neck coil	• Single voxel, C2	• PRESS • NSA=256 • Shim method: manual (18-28 Hz)	10x10x20mm^3 (variable to fit cord); 1500 or 3000/30; no; 3-5m shimming + 3m40s	NAA/Cre, Cho/Cre, presence of Lac peak	• mJOA	• Decreased NAA/Cre: 1.27 vs. 1.83, P<0.0001 • No difference in Cho/Cre • No correlation between NAA/Cre and mJOA • 7/21 CSM patients had lactate peak vs. no controls, P<0.05	High (diagnostic), moderately high (correlation); boxplot shows low SE/SP
Ciccarelli et al. (2010a); prospective, cross-sectional	MS (14, 6m within lesion onset at C1-C3) vs. HCs (13)	Same as Ciccarelli et al. (2007)				ResNAA (NAA not explained by AD, CSA parameters)	Same as Ciccarelli et al. (2007)	• Decreased NAA: 4.2 vs. 5.9, P=0.03 • ResNAA correlates with EDSS (R^2=0.5, P=0.03), TWT (R^2=0.4, P=0.02), and MSWS-12 (R^2=0.4, P=0.01)	High; high variance of metrics, requires MRS, DTI in same ROI
Ciccarelli et al. (2010b); prospective, longitudinal	Same as Ciccarelli et al. (2007)					Absolute NAA; FU MRS studies at 1, 3, 6 months	Same as Ciccarelli et al. (2007)	• Increase in NAA from 1 month to 6 months in patients that recover following acute MS: P=0.001 • Baseline NAA and NAA change over 1st month not predictive of outcome	High; weak results for correlation and prediction
Marliani et al.(2010); prospective, cross-sectional	RRMS (15) vs. HCs (10)	3T; GE; 8-channel spine PAC (upper 4 elements)	• Single voxel, C2-C3	• PRESS • NSA=400 (CHESS), 16 (no water suppression) • Automatic shimming	7x9x35mm^3 (variable); 2000/35; no; 14m	NAA/Cre, NAA/Cho, Cho/Cre, Myo/Cre	• EDSS	• All metabolite ratios significantly altered in RRMS (P=0.002 to 0.04) • No metabolite ratios correlate with EDSS	High; no correlation with EDSS found, diagnostic accuracy NR
Carew et al. (2011b); prospective, cross-sectional	ALS (14) vs. HCs (16)	3.0T; Siemens; Head/neck/ spine PACs	• C1-C2	• PRESS • NSA=256 (CHESS), 4 (no water suppression) • Automatic shimming with B0 mapping	8x5x35mm^3; 2000/35; no; 12m	Ratios between Cho, Myo, NAA, Cre	• ALSFRS-R • FVC	• Decreased NAA/Cre: 0.75 vs. 1.25, P=0.0007 • Decreased Cho/Cre: 0.40 vs. 0.50, P=0.007 • NAA/Myo correlates with FVC: r=0.66, P=0.01 • Metrics not significantly correlated with ALSFRS-R	High; 4/30 subjects excluded due to technical problems, no correlation with ALSFRS-R found
Carew et al. (2011a); prospective, cross-sectional	SOD1 (24) vs. ALS (23) vs. HCs (29)	Same as Carew at al. (2011)a					• None (asymptomatic population)	• SOD1 vs. HCs shows decreased NAA/Cre (P=0.001), decreased Myo/Cre (P=0.02) • SOD1 vs. ALS shows increased NAA/Cho (P=0.002)	High; 12 metric calculations excluded due to technical issues
Bellenberg et al. (2013); prospective, longitudinal	MS (22) vs. HCs (17)	1.5T; Siemens; head/neck coil PAC	• Single voxel, C3-C5 (variable, to include MS lesions)	• PRESS • 8 adjacent sat bands • NSA=128 (CHESS), 16 (no water suppression) • Shim method: NR	8x10x40mm^3; 1500/30; yes (300ms delay); AT NR	Absolute values and ratios for: NAA, Cre, Cho, Myo; MRI study repeated at 1 year FU	• EDSS • Max. walking distance • MSFC • 25-foot TWT • 9-hole peg • FU at 1y, 2y	• Decreased NAA, NAA/Cre (P<0.01), Cho/Cre (P=0.026) • Increased Myo (P=0.001), Myo/Cre (P=0.002) • NAA correlates with age: r=-0.482, P=0.003 • No correlation with clinical measures • No significant changes in MRS metrics over 1 year FU • MS patients that worsened after 1 year had lower baseline NAA/Cre (P=0.024) and higher Cho (P=0.021)	High (diagnostic, prognostic), moderately high (correlation); no correlation found, weak prediction of outcome
Ikeda et al. (2013); prospective, longitudinal	ALS (19) vs. HCs (20)	1.5T; Siemens; NR	• Single voxel, C1-C3	• PRESS • NSA=400 (CHESS) • Shim method: automatic	6x8x40mm^3; 1500/50; no; 15m	NAA/Cre, Cho/Cre, Myo/Cre, NAA/Myo	• ALSFRS-R • FVC • EMG • Data captured 6m prior, 6m after	• Decreased NAA/Cre, NAA/Myo, increased Myo/Cre: ALS vs. HCs and with vs. without EMG denervation (P<0.01) • NAA/Cre and NAA/Myo correlate with ALSFRS-R: r=0.79, P<0.01 and ρ=0.76, P<0.01 respectively • NAA/Cre and NAA/Myo predict decline of ALSFRS-R: r=-0.70, P<0.01 and ρ=-0.78, P<0.01	High (diagnostic, prognostic), moderately high (correlation); long acquisition time difficult for ALS population
Salamon et al. (2013); prospective,	CSM (21 total, 11 with T2w-HI, 10 without) vs.	3T; Siemens; NR	• Single voxel, C2	• PRESS • NSA=256 (CHESS), 4 (no water suppression)	7x7x35mm^3; 2000/30; no; NR	NAA/Cre, Glu/Cre, Cho/Cre, Myo/Cre, (Lip+Lac)/Cre,	• mJOA	• Cho/NAA increased in CSM (P<0.01) • Cho/NAA correlates with mJOA: R=-0.45, P<0.01	High; coarse clinical data, age/gender of HCs NR

cross-sectional	HCs (11)			• 6 sat bands • Shim method: manual		Cho/NAA			
Taha Ali et al. (2013); prospective, cross-sectional	CSM (24) vs. HCs (11)	1.5T; Siemens; neck circular surface coil	• Single voxel, C2	• PRESS • NSA=512 (CHESS) • Multiple very selective sat bands placed	10x10x15-20mm^3; 2000/36; yes, 4m54s	NAA, Cho, Cre, Lac, NAA/Cre, Cho/Cre	• None	• NAA/Cr decreased: 1.34 vs. 1.82, P<0.0001 • Lactate peak present in 9/24 CSM subjects, no HCs	High; no clinical data, diagnostic accuracy only provided for lactate

Table 1.8: Summary of fMRI Studies.

Authors (Year); Design	Subjects	B_0; Vendor; Coil	Anatomical Region/ Position	fMRI Acquisition	FOV; Matrix; Voxel size; TR/TE (ms); Cardiac Gating; AT	fMRI Metrics	ROI	Clinical Measures	Key Results	Risk of Bias; Key Barriers to Translation
Stroman et al. (2004); prospective, cross-sectional	cSCI (27) vs. HCs (15)	1.5T; GE; spine PAC	• T11-conus • 5 axial slices, mid-disc or mid-VB	• Single-shot FSE • PD-weighted, SEEP contrast • 3 sat bands: ant, L, and R • 8.25s/volume • Block-design, thermal stimulus (10C, 32C) to legs	120x120mm^2; 128x128; 0.9x0.9mm^2, thickness NR; 8250/34; No; NR	Activation maps; co-registered with template, group activation for voxels active in >= 3 subjects	L1-S1 cord	• AIS grade	• Activation in lumbar cord seen in all cSCI subjects • Complete SCI subjects showed decreased ipsilateral dorsal activation and increased bilateral ventral activation (P values NR)	High; minimal clinical data, activations not corrected, only qualitative analysis of group activations
Agosta et al. (2008b); prospective, cross-Sectional	RRMS or SPMS (24) vs. HCs (10)	1.5T; Siemens; Phased-array spine coil	• C5-C8 cord • 9 axial slices (mid-VB or mid-disc), gap adjusted to fit	• Multishot Turbo SE, FA=120° • PD-weighted, SEEP contrast • 2 sat bands (ant. and post.) • 13s/volume • Block-design, tactile stimulus to right hand	100x100mm^2; 256x244; 0.4x0.4x7mm^3; 2850/11; No; NR	Frequency of activation; mean SI change (active voxels)	Manual, 5 regions (R ant., L ant., R post., L post., central)	• EDSS	• Increased mean SI change (active voxels): 3.4% vs. 2.7%, P=0.03 • Decreased frequency of ipsilateral activation: P=0.003 • Decreased frequency of posterior activation: P=0.02	High; coarse clinical data, activations not corrected, correlation with EDSS NR
Agosta et al. (2008a); prospective, cross-Sectional	RRMS or SPMS (25) vs. HCs (12)	Same as Agosta et al. (2008)a							• Increased mean SI change (active voxels): 3.9% vs. 3.2%, P=0.02 • Mean SI change correlates with mean cord FA: r=-0.48, P=0.04 • Average SI change correlates with cord FA: r=-0.48, P=0.04	High; coarse clinical data, activations not corrected, correlation with EDSS NR
Agosta et al. (2009b); prospective, cross-Sectional	PPMS (23) vs. HCs (18)	Same as Agosta et al. (2008)a							• Increased mean SI change (active voxels): 3.3% vs. 2.6%, P=0.05 • Decreased frequency of posterior activation (P<0.001) • Mean SI change correlates with mean cord FA: r=-0.58, P=0.001	High; coarse clinical data, activations not corrected, correlation with EDSS NR
Valsasina et al. (2010); prospective, cross-sectional	MS (49 total, 30 RRMS, 19 SPMS) vs. HCs (19)	Same as Agosta et al. (2008)a							• RRMS (P=0.05) and SPMS (P=0.02) had increased cord activation • Severe disability corresponded to increased activation vs. controls (P=0.004) and mild disability (P=0.04)	High; coarse clinical data, activations not corrected, correlation coefficients NR
Cadotte et al. (2012a); prospective, cross-sectional	cSCI (18) vs. HCs (20)	3.0T; GE and Siemens; NR	• Brainstem and C1-T1 • 9 sagittal slices, contiguous	• ssFSE (HASTE) multi-echo, partial Fourier • PD-weighted, SEEP contrast • 9s/volume • Thermal (44C) stimulus, L/R above and below injury	280x210mm^2; 192x144; 1.5x1.5x2mm^3; 9000/38; No; 7m12s	Number of positive and negative active voxels per dermatome; connectivity analysis	Manual, 4 quadrants	• ASIA sensory score	• Increased number of active voxels in incomplete cSCI in dermatome of normal sensation • Number of active voxels correlates with degree of sensory impairment: R^2 = 0.93, P<0.001 • Increased number of intraspinal connections in cSCI vs. HCs	High; sensory-only paradigm, requires thermal stimulator
Rocca et al. (2012); prospective, cross-sectional	MS (35 total, 20 with fatigue, 15 without) vs.	Same as Agosta et al. (2008)a						• EDSS • Fatigue Severity	• No difference in number of active voxels between MS groups or HCs • MS without fatigue had more distributed activation	High; activations not corrected (no activations in 30% of subjects at p<0.001), altered

	HCs (20)		Scale	outside ipsilateral dorsal quadrant vs. MS with fatigue and HCs (P<0.05) • Bilateral recruitment correlated with severity of fatigue: r=-0.34, P=0.04	recruitment not clearly defined
Valsasina et al. (2012); prospective, cross-sectional	Progressive MS (34 total, 18 SPMS, 16 PPMS) vs. HCs (17)	Same as Agosta et al. (2008)a		• Activation increased vs. HCs: P=0.003 • Activation increased in SPMS vs. PPMS: P=0.05 • No correlation between activation and EDSS	High; coarse clinical data, activations not corrected, no correlation with EDSS found

7.2 APPENDIX B – Updated Electronic Literature Search

The following search terms were used in a PubMed electronic database search:

(((((((((DTI[Title/Abstract]) OR Diffusion tensor imaging[Title/Abstract]) OR Magnetization transfer[Title/Abstract]) OR MT[Title/Abstract]) OR Myelin water fraction[Title/Abstract]) OR MWF[Title/Abstract]) OR functional MRI[Title/Abstract]) OR fMRI[Title/Abstract]) OR MR spectroscopy[Title/Abstract]) OR MRS[Title/Abstract]) AND (((spine[Title/Abstract]) OR spinal[Title/Abstract]) OR cervical[Title/Abstract])

Following the search, a filter was applied to restrict results to the following dates: 2015-06-01 to present (2017-02-06). This search returned 374 citations, of which _ were selected for narrative review.

7.3 APPENDIX C: Curriculum Vitae

The following pages are Allan R. Martin's Curriculum Vitae as of April 17, 2017.

EDUCATION

Formal Education:
University of Toronto, PhD student, Institute of Medical Science (Surgeon Scientist Program)
9/2014-6/2017
University of Toronto, Neurosurgery Residency Training Program
7/2011-6/2019
University of Toronto, Doctor of Medicine (MD)
9/2007-4/2011
University of Toronto, Part-time undergraduate
9/2001-5/2007
University of Toronto, Bachelor of Applied Science (BASc), Engineering Science (Honours)
9/1994-5/1999

PUBLICATIONS

Peer-reviewed journal publications (31):

- **Martin AR**, Cohen-Adad J, De Leener B, Cadotte DW, Crawley A, Ginsberg H, Mikulis DJ, Fehlings MG. Clinically Feasible Microstructural MRI to Quantify Cervical Spinal Cord Tissue Injury using DTI, MT, and T2*-weighted Imaging: Assessment of Normative Data and Reliability. AJNR, 2017 Apr 20. doi: 10.3174/ajnr.A5163. [Epub ahead of print].
- **Martin AR**, De Leener B, Cohen-Adad J, Cadotte DW, Kalsi-Ryan S, Lange SF, Tetreault L, Nouri A, Crawley A, Mikulis DJ, Ginsberg H, Fehlings MG. A Novel MRI Biomarker of Spinal Cord White Matter Injury: T2*-weighted White Matter to Grey Matter Ratio. Submitted to AJNR 2016-10-03, AJNR, 2017 Apr 20. doi: 10.3174/ajnr.A5162. [Epub ahead of print].
- Nouri A, **Martin AR**, Tetreault L, Nater A, Kato S, Nakashima H, Nagoshi N, Reihani-Kermani H, Fehlings MG. The Relationship Between MRI Signal Intensity Changes, Clinical Presentation, and Surgical Outcome in Degenerative Cervical Myelopathy: Analysis of a Global Cohort. Spine, 2017, in press.
- Kurpad S, **Martin AR**, Fischer DJ, Skelly AC, Mikulis DJ, Flanders A, Aarabi B, Mroz T, Tsai E, Tetreault L, Fehlings MG. Role of baseline magnetic resonance imaging upon neurologic, functional, and safety outcomes in patients with acute traumatic spinal cord injury. Global Spine Journal, 2017; in press.
- Fehlings MG, **Martin AR**, Tetreault L, Aarabi B, Anderson P, Arnold P, Brodke D, Burns A, Chiba K, Dettori J, Furlan J, Hawryluk G, Holly LT, Howley S, Jeji T, Kalsi-Ryan S, Kotter M, Kurpad S, Kwon B, Marino R, Massicotte EM, Merli G, Nakashima H, Nagoshi N, Palmieri K, Singh A, Skelly AC, Tsai E, Vaccaro A, Wilson JR, Yee A, Harrop J. A Clinical Practice Guideline for the Management of Patients with Acute Spinal Cord Injury: Recommendations on the Role of Baseline Magnetic Resonance Imaging in Clinical Decision Making and Outcome Prediction. Global Spine Journal, 2017; in press.
- Fehlings MG, Tetreault L, Wilson JR, Aarabi B, Anderson P, Arnold P, Brodke D, Burns A, Chiba K, Dettori J, Furlan J, Hawryluk G, Holly LT, Howley S, Jeji T, Kalsi-Ryan S, Kotter M, Kurpad S, Kwon B, Marino R, **Martin AR**, Massicotte EM, Merli G, Nakashima H, Nagoshi N, Palmieri K, Singh A, Skelly AC, Tsai E, Vaccaro A, Yee A, Harrop J. A Clinical Practice Guideline for the Management of Patients with Acute Spinal Cord Injury and Central Cord Syndrome: Recommendations on the Timing (≤24 hours versus >24 hours) of Decompressive Surgery. Global Spine Journal, 2017; in press.
- Fehlings MG, Wilson JR, Tetreault L, Aarabi B, Anderson P, Arnold P, Brodke D, Burns A, Chiba K, Dettori J, Furlan J, Hawryluk G, Holly LT, Howley S, Jeji T, Kalsi-Ryan S, Kotter M, Kurpad S, Kwon B, Marino R, **Martin AR**, Massicotte EM, Merli G, Nakashima H, Nagoshi N, Palmieri K, Singh A, Skelly AC, Tsai E, Vaccaro A, Yee A, Harrop J. A Clinical Practice Guideline for the Management of Patients with Acute Spinal Cord Injury: Recommendations on the Use of Methylprednisolone Sodium Succinate. Global Spine Journal, 2017; in press.
- Fehlings MG, Tetreault L, Aarabi B, Anderson P, Arnold P, Brodke D, Burns A, Chiba K, Dettori J, Furlan J, Hawryluk G, Holly LT, Howley S, Jeji T, Kalsi-Ryan S, Kotter M, Kurpad S, Kwon B, Marino R, **Martin AR**, Massicotte EM, Merli G, Nakashima H, Nagoshi N, Palmieri K, Singh A, Skelly AC, Tsai E, Vaccaro A, Wilson JR, Yee A, Harrop J. A Clinical Practice Guideline for the Management of Patients with Acute Spinal Cord Injury: Recommendations on the Type and Timing of Anticoagulant Thromboprophylaxis. Global Spine Journal, 2017; in press.
- Fehlings MG, Tetreault L, Aarabi B, Anderson P, Arnold P, Brodke D, Burns A, Chiba K, Dettori J, Furlan J,

Hawryluk G, Holly LT, Howley S, Jeji T, Kalsi-Ryan S, Kotter M, Kurpad S, Kwon B, Marino R, **Martin AR**, Massicotte EM, Merli G, Nakashima H, Nagoshi N, Palmieri K, Singh A, Skelly AC, Tsai E, Vaccaro A, Wilson JR, Yee A, Harrop J. A Clinical Practice Guideline for the Management of Patients with Acute Spinal Cord Injury: Recommendations on the Type and Timing of Rehabilitation. Global Spine Journal, 2017; in press.

- Fehlings MG, Tetreault L, Aarabi B, Arnold P, Brodke D, Burns A, Carette S, Chen R, Chiba K, Dettori J, Furlan J, Harrop J, Holly L, Kalsi-Ryan S, Kotter M, Kwon B, **Martin AR**, Middleton J, Milligan J, Nakashima H, Nagoshi N, Rhee J, Riew D, Singh A, Skelly AC, Sodhi S, Wilson JR, Yee A. A Clinical Practice Guideline for the Management of Patients with Degenerative Cervical Myelopathy: Recommendations for Patients with Mild, Moderate and Severe Disease and Non-myelopathic Patients with Evidence of Cord Compression. Global Spine Journal, 2017; in press.
- Fehlings MG, Tetreault L, Wilson JR, Kwon B, Burns A, **Martin AR**, Hawryluk G, Harrop J. A Clinical Practice Guideline for the Management of Acute Spinal Cord Injury: Introduction, Rationale and Scope. Global Spine Journal, 2017; in press.
- Tetreault L, Skelly AC, Dettori JR, Wilson JR, **Martin AR**, Fehlings MG. Guidelines for the Management of Degenerative Cervical Myelopathy and Acute Spinal Cord Injury: Development Process and Methodology. Global Spine Journal, 2017; in press.
- Rhee J, Tetreault L, Chapman J, Wilson JR, Smith JS, **Martin AR**, Dettori JR, Fehlings MG. Update to Rhee et al 2013, "Nonoperative Management of Degenerative Cervical Myelopathy: A Systematic Review." Global Spine Journal, 2017; in press.
- Tetreault L, Rhee J, Prather H, Kwon B, Wilson JR, **Martin AR**, Andersson IB, Dembek AH, Pagarigan KT, Dettori JR, Fehlings MG. Change in Function, Pain and Quality of Life following Structured Nonoperative Treatment in Patients with Degenerative Cervical Myelopathy: A Systematic Review. Global Spine Journal, 2017; in press.
- Nater A, **Martin AR**, Sahgal A, Choi D, Fehlings MG. Symptomatic Spinal Metastasis: A systematic literature review of the preoperative prognostic factors for survival, neurological, functional and quality of life in surgically treated patients and methodological recommendations for prognostic studies. PLOS ONE, 2017, in press.
- De Leener B, Mangeat G, Dupont S, **Martin AR**, Callot V, Stikov N, Fehlings MG, Cohen-Adad J. Topologically-preserving straightening of spinal cord MRI. Journal of Magnetic Resonance Imaging, 2017;12(2):e0171507.
- Nouri A, **Martin AR,** Lange SF, Kotter MRN, Mikulis DJ, Fehlings MG. Congenital Cervical Fusion as a Risk Factor for Development of Degenerative Cervical Myelopathy. World Neurosurgery, 2017;100:531-539.
- Nouri A, **Martin AR**, Tetreault L, Nater A, Kato S, Nakashima H, Nagoshi N, Reihani-Kermani H, Fehlings MG. MRI analysis of the combined prospectively collected AOSpine North America and International Data: The Prevalence and Spectrum of Pathologies in a Global Cohort of Patients with Degenerative Cervical Myelopathy. Spine (Phila Pa 1976). 2016 Nov 16. [Epub ahead of print].
- **Martin AR**, Aleksanderek I, Cohen-Adad J, Tarmohamed Z, Tetreault L, Smith N, Cadotte DW, Crawley A, Ginsberg H, Mikulis D, Fehlings MG. Translating State-Of-The-Art Spinal Cord MRI Techniques To Clinical Use: A Systematic Review Of Clinical Studies Utilizing DTI, MT, MWF, MRS, and fMRI. Neuroimage: Clinical, 2016;10:192–238.
- Ahuja CS, **Martin AR,** Fehlings MG. Recent advances in managing a spinal cord injury secondary to trauma. F1000 Faculty Rev. 2016;5:1017.
- Nouri A, **Martin AR**, Mikulis DJ, Fehlings MG. Magnetic resonance imaging assessment of degenerative cervical myelopathy: A review of structural changes and measurement techniques. Neurosurgical Focus, 2016;40(6):E5.
- **Martin AR**, Aleksanderek I, Fehlings MG. Diagnosis and Acute Management of Spinal Cord Injury: Current Best Practices and Emerging Therapies. Current Trauma Reports. 2015;1(3):169-181.
- Mansouri A, Nader A, **Martin AR**. Journal Club: 5-Aminolevulinic Acid-derived Tumor Fluorescence: The Diagnostic Accuracy of Visible Fluorescence Qualities as Corroborated by Spectrometry and Histology and Postoperative Imaging. Neurosurgery 2015;76(2):227-229.
- **Martin AR**, Cruz JP, O'Kelly C, Kelly M, Spears J, Marotta TR. Small pipes: preliminary experience with 3mm or smaller Pipeline flow-diverting stents for aneurysm repair prior to regulatory approval. AJNR 2015 Mar;36(3):557-561.
- Ayling O, **Martin AR**, Roch-Nagle G. Primary repair of a traumatic superficial temporal artery pseudoaneurysm: case report and literature review. Vascular and Endovascular Surgery. 2014;48(4):346-8.
- Cruz JP, O'Kelly C, Kelly M, Wong JH, **Martin AR**, Spears J, Marotta TR. Pipeline embolization device in

aneurysmal subarachnoid hemorrhage. AJNR 2013;34(2):271-276.

- **Martin AR**, Cruz JP, Matouk C, Spears J, Marotta TR. The Pipeline flow-diverting stent for exclusion of ruptured intracranial aneurysms with difficult morphologies. Neurosurgery. 2012;70(1 Suppl Operative):21-28.
- **Martin AR**, Sankar T, Lipsman N, Lozano AM. Brain-machine interfaces for motor control: a guide for neuroscience clinicians. Can J Neurol Sci 2012;39(1):11-22.
- **Martin AR**, Reddy R, Fehlings MG. Dropped-head syndrome: diagnosis and management. Evidence-Based Spine-Care Journal.2011;2(2):1-5.
- **Martin AR**, Klemensberg J, Klein L, Urbach D, Bell CM. Comparing public and private bariatric surgery facilities in Canada. Canadian Journal of Surgery. 2011;54(3):154-69.
- Podolsky DJ, **Martin AR**, Whyne CM, Massicotte EM, Hardisty MR, Ginsberg HJ. Exploring the role of 3-dimensional simulation in surgical training: feedback from a pilot study. Journal of Spinal Disorders and Techniques. 2010;23(8):e70-4.

Manuscripts in progress (5):

- **Martin AR**, De Leener B, Cohen-Adad J, Cadotte DW, Kalsi-Ryan S, Lange SF, Tetreault L, Nouri A, Crawley A, Mikulis DJ, Ginsberg H, Fehlings MG. Monitoring for Myelopathic Progression with Multiparametric Quantitative MRI. Under review, Journal of Neurology, Neurosurgery, and Psychiatry.
- **Martin AR**, De Leener B, Cohen-Adad J, Cadotte DW, Wilson JR, Tetreault L, Nouri A, Crawley A, Mikulis DJ, Ginsberg H, Fehlings MG. Quantitative MRI Detects Tissue Injury in Asymptomatic Spinal Cord Compression. Under review, Annals of Neurology.
- **Martin AR**, De Leener B, Cohen-Adad J, Cadotte DW, Kalsi-Ryan S, Lange SF, Tetreault L, Nouri A, Crawley A, Mikulis DJ, Ginsberg H, Fehlings MG. Multiparametric Microstructural Spinal Cord MRI Correlates with Global and Focal Impairment and Predicts Outcomes in Degenerative Cervical Myelopathy.
- **Martin AR**, De Leener B, Cohen-Adad J, Cadotte DW, Kalsi-Ryan S, Lange SF, Tetreault L, Nouri A, Crawley A, Mikulis DJ, Ginsberg H, Fehlings MG. Development and Validation of a Multivariate Microstructural MRI Diagnostic Tool for Mild Degenerative Cervical Myelopathy.
- Nouri A, Tetreault L, Nori S, **Martin AR**, Nater A, Shamji MF, Fehlings MG. Congenital Cervical Spine Stenosis in a Global Cohort of Patients with Degenerative Cervical Myelopathy: A Report Based on a MRI Diagnostic Criterion.

Textbook chapters and non-peer-reviewed publications (5):

- **Martin AR**, Cohen-Adad J, Fehlings MG. AOSpine Masters Series: Spinal Cord Injury. Chapter 4: Magnetic Resonance Imaging of the Injured Spinal Cord: The Present and the Future. Editor: Dr. Luis Vialle. In press.
- **Martin AR,** Fehlings MG. American Academy of Orthopedic Surgeons: Athlete's Spine. Chapter: Spinal Cord Injury: Pharmacologic Agents, Thermal Cooling, and Timing of Interventions. Editor: Dr. Andrew Hecht. In press.
- Lange SF, **Martin AR**, Fehlings MG. Neurosurgery Case Series: The Impact of Kyphosis in Patients with Degenerative Cervical Myelopathy. Editor: Dr. Nathan Selden. In press.
- **Martin AR**, Fehlings MG. A Review of Anterior Surgery for Cervical Disc Disease, by Lunsford et al. (1980). *Essential Papers in Neurosurgery.* Editor: Zoher Ghogawala. In press.
- Enenkel RF, Fitch BG, Germain RS, Gustavson FG, **Martin AR**, Mendell MP, Pitera JW, Pitman MC, Rayshubskiy A, Suits F, Swope WC, Ward TJC. Custom math functions for molecular dynamics. IBM Journal of Research and Development. 2005; 49(2/3): 465.

PATENTS

Issued patents (9):

- Inventors: Archambault RG, Gao Y, **Martin AR**, Mendell MP, Silvera RE, Yiu G. Owner: IBM Canada Ltd. Title: Multiple Pass Compiler Instrumentation Infrastructure. US patent: US20110016460 A1. Filed 2010-06-06. Granted: 2011-01-20. Canadian patent: CA2672337 A1. Filed: 2009-07-15. Granted: 2011-01-15.
- Inventors: Gao Y, O'Connell FP, Archambault RG, **Martin AR**, Blainey RJ, McInnes JL. Owner: IBM Corp. Title: Fine-grained software-directed data prefetching using integrated high-level and low-level code analysis optimizations. United States Patent: 7669194. Filed: 2004-08-26. Granted: 2010-02-23.
- Inventor: **Martin AR**. Owner: IBM Corp. Title: System and method for optimized swing modulo scheduling based on identification of constrained resources. United States Patent: 7546592. Filed: 2005-07-21. Granted: 2009-06-09.

- Inventors: **Martin AR**, McInnes JL, Archambault RG, Enenkel RF, Hay RW, McIntosh RI, Mendell MP. Owner: IBM Corp. Method and apparatus for determining the profitability of expanding unpipelined instructions. United States Patent: 7506331. Filed: 2004-08-30. Granted: 2009-03-17.
- Inventor: **Martin AR**. Owner: IBM Corp. Title: Method, apparatus, and program for pinning internal slack nodes to improve instruction scheduling. United States Patent: 7493611. Filed: 2004-08-30. Granted: 2009-02-17.
- Inventors: **Martin AR**, McInnes JL. Owner: IBM Corp. Title: Extension of swing modulo scheduling to evenly distribute uniform strongly connected components. United States Patent: 7444628. Filed: 2004-08-30. Granted: 2008-10-28.
- Inventors: Gao Y, Mendell M, McInnes JL, Archambault RG, **Martin AR**. Owner: IBM Corp. Uniform external and internal interfaces for delinquent memory operations to facilitate cache optimizations. International patent: WO/2008/110418. Filed: 2008-02-08.
- Inventors: **Martin AR**, McInnes JL. Owner: IBM Corp. Title: Scheduling technique for software pipelining. US patent: US20080104373 A1. Filed: 2008-01-03. Granted: 2008-05-01. Canadian patent: CA2439137 A1. Filed 2003-08-08. Granted: 2005-02-08.
- Inventor: **Martin AR**. Owner: IBM Corp. Title: Method for generating instruction sequences for integer multiplication. United States Patent 6748590. Filed: 2000-11-21. Granted: 2004-06-08. Canada Patent: CA/2319888. Filed: 2000-09-18.

Patent application filed, subsequently abandoned (2):

- Inventor: **Martin AR**. Owner: IBM Corp. Title: Modification of swing modulo scheduling to reduce register usage. US patent application: 20060048123. Filed: 2004-08-30. Abandoned: 2006-03-02.
- Inventors: **Martin AR**, McInnes JL. Owner: IBM Corp. Title: Modulo scheduling of multiple instruction chains. US patent application: 20040268335. Filed: 2003-11-06. Abandoned: 2004-12-30.

CONFERENCES AND PRESENTATIONS

Podium Presentations (24):

- **Martin AR**, De Leener B, Cohen-Adad J, Cadotte DW, Wilson JR, Tetreault L, Nouri A, Lange SF, Crawley A, Mikulis DJ, Ginsberg H, Fehlings MG. Multi-Parametric Spinal Cord MRI Detects Subclinical Tissue Injury in Asymptomatic Cervical Spinal Cord Compression. International Society for Magnetic Resonance in Medicine (ISMRM), April 25th, 2017, Honolulu, HI, USA.
- **Martin AR**, De Leener B, Cohen-Adad J, Cadotte DW, Wilson JR, Tetreault L, Nouri A, Lange SF, Crawley A, Mikulis DJ, Ginsberg H, Fehlings MG. Multi-Parametric Cervical Spinal Cord MRI Provides An Accurate Diagnostic Tool for Detecting Clinical Myelopathy. International Society for Magnetic Resonance in Medicine (ISMRM), April 25th, 2017, Honolulu, HI, USA.
- **Martin AR**, De Leener B, Cohen-Adad J, Cadotte DW, Wilson JR, Tetreault L, Nouri A, Lange SF, Crawley A, Mikulis DJ, Ginsberg H, Fehlings MG. Multi-Parametric Spinal Cord MRI Detects Subclinical Tissue Injury in Asymptomatic Cervical Spinal Cord Compression. AANS/CNS Joint Section on Disorders of the Spine and Peripheral Nerves, March 9th, 2017, Las Vegas, NV, USA.
- **Martin AR**, De Leener B, Cohen-Adad J, Cadotte DW, Wilson JR, Tetreault L, Nouri A, Lange SF, Crawley A, Mikulis DJ, Ginsberg H, Fehlings MG. Multi-Parametric Spinal Cord MRI Detects Subclinical Tissue Injury in Asymptomatic Cervical Spinal Cord Compression. Global Spine Congress, May 5th, 2017, Milan, Italy.
- **Martin AR**, De Leener B, Cohen-Adad J, Cadotte DW, Wilson JR, Tetreault L, Nouri A, Lange SF, Crawley A, Mikulis DJ, Ginsberg H, Fehlings MG. Multi-Parametric Microstructural Spinal Cord MRI Applied to Degenerative Cervical Myelopathy. Global Spine Congress, May 5th, 2017, Milan, Italy.
- **Martin AR**, De Leener B, Cohen-Adad J, Cadotte DW, Wilson JR, Tetreault L, Nouri A, Lange SF, Crawley A, Mikulis DJ, Ginsberg H, Fehlings MG. Multi-Parametric Cervical Spinal Cord MRI Provides An Accurate Diagnostic Tool for Detecting Clinical Myelopathy. Candian Spine Society (CSS), February 24th, 2017, Montreal, QC.
- **Martin AR**, De Leener B, Cohen-Adad J, Cadotte DW, Wilson JR, Tetreault L, Nouri A, Lange SF, Crawley A, Mikulis DJ, Ginsberg H, Fehlings MG. Multi-Parametric Spinal Cord MRI Detects Subclinical Tissue Injury in Asymptomatic Cervical Spinal Cord Compression. Candian Spine Society (CSS), February 24th, 2017, Montreal, QC.
- **Martin AR**, Fehlings MG. Seed Starter Grant Progress Update: Spinal Cord Spectroscopy. Cervical Spine

Research Society (CSRS) 2016 Meeting, Toronto, ON, December 3, 2016.

- **Martin AR**, De Leener B, Cohen-Adad J, Aleksanderek I, Cadotte DW, Kalsi-Ryan S, Tetreault L, Crawley A, Mikulis DJ, Ginsberg H, Fehlings MG. A clinically feasible quantitative MRI protocol to assess tissue injury in the cervical spinal cord using DTI, MT, and T2*-weighted imaging: reliability and variations with confounding variables. North American Spine Society (NASS) 31st Annual Meeting, Boston, MA, October 27, 2016.
- **Martin AR**, De Leener B, Cohen-Adad J, Aleksanderek I, Cadotte DW, Kalsi-Ryan S, Tetreault L, Crawley A, Mikulis DJ, Ginsberg H, Fehlings MG. Microstructural MRI Quantifies Tract-Specific Injury And Correlates with Global Disability and Focal Neurological Deficits in Degenerative Cervical Myelopathy. Congress of Neurological Surgeons (CNS) 2016 Annual Meeting, San Diego, September 27, 2016.
- **Martin AR**, Fehlings MG. Management of Degenerative Cervical Myelopathy: Current Evidence, Clinical Practice Guidelines, and Future Treatment Options. 55th International Spinal Cord Society (ISCoS) Annual Scientific Meeting, Vienna, Austria, September 14, 2016.
- **Martin AR**, Fehlings MG. Clinical Trials Update: Riluzole as a neuroprotective agent in traumatic and non-traumatic spinal cord injury. 55th International Spinal Cord Society (ISCoS) Annual Scientific Meeting, Vienna, Austria, September 12, 2016.
- **Martin AR**, De Leener B, Aleksanderek I, Cohen-Adad J, Cadotte DW, Kalsi-Ryan S, Tetreault L, Crawley A, Ginsberg H, Mikulis DJ, Fehlings MG. A Prospective Longitudinal Study in Degenerative Cervical Myelopathy Using Quantitative Microstructural MRI with Tract-Specific Metrics. International Society for Magnetic Resonance in Medicine (ISMRM) Annual Meeting, Singapore, May 12, 2016.
- **Martin AR**, Aleksanderek I, Cohen-Adad J, Tarmohamed Z, Tetreault L, Smith N, Cadotte DW, Crawley A, Ginsberg H, Mikulis D, Fehlings MG. Translating State-Of-The-Art Spinal Cord MRI Techniques To Clinical Use: A Systematic Review Of Clinical Studies Utilizing DTI, MT, MWF, MRS, and fMRI. International Society for Magnetic Resonance in Medicine (ISMRM) Annual Meeting, Singapore, May 12, 2016.
- **Martin AR**, Aleksanderek I, Cohen-Adad J, Cadotte DW, Kalsi-Ryan S, Nugaeva N, De Leener B, Tetreault L, Mikulis DJ, Crawley A, Ginsberg H, Fehlings MG. 2-minute oral presentation: A Prospective Longitudinal Study in Degenerative Cervical Myelopathy (DCM) Using Next-Generation Multimodal Quantitative MRI with Tract-Specific Metrics. AANS/CNS Joint Section on Disorders of the Spine and Peripheral Nerves, Spine Summit, Orlando, FL, March 19, 2016.
- **Martin AR**, Aleksanderek I, Cohen-Adad J, Cadotte DW, Kalsi-Ryan S, Nugaeva N, De Leener B, Tetreault L, Mikulis DJ, Crawley A, Ginsberg H, Fehlings MG. Next-Generation MRI Identifies Tract-Specific Injury And Predicts Focal Neurological Deficits in Degenerative Cervical Myelopathy: Development and Characterization of Accurate Imaging Biomarkers for Spinal Cord Pathologies. Canadian Spine Society (CSS) Annual Meeting, Whistler, BC, February 27, 2016.
- **Martin AR**, Aleksanderek I, Cohen-Adad J, Tarmohamed Z, Tetreault L, Smith N, Cadotte DW, Crawley A, Ginsberg H, Mikulis D, Fehlings MG. Translating State-Of-The-Art Spinal Cord MRI Techniques To Clinical Use: A Systematic Review Of Clinical Studies Utilizing DTI, MT, MWF, MRS, and fMRI. Canadian Spine Society (CSS) Annual Meeting, Whistler, BC, February 27, 2016.
- **Martin AR.** Next-Generation MRI of the Human Spinal Cord: Translating Quantitative Measures of Tissue Injury to Clinical Use in Traumatic and Non-Traumatic SCI. 2015 Ontario Spinal Cord Injury Research Network (OSCIRN) Meeting, Toronto, ON, October 23, 2015.
- **Martin AR**, Aleksanderek I, Cohen-Adad J, Cadotte DW, Kalsi-Ryan S, Nugaeva N, De Leener B, Tetreault L, Mikulis DJ, Crawley A, Ginsberg H, Fehlings MG. Power-Pitch Session: A Prospective Longitudinal Study in Degenerative Cervical Myelopathy (DCM) Using Multimodal Advanced MRI with Tract-Specific Quantitative Metrics. International Society for Magnetic Resonance in Medicine (ISMRM) Spinal Cord MRI Workshop, Toronto, ON, June 5, 2015.
- **Martin AR**, Aleksanderek I, Cohen-Adad J, Cadotte DW, Kalsi-Ryan S, Nugaeva N, Mikulis DJ, Crawley A, Ginsberg H, Fehlings MG. Next-generation MRI of the human spinal cord: methods of a longitudinal translational study to develop quantitative imaging biomarkers in cervical spondylotic myelopathy (CSM). SpineFEST, University of Toronto Spine Program, June 2015.
- **Martin AR**, Aleksanderek I, Cohen-Adad J, Cadotte DW, Kalsi-Ryan S, Nugaeva N, Mikulis DJ, Crawley A, Ginsberg H, Fehlings MG. Next-generation MRI of the human spinal cord: Translating measures of microarchitecture and function to clinical utilization. Imaging Network of Ontario (ImNO), 13th Symposium, March 2015.
- **Martin AR**. IBM Blue Gene Compilers and Optimizations. 3rd Blue Gene Systems Software and Applications Workshop, Tokyo, Japan. April 2006. http://www.cbrc.jp/symposium/bg2006/PDF/ Martin.pdf
- **Martin AR**. Profitability Analysis of Instruction Replacement Sequences, IBM CASCON Conference 2005

- **Martin AR**. Modulo Scheduling, IBM CASCON Conference 2004

Conference Posters/Abstracts (16):

- **Martin AR**, De Leener B, Cohen-Adad J, Cadotte DW, Wilson JR, Tetreault L, Nouri A, Lange SF, Crawley A, Mikulis DJ, Ginsberg H, Fehlings MG. Toward Clinical Translation of Quantitative Spinal Cord MRI: Serial Monitoring to Identify Disease Progression in Patients with Degenerative Cervical Myelopathy. International Society for Magnetic Resonance in Medicine (ISMRM), April 25th, 2017, Honolulu, HI, USA.
- **Martin AR**, De Leener B, Cohen-Adad J, Aleksanderek I, Cadotte DW, Kalsi-Ryan S, Tetreault L, Crawley A, Mikulis DJ, Ginsberg H, Fehlings MG. Clinically Feasible Microstructural MRI to Assess Tissue Injury in the Cervical Spinal Cord: Normative Data, Variations with Confounding Variables, and Reliability. Congress of Neurological Surgeons (CNS) 2016 Annual Meeting, San Diego, September 24-28, 2016.
- **Martin AR**, Aleksanderek I, Cohen-Adad J, Tarmohamed Z, Tetreault L, Smith N, Cadotte DW, Crawley A, Ginsberg H, Mikulis D, Fehlings MG. Translating State-of-the-Art Spinal Cord MRI Techniques to Clinical Use: a Systematic Review of Clinical Studies Utilizing DTI, MT, MWF, MRS, and fMRI. Congress of Neurological Surgeons (CNS) 2016 Annual Meeting, San Diego, September 24-28, 2016.
- **Martin AR**, De Leener B, Cohen-Adad J, Cadotte DW, Kalsi-Ryan S, Lange SF, Tetreault L, Nouri A, Crawley A, Mikulis DJ, Ginsberg H, Fehlings MG. Microstructural Cervical Spinal Cord MRI Quantifies White Matter Injury And Correlates with Global and Focal Deficits. National Neurotrauma Society (NNS) 2016 Symposium, Lexington, KY, June 26-29, 2016. Awarded Top 20 Abstract Finalist and Murray Goldstein Award.
- **Martin AR**, De Leener B, Cohen-Adad J, Aleksanderek I, Cadotte DW, Kalsi-Ryan S, Tetreault L, Crawley A, Mikulis DJ, Ginsberg H, Fehlings MG. Clinically Feasible Microstructural MRI to Assess Cervical Spinal Cord Tissue Injury: Methods, Normative Data, and Reliability. National Neurotrauma Society (NNS) 2016 Symposium, Lexington, KY, June 26-29, 2016.
- Alcaide-Leon P, Sankar S, Cybulsky K, Ahn B, Leurer C, **Martin AR**, Bharatha A, Oh J. Quantitative Spinal Cord MRI in Radiologically Isolated Syndrome: Preliminary Results of a Prospective Study. 31st Congress of the European Committee for Treatment and Research in Multiple Sclerosis, Barcelona, Spain, October 2015.
- **Martin AR**, Aleksanderek I, Cohen-Adad J, Cadotte DW, Kalsi-Ryan S, Nugaeva N, De Leener B, Mikulis DJ, Crawley A, Ginsberg H, Fehlings MG. Next-Generation MRI of the Human Spinal Cord: A Prospective Longitudinal Study in Cervical Spondylotic Myelopathy (CSM) to Develop Quantitative Imaging Biomarkers. Congress of Neurological Surgeons (CNS), New Orleans, LA, Sept 2015.
- Wang J, Smith S, Kalsi-Ryan S, **Martin AR,** Massicotte EM, Fehlings MG. The Role of Surgery in Gait Improvement. University of Toronto, University of Toronto, Institute of Medical Sciences (IMS) SURP Research Day, August 2015.
- **Martin AR**, Aleksanderek I, Cohen-Adad J, Cadotte DW, Kalsi-Ryan S, Nugaeva N, Mikulis DJ, Crawley A, Ginsberg H, Fehlings MG. Next-generation MRI of the human spinal cord: methods of a longitudinal translational study to develop quantitative imaging biomarkers in cervical spondylotic myelopathy (CSM). SpineFEST, University of Toronto Spine Program, June 2015.
- Aleksanderek I, **Martin AR**, Cohen-Adad J, Kalsi-Ryan S, Nugaeva N, Mikulis DJ, Crawley A, Fehlings MG. Imaging biomarkers of the spinal cord in cervical spondylotic myelopathy quantified using MR spectroscopy. SpineFEST, University of Toronto Spine Program, June 2015.
- **Martin AR**, Aleksanderek I, Cohen-Adad J, Cadotte DW, Kalsi-Ryan S, Nugaeva N, Mikulis DJ, Crawley A, Ginsberg H, Fehlings MG. Next-generation MRI of the human spinal cord: methods of a longitudinal translational study to develop quantitative imaging biomarkers in cervical spondylotic myelopathy (CSM). Gallie Day, Department of Surgery, University of Toronto, May 2015.
- Aleksanderek I, **Martin AR,** Cohen-Adad J, Kalsi-Ryan S, Nugaeva N, Mikulis DJ, Crawley A, Fehlings MG. Imaging biomarkers of the spinal cord in cervical spondylotic myelopathy quantified using MR spectroscopy. Gallie Day, Department of Surgery, University of Toronto, May 2015.
- Aleksanderek I, **Martin AR**, Cohen-Adad J, Kalsi-Ryan S, Nugaeva N, Mikulis DJ, Crawley A, Fehlings MG. Imaging biomarkers of the spinal cord in cervical spondylotic myelopathy quantified using MR spectroscopy. Toronto Western Research Institute (TWRI) Research Day, May 2015.
- **Martin AR**, Aleksanderek I, Cohen-Adad J, Cadotte DW, Kalsi-Ryan S, Nugaeva N, Mikulis DJ, Crawley A, Ginsberg H, Fehlings MG. Next-generation MRI of the human spinal cord: Translating measures of microarchitecture and function to clinical utilization. Imaging Network of Ontario (ImNO), 13th Symposium, March 2015.
- **Martin AR**, Cruz JP, Spears J, Marotta TR. Small pipes: the use of small diameter flow diversion in the Circle

of Willis and beyond. 12th Congress of the World Federation of Interventional and Therapeutic Neuroradiology.
- **Martin AR**, Whyne CM, Ginsberg HJ. Evaluating the Role of 3D Simulation in Surgical Training. 55th Annual Meeting of the Orthopedic Research Society Conference, Las Vegas, Nevada, February 2009
- **Martin AR**, Whyne CM, Ginsberg HJ. Evaluating the Role of 3D Simulation in Surgical Training. Ontario Medical Student Research Day, Toronto, April 2009
- **Martin AR**, Modulo Scheduling at IBM Application and Integration Middleware conference in Raleigh, NC, 2004

Clinical Grand Rounds Presentations (7):
- IgG4-related hypetrophic pachymeningitis. Neurology Rounds, July 20, 2013.
- Delayed vasospasm following epidermoid tumour resection. Krembil Combined Krembil Neurology/Neurosurgery Rounds, Toronto Western Hospital, November 10, 2012.
- Brain-Machine Interfaces. Krembil Combined Krembil Neurology/Neurosurgery Rounds, Toronto Western Hospital, August 3, 2012.
- Choroid Plexus Tumours at Combined Neurology/Neurosurgery Rounds at Hospital for Sick Children, April 14, 2010
- The Liberation Procedure: Hope or Hype? Presented at Family Medicine Rounds, Toronto East General Hospital and Flemingdon Park Health Centre, December 2009
- Adrenal Suppression in a 17-year-old Asthmatic. Presented at Pediatric Rounds, Toronto East General Hospital. October 2009
- Brain-Machine Interfaces. Presented at Neurosurgery Journal Club, Toronto Western Hospital, August 2009

HONOURS AND AWARDS

Grants/Fellowships:
- Canadian Institutes of Health Research (CIHR) Fellowship: salary support 2016-2017 ($50,000/year + $5000 allowance, up to 3 years)
- Cervical Spine Research Society (CSRS) Seed Starter Grant: operating funding for investigation of MR spectroscopy in the cervical spinal cord ($25,000 USD).
- Edward Christie Stevens Fellowship in Medicine 2015-2016 ($4000)
- Surgeon Scientist Training Program, University of Toronto (salary support, 07/2015 - 06/2016)
- Edward Christie Stevens Fellowship in Medicine 2014-2015 ($1750)
- Joseph M. West Family Memorial Fund Award 2014-2015 ($1750)
- Ministry of Health Clinician Investigator Program (salary support, 07/2014 – 06/2015)
- Rick Hansen Institute: Optimizing Neurorecovery Following SCI: Deep Brain Stimulation of the Pedunculopontine Nucleus to Improve Walking After Spinal Cord Injury. Under PI Dr. Andres Lozano ($150,000)
- St. Michaels Hospital Trauma/Neurosurgery Multi-disciplinary Grant 2008. Under PI Dr. Howard Ginsberg ($2000)

Research Awards:
- Charles Kuntz Scholar Award 2016, AANS/CNS Joint Section on Disorders of the Spine and Peripheral Nerves ($500 USD)
- National Neurotrauma Society (NNS) 2016 Symposium, Murray Goldstein Award ($500 USD, Elselvier Textbook Gift Certificate: $400 USD)
- International Society for Magnetic Resonance in Medicine (ISMRM) 2016 Magna Cum Laude Merit Award
- Canadian Spine Society (CSS) 2016 Annual Meeting, Best Resident Paper ($500)
- SpineFEST 2016 Abstract Competition: 3rd Place ($250)
- Office of Research Trainees, University Health Network, Conference Travel Award for ISMRM 2016 ($500)
- SpineFEST 2015 Abstract Competition: 3rd Place ($150)

Academic Honours/Awards:

- University Scholarships: Canada Scholar ($5,000 x 4 years), University of Toronto Scholar ($2,500), Wallberg Award ($1,000), J.P. Bickell Foundation Scholarship ($1,000)
- Governor General's Bronze Medal for highest grade-point average in graduating high school class (97%)
- Honours Standing for all preclerkship medical school blocks
- Achieved top mark in individual undergraduate classes: MAT194 (98%), ECE150 (100%), CHE150 (94%), ECE250 (96%), MIE301 (96%), ECE443 (95%), BIO150 (90%, top 1% of class)
- Dean's List for all 8 semesters of undergraduate Engineering Science program
- University of Waterloo Math Contests: highest mark in high school, and top 5% of all contestants in all 5 years of high school
- Achieved score of 39Q on MCAT (VR13, BS12, PS14)

Clinical Honours:

- Received Gold Star award from nurses on 5A unit for excellent collaboration and patient care, 2012.
- Recognized for excellent patient care in letter to TWH patient affairs by patient, 2012

Industry Honours/Awards:

- 11 IBM Invention Achievement Awards totalling $10,500
- IBM Outstanding Technical Achievement Award for industry leading Power4 performance: $5,000 USD
- 2 IBM Bravo Awards for outstanding technical contributions totalling $1,000
- 2 sets of IBM stock options of high achievement, exercised for total of $20,000
- Invited to 3 IBM Toronto Lab Gala dinners for outstanding technical performance

---

RESEARCH AND TEACHING INTERESTS

Research interests:

- Innovation and application of emerging technology to the field of neurosurgery
- Functional and anatomical neuroimaging
- Computational analysis of medical imaging
- Intraoperative navigation and image-guided surgery
- Design of surgical instruments and robotics systems

Teaching interests:

- Helping medical students and junior residents become proficient in the basics of clinical neurosurgery including knowledge, operative skills, and patient management
- Providing a friendly and low-stress learning environment for students
- Improving formal resident education by being an active voice in design of curriculum and lecture formats

---

RESEARCH EXPERIENCE

Research Fellow, Institute of Medical Sciences PhD Program
7/2014-Present

- Supervised by Dr. Michael G. Fehlings
- Leading several clinical studies using advanced MRI techniques to quantify injury to the human spinal cord and translate these novel tools to clinical utilization

Research Consultant, Ryerson Biomechanics and Photonics Laboratory
5/2011-9/2011

- Supervised by Dr. Victor Yang
- Investigating alternative techniques for neuro-navigation
- Developing software for surgical planning and navigation

Student Researcher, Investigating Deep Brain Stimulation Recordings for Brain-Machine Interfaces
5/2009-9/2009

- Supervised by Dr. Andres Lozano
- Worked on signal analysis of EEG and local field potential recordings for possible use in a brain-machine interface
- Wrote a review paper on subject of neuroprosthetics, accepted by Canadian Journal of Neurological Sciences

Student Researcher, Evaluation of Public/Private Bariatric Surgery Clinics in Canada
9/2008-5/2009
- Supervised by Dr. Chaim Bell, project part of Determinants of Community Health 2 course
- Research comparing cost, wait-times, and outcomes between public and private bariatric surgery clinics
- Wrote a research manuscript, accepted for publication in Canadian Journal of Surgery

Student Researcher, Development and Evaluation of a 3D Surgical Simulator, CREMS
1/2008-12/2008
- Supervised by Dr. Howard Ginsberg and Dr. Cari Whyne
- Designed and conducted a study to evaluate the efficacy of the simulator as a teaching tool for surgical residents
- Applied and received Research Ethics Board approval from University of Toronto and Mount Sinai Hospital
- Secured $2000 grant from St. Michael's Hospital Neurosurgery/Trauma Small Grant Program
- Created a prototype for a standalone program and with additional functionality

Research Assistant, University of Toronto (10 hrs/wk)
5/1998-9/1998
- Supervised by Professor Mark Chignell in paid Research Assistant position
- Created a software document categorization system based on a clustering algorithm from a technical paper

---

GRANT WRITING EXPERIENCE

Research Operating Grants (8):
- Cervical Spine Research Society (CSRS) Seed Starter Grant: operating funding for investigation of MR spectroscopy in the cervical spinal cord ($25,000 USD).
- As lead assistant to Dr. Michael Fehlings: Wings for Life (2), Canadian Institute of Health Research (CIHR) (2), CIHR/National Science and Engineering Research Council (NSERC) (1), Rick Hansen Institute (2)

JOURNAL/GRANT REVIEWER EXPERIENCE

Journal Manuscript Reviews (30):
- As independent reviewer (2): Functional Neurology (1), Journal of Neuroimaging (1)
- As assistant reviewer to Dr. Michael Fehlings (26): European Spine Journal (3), Lancet Neurology (3), Neurosurgery (3), PLOS One (7), Spine (8), Spinal Cord (1), Journal of Neurosurgery: Spine (1)

Grant Reviews (1):
- As assistant reviewer to Dr. Michael Fehlings: Wings for Life (1)

TEACHING EXPERIENCE

- Art and Science of Clinical Medicine (ASCM) Tutor for Brain & Behaviour, for first-year University of Toronto medical students (March-April 2015)
- Formal mentor to 3 junior neurosurgery residents (Jetan Badhiwala, Kyle Juraska, Francois Mathieu)
- Formal preceptor/advisor to 6 undergraduate research students in Dr. Fehlings' lab (Zenovia Tarmohamed, Nathaniel Smith, Samantha Smith, Justin Wang, Ashima Agarwal, Stefan Lange), July 2014 – present.

- CSC490/2900H (Undergraduate Engineering Design Project Course) – Group Mentor, January – June, 2016
- Course instructor and co-administrator for University of Toronto PGY1 Neurosurgery Crash Course, July 2014 and July 2015
- Surgical Exploration and Discovery (SEAD) Program Lecturer, University of Toronto Medical School, June 2014
- Suturing Instructor, University of Toronto Medical School Suturing Workshop, 2013, 2014, 2015
- Informal preceptor to numerous medical students (approximately 20) completing neurosurgery electives, July 2011 – June 2014
- Course instructor for University of Toronto Surgical Exploration and Discovery (SEAD) Program, Neurosurgery, April 2014
- Sailing Instructor for Oakville Yacht Squadron (OYS), teaching basic and advanced sailing skills to children and adults,1992-1995

PROFESSIONAL EXPERIENCE

Software Developer, Compiler Optimization, IBM Canada (10 hrs/wk)
9/2007-3/2009
- Completed several work items, maintenance of previously written code, and mentorship of new team members

Software Developer, Compiler Optimization, IBM Canada (40 hrs/wk)
5/1999-8/2007
- Excelled in this highly technical area, earning two promotions in first four years of employment
- Acted as Technical Lead of a team of 20 engineers and researchers developing Blue Gene compiler products
- Participated in high-level hardware design discussions for upcoming IBM processor chips
- Owned several compiler optimizations such as modulo scheduling and loop unrolling

Landlord
5/2003-8/2008
- Purchased and extensively renovated a 70-year-old duplex, renting one bedroom apartment
- Learned all aspects of property management, including maintenance and tax implications of rental income

Software Developer, Netron Incorporated (40 hrs/wk)
5/1997-8/1998
- Worked in Research and Development department of software tools company
- Successfully created a standalone component of Netron Fusion product

CLINICAL EXPERIENCE

Licensure, certifications, and specialized skills:
- University of Toronto: Microsurgery (Dr. Julian Spears), Aug 2013
- University of Toronto: Spinal Instrumentation (Dr. Eric Massicotte), Jun 2012, June 2013
- University of Toronto: Fundamentals of Spinal Surgery: An Introductory Course of Advanced Spinal Techniques for Spinal Fellows, August 2014
- AOSpine: Spine Trauma and Instrumentation Principles Course, Oct 2011
- Midas Rex: Drill Techniques and Equipment, Jul 2011
- College of Physicians and Surgeons of Ontario, Postgraduate Medical Certificate: July 1, 2011
- Medical Council of Canada Qualifying Exam, Part 1: completed May 2011
- Medical Council of Canada Qualifying Exam, Part 2: completed Oct 2012
- Royal College of Physicians and Surgeons: Surgical Foundations Exam: completed Apr 2013
- Advanced Cardiac Life Support (ACLS): completed June 2011
- Advanced Trauma Life Support (ATLS): completed August 2011
- Trained in Standard First Aid and CPR Level C (St. John Ambulance, completed in 2006)

University of Toronto Neurosurgery Residency Program clinical rotations:

- Neurosurgery (St. Michael's Hospital): 6 months under Dr. Julian Spears
- Neurosurgery (Toronto Western Hospital): 9 months under Dr. Eric Massicotte
- Neurosurgery (Sunnybrook Health Sciences Centre): 3 months under Dr. Todd Mainprize
- Neurology: 3 months under Dr. David Chan
- Spine/Orthopedic Surgery: 2 months under Dr. Henry Ahn
- Trauma/General Surgery: 3 months under Dr. Teodor Grantcharov
- Vascular Surgery: 2 months under Dr. George Oreopoulos
- Emergency: 2 months under Dr. Martin Horak
- ICU: 3 months under Dr. Natalie Wong and Dr. Simon Abramson

---

LEADERSHIP EXPERIENCE

- Co-organizer of International Society for Magnetic Resonance in Medicine (ISMRM) Spinal Cord MRI Workshop, Toronto, ON, June 5, 2015.
- Resident Program Committee (RPC) member, University of Toronto Neurosurgery Program 7/2012-6/2014. Led Junior resident subgroup with Brian Drake to improve junior residency. Participated in CaRMS selection committee 2013, 2014.
- Core Surgery Committee member, University of Toronto Department of Surgery 9/2011-6-2013. Attended monthly meetings regarding improving surgical education including revising Surgical Foundations curriculum.
- Formal mentor to 2 junior neurosurgery residents (Jetan Badhiwala, Kyle Juraska)
- Acted as informal preceptor to numerous elective medical students at both TWH and SMH who were interested in Neurosurgery, teaching skills in performing emergency consults, floor duties, order entry, and basic OR skills.
- Co-president of Student Interest Group in Neurology (SIGN), University of Toronto working with Dr. Liesly Lee 9/2008-5/2009
- Neurosurgery/Neuroradiology Representative for Students for Technology and Engineering in Medicine (STEM) 9/2008-5/2009
- Acted as IBM Blue Gene Compiler Technical Lead, heading a team of 25 engineers and researchers developing fundamental software that helped implement the world's fastest supercomputer (2005-2007).
- Acted as IBM TOBEY Department Assistant Team Lead, running weekly team meetings and overseeing individual performance goals of 20 technical employees

---

VOLUNTEER EXPERIENCE

Volunteer, Hospital for Sick Children (3 hrs/wk)
12/2005-5/2007

- Spent time with kids with severe illnesses on neurosurgery and multi-organ transplant units
- Provided entertainment and a sense of normalcy for the children and their parents

Crew Leader, Habitat for Humanity Toronto (4-8 hrs/wk)
9/2005-12/2006

- Helped build affordable housing for low-income families, participating in all aspects of construction
- Asked to become crew leader on first volunteer shift
- Led groups of 6-10 volunteers, teaching skills and monitoring safe practices

Volunteer, Employee Charitable Fund, IBM Canada (100 hrs)
9/2001-10/2006

- Represented area for 3 years, organizing events such as hockey pool, table tennis tournament, and CN Tower stair climb team

Team Member, Sean Lough Campaign for City Counselor (3-5 hrs/wk)
6/2003-11/2003

- Helped organize aspects of campaign including fundraising and canvassed to increase awareness of issues

---

ACADEMIC AFFILIATIONS

- Resident Member: American Academy of Neurological Surgeons (AANS), Congress of Neurological Surgeons (CNS)
- Student Member: Society for Neuroscience (SfN), International Society for Magnetic Resonance in Medicine (ISMRM)
- OMA, CMA

MISCELLANEOUS

Specialized skills and other training:

- National Coaching Certification Program: Level 2 (completed in 1996)
- Software training in: C, C++, Fortran, Plix, Cobol, Java, KSh, compiler optimization, UNIX admin
- Canadian Yachting Association: Gold Sail (highest possible) and Blue Sail (advanced instructor) levels

Interests and other skills

- Hobbies: parenting, home renovations, music (drums and bass guitar), travel
- Sports: long distance running, sailing, skiing, snowboarding, floor hockey, soccer, tennis, golf, cycling

Copyright Acknowledgements

Permission was obtained to reproduce Figure 1.1 from Nouri et al. (2015) from artist Diana Kryski (Kryski Biomedia), who holds copyright of this image.

Permission was obtained to reproduce Figure 1.4 from Cohen-Adad et al. (2012) from Wolters Kluwer Health, Inc.

Permission was requested from American Journal of Neuroradiology (AJNR) to reproduce Martin et al. (2017a) and Martin et al. (2017b), and this was informally granted (via email), and official permission will be granted following publication of these manuscripts in June 2017.

Permission will be requested for the articles that represent Chapters 4 and 5, once they are accepted for journal publication.